The Development of Point Doppler Velocimeter Data Acquisition and Processing Software

Angelo A. Cavone
ATK Space, Hampton, Virginia

The NASA STI Program Office . . . in Profile

Since its founding, NASA has been dedicated to the advancement of aeronautics and space science. The NASA Scientific and Technical Information (STI) Program Office plays a key part in helping NASA maintain this important role.

The NASA STI Program Office is operated by Langley Research Center, the lead center for NASA's scientific and technical information. The NASA STI Program Office provides access to the NASA STI Database, the largest collection of aeronautical and space science STI in the world. The Program Office is also NASA's institutional mechanism for disseminating the results of its research and development activities. These results are published by NASA in the NASA STI Report Series, which includes the following report types:

- TECHNICAL PUBLICATION. Reports of completed research or a major significant phase of research that present the results of NASA programs and include extensive data or theoretical analysis. Includes compilations of significant scientific and technical data and information deemed to be of continuing reference value. NASA counterpart of peer-reviewed formal professional papers, but having less stringent limitations on manuscript length and extent of graphic presentations.

- TECHNICAL MEMORANDUM. Scientific and technical findings that are preliminary or of specialized interest, e.g., quick release reports, working papers, and bibliographies that contain minimal annotation. Does not contain extensive analysis.

- CONTRACTOR REPORT. Scientific and technical findings by NASA-sponsored contractors and grantees.

- CONFERENCE PUBLICATION. Collected papers from scientific and technical conferences, symposia, seminars, or other meetings sponsored or co-sponsored by NASA.

- SPECIAL PUBLICATION. Scientific, technical, or historical information from NASA programs, projects, and missions, often concerned with subjects having substantial public interest.

- TECHNICAL TRANSLATION. English-language translations of foreign scientific and technical material pertinent to NASA's mission.

Specialized services that complement the STI Program Office's diverse offerings include creating custom thesauri, building customized databases, organizing and publishing research results ... even providing videos.

For more information about the NASA STI Program Office, see the following:

- Access the NASA STI Program Home Page at *http://www.sti.nasa.gov*

- E-mail your question via the Internet to help@sti.nasa.gov

- Fax your question to the NASA STI Help Desk at (301) 621-0134

- Phone the NASA STI Help Desk at (301) 621-0390

- Write to:
  NASA STI Help Desk
  NASA Center for AeroSpace Information
  7115 Standard Drive
  Hanover, MD 21076-1320

The Development of Point Doppler Velocimeter Data Acquisition and Processing Software

Angelo A. Cavone
ATK Space, Hampton, Virginia

ACKNOWLEDGMENTS

PREFACE

This report details the development of the Point Doppler Velocimeter and is a deliverable for task order NNL07AM34T of the NASA Langley Research Center TEAMS contract NNL07AA00B. It satisfies a portion of the final report deliverable as defined in Sections 1.0 and 2.0 of the statement of work. This report is a slightly modified version of the thesis prepared by Angelo Cavone that was successfully defended in November 2005 in pursuit of a Master's Degree in Computer Science from Christopher Newport University. The thesis committee was chaired by Dr. A. Martin Buoncristiani, PhD, Professor, and Department Chair, Department of Physics, Computer Science and Engineering at Christopher Newport University. The thesis committee also included Drs. John Hardie and Raouf Selim of Christopher Newport University and Mr. James Meyers of NASA Langley Research Center. Mr. Meyers directed the laboratory research described in this report.

ABSTRACT

In order to develop efficient and quiet aircraft and validate Computational Fluid Dynamic predications, aerodynamic researchers require flow parameter measurements to characterize flow fields about wind tunnel models and jet flows. A one-component Point Doppler Velocimeter (pDv), a non-intrusive, laser–based instrument, was constructed using a design/develop/test/validate/ deploy approach. A primary component of the instrument is software required for system control/management and data collection/reduction. This software along with evaluation algorithms, advanced pDv from a laboratory curiosity to a production level instrument. Simultaneous pDv and pitot probe velocity measurements obtained at the centerline of a flow exiting a two-inch jet, matched within 0.4%. Flow turbulence spectra obtained with pDv and a hot-wire detected the primary and secondary harmonics with equal dynamic range produced by the fan driving the flow. Novel, hardware and software methods were developed, tested and incorporated into the system to eliminate and/or minimize error sources and improve system reliability.

TABLE OF CONTENTS

LIST OF TABLES

LIST OF FIGURES

SYMBOLS

$BG_R[i]$ = Background light level at reference camera pixel location i

$BG_S[i]$ = Background light level at signal camera pixel location i

c = Speed of light

$e[I]$ = Voltage measured at output of hot-wire anemometer

$E_R \cos \omega_R t$ = Reference electromagnetic wave, volts/meter

$E_S \cos \omega_S t$ = Scattered light electromagnetic wave, volts/meter

$E(t)$ or ET = Total electromagnetic wave $E_R \cos \omega_R t + E_S \cos \omega_S t$

F = Measured frequency

f_D = Doppler shift in laser optical frequency, Hz

f_S = Laser light source optical frequency, Hz

$FFR[i]$ = Flat field correction factor for reference camera pixel at location i

$FFS[i]$ = Flat field correction factor for signal camera pixel at location i

FSR = Free Spectral Range

$\hat{\imath}$ = Laser light sheet propagation direction unit vector

$i(t)$ = Total photomultiplier output current, amperes

$i_{ac}(t)$ = ac component of photomultiplier output current, amperes

$i_{dc}(t)$ = dc component of photomultiplier output current, amperes

ii = IVC Input Light Intensity Level

k_O = Incident laser beam wave vector (unit vector)

k_S = Scattered laser light wave vector (unit vector)

L = Laser cavity length

Le = Effective laser cavity length

L_{fr} = Fringe spacing

m = integer number of half-wavelengths

N = Normalized Light transmission ratio

$N[i,j]$ = Normalized signal level for a correspond pair of Signal and Reference camera pixels at position i, j

n = number of digitizer bits

pA = Atmospheric pressure – standard (29.92 in/Hg)

pMA = Atmospheric pressure – measured

pD = Differential pressure (pT– pS)

P_S = Static pressure

P_T = Total pressure

r_w = Wheel radial location (inches)

R = Gas Constant 286J/kg °K

Rw = Rotational speed of wheel (Hz)

RPS = Revolutions Per Second

$R[i]$ = Reference camera intensity level at pixel location i

$R[i,j]$ = Amplitude of pixel at location i, j on the Reference camera

$S[i]$ = Signal camera intensity level at pixel location i

$S[i,j]$ = Amplitude of pixel at location i, j on the Signal camera

$TICL$ = Turbulence intensity based on centerline pipe exit velocity

TM = Temperature measured at time of data acquisition, °C

t = etalon thickness

v = Velocity of the scattering particle (unit vector)

vB = Velocity obtained using Bernoulli's equation, m/s

vCL = Centerline velocity at pipe exit, m/s

$vHW[i]$ = Instantaneous flow velocity measured with a hot-wire

vR = Velocity of moving receiver (detector)

v_{LFM} = Optical frequency observed by laser frequency monitor component

v_{MC} = Optical frequency observed by measurement component

v_O = Optical frequency

v_R = Velocity of moving receiver (detector)

v_{RMS} = RMS velocity measured with a hot-wire

V_s = Velocity of moving source

$VPP[i]$ = Voltage measured at output of pitot probe manometer

V = Velocity vector

V_P = Particle velocity, m/s

V_S = Particle velocity, m/s

VW = Velocity of rotating wheel

$WSRPM$ = Rotating wheel speed, Revolutions Per Minute (rpm)

ω_r = Angular frequency of reference electromagnetic wave, radians/second

ω_s = Angular frequency of signal electromagnetic wave, radians/second

Δv = Doppler shift in laser optical frequency

$\hat{o}$ = Propagation direction of detected scattered light unit vector

oi = IVC Output Light Intensity Level

β = Proportionality constant of a photomultiplier tube

θ = Beam pair intersection angle

θw = Rotating wheel light scattering angle

ρ = Density

ρa = Density of air at time of data acquisition

σv = Standard deviation for resolved local velocity

ϕ_2 = Angle between two, crossed laser beams, deg

λ = Laser wavelength, m

λi = Illumination laser wavelength, m

λo = Wavelength observed at detector, m

$\Delta\lambda$ = Change in wavelength, m

ACRONYM TABLE

A/F – light attenuation-to-light frequency conversion
CCD – Charge Couple Device
CFD – Computational Fluid Dynamics
DAQ – Data Acquisition (Board)
DC – Direct Current
DGV – Doppler Global Velocimetry
DLR – German acronym for the German Aerospace Research Center and Space Agency
[German] Deutsche Forschungsanstalt fuer Luft- und Raumfahrt
DPIV – Digital Particle Image Velocimetry
DSP – Digital Signal Processing
FDP – Frequency Domain Processor
FFT – Fast Fourier Transform
FL – Focal Length
FPAA – Field Programmable Analog Array
FS – Full Scale
FSR – Free Spectral Range
GHz – gigahertz
GPIB – General Purpose Interface Bus
GUI – Graphical User Interface
He-Ne – Helium Neon
HW – Hardware
Hz – Hertz
kHz – kilohertz
IVC – Iodine Vapor Cell
LFM – Laser Frequency Monitor
LSB – Least Significant Bit
LUT – Lookup Table
LV – Laser Velocimetry
LVABI – Laser Velocimetry Autocovariance Buffer Interface
MHz – Megahertz
Nd:YAG –Neodymium-doped Yttrium Aluminum Garnet (Lasing Medium)
NTF – National Transonic Facility (at NASA Langley Research Center)
pDv – Point Doppler Velocimetry
PID – Proportional Integral Derivative
PIV – Particle Imaging Velocimetry
PMT – Photomultiplier Tube
SDPIV – Stereo Digital Particle Imaging Velocimetry
TEM_{00} – Transverse Electromagnetic Mode
VMR – Voltage Mid-Rail

CHAPTER I - INTRODUCTION

A. Problem Statement (Research Motivation)

Aerodynamicists employ flow measurement technologies to characterize flow fields around aerodynamic models and jet flows, and to validate computational fluid dynamic (CFD) predictions. Measurements obtained using these technologies provide researchers with temperature, pressure, density, velocity and turbulence characterizations, enabling them to gain a better understanding of the physics associated with the flow. This knowledge is then applied to develop or modify airfoil and jet engine configurations, investigate novel flight concepts, study advanced materials, improve fuel efficiency, reduce noise emissions and minimize structural fatigue. The anticipated effects of the new or modified designs are then verified with further measurements. The test-modify-verify cycle is repeated until the desired performance goals are achieved. Flow characterization data is also used to improve or verify CFD prediction models that are used to estimate the effects of new and modified configurations to be tested in the next design cycle.

Although traditional intrusive flow measurement instruments such as pitot probes and hot-wire anemometers are still used, they are losing favor to non-intrusive laser based techniques which permit researchers to more accurately map the flow being investigated without the influence of the measurement probe. To date, several laser based flow velocity measurement systems, such as the Laser Velocimeter (LV) (Reference beam configuration - Yeh and Cummins, 1964, Fringe configuration – Lennert, Brayton, and Crosswy, 1970) which provides three-component velocity and turbulence intensity measurements at a point, and Particle Image Velocimetry (PIV) (Adrian and Yao, 1983) which provides two-component measurements within a plane have been developed. At present, these two techniques are routinely employed in flow field investigations of fundamental fluid mechanic phenomena, aircraft configurations, and engine and jet flows.

Many factors influence the decision of an aerodynamic research team to select a given flow measurement technique. These include the ability of the instrument to make the desired measurement, perturbation of the flow, survivability in harsh environments, operating costs, ease of use and measurement confidence. Of these concerns, the most critical factor is the degree of confidence that the resulting measurements accurately characterize the target flow parameter. For this reason, acceptance of any new flow measurement technology is predicated on the degree to which it yields information that compares favorably with the measurements obtained using accepted standards.

The goal of the present research is to investigate the application of Point Doppler Velocimetry (pDv) to measure the turbulent frequency content of a flow. At present, the only instrument capable of making these measurements with any degree of fidelity is the hot-wire anemometer. Because the hot-wire is physically placed into the flow, its disruptive nature introduces a degree of flow measurement uncertainty. Point Doppler Velocimetry is currently being investigated at the NASA Langley Research Center in Hampton, Virginia, in hopes of achieving an *optical hot-wire* that would provide non-intrusive flow spectral measurements. Researchers at West Virginia University (Kuhlman, et. al., 2002) and the German Aerospace Center – DLR (Schodl, et. al., 2002) are also investigating Point Doppler Velocimetry for application to circular jets and engine testing respectively.

As with any measurement technology, the effects of potential error sources must be characterized, and then minimized to lower the degree of uncertainty in the measurement (Sydenham, 1979). This exercise is even more critical as the desired statistical order is increased, which amplifies the influence of any error source on the resultant measurement. Thus, a comprehensive and carefully constructed series of experiments must be developed to identify and mitigate the influence of error sources in an instrument as complicated as a Point Doppler Velocimeter, especially when the desired measurement is turbulence power spectra. The goal of this effort is to work through the concept of Point Doppler Velocimetry at each level and develop a system that fulfills the theoretical promise of non-intrusively obtaining continuous velocity measurements.

B. Point Doppler Velocimetry

Point Doppler Velocimetry (pDv) is a non-intrusive, laser based, flow measurement technique capable of measuring the velocity of embedded particles at a point. This point, or sample volume, is defined as the intersection of a focused laser beam and the optical axis of an optical receiver system. This geometry defines the component of flow velocity measured - along the direction of the bisector of the angle defined by the two optical axes, Figure 1-1. The technique utilizes the absorption characteristics of Iodine vapor to act as an optical frequency discriminator on the collected laser light, which is scattered by small particles passing through the sample volume. The optical frequency difference between the output of a single-frequency (Argon ion or doubled Nd:YAG) laser and the collected scattered light is the Doppler frequency induced by the motion of the particles as they pass through the laser beam. Thus, the frequency dependent absorption of optical energy as the collected scattered light passes through an Iodine Vapor Cell (IVC), Figure 1-2, provides a velocity dependent transfer function that can be measured. Calibration tables relating light absorption to optical frequency are required for each IVC as the absorption characteristics of each cell will differ based on the internal vapor pressure obtained during cell construction. The instantaneous transfer function is obtained by using two high response photodetectors – one for sampling the collected light before the cell (reference) and another for following the cell (signal). Normalizing the signal intensity with respect to the reference intensity yields a signal that is dependent only on optical frequency, and thus to velocity through the Doppler Effect. The laser frequency, measured with an IVC in a second optical system, is then subtracted from the pDv-measured frequency to yield the Doppler frequency.
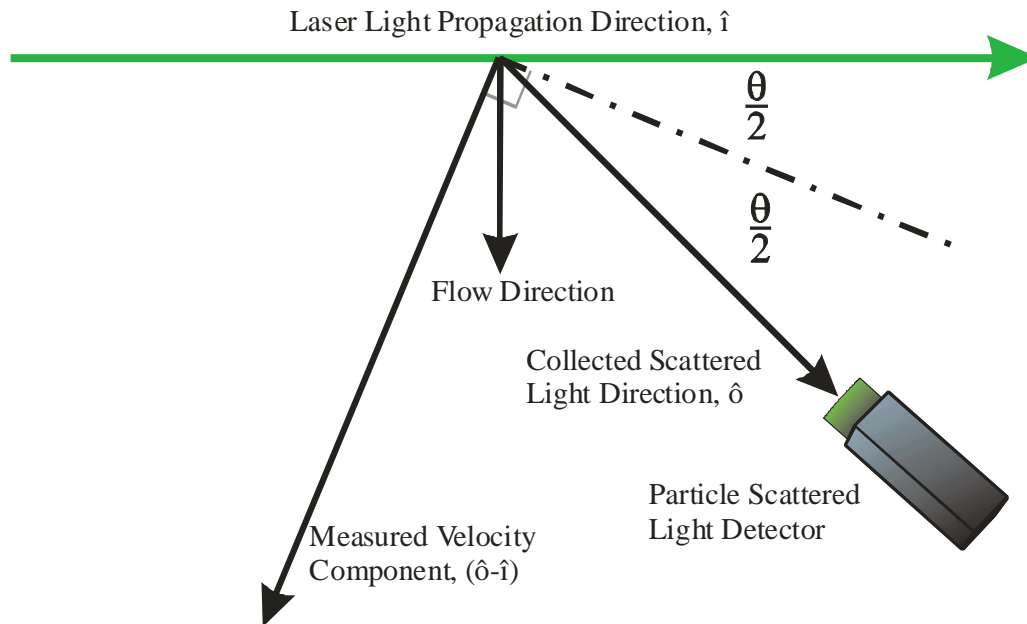
Figure 1-1 – Determination of the measured velocity component.

The figure shows a plot with y-axis labeled "Percent Light Transmission" ranging from 0 to 100.0, and x-axis labeled "Optical Frequency, Mhz". Dashed reference lines mark $T(\nu_0 - \nu_D)$ at about 72%, $T(\nu_0)$ at about 48%, and $T(\nu_0 + \nu_D)$ at about 22%, with corresponding x-axis values $\nu_0 - \nu_D$, ν_0, and $\nu_0 + \nu_D$. A double arrow indicates ~1 GHz across the absorption dip.
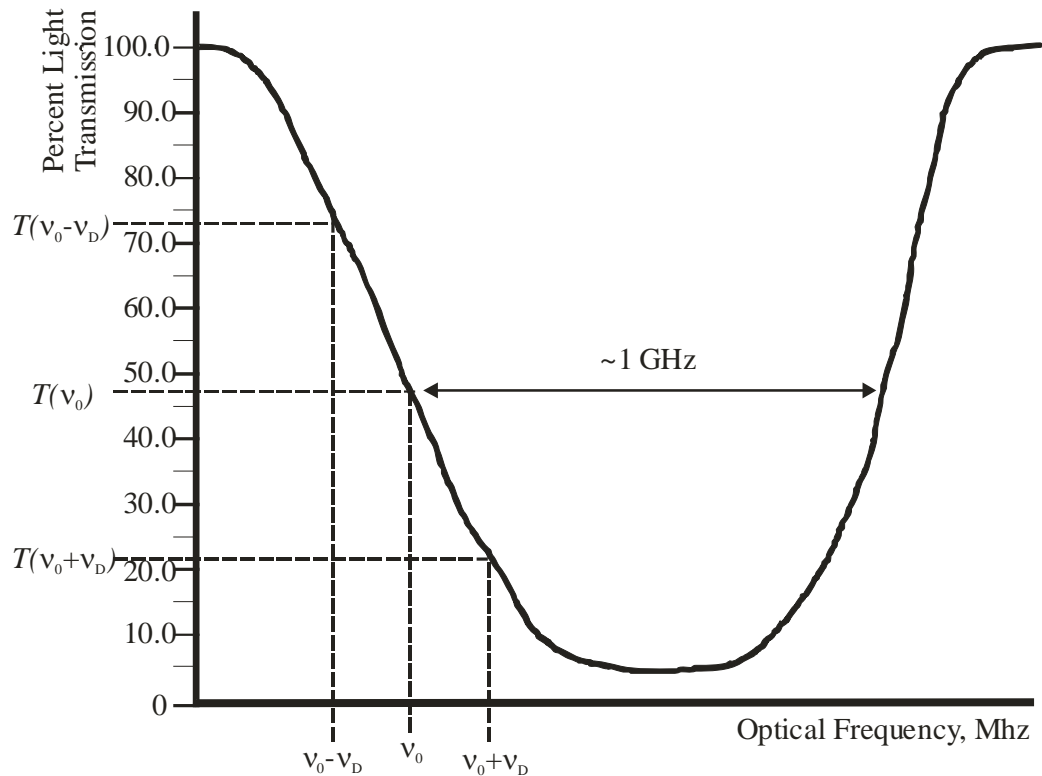
Figure 1-2 – Transfer function of an iodine vapor absorption line

Since pDv is capable of making velocity measurements from scattered light, regardless of its source, it does not suffer from the limitation of single particle scatter necessary for LV or PIV. The LV and PIV techniques require seeding particles sufficiently large to resolve optically, but small enough to faithfully follow the flow field. These conflicting requirements are rarely satisfied, leading to measurement errors - especially in the higher order statistics. In contrast, pDv only requires sufficient photons to activate the detectors to yield velocity measurements. Thus many very small smoke particles may be used as the scattering source. This characteristic eliminates particle dynamic limitations while providing the potential for the continuous acquisition of data points needed for turbulence power spectra measurements.

These characteristics make pDv of particular interest to aerospace researchers since the potential ability to non-intrusively measure flow spectra offers the additional potential to make spatial cross correlation measurements. To date, the accepted standard for measuring flow spectra, the hot-wire anemometer, can be used for spatial cross correlation measurements only in a limited way. The anemometers can only obtain these measurements when the wake of one probe does not influence the measurements of the second probe. Additionally, the two traversing mechanisms must not interfere with each other, typically limiting the potential measurement locations.

C. Research Goals

The presented research concentrates on two areas: (a) demonstrating that pDv is a reliable instrument capable of providing precise and repeatable average velocity, flow statistical, and spectral measurements, and (b) the development and validation of hardware and software needed to conduct the research necessary to refine a deployable instrument providing quality measurements with a high degree of confidence.

D. Point Doppler Velocimetry – Measurement Accuracy

The pDv system must be thoroughly scrutinized so that reliable average velocity, statistical and spectral measurements are obtained in a straightforward robust manner. Investigations were

conducted to address the three parameters that ultimately describe the performance of a measuring instrument (Sydenham, 1979):

- *Resolution* – the finest interval of the measurement scale that can be discerned in the measurement process
- *Precision* – the proximity to a particular value that an individual measurement in a series of identically performed measurements has
- *Accuracy* – the degree to which an individual or collection of measurements matches the value obtained using the accepted standard for making the desired measurement

pDv is a complex instrument that employs a number of subsystems: laser, optics, signal conditioning and data acquisition electronics, and control, acquisition and processing software. The process of bringing these components together to form a cohesive instrument can potentially introduce many types of errors. Accordingly, a methodical series of tests is required at several levels in order to isolate potential error sources, minimize their influence on the velocity measurements, and document the levels of the remaining influence and resulting measurement resolution. To date, testing has been focused in three areas: system component validation, physics and algorithm validation, and overall system validation.

Component validation is concerned with breaking the system down to the smallest element and examining its response to a known stimulus. Known synthetic signals, such as those produced by electronic signal generators and illumination sources, were used to test each component individually and as part of a larger group. Individual and group responses were investigated to establish the operating characteristics, limits, and noise added by the component.

Physics and algorithm validation concentrates on determining how well the system performs as predicted by the theory and whether the theory actually produces the desired measurement characteristics. These efforts will make it possible to determine how the instrument must be implemented to attain the measurement capabilities predicted by theory, develop system calibration schemes and develop efficient data reduction processes.

System operation focuses on the validity of Point Doppler Velocimetry velocity measurements through comparative testing. To date, two research scenarios were employed. In the first series of tests, pDv was used to measure the velocity of a rotating wheel. The rotating wheel provided a *primary standard* to yield known velocities, wherein only measures of distance and rotation speed were needed to determine the velocity at a point on the wheel. The wheel was used to perform two functions; (a) to provide known Doppler shifts to calibrate the IVCs, and (b) to provide a cross check on the overall system accuracy. A description of the calibration procedures is presented in Chapter 5.

The second level of testing provided a means for comparing pDv velocity measurements with those obtained using accepted flow measurement standards. The two standards chosen were a pitot probe to obtain mean velocity measurements, and a hot-wire anemometer to obtain statistical and temporal measurements of turbulence. The ultimate goal was to obtain turbulence power spectra measurements with the pDv that compared favorably with hot-wire measurements. These measurements were made in the jet flow exiting from a 2-inch diameter pipe with a mean centerline velocity of 50 m/s.

A one-component pDv system was constructed, along with the Laser Frequency Monitor (LFM), to conduct these investigations. An Argon ion laser was operated in single frequency mode to provide illumination for the wheel and the pipe flow. For the rotating wheel investigation, the laser beam was focused onto the wheel surface at an angle of 13.9-degrees and the receiver system was aligned in the same plane at an angle of 23.5-degrees Figure 1-3. This configuration yielded velocity measurements in the horizontal plane based on Doppler theory.
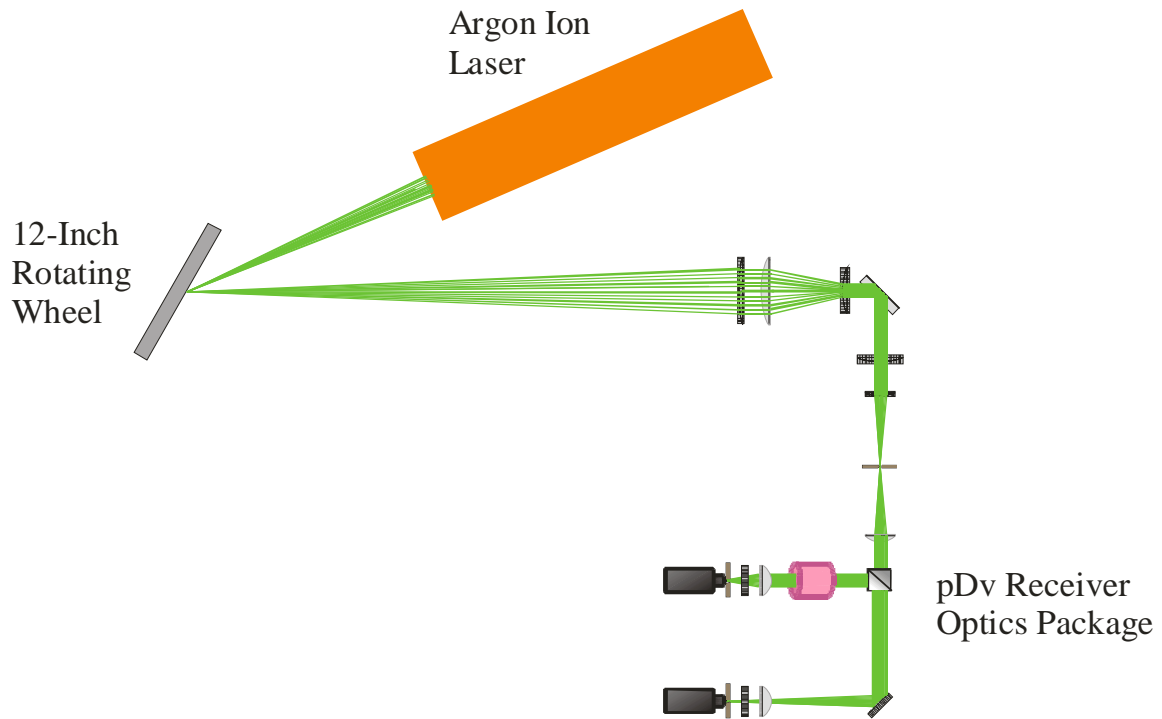
Figure 1-3 – Schematic of the 12-inch rotating wheel configuration.

Once the wheel investigations were completed, the system was moved to the 2-inch pipe flow, Figure 1-4. The weaker scattered light obtained from the smoke particles necessitated a change of detectors from avalanche photodiodes to photomultipliers. The optical arrangement was set to yield a direct measure of the on-axis, U-component, of velocity. Thus, no conversions were necessary when comparing the measurements with the data obtained by the pitot probe and the hot-wire anemometer.
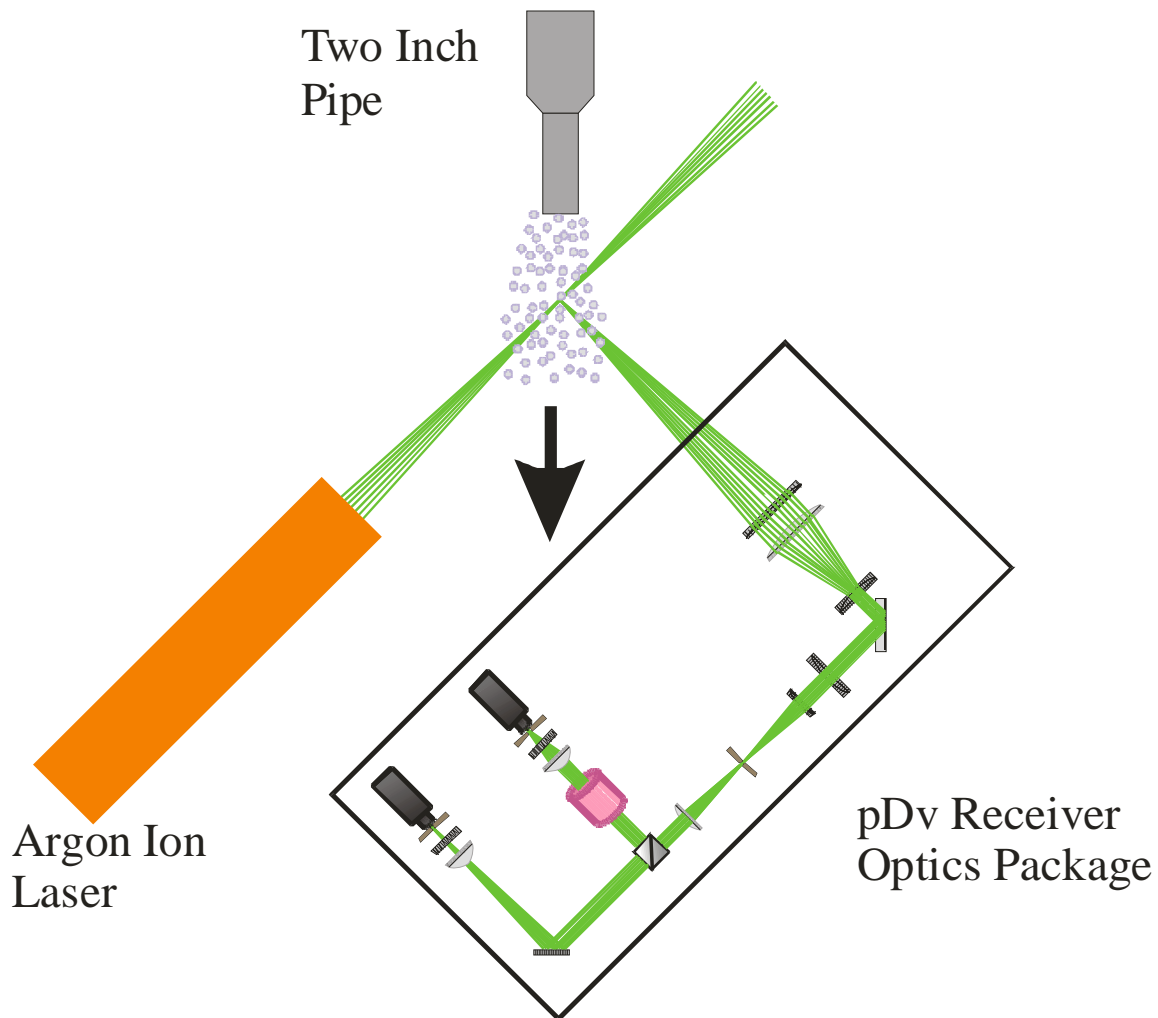
Figure 1-4 – Configuration used to measure the exit velocity of a two-inch pipe.

E. pDv Data Acquisition and Processing Software

Most advanced instrumentation, including pDv, is dependent on the availability of state-of-the-art electronics and sophisticated control, acquisition, and processing software. The theoretical process to translate collected scattered laser light into a measure of the flow velocity was dissected and electronic systems and/or software procedures were chosen appropriately for each segment to obtain efficient and accurate conversions from light levels to velocity. Additionally, system control software was developed to insure stable operation of the laser, translate the three-dimensional scan rig to place the sample volume (and probe) in the desired position, control/setup/operate custom signal processing electronics, and monitor system parameters to insure proper operation prior to data acquisition.

The data acquisition and processing software was developed to satisfy two objectives; pDv technology research and the routine application of the technique for flow characterization. A versatile research version was developed that can be easily modified to adapt to the needs determined by pDv research investigations. This version provides the monitoring capabilities necessary to investigate subtle changes in system functions. The planned deployable version will be an easy-to-use program for aerodynamic researchers who are not skilled in the details of the pDv technology.

Current efforts are focused on the development of the research version. This software provides mechanisms necessary for validating the operational characteristics of system components, developing algorithms used to convert detector output signals to velocity, validating system operating

characteristics and identifying and resolving system limitations and error sources. The statistical and time dependent data obtained with this software provides the insight needed to validate the functionality of pDv technology, and investigate potential modifications to yield a robust instrument that produces flow velocity measurements with the desired confidence levels.

The deployable version of the data acquisition and processing software will be based on the research version. However, many of the detailed monitoring capabilities will be replaced with a graphical user interface (GUI) hosting controls that support only the major system functionality. Additionally, processing software will be modified for production use, where processing speed and measurement accuracy are paramount. Client/server mechanisms will be incorporated to permit real time interaction between the acquisition and processing programs running on networked computers. This approach will provide the aerodynamicists with real time feedback of flow characteristics enabling them to adjust their test matrix in-situ. This will enable them to concentrate on research activities obtaining details of the flow field anomalies instead of exhausting test time using a fine mesh to measure benign areas.

CHAPTER II - LASER BASED FLOW MEASUREMENT INSTRUMENTATION REVIEW

A. Introduction

Since the development of lasers in the early 1960's, researchers have investigated their application to velocity flow field characterization. This research has resulted in the development of instruments capable of characterizing blood flows, flame activity, chemical vapor deposition processes and low-speed to hypersonic airflows. The non-intrusive nature of laser-based flow measurements was attractive to aerodynamicists who employed these techniques to characterize flow fields around classical airfoils, aircraft models, rotating machinery and jet engine inlets and exhausts. Laser based instruments provide accurate velocity measurements in separated, rotating and reverse flow fields, since the measurement probes do not disrupt flow progression. In addition, optical based probes are used to investigate flows in harsh environments such as combustible gases, corrosive fluids or extreme temperature regimes without concern for any probe damage.

Several techniques have been developed to date that exploit the coherent and single frequency nature of laser light to measure the velocity of small particles at a point or in a plane in the same manner that Doppler radar measures the velocity of aircraft. A comparison of the capabilities and limitations of traditional and laser-based flow measurement instruments is presented in Table 2-1. This section provides historical and background information regarding the laser based techniques listed as their operating principles provide the basis for the research in pDv technology.

Attributes	Techniques					
	Pitot-Probe	Hot-Wire	LV	PIV	DGV	pDv
Mean Velocity	Yes	Yes	Yes	Yes	Yes	Yes
Turbulence Intensity	No	Yes	Yes	Limited	No	Yes
Spectral	No	Excellent	Limited	No	No	Potential
Response	<1 Hz	>10kHz (400kHz max.)	Instan-taneous Random Samples	Instan-taneous @ CCD Rates	CCD ~1Hz-30Hz, Limited By Smoke	Limited by DAQ HW
Advantage	Simple, Reliable	Spatial Resolution	Simul taneous, 3-Comp.	2D/3D Velocity	3D Velocity, Large View Plane, High Velocity	Uniform Samples, Direct Velocity Measure
Disadvantage	Invasive	Invasive	Random Sample	Limited View Plane, Low Velocity	Flare, Absolute Measure	Flare, Absolute Measure
Acceptance	Std.	Std.	Std.	Std.	R & D	R & D

Table 2-1 – Comparison of flow parameter measurement techniques.

B. The Laser Velocimeter – A Point Measurement Technique

Yeh and Cummins (1964), who developed what they referred to as a *Laser Spectrometer*, reported the first research on the application of lasers for measuring flow velocity. The goal of their research, conducted at Columbia University under a National Science Foundation Grant, was to develop a flow measuring system to overcome inaccuracies resulting when dye molecules used to study flow streamlines of 50 mm/s or less became diffuse. Their system, now more commonly referred to as a reference beam Laser Velocimeter (LV), leveraged the technologies employed in Doppler radar to measure the velocities of micron-sized, polystyrene particles in water. The geometry of the configuration they employed to make these measurements is shown in Figure 2-1.
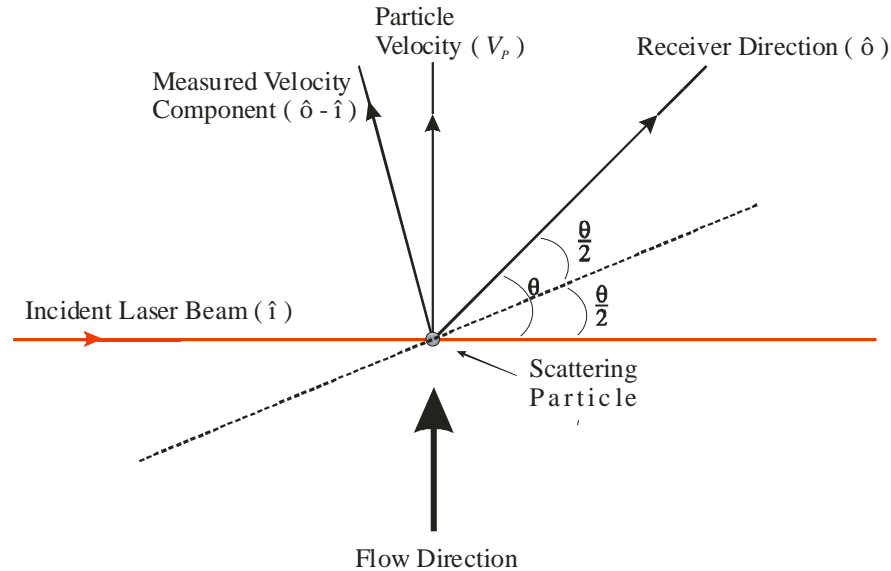
Figure 2-1 – Geometry used to make the first Laser Velocimetry measurements.
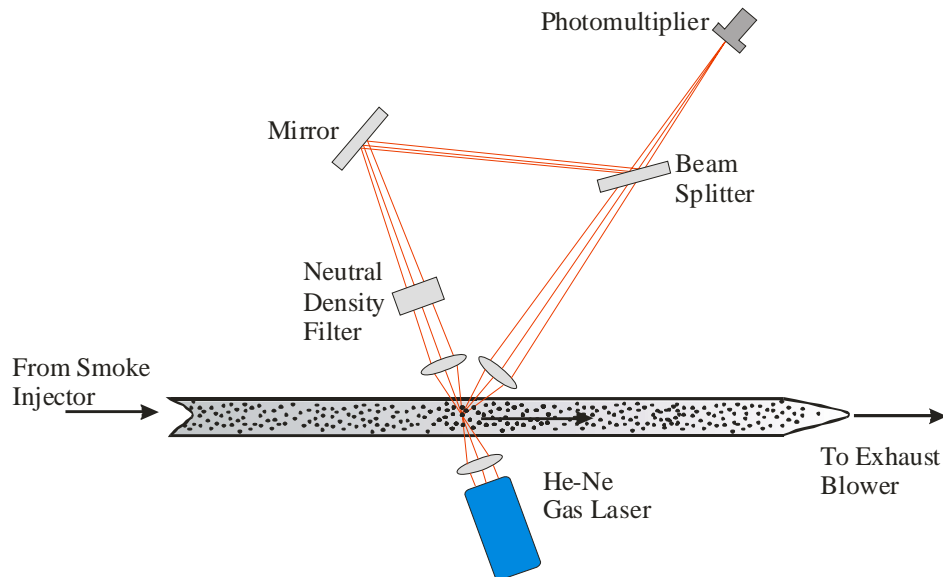
Figure 2-2 – Schematic of reference beam LV system developed by Foreman, et al.

The first documented application of a reference beam LV system to measure the velocity of tracer particles in a gas is credited to Foreman, et al., (1965). The optical configuration employed by them to measure particle velocities in a glass flow-tube is shown in Figure 2-2. Here, the light beam exiting

9

a Helium-Neon (He-Ne) laser was focused at the center of the tube. The original (reference) laser beam, which exited the test section at the emitted laser frequency, was attenuated with a neutral density filter to balance the amplitude level to the particle-scattered light intensity levels. The reference beam was then focused onto the photocathode surface of a photomultiplier tube (PMT). Particles entrained in the flow scattered the laser light in all directions. Some of the scattered light was collected at an angle θ, and focused onto the PMT overlaying the reference beam. The PMT acted as a square law detector in that the electromagnetic waves of the unscattered and scattered laser light were summed and squared (heterodyned) at the photocathode surface as described in Equation 2.1:

$$E(t) = \left(E_S \cos(\omega_S t) + E_R \cos(\omega_R t)\right)^2 \qquad (2.1)$$

The heterodyned signal produced (Equation 2.2) by the PMT was a current whose ac component had a frequency equal to the difference of the optical frequencies of the two input laser signals:

$$i(t) = i_{dc}(t) + i_{ac}(t) \qquad (2.2)$$

Where:

the DC component $i_{dc}(t)$ was determined from:

$$i_{dc}(t) = \beta \left[\frac{E_R^2}{2} + \frac{E_S^2}{2} \right] \qquad (2.3)$$

and the AC component $i_{ac}(t)$ was determined from:

$$i_{ac}(t) = \beta(E_S E_R \cos(\omega_S - \omega_R)t) \qquad (2.4)$$

Where:

β, the proportionality constant, is the response factor of the PMT.

The difference frequency is the Doppler shift frequency, which is directly related to the velocity of the particle that scattered the light. During data acquisition operations, the Doppler frequency was measured directly by a spectrum analyzer, displayed and manually recorded (Foreman, et al. 1965).

The velocity component measured was along the axis in the direction determined by the difference of the incident and scattered light vectors as shown in Figure 2-1. Alignment of the two beams on the photocathode surface was critical, since they were required to be parallel to within $\lambda/4$ to achieve heterodyning. The Doppler frequency shift realized in this configuration is given in Equation 2.5:

$$\Delta v = \left(\frac{v_S - v_0}{2\pi} \right) \bullet V_P \qquad (2.5)$$

During the proof-of-concept tests, this LV system successfully measured the velocity of smoke particles entrained in the glass flow-tube to be about 1 m/s. Subsequently the system was applied to make velocity measurements ranging from 12- to 24-m/s in a vertical wind tunnel. The measured values compared favorably to simultaneously measured velocities using a pitot static probe.

Problems such as optical alignment, component vibration and path length equalization limited the application of the reference beam approach and prompted researchers to investigate alternative configurations. In 1967, Goldstein and Kreid introduced the cross-beam, reference-beam type LV system. Lennert, et al., (1970) extended this work and developed a more robust system that could easily be aligned as shown in Figure 2-3. In this arrangement, the beam exiting the laser was split into two paths using a beam splitter. One beam (reference) contained 1% of the total light energy exiting the laser, while the second beam (probe) contained the remaining 99%. At the point in the flow where these two beams crossed, passing particles scattered the laser light. By positioning a PMT along the same axis as the reference beam, a reference-scatter arrangement was developed as the

10

PMT also collected some of the particle-scattered light from the second beam at the cross over point. As in the original configuration, a heterodyned signal representing the resultant Doppler frequency was the output by the PMT and was measured using a spectrum analyzer. This system was self-aligning since all of the wavefronts of the scattered light from the cross over point were parallel with the reference beam, satisfying the $\lambda/4$ requirement for heterodyning. Their system was used to map the velocity distributions of the flow field around a wing section in a flow with free stream velocities set to both 90- and 300-m/s.
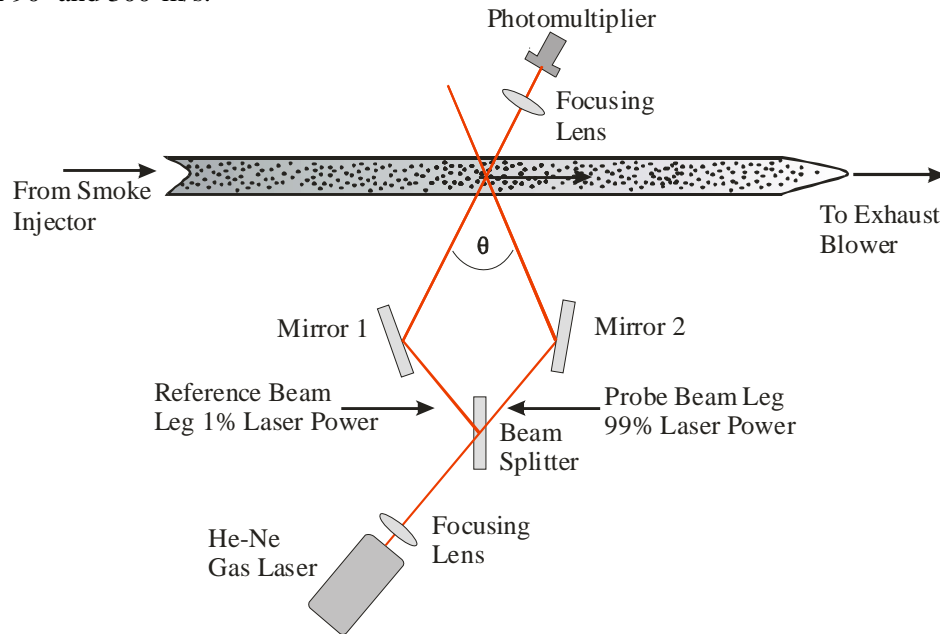
Figure 2-3 – Cross-beam, reference-beam LV system developed by Lennert, et al.

Follow on work on the cross-beam system by several research teams suggested that higher quality Doppler frequency shift signals would be obtained, if only particle scattered light was collected. Brayton and Goehart (1970) developed systems (Figure 2–4 and Figure 2–5) based on this concept that they referred to as "crossed beam, dual scatter" LV; more commonly known as the fringe-based LV technique, the configuration primarily used today. In this arrangement, they equalized the power in both of the laser transmission legs and rotated the receiver optics package so that only particle-scattered light was collected. This resulted in improvements in signal level, signal-to-noise ratio, and sensitivity enabling velocity measurements to be made from single particle transits.
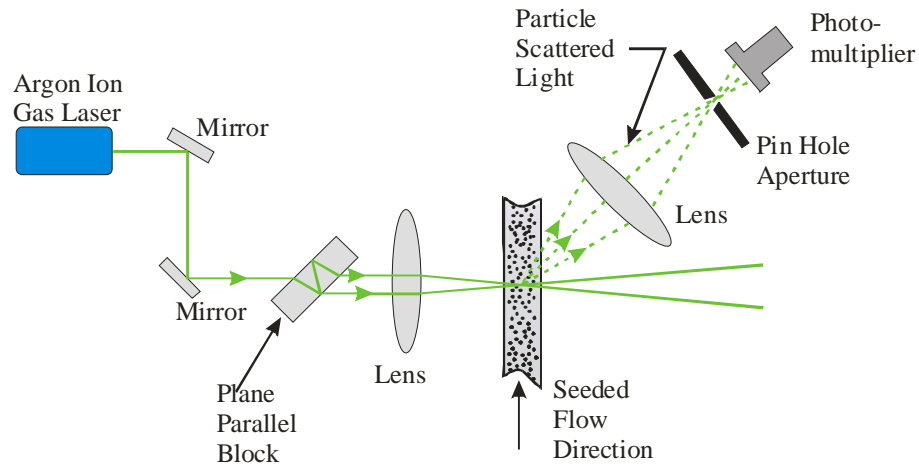
Figure 2–4 – Forward scatter, crossbeam, dual scatter LV system.
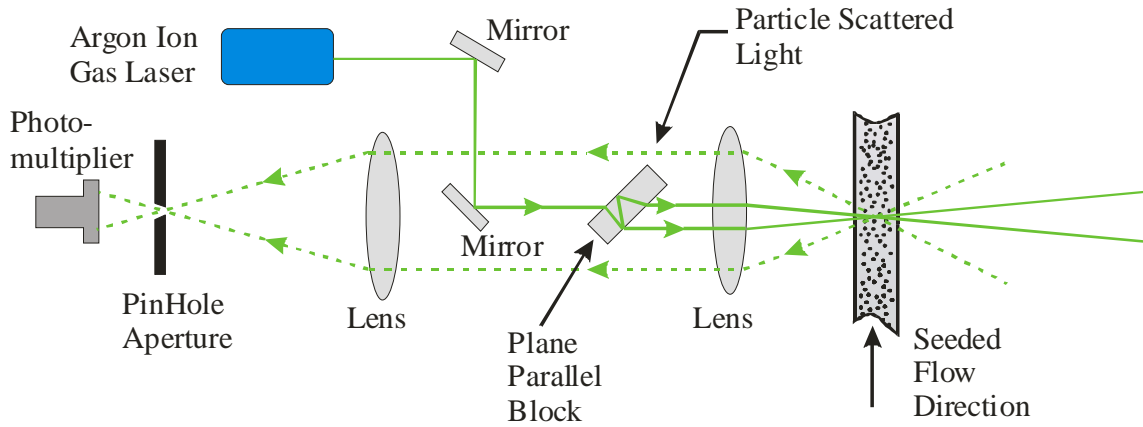
Figure 2–5 – Backscatter, crossbeam, dual scatter LV system (Brayton & Goehart).

The stated improvements were realized using this technique since the detected Doppler frequency is independent of the viewing angle. This permits the collection of scattered light over large solid angles overcoming restrictions in reference beam techniques, where alignment and scattered light collection were limited by beam overlap (Brayton, et al. (1970)). For dual-scatter based LV techniques, the Doppler frequency is dependent only on laser wavelength and the angle between the two laser beams (Meyers, 1971):

$$\Delta f_D = \frac{2V_S}{\lambda}\sin\frac{\Phi_2}{2} \tag{2.6}$$

This arrangement may also be analyzed as if it was an optical interferometer. As illustrated in Figure 2-6, at the location where the two identically coherent and polarized laser beams cross, evenly spaced fringes are formed due the constructive and destructive nature of the light wave fronts (Rudd, 1969).

(b) The constructive and destructive interaction of light waves produces a fringe pattern in the LV sample volume.

(a) Flow entrained particles scatter light as they pass through LV sample volume.

(c) PMT output signal representing a Doppler signal burst resulting from a single particle passage
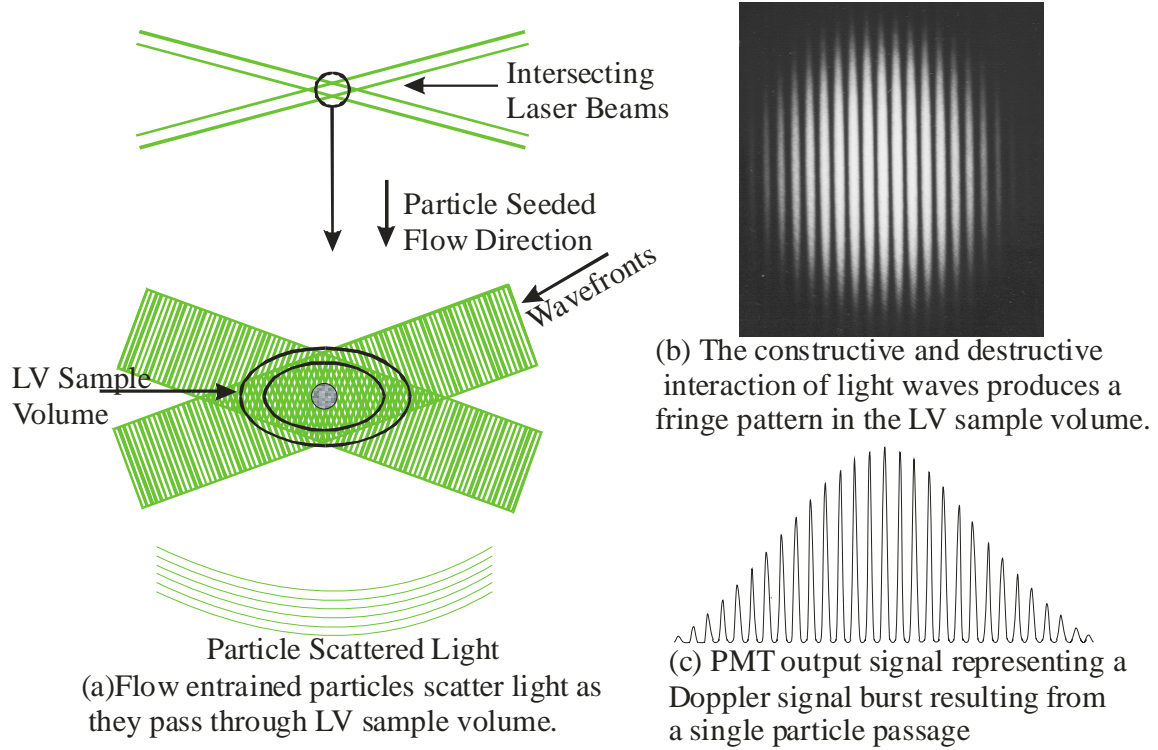
Figure 2-6 – Characteristics of the fringe type Laser Velocimeter (LV).

These fringes produce an alternating pattern of parallel minimum and maximum light levels. Particles passing through the light and dark regions of these fringes scatter light in an oscillatory manner. The frequency of these oscillations is proportional to the velocity of the particle scattering the light. A portion of the light scattered when a particle passes through the sample volume is gathered using collection optics and directed to the off-axis PMT. The PMT output is an oscillating voltage signal representing the intensity of the light scattered by the particle passing through the fringes. Fringe spacing (L_{fr}) is dependent on the angle (θ) at which the two laser beams cross and laser wavelength (λ) as related by Equation 2.7:

$$L_{fr} = \frac{\lambda}{2\sin\left(\dfrac{\theta}{2}\right)} \tag{2.7}$$

With the fringe spacing established, the velocity of a particle in the plane normal to the fringe pattern is obtained through Equation 2.8:

$$V_p = \frac{\lambda F}{2\sin\left(\dfrac{\theta}{2}\right)} \tag{2.8}$$

Notice that Equation 2.6 developed from Doppler theory matches Equation 2.8 based on the interference fringe model. Thus:

$$V_S = V_P \tag{2.9}$$

and

$$\Delta f_D = F \tag{2.10}$$

The measurement of a second velocity component is made possible by orienting a second pair of laser beams along the same optical axis, but orthogonal to the first pair of crossed laser beams.

A third pair of crossed laser beams orthogonal to the original optical axis provides a third measurement component. Multi-measurement component configurations require each beam pair to be unique in some manner. LV systems based on polarization separation (Brayton, et al., 1972), Bragg induced frequency bias (Lennert, et al., 1970) and laser wavelengths (Grant and Orloff, 1973) were developed to address the need for multiple component measurements. Of these approaches, only the laser wavelength technique is capable of providing simultaneous three component measurements. The wavelength implementation has become the dominant approach and it is currently employed in all multiple component, fringe-type LV systems. The first three dimensional velocity measurements obtained using LV were reported by Huffaker, Fuller and Lawrence (1969), who used a very complicated reference beam LV to measure the velocity of particles exiting a supersonic jet. The first three component fringe-based LV system was developed by Yanta and Aushermann (1981) to measure high speed flows. A similar configuration developed by Meyers and Wilkinson (1982) is shown in Figure 2-7.
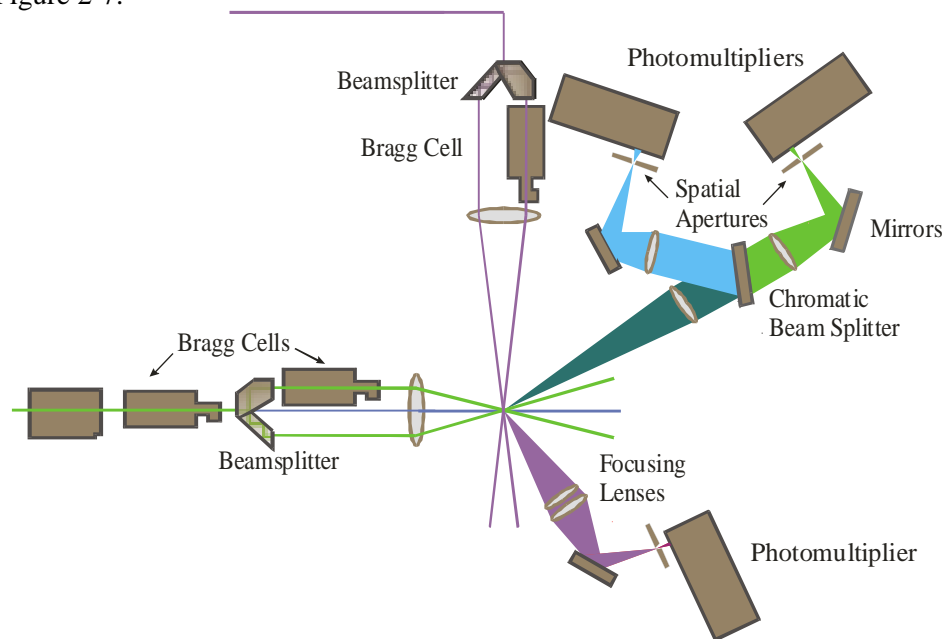
Figure 2-7 – Three component fringe-type Laser Velocimeter.

Current configurations of fringe-type LV systems provide a simultaneous three-component velocity measurement of particles entrained in flow fields and is now an accepted standard for determining statistical turbulence parameters for these flows. Although these three component measurements are simultaneous, they occur only when a particle passes through the fringe patterns. In general, this occurs randomly in time (Poisson distributed). If multiple particles are in the sample volume, a high degree of uncertainty is found within the velocity measurements due to the constructive and destructive mixing between the individual signals. This random spacing between particle arrivals is the primary limitation in successfully measuring temporal parameters, since standard data processing techniques such as FFT analyses require uniform sampling.

Flow directionality in fringe-based LV velocity measurements was achieved with frequency bias using an acoustic-optic Bragg cell (Lennert, et al., 1970). By inserting a Bragg cell into one of the original laser beams, the optical frequency for that leg is shifted by the acoustic frequency, typically on the order of 40 MHz. When the frequency-shifted beam is crossed with the second beam the resulting fringe pattern will move. In the zero velocity condition, the PMT outputs a signal with a Doppler frequency equal to the shift frequency. When the passing particle flows against the direction

of the moving fringes, a higher frequency is realized and when the particle moves in the direction of the fringes, a lower frequency is realized. The ability to establish flow direction enables the application of LV for making velocity measurements in recirculating and turbulent flows.

1. LV Signal Processing Instrumentation

As the purpose of the LV instrument was to measure the velocities contained in a flow field, instruments are required to convert the output current of the PMT to flow velocity information. In order to realize accurate flow velocity information from a very complex PMT output signal, the researcher needed to understand the characteristics inherent to the LV signal:

a. Reference Beam LV Signal Characteristics:

- The PMT output signal is composed of a Doppler burst indicating particle passage riding atop a shot noise limited DC level (~200 MHz – nearly white noise) resulting from photon pile-up due to the constant impingement by the reference beam on the PMT surface
- Particle dropout is a consequence of no particle passages during the sampling interval in certain areas such as those near flow boundaries. During these instances, only the shot/electronic noise riding on top of the DC level is processed
- Intensity variations at the PMT surface due to light scattered (flare) off structures in the field of view of the measurement volume are problematic. The blending of the targeted signal (Doppler burst) and any undesired signal (background light level) results in low signal-to-noise ratios under some flow conditions making the determination of the burst signal frequency difficult
- Doppler signal broadening due to the finite time of the signal burst and the inability to identify the location of the peak frequency (too few cycles) - a problem for general-purpose frequency characterization instruments used to process reference beam LV signals, since these systems employed scanning filters to locate signal peaks. If the signal is not present during the scan interval, inaccurate frequency measurements are obtained

The occurrence of multiple particles in the sample volume during the sampling interval introduced a degree of measurement uncertainty due to the constructive and destructive mixing of the burst frequencies generated by the particles; i.e. square law with more than one signal as shown in Equation 2.1. Here, each particle in the sample volume introduces a new $E_S(n)$ term.

b. Fringe Type LV Signal Characteristics:

- The PMT output signal burst consists of a Doppler burst representing a particle passage riding atop a pedestal voltage. Prior to processing this signal burst, the pedestal component, which results from the Gaussian intensity profile of the crossed laser beams, requires suppression. High-pass filters are used to remove the pedestal signal so that only the burst signal resulting from a particle passage is processed.
- Light scattered off surfaces in the field of view of the collection optics.
- Multiple particles in the sample volume.

These LV signal attributes make the realization of accurate flow-field velocity measurements challenging. As such, several instruments have been employed to measure the Doppler frequency of "burst" signals produced when a particle traverses the probe volume during LV experiments. With these instruments, the flow measurement data are recorded, processed and analyzed, and accurate velocity flow field maps are developed.

2. Spectrum Analyzer

In early LV investigations, swept frequency spectrum analyzers were used to measure the frequency content of LV bursts. The spectrum analyzer was used in all three of the primary LV

techniques; reference beam, cross beam and crossed beam- dual scatter. A narrow spike in the resultant amplitude vs. frequency plot provided an indication of the average Doppler frequency content of the burst signals, which was then translated by hand to a measurement of the mean flow velocity. A measure of flow turbulence intensity was estimated by measuring the width of the Doppler spectrum.

Although the spectrum analyzer provided the desired measurement quantities, it had several difficulties. Among these was that the accuracy of the recorded measurement was dependent on the care taken in reading the displayed information. Another problem was associated with the method used to measure the energy content of a series of bursts and establish its frequency spectrum, which entailed scanning through a range of frequencies. The time needed to perform these scans introduced latency in sampling the PMT output signal, precluding a continuous spectrum analyzer output. In spite of these limitations, the application of this common, general purpose, laboratory device enabled researchers to concentrate on the development of the LV technique rather than on the design of an instrument dedicated to processing LV signals.

3. Frequency Tracker

The desire to extend LV measurement capability and overcome limitations imposed by spectrum analyzers, encouraged the development of custom electronic circuits to process LV signals. The first LV application specific instrument was the Raytheon Wide Band Frequency Tracker, described by Friedman, et al., (1971), which was used to process reference beam LV signals. The tracker, which processed burst signals in the frequency domain in a manner analogous to an FM radio tuner, applied negative feedback to compress bandwidth and adjust signal threshold as system noise fluctuated. Similar in operation to the spectrum analyzer, the tracker employed a frequency-to-voltage discriminator to extract Doppler frequency information from the PMT output signal. A one-second time average voltage output produced by the discriminator yielded a measure of the average Doppler frequency (mean flow velocity). An additional flow related parameter, turbulence intensity, which was related to the Doppler frequency fluctuations, could also be obtained from the rms of the frequency tracker output signal.

As the frequency tracker was designed to operate on signals in the frequency domain, it processed the signal with the highest energy content. Since the PMT signal of reference beam LV systems contained a Doppler burst indicating particle passage riding on top of shot noise, a high signal-to-noise ratio was required to extract Doppler frequency information. In addition, when no particle passage was observed, the tracker processed any peak noise riding on the DC level leading to erroneous results. The original frequency tracker, which employed an analog hold circuit, required that the PMT output signal have a 50% or greater duty cycle to produce accurate frequency measurements. A later version of the tracker, which used a digital hold circuit, reduced the duty cycle requirement to 15%. For these reasons, the frequency tracker was typically employed only when signal to noise ratio and data rate were high and the PMT output signal was nearly continuous such as in heavily seeded or liquid flows.

4. LV High-Speed Burst Counter

Application of the spectrum analyzer and frequency tracker for processing LV signals provided a means for characterizing PMT output signals produced in reference beam LV systems. However, the analog circuits (frequency discriminators) they employed were designed to process continuous signals such as those encountered in liquid flows limiting their ability to accurately measure the Doppler frequency of burst signals encountered in air flows. In addition, the validation circuitry necessary to insure processing of only LV signal bursts was not available.

As LV technologies matured, and the fringe type LV method became the most prevalent implementation, a new signal-processing scheme was required. The processing of fringe type LV type signals was accomplished using a high-speed burst counter, introduced by Lennert, et al. (1971) and refined by Asher (1972). This was the first device that incorporated circuitry specifically

designed to process LV burst signals. Operating in the time domain, this device conditioned the incoming burst signal to form a digital pulse train (Asher, 1972). The leading edge of the first pulse in the train enabled a 100 MHz clock that drove two counters. After the passage of the first four pulses in the modified burst pulse train, one counter was stopped, while the other counter continued until the occurrence of the eighth pulse. The 4- and 8-counter outputs were passed through a D/A converter and resolved voltages compared to determine if the 4 to 8 ratio satisfied the acceptance criteria set by the operator via the unit front panel. Data points outside of the limit were considered noise and rejected, while the count values associated with valid data samples were output over a digital data bus that was interfaced to a computer. The validation process minimized shot noise effects and irregular Doppler signals that occurred when multiple particles were in the sample volume or when a particle passed through the edges of the sample volume. Indication of a valid measurement data output word was provided using a Data Valid signal. The active state of this signal was used to instruct the data collection computer to save the data representing the valid measurement. Analysis of the time spacing between Data Valid pulse activations yielded a measure of data rate and dead time.

The original LV counter was capable of detecting and processing Doppler burst signals in the range of 100 kHz to 25 MHz with a data update rate of up to 100 kHz and provided average flow velocity, turbulence intensity and limited turbulence frequency spectral measurements. The requirement of single particle presence in the sample volume limited the use of LV counters to flows with low particle concentrations and the irregularity in the time between successive measurements limited turbulence spectra analyses.

Later versions of the LV burst counter were wholly based on digital circuitry, employed advanced error detection circuitry, and used a 1 GHz clock to drive the comparison counter chains. This increased burst frequency resolution and reduced measurement uncertainty to 0.5% per burst. The higher speed circuitry also increased the measurement frequency limit to 100 MHz.

5. *Laser Velocimetry Autocovariance Buffer Interface (LVABI) / LV Counter Buffer*

The slow acquisition speeds of minicomputers of the 1970's motivated the development of a custom, high speed, data acquisition unit to accommodate the data rates of the LV burst counter. This unit, called the Laser Velocimetry Autocovariance Buffer Interface (LVABI), (Cavone, et al., 1987), was used to buffer the LV counter data stream during the data acquisition phase, so that it could later be transferred to the host computer in a speed compatible manner. In addition, this system extended LV measurement capability through the following enhancements (Clemmons, 1981):

- Buffered the measurement data to minimize data loss as a result of speed incompatibilities between the LV counter (data rates up to 100 kHz) and slow data acquisition computers of that time period
- Determined and saved the interarrival time between successive velocity measurements up to 1.6 sec. with a resolution of 50 nsec
- Enabled the acquisition of LV data from up to 6 LV counters in parallel with interarrival time measurements for each LV data stream
- Provided an optional data coincidence (within programmable aperture) requirement prior to data acceptance for multiple channel measurements
- Conditionally sampled analog and/or digital data streams produced by other devices such as rotary position encoders, pitot probes and hot-wire anemometers in parallel with the acquisition of the LV data stream, enabling LV measurements to be correlated with position or other measured flow parameters

6. *Frequency Domain Signal Processors*

Use of high-speed LV burst counters remained the predominate method for processing LV signals until the late-1980s, when researchers leveraged the combination of advanced electronic circuits and software to develop instruments employing FFT methods to process LV signals in the

frequency domain. The first of these devices called the Frequency Domain Processor (FDP) (Meyers, et al., 1988), (Baker, et al., 1988) applied high speed A/D converters in combination with higher density memories, and Digital Signal Processors (DSP) and their associated signal processing libraries to improve LV burst signal frequency measurements. These systems overcame the limitations associated with using analog circuits (spectrum analyzers and LV frequency tracker) to process signals in the frequency domain yet maintained the single burst measurement characteristics of the LV burst counter. Technologies used in the FDP also overcame two limitations of LV counters – two points per burst determined the signal frequency and the LV burst must fit a standard signal burst model. Since the FDP acquired multiple samples per burst signal (i.e. > Nyquist sampling rate), single burst measurement uncertainty was reduced to 0.20%.

C. Planar Measurement Techniques

The application of LV afforded a better understanding of the development and progression of flow structures within various flow regimes. In some cases the characterization of some flows was not possible prior to the introduction of LV due to limitations imposed by intrusive probes. During the 1980s, limitations of LV were becoming apparent as aerospace researchers sought additional flow information.

The need for flow measurement systems with expanded measurement capabilities was driven by several factors. First, in order to gain an accurate understanding of turbulent and other unsteady flows, the targeted flows must be considered on a global scale with sufficient spatial resolution to obtain insight into the generation and interaction of flow structures. Secondly, the development of higher power computer hardware helped to make computational fluid dynamics (CFD) a viable tool for predicting velocity flow fields. Thirdly, the costs associated with operating aerodynamic research facilities increased significantly, reducing the time available for researchers to carry out aerodynamic studies. These circumstances made point velocity measuring techniques such as LV less desirable for large wind tunnel applications, since they require a great deal of time to map out large grids with the desired spatial resolution. Further, cause and effect measurements were not possible. These issues required instrumentation engineers to develop whole field or planar velocity measurement techniques.

By inserting a thin sheet of laser light into a flow, the structures embedded within that flow are easily observed through variations in scattering intensity that result when the concentrations of particles embedded within the flow fluctuate as a function of flow structure development and abatement. This property has been exploited to obtain insight into flow fields on large scales. A first approach, known as light sheet flow visualization, used a standard video camera to view and record the scattered light levels. It did not, however, provide a quantitative measure of flow parameters. The concept of viewing the flow field illuminated by a light sheet was expanded to measure the velocity field from particles contained in a flow. Two approaches of particular interest are Particle Imaging Velocimetry (PIV) (Adrian and Yao, 1983) and Doppler Global Velocimetry (DGV) (Komine, 1991).

1. Particle Image Velocimetry (PIV)

Particle Image Velocimetry (PIV) is a two-dimensional whole flow field mapping technique that instantaneously tracks the progression of particles entrained in a flow. Within a selected measurement plane, two time staggered, short duration (~10 ns), Nd:YAG, laser light pulses form two temporally separated thin light sheets that illuminate the particle field and enable time of flight measurements. The time separation of these laser light sheets was adjusted to match velocities anticipated to be in the flow and to keep the viewed particle motion distances small. The displacement of particles that scatter the laser light was originally recorded by double exposing photographic film (Adrian and Yao, 1983) and later on two successive images grabbed from large-area Charge Coupled Device (CCD) cameras. Since the time separation of the light sheets was known, it was possible to determine the velocity of each particle based on the recorded displacement. Registration patterns were used to accurately scale and locate the developed flow maps with respect to a wind tunnel model location or other boundaries.

In their original PIV work, Adrian and Yao, (1983), applied autocorrelation techniques to extract velocity information from a single photographic image used to record the laser pulse pairs. In 1991, Humphreys developed an alternative implementation, which was faster but not as robust. In this approach, the movement of particles between laser pulses recorded on double exposed film was tracked using histogram and pattern matching techniques. As with the autocorrelation method, velocity information was extracted by analyzing the photographs in small interrogation blocks (1 mm x 1 mm) and determining the centroid of each particle imaged. Guided by each centroid in the developed centroid map, a circular neighborhood of all possible pairings between the centroid at the center of the neighborhood and all other centroids within the radial bounds was established for image pairings. The process was repeated until all of the centroids within the map were analyzed. This yielded the collection of possible vectors associated with the centroid pairings. For each neighborhood, there is only one valid pairing and many incorrect pairings. Correct pairings are identified by finding the peaks in magnitude and angle histograms generated from the data ensemble (Humphreys, 1991). Smooth transitions between interrogation regions were realized by overlapping the interrogation blocks by 50% which results in each of the quadrants of an interrogation block away of the edge of the image being processed four times.

Once the velocity vectors of the entire particle field were established, adjacent vectors were compared and wildly different vector values between neighbors were rejected. Using a weighted average of the distance from a given grid point, validated vectors were then projected onto a uniform grid, producing a velocity map of the image flow plane.

Establishing flow velocity maps through autocorrelation and film image pairings was a time consuming (4 to 5 hours) process that was alleviated with the introduction of large-area CCD cameras for imaging the particle planes. This modern approach called Digital Particle Image Velocimetry (DPIV) employs a CCD camera in combination with a frame grabber and advanced cross-correlation signal processing techniques. Algorithms implemented in high-speed computers provide an order of magnitude speed increase in processing capability enabling near real-time velocity measurements of flow cross-sections. The concept of frame straddling (Wernet 2000), where by the first light pulse is imaged near the end of the electronic shutter period of the camera and the second light pulse imaged at the start of the electronic shutter period on the subsequent image frame, enables a single CCD camera to be used to image both laser pulses. This reduces system cost and component count, since a single large area CCD camera can be used to perform the function of two cameras. This approach has become the defacto standard as frame straddling specific cameras are being manufactured by several companies, e.g. Kodak, Sensicam, etc.

An early limitation of PIV was that it could only provide two-dimensional, in plane measurements. This restriction was overcome with an advanced implementation of PIV called Stereo Digital PIV (SDPIV). This system uses two CCD cameras mounted in a stereo viewing arrangement to enable the measurement of the out-of-plane velocity component through the determination of the difference in the in-plane velocity measurements (Wernet, 1996). Errors associated with the out-of-plane velocity measurements are ten times greater than those of the in-plane components.

The ability of PIV to simultaneously measure an entire flow plane with high grid resolution satisfies CFD code validation requirements and reduces aerodynamic research facility run times. PIV has been applied to measure velocity planes around aerodynamic models in wind tunnels (Fleming, et al, 2002), in jet flows, engine inlets and exhausts and rotating machinery (Wernet, 2000) and is now a standard planar flow measurement technology.

In spite of the advanced measurement capability afforded by PIV, several constraints make PIV unattractive for some aerodynamic research applications. The limitations include: (a) susceptibility to the effects of seeding particle dynamics, (b) limited viewing plane (0.5 m x 0.5 m max.), (c) flare from scattering surfaces in the viewing plane, and, (d) inability to make cross-flow measurements since the in-plane time of the particle must be longer than the time between laser pulses. The characteristics of particle dynamics combined with small viewing regions are firmly tied to each other, since PIV requires that the blur circle produced by a given particle fill a minimum area of

3-by-3 pixels to achieve accurate centroid weighting. The requirement of 3-by-3 pixel areas for each particle quickly consumes the surface area of even large format CCD cameras, thus limiting the viewing plane size.

2. Doppler Global Velocimetry (DGV)

In the late 1980's, a team of researchers at the Northrup Research and Technology Center applied their knowledge of spectroscopy and the light absorption characteristics of various gases to detect scattered light frequency variations in particle seeded flows. This research resulted in the creation of an optical frequency discriminator based on the light absorption characteristics of molecular Iodine. As light passed through the Iodine vapor, it was attenuated as a function of optical frequency. Komine, et al. applied their optical frequency discriminator to develop a planar velocity measurement technique called Doppler Global Velocimetry (DGV) for which Northrup was awarded a U.S. patent in 1990. As in PIV, DGV, a thin sheet of laser light is applied to illuminate flow-entrained particles and CCD cameras image the resulting scattered light. However, rather than measuring velocity through particle displacement, DGV measured the optical frequency of the light scattered by concentrated collections of small particles. As long as sufficient scattered light to activate the CCD cameras is collected, velocity measurements can be obtained. This eliminates the requirement for individual particle resolution overcoming two limitations in PIV, particle lag effects and the limited viewing area.

Like the reference beam LV system, introduced by Yeh and Cummins (1964), the physics behind DGV are based on the principles of Doppler theory as related to the shift in optical frequency observed when light is scattered by flow driven particles passing through a laser beam. Instead of using heterodyning to isolate the Doppler frequency, DGV measures the absolute optical frequency by applying the absorption characteristics of Iodine vapor. By taking the ratio of scattered light intensity measurements before and after passage through the Iodine vapor, the absolute optical frequency resulting from particles passing within the laser light sheet is determined. The difference between the observed frequency and the frequency of the light emitted by the laser provides the Doppler frequency shift resulting from particle motion.

At multiple optical wavelengths within the green spectra, Iodine vapor has numerous absorption bands, each with a linewidth of about 1 GHz. In a manner analogous to band-reject (notch) filters used to condition electronic signals, light with frequencies falling between the frequency extremes of one of these absorption lines is attenuated to varying degrees. This characteristic is the basis for using Iodine vapor as an optical frequency-to-transmission converter. Two bands of particular interest are the 514.5 nm line of an Argon Ion laser and the 532.0 nm line of a frequency doubled Nd:YAG laser. Each of these lasers has been used in DGV research. In practice, Iodine granules are placed into an evacuated sealed cell referred to as an Iodine Vapor Cell (IVC)[1] (Figure 2–8(G&K)). The IVC is then heated to a stable temperature of 40°C, where the Iodine granules are converted to a gaseous state filling the sealed cell with Iodine vapor at a desired molecular density. This yields the maximum absorption difference between optical frequencies located outside of and at the center of the absorption line.

---

[1] Letter designations refer to labeled items on the referenced figure.

Measurement Component:
{I} Image Steering Mirror
{J} Beam Splitter Cube
{K} Iodine Vapor Cell
{L} Reference Leg CCD Camera
{M} Signal Leg CCD Camera

Laser Transmission Optics:
{A} Beam Steering Mirror
{B} BK7 Beam Sampler
{C} Light Sheet Forming Optics

LFM Component:
{D} Beam Steering Mirror
{E} Beam Splitter Cube
{F} Reference Leg PIN Photodiode
{G} Iodine Vapor Cell
{H} Signal Leg PIN Photodiode

Figure 2–8 – Schematic of the Doppler Global Velocimeter optical arrangement.

The Doppler frequency as well as the velocity component measured by DGV is dependent on the location of the laser light sheet with respect to the receiving optics package. The velocity component measured, ô – î, is parallel to the difference between the unit vector in the propagation direction of the laser light î, and the unit vector in the propagation direction of the collected scattered light, ô. As depicted in Figure 1-1, the measured velocity vector, ô - î, is the vector perpendicular to the bisector of vectors ô and î, which lie in the plane defined by the vectors ô and î. For a given flow, velocity vector *V*, the collected scattered laser light frequency shift, Δν, is dependent on the dot product between the velocity vector *V* and the measurement vector ô - î as shown in Equation (2.11) (Meyers, Komine, 1991):

$$\Delta \nu = \frac{\nu_o \left(\hat{o} - \hat{i} \right) \bullet V}{c} \tag{2.11}$$

Where:
vo = Optical frequency
c = Speed of light

Recognize that Equation (2.11) is the same as the Equation (2.5) used in the reference LV system to compute the Doppler frequency shift resulting from particles passing through a laser light beam. Also note that in Equation (2.11), the Doppler frequency and accordingly the velocity quantity measured depends on the scattering angle; thus, multiple views or light sheet directions provide velocity measurements that are translated to standard Cartesian three component measurements.

The transfer function for each IVC is determined by normalizing the light level measured at the exit of the IVC by the light level impinging its front surface. An accurate and stable description of this transfer function (absorption profile), relating the laser light transmission characteristics of an IVC as a function of optical frequency, is critical for precise Doppler frequency shift and flow velocity measurements. Continuous measurement of the IVC transfer function yields a time record of the scattered laser light optical frequency.

Because each IVC has a unique light absorption profile, a calibration procedure is required to ascertain the transfer function for each IVC employed in the DGV instrument. The transfer function for a given IVC is obtained by tuning the laser through approximately thirty frequency or longitudinal modes centered about the absorption band in the Iodine vapor most sensitive to frequencies about the 514.5 nm line of an Argon Ion laser. These thirty frequency modes spanned 4 GHz, which is wider than the line width of iodine vapor. The distance in optical frequency from one mode to the next or the Free Spectral Range (FSR) is determined as follows:

$$\text{FSR} = \frac{c}{2L_e} \tag{2.12}$$

Where:
$\quad$ c = Speed of light
$\quad$ L_e = Effective laser cavity length

The 1.5-meter long tube installed in the employed Argon Ion laser, produced a FSR of approximately 129 MHz. By tuning or *mode hopping* the laser through these frequency modes and computing the resultant normalized light level, a calibration curve relating light transmission to optical frequency, or the transfer function of an IVC, was developed by fitting the ensemble of points.

The absorption profile developed by scanning through the various frequency modes and recording the extent of light attenuation was neither smooth nor continuous, hampering its application for sensing frequency variations in collected scattered light. An improved calibration of the absorption profile, having better optical frequency resolution, was provided by a constant speed, 12-inch. diameter rotating wheel. The 12-inch diameter wheel, with an adjustable rotational speed of up to 3000 rpm, was selected because it provided a Doppler shift of the emitted laser frequency that spanned three laser modes, providing an overlap in line segments describing light absorption. The surface of the wheel was illuminated with a cone of laser light originating from a source located normal to the wheel surface in the horizontal plane. Fine grit sandpaper covering the wheel surface acted as a light scattering medium. A DGV receiver optics package located in the same plane at a position 60 degrees from the laser was used to measure scattered light variations produced by the rotating wheel. In this configuration, the velocity vector measured, ô – î, was along the horizontal direction of the wheel, which was stationary in the x plane and was not sensitive to motions in the z plane. Since each pixel in the CCD array acted as an independent detector, it had a unique spatial ô – î relationship or mapping to the impinging scattered light. This characteristic produced a unique Doppler frequency shift along each horizontal line of the rotating wheel.

For each of the laser frequency modes about the absorption line, several images of light scattered from the rotating wheel were acquired. The collection of images acquired at each of the investigated laser frequency settings was then normalized and averaged. From the resulting average image, Doppler shift frequencies were computed for each pixel location in the region of the image where the wheel was located. Accurate computation of the Doppler frequency shift profile using Equation (2.11) was possible since: (a) the physical mapping of CCD pixel locations to wheel surface positions was obtained by imaging a spatial calibration grid or *dot card,* which contained dots of a known uniform spacing prior to imaging the rotating wheel thus providing a means for determining the ô – î relationship for each pixel position; and, (b) an optical tachometer was used to measure the speed of the rotating wheel (Meyers and Lee, 2000).

The resolved Doppler frequency shifts at all pixel locations along each row were then averaged yielding a profile of the Doppler frequency shift along the vertical diameter of the wheel, which spanned 258 MHz or two laser frequency modes.

Plotting the normalized pixel values along the vertical center of the wheel against the computed Doppler frequency shift profile provided a 258 MHz segment of the IVC absorption profile. By combining the segments obtained at each laser frequency mode about the absorption line, the transfer function of the targeted IVC was obtained. The overlapping segments were shifted along the frequency axis to minimize errors and a B-spline fitting algorithm was applied to improve the smoothness of the absorption profile. The scattered light level-to-optical frequency transfer function was realized practically by scaling the normalized scattered light levels to produce a 1024-element lookup table (LUT). As part of the DGV processing sequence, scaled normalized pixel values were used to address the LUT to obtain the frequency it corresponded to. Since floating-point processing operations were employed to improve measurement resolution, a linear interpolation algorithm was applied to adjacent points in the LUT to determine the optical frequency.

For DGV investigations the frequency of the laser was tuned to a region of the absorption line, where the optical frequency shifts observed due to particle velocity would be measured in a linear region of the IVC calibration curve. During these experiments, light scattered by particles moving through the laser light illuminated viewing plane was attenuated as it passed through the IVC to a degree proportional to the Doppler shift frequency resulting from particle motion. The direction of the particle movement was ascertained by noting the increase or decrease in light attenuation level relative to the referenced midpoint set by the laser frequency (Meyers, Komine, 1991).

The receiver package for each DGV measurement component employed reference and signal CCD cameras (K&M in Figure 2–8) to view the particle field to accurately resolve the optical frequency of the particle scattered light. Collection optics at the front of the DGV receiver system gathered a portion of the scattered light and directed it to a non-polarizing beam splitter that guided this light down the two detector paths. Light directed down one optical path was passed through the IVC to the signal CCD camera that sensed the scattered light level variations caused by the particle-induced optical frequency shifts. Light that was directed down the reference CCD camera path provided a measurement of absolute scattered light level variations across the imaged plane.

The output signal for a given pixel on the signal leg CCD camera is proportional to the velocity of objects or particles passing through the laser light sheet where that pixel is focused. However, the level of this signal is also proportional to the extent of the light scattered in the imaged plane. Particle size and number density influences, along with light sheet intensity variations are accounted for by the reference CCD camera image. Normalization of corresponding pixel locations in time-coincident signal and reference camera images provides a direct measurement of the IVC transfer function, as scattered light levels varied in response to flow conditions. Normalized pixel levels are obtained using Equation (2.13):

$$N[i, j] = \frac{S[i, j]}{R[i, j]} \qquad (2.13)$$

Where:

$N[i, j] =$ Normalized signal level for a corresponding pair of Signal and Reference camera pixels at position *i, j*

$S[i, j] =$ Amplitude of pixel at location *i, j* on the Signal camera

$R[i, j] =$ Amplitude of pixel at location *i, j* on the Reference camera

The potential for errors in flow field velocity resolution is high, if collected scattered light along the signal and reference paths is modified for any reason due to the sensitivity of the normalization process that converts light intensity variations to optical frequency information. In order to obtain accurate frequency and velocity measurements from raw image data sets, a series of data processing

operations is required. Time coincident signal and reference image pairs are pixel-by-pixel corrected for background light level removal, spatial misalignment, and flat-field correction.

Background light resulting from ambient lighting conditions, secondary light scatter resulting from laser flare off of models or other objects in the receiver field of view and CCD camera dark currents introduced unknown offsets in the sensed light energy. As DGV velocity measurements are dependent on light intensity ratios, photons produced by anything other than tracer particles represented an error source. Background light contributions were accounted for by acquiring a series of images with the apparatus required for the investigation installed, seeding particle generator turned off, and the flow field illuminated by the laser light. In addition, light sources required during the experiment were turned on. Acquired images were then averaged and the background level at each pixel location of the CCD determined. The resultant images were subtracted from each raw signal and reference data image to minimize background contributions.

Optical distortions resulting from viewing perspective mismatches, imperfections in optical components and test facility windows and pixel misalignments in reference and signal camera images introduced an element of error, as particle scattered light was not viewed at spatially corresponding pixel locations. Additionally, in order to resolve standard orthogonal velocity components in multiple component configurations, each component required pixel-by-pixel alignment to assure that the same regions of the flow plane were imaged. Piecewise bilinear image-dewarping algorithms were used to align the corresponding pixels on the reference and signal camera images to account for incurred spatial, geometric and optical distortions. Image dewarping coefficients for each pixel position on each reference/signal CCD camera pair were determined by processing a series of images of a white-light illuminated calibration grid consisting of uniformly located dots inserted into the light sheet plane. The dewarping process enabled temporally corresponding normalized images across multiple components to be overlaid producing velocity maps that represented the same measurement region (Meyers and Lee, 2000).

A third source of error was associated with the detection and sampling of particle scattered light. As shown in Figure 2–8, the optical components used to deliver the scattered light to each CCD camera were different along the signal and reference paths. Even with attenuation effects of the Iodine vapor minimized, the optical energy transfer through the optical components (beam splitter, IVC system windows and camera lenses), variations in CCD sensor pixel sensitivity and differences in the detection and sampling electronics (cameras and frame grabbers) affected the light level measurement. If the light and signal paths were matched perfectly, the signal/reference ratio at any pixel location would be unity, and the normalized images would represent only the intensity variations caused by particle motion. A *flat-field* calibration procedure was used to establish scaling factors that drove the signal/reference ratio to unity to equalize normalized data images and account for these mismatches.

Consider a pair of corresponding pixels of the signal and reference CCD cameras and the path taken by the scattered light that impinged them. From Figure 2–8, recognize that light passing down the signal path was attenuated by the additional glass surfaces of the IVC. In addition, items such as irregularities within, and dust, fingerprints or scratches on the surfaces of optical components affected the intensity of the light reaching either or both pixels. Along the optical path, the position and effect of obstacles similar to these varied across the CCD surface that degraded the scattered light levels, requiring that unique flat-field scaling factors be computed for each pixel location.

Flat-field correction factors were developed from images acquired with the particle field illuminated by laser light of a particular frequency, where the effects of the Iodine vapor were negated. This was achieved by tuning the laser to a frequency lying outside of the Iodine absorption line. For corresponding pairs of the flat-field images, the scaling factor at each pixel location was established by normalizing the intensity level of a pixel on the signal camera by the level at the spatially coinciding pixel on the reference camera. Averaging the individual pixel scaling factors for the collection of calibration images produced an average flat field image.

Removal of background light contribution and application of the flat-field correction factors modified normalization Equation (2.13) as follows:

$$N[i,j] = \left[\frac{S[i,j] - BG_S[i,j]}{R[i,j] - BG_R[i,j]} \right] * \left[\frac{FF_R[i,j] - BG_R[i,j]}{FF_S[i,j] - BG_S[i,j]} \right] \qquad (2.14)$$

Note that flat-field scaling factors are the inverted normalized values. Applying these factors in this manner reduced processing time as multiplication operations did not incur the computational overhead of division procedures.

Resultant normalized values at each pixel location were scaled to 1024 (Equation 2.15) and used to address the IVC calibration LUT to extract the corresponding optical frequency in the manner previously discussed:

$$N[i,j] = N[i,j] * 1024 \qquad (2.15)$$

The collection of individual frequency values was combined to produce an image representing the optical frequency observed at the measurement component (ν_{MC}).

An additional receiver system referred to as the Laser Frequency Monitor (LFM) was used to monitor the frequency of the laser output. Video signals produced by this system were digitized simultaneously with the digitization of the video signals produced by the measurement component. LFM data images were corrected and normalized in the same manner as those of the measurement component to extract frequency information contained within the LUT for the IVC employed in the LFM. The LFM measured the laser frequency (ν_{LFM}) at the same instant each measurement component image pair was acquired. LFM frequency values were subtracted from those of the measurement component to obtain the Doppler shift frequency (Equation 2.16):

$$\Delta\nu[i,j] = \nu_{MC}[i,j] - \nu_{LFM}[i,j] \qquad (2.16)$$

The velocity observed at the measurement component was then computed using Equation 2.17:

$$V[i,j] = \frac{\Delta\nu[i,j] * \lambda}{\left(\hat{o}[i,j] - \hat{i}[i,j] \right)} \qquad (2.17)$$

Since the original DGV research conducted by Komine, et al, the technology behind DGV has been refined and advanced at several aerodynamics research facilities including; NASA Langley Research Center, (Meyers, et al., 1991,1992, 2000 and Smith et al. 1998), NASA Ames Research Center (McKenzie, 1997 and Reinath, 1997), Wright Patterson Air Force Base (Beutner et al., 2001) and the German Aerospace Center – DLR (Schodl, et al., 2002). DGV has been used to measure velocity flow fields at various locations around basic aerodynamic models, helicopter rotors, high-speed jets, inside of pipes and within engine piston cylinders and turbomachinery to date.

The goal of this experimental research has been to mature DGV technology to the degree that it becomes a flow velocity measurement technique, routinely employed by aerodynamicists to investigate flow phenomena over a large plane. Current research efforts continue in several areas including:

- Data image processing, where researchers are focusing on increasing the velocity measurement accuracy through improvements in IVC calibrations, and minimization of speckle noise, flare and secondary scattered light effects. Processing schemes that provide near real-time feedback of velocity flow field measurements are also being investigated to permit test progress monitoring (Meyers and Lee, 2000)
- Laser frequency stabilization techniques to maintain the frequency of the laser at the center of the edge of an IVC absorption line during DGV experiments. Stabilization is desirable, as temperature variations and test area vibrations will cause the laser to deviate from the initial laser frequency setting, limiting flow measurement resolution (Roehle and Schodl, 1994)

- Application of DGV to large-scale flow research facilities, where complex flow fields around full-scale automobile, airplane and helicopter models need to be investigated (Reinath, 1997)
- Detector upgrades to improve system measurement capabilities through the application of low noise, high-resolution CCD cameras. These CCD cameras improve the image quality in two ways. Larger numbers of detector pixels extend the image spatial resolution enabling larger viewing planes to be investigated and the deeper charge wells at each pixel location enable increased measurement sensitivity as more digitization levels are possible (i.e. 10-, or more vs. 8-bits/pixel)
- Optical system improvements, which minimize polarization effects and reduce angular dependence due to Mie scattering
- The application of optical fiber image delivery systems enabling DGV measurements in locations with limited optical access. The optical fiber image delivery system also reduces component count, since multiple measurement components may be imaged using a single measurement component system (Nobes, et al.)

D. Summary

Laser-based flow measurement instruments have provided researchers with tools enabling flow fields to be investigated in a non-intrusive manner at specific locations over measurement planes. The LV, PIV and DGV techniques discussed are only a sampling of laser based flow measurement technologies. Detailed discussions regarding these technologies have been presented as their underlying physics, implementation, measurement capabilities, applications, and limitations form the foundation of pDv.

CHAPTER III - POINT DOPPLER VELOCIMETRY

A. Introduction

The measurement of turbulence power spectra quantifies the frequency content of unsteady and turbulent flows; conditions typically encountered at flow edges, in shear regions and boundary layers, and in jet flows. At present the accepted standard for making these measurements is the hot-wire anemometer.

Although the hot-wire anemometer is a proven technique providing accurate velocity and spectral measurements, the intrusive nature of the probe introduces a degree of measurement uncertainty that might be overcome using a laser-based approach. However, a fundamental limitation of current laser-based techniques is in their ability to measure time dependent flow quantities, prohibiting them from being used to make accurate spectral measurements. The need to resolve random, Poisson-distributed, single particle passages through the fringe-type LV probe volume precludes sampling of the PMT output signal at regular intervals, making spectral measurements with LV inaccurate. Frame rates of commercially available CCD cameras can not satisfy the Nyquist sampling criteria necessary to investigate rapidly changing flows precluding the use of PIV and DGV for these types of investigations.

At present, a laser-based instrument called the Point Doppler Velocimeter (pDv) is being developed to address the need for turbulence power spectra measurements. pDv applies many of the technologies of LV, PIV and DGV to make velocity measurements at regular intervals, thus facilitating the possibility for temporal measurements. The non-intrusive nature of a laser-based technique capable of measuring temporal velocity quantities also presents the prospect for making spatial cross-correlation measurements in flows. Cross-correlation measurements using hot-wire anemometers, are limited since the probes disturb the flow and interfere with one another.

The goal of the current research is to assess the feasibility of making turbulence spectra measurements using pDv. This chapter presents the physics, components, capabilities, limitations and errors sources identified during the present pDv development effort. In addition, the process of advancing this technology from the prototype phase into an instrument capable of delivering the required measurements in a reliable and accurate manner is explained.

B. The Point Doppler Velocimeter – A New Point Measurement Instrument

Point Doppler Velocimetry (pDv) is an alternative embodiment of the DGV technology that trades the ability to make spatial velocity measurements across a plane for the ability to make temporal velocity measurements at a point. This point, (probe or sample volume), is situated where a focused beam of Argon Ion laser light and the optical axis of the receiving optics package intersect (Figure 3-1). Given that pDv velocity measurements are obtained by measuring the Doppler shift of light scattered by one or more particles collected by the receiving optics rather than single particle passages as is in LV, it appears that the temporal measurements might be possible. Realization of continuous velocity and temporal measurements is probable with the fulfillment of three conditions:

- Fast response, high sensitivity detectors capable of being sampled at uniform intervals dictated by flow conditions
- A steady stream of particles that are large enough to scatter sufficient laser light for detection, but small enough to accurately follow the flow
- Laser frequency stabilization to eliminate drift

Measurement Component:
{H} Image Steering Mirror
{I} Beam Splitter Cube
{J} Reference Leg PMT
{K} Iodine Vapor Cell
{L} Signal Leg PMT

LFM Component:
{C} Beam Steering Mirror
{D} Beam Splitter Cube
{E} Reference Leg PIN Photodiode
{F} Iodine Vapor Cell
{G} Signal Leg PIN Photodiode

Laser Transmission Optics:
{A} Beam Steering Mirror
{B} BK7 Beam Sampler
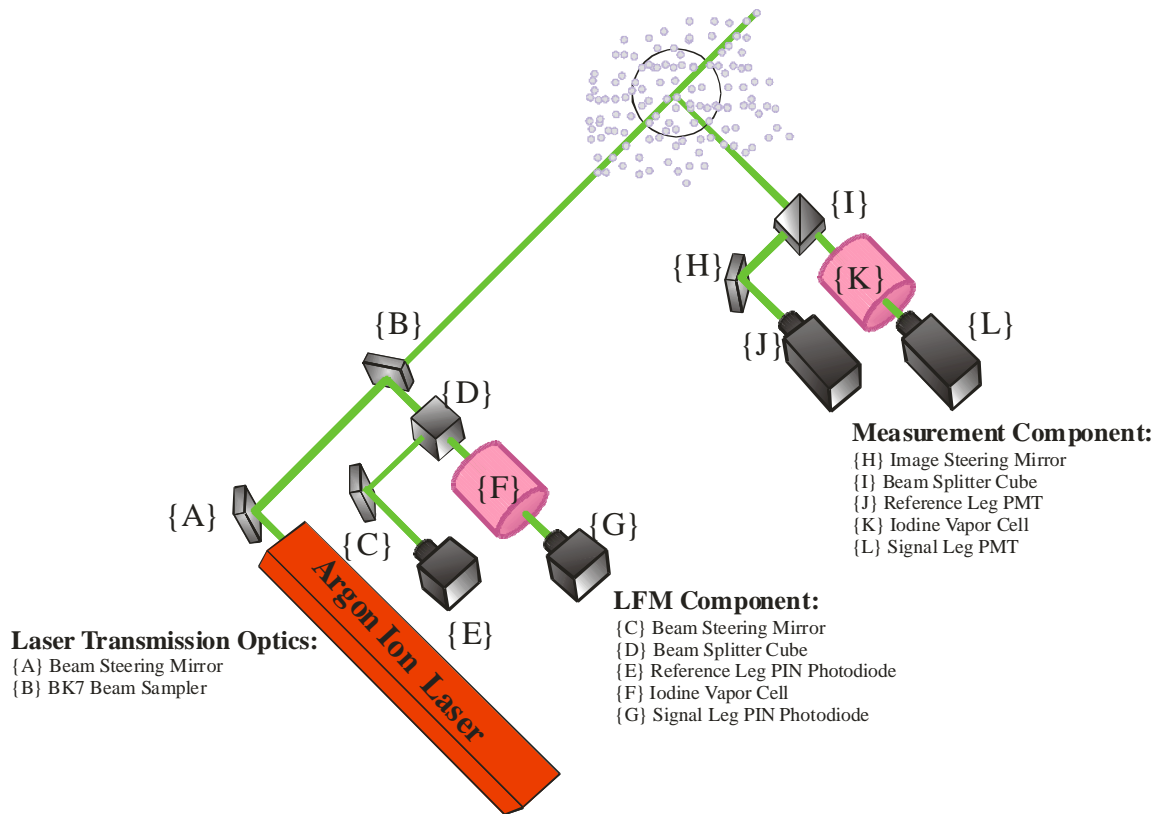
Figure 3-1 – Schematic of the pDv transmission and receiver optics packages.

The foundation of this research is based upon the work of others who have previously investigated pDv. Hoffenberg and Sullivan (1993), who employed an IVC to detect the Doppler frequency shift of particle scattered laser light at a point, conducted the first documented pDv research. The pDv velocity measurements they obtained compared favorably with earlier LV measurements for the investigated flow conditions. A graduate student research team led by Kuhlman (1997) continued this work at West Virginia University under a NASA Langley research grant. In this work, a 2-D system was constructed and used to measure the velocity of a rotating wheel to an accuracy of ±0.5 m/sec. Later two-dimensional pDv measurements obtained by Kuhlman and Scarberry (2002) in the flow exiting a one-inch diameter pipe were within ± 3 m/sec of average velocity measurements obtained using a pitot probe and hot-wire anemometer. RMS velocities measured using pDv for the same flow were approximately 1 m/sec higher than those obtained using a hot-wire anemometer. In addition, pDv spectral measurements were attempted and the resultant spectral plots were similar to the shape produced using hot-wire samples; however, no quantitative comparisons were presented. These research efforts identified three fundamental limitations in the pDv technique:

- A high particle number density was required in order to obtain continuous velocity measurements
- Laser frequency instability compromised the system measurement capability
- Without precise calibrations of the transfer function for the employed IVCs, accurate Doppler frequency resolution and subsequently velocity measurements were not feasible

The present research extends this work to investigate these limiting factors and develop schemes to improve system operation. By eliminating or minimizing these error sources, it will be possible to realize a robust instrument capable of making accurate/reliable velocity and turbulence power spectra measurements.

C. pDv System Principles

pDv is based on technologies employed by other laser-based flow measuring instruments, in particular LV and DGV. The geometry used by pDv to measure particle velocities is identical to the configuration used in LV systems dating back to the work of Yeh and Cummins (1964) (Figure 2-1) and those used in DGV (Figure 1-1). Particle velocity measurements are realized where the focused laser beam and the optical axis of the receiving optics package intersect. In this configuration, the measured velocity vector, v_o, for particles passing through the sample volume is proportional to the vectorial difference, $\hat{o}$-$\hat{\imath}$, between the laser beam propagation direction $\hat{\imath}$ and the viewing direction of the receiver optical package $\hat{o}$ (Appendix A):

$$\Delta \nu = \frac{v_o\left(\hat{o} - \hat{i}\right) \bullet V}{c} \tag{3.1}$$

The fundamental problem with using DGV to measure temporally dependent flow quantities is the low frame rates of commercially available CCD cameras (10- to 30- Hz). To overcome low sampling rates and facilitate the uniform sampling of scattered light levels, pDv replaces the CCD cameras (Figure 2-8(K&M)) used in DGV with fast-response photomultiplier tubes (PMTs), Figure 3-1(K&L) in combination with spatial filtering techniques that limit the size of the viewing volume. The PMTs are analogous to a corresponding pair of pixels in the CCD cameras in that they view the same small volume of the laser light. However, since the response time of the PMT is orders of magnitude faster than the CCD, the potential for temporal measurements exists.

Like fringe-type LV, pDv is capable of simultaneous three component velocity measurements at a single spatial location. However, pDv potentially offers several advantages over the fringe-type LV technique. First, the particle size/lag limitations associated with single particle resolution are overcome, as pDv velocity measurements are obtained by quantifying the intensity of light scattered by one or more particles. This characteristic affords a second advantage - the potential to uniformly sample PMT output signals. Uniform sampling eliminates the variability error associated with Poisson distributed particle arrivals (random quantizing in time) of fringe-type LV. If the signal/noise ratio in pDv is high, turbulence power spectra and spatial cross correlation measurements should be possible.

D. pDv Instrument Implementation

The pDv instrumentation system was constructed in a manner that addressed limitations identified during previous research activities to investigate pDv measurement capability. The system consists of:

- Highly sensitive, fast response detectors
- Custom circuits to provide continuous signals for velocity measurements
- Closed-loop, laser frequency drift minimization system

The implementation of the pDv instrument was nearly identical to the configuration used in DGV and as such employs six hardware subsystems:

- Argon Ion laser for flow entrained particulate illumination
- Frequency discriminating Iodine Vapor Cells (IVCs)
- Laser frequency-monitoring (LFM) system
- Measurement component for scattered light collection/detection
- Signal conditioning and data acquisition hardware/software
- Positioning system for locating the measurement volume

Additionally, an integral part of the pDv instrument is the data acquisition and processing software subsystems, covered in depth in Chapter 4.

1. Laser System

In the manner of DGV, pDv requires that the laser light source be operated in single frequency mode. Stable, single frequency operation is paramount to the accurate resolution of the Doppler frequency shift in light resulting from particle motion as it is determined by subtracting the frequency of the light exiting the laser from that of the frequency in the collected scattered light (Equation 2.11). Any variation in laser frequency will compromise measurement accuracy, thus requiring the frequency of the light exiting the laser be continuously recorded. This is the rationale for the Laser Frequency Monitor (LFM) (Figure 3-1). In addition, the laser must be frequency tunable to enable scattered light frequency measurements to be made in the linear region of the intensity-to-frequency transfer function of a given IVC.

A fundamental property of a light beam produced by a laser is that it is *monochromatic* by nature, implying that it is composed of a single wavelength or light frequency. However, a detailed examination of the light spectra produced consists of a Gaussian distributed range of closely spaced frequencies centered about the theoretical color (Figure 3-2(c)). A brief review of laser construction and operation will provide more insight into this characteristic and introduce the methods employed to narrow the spectral width to a single frequency.

FWHM =l
Gain Bandwidth = 6.5 Ghz

l_0

Frequency

(a) Doppler Broadened Emission Line

c/2L

l_0

Frequency

(b) Laser Cavity Resonating Modes

c/2L

l_0

Frequency

(c) Envelop of Actual Output Frequency Modes

c/2L

λ_0

Frequency

(d) Etalon Resonating Modes

λ_0

Frequency

(e) Single Mode Laser Output
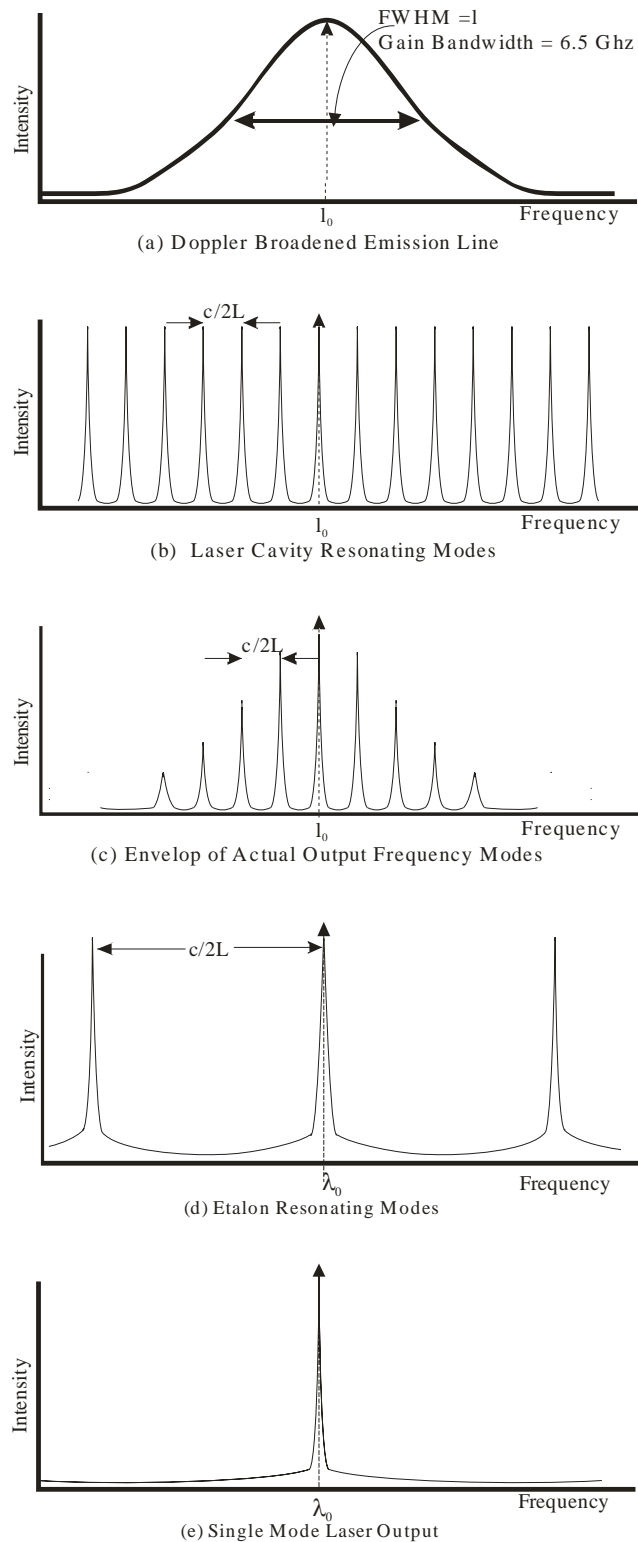
Figure 3-2 – Spectral characteristics of the light produced by a laser.

A gas laser will produce light when a high-voltage potential is placed across the conduction terminals located on each end of a sealed tube, (Figure 3-3), containing an inert gas such as Argon. The potential difference across the terminals causes an electrical discharge resulting in collisions

31

between the electrons displaced from the high-voltage input conductors and the atoms/molecules in the lasing medium; Argon gas in Figure 3-3. The kinetic energy resulting from these collisions pumps some of the Argon atoms into a higher or *excited atomic state* (ionization). The generated ions are unstable and spontaneously release excess energy in the form of *photons* as they fall to lower energy states. When generated photons pass other excited atoms, a new photon is produced in phase with a passing photon as that atom falls to the next lower ground state. The photons generated through this process, known as *stimulated emission*, have the same energy, wavelength, phase and direction of travel as the stimulating photons. Thus, the resultant light is *monochromatic*, *directional* and *coherent*.
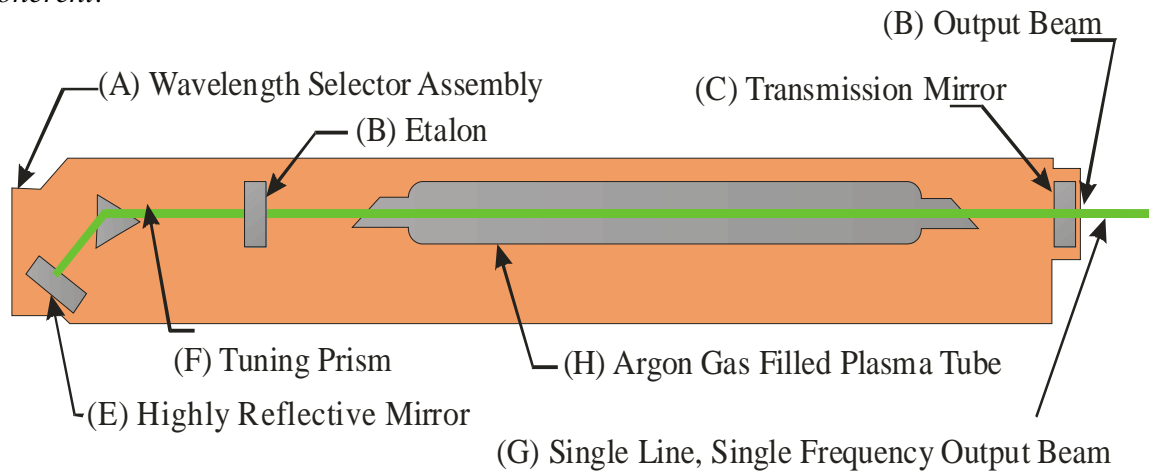
Figure 3-3 – Schematic identifying the major subsystems of an Argon Ion laser.

This process continues among other atoms resulting in a *population inversion,* as most of the atoms enter the excited state and generate more photons as they fall to the ground state. Mirrors located at either end of the resonator cavity of the laser cause these photons to be reflected back and forth creating a chain reaction of photon emissions along the tube axis. In the process of passing between the mirrors, light energy is increased by the additional photons from the *active medium*, which acts as an optical amplifier. The mirror located at the front of the laser cavity is approximately 90% reflective, enabling about 20% of the generated light to exit the laser cavity in the form of a light beam.

An Argon atom has several available energy states as shown in Figure 3-4. If the atom is excited to the highest energy state, photons will be generated at each level all the way to the ground state. Since the interval between the energy levels is not constant, photons of different wavelengths, corresponding to the energy level differences, are generated; an Argon laser produces six simultaneous wavelengths in the range of 457.9 nm to 514.5 nm.
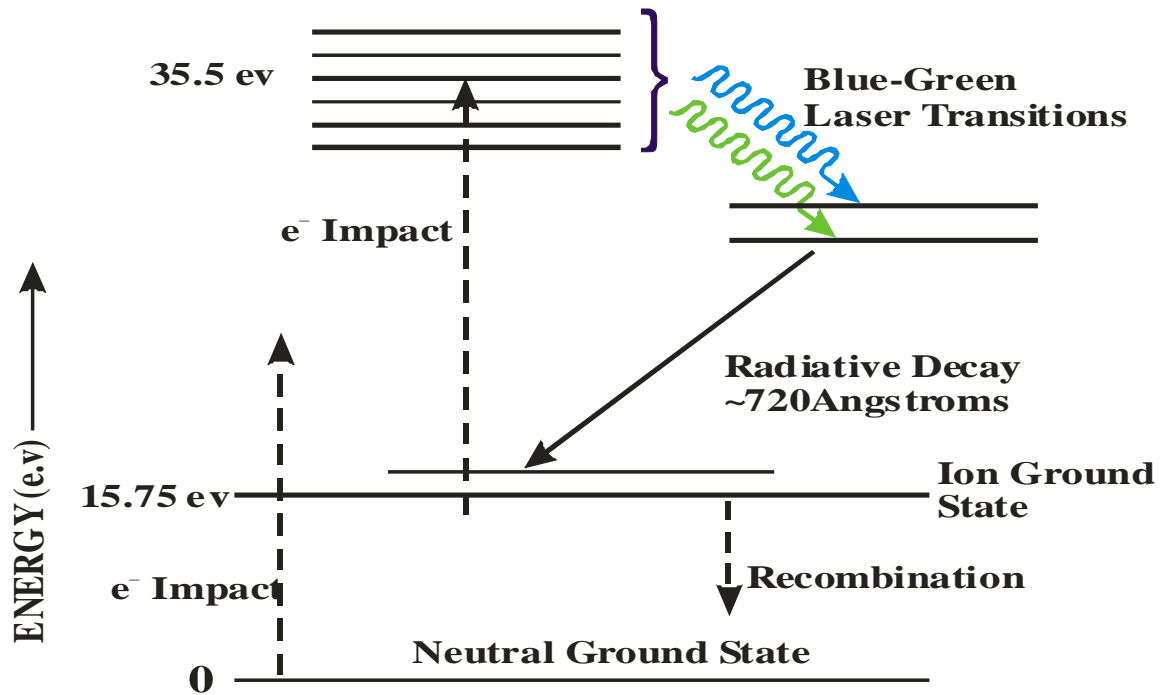
Figure 3-4 – Energy states of an Argon Ion laser.

Incorporation of a prism wavelength selector (Figure 3–3) in the resonator cavity enables an individual color to be chosen. Through a mechanical adjustment of the selector, the tilt angle of the prism is changed which separates the colors allowing the selection of a desired color. The 514.5 nm wavelength was selected for the current research, since the Argon laser outputs the greatest optical power at this wavelength and the best absorption lines in Iodine are in the green wavelengths.

The green light emitted at this wavelength has a single transverse mode (TEM$_{00}$) with a Gaussian shaped gain profile or intensity distribution. The light beam however is not truly monochromatic or single wavelength, since the thermal motion of the Argon ions Doppler broadens the light as depicted in Figure 3-2(a).

This continuum Doppler broadened spectrum is only amplified at the resonant frequencies imposed by the laser resonator cavity. These resonating frequencies, shown in Figure 3-2(b), produce a comb shaped version of the Doppler broadened signal as shown in Figure 3-2(c). The spacing of these frequencies (v_o) is related to the distance between the front and rear mirrors of the optical cavity (*L*) as given in Equation 3.2:

$$v_0 = m * \frac{c}{2L} \tag{3.2}$$

Where:
  m =   Integer number of half-wavelengths
  c =   Speed of light

These resonances are commonly referred to as longitudinal modes. The laser used in the present research had approximately 50 longitudinal modes within the Doppler broadened laser light. Each mode was separated by 129 MHz (v_0) or the Free Spectral Range (FSR) of the laser indicating that the Doppler broadened bandwidth of the laser was approximately 6.5 GHz.

Since the multi-mode bandwidth was much larger than the 1 GHz line width of the IVC absorption line, additional frequency refinement was necessary for optical frequency discrimination. To satisfy this requirement, a temperature-controlled etlaon,

Figure 3 – 3, was inserted into the laser cavity to enable selection of a single longitudinal frequency mode. The etalon, a Fabry-Perot interferometer, is a 1-cm thick quartz window with parallel flat surfaces housed inside a temperature stabilized optical mount or oven. When placed inline with the axis of the laser cavity as shown in Figure 3–3, the etalon acts as a second resonator passing only the longitudinal modes that produce an integer number of wavelengths within its thickness as given by Equation 3.2 and shown in Figure 3-2(d). Selection of a resonating frequency mode, Figure 3-2(b), is accomplished by either adjusting the temperature of the etalon oven or by varying the etalon tilt angle, causing the effective thickness of the etalon to change. Either approach modifies the path length of the beam through the etalon, thus changing the overall resonating frequency. For the pDv application, frequency selection was achieved by tilting the etalon while the oven temperature was held constant. Aligning a mode resonating within the etalon with the one resonating in the laser cavity enables the selection of a single frequency, as only the mode common to both the resonators is amplified, Figure 3-2(e). In this configuration, commonly referred to as *Single Longitudinal Mode*, laser power is concentrated in the single resonating frequency present in both resonators and the laser emits a beam that is of a single wavelength. When an etalon is used, approximately 50% of the total power available from the 514.5 nm line is output.

The prism wavelength selector in combination with the intracavity etalon provides the ability to select a single laser frequency to satisfy pDv requirements. For the present research, the spectral linewidth was narrowed to 14.64 MHz. It was observed however that during pDv investigations the frequency of the laser drifted about the desired longitudinal mode. The cause of this frequency drift was attributed to temperature variations in the water used to cool the laser and to a lesser extent to the ambient air temperature in the test area. The water temperature changes caused the length of the laser cavity to grow or shrink microscopically, resulting in a change in the resonating frequency. Short term frequency deviations were on the order of several MHz, while longer term drifts could cause the frequency to change as much as the laser FSR. If the conditions caused the etalon resonance frequency to become unstable at the selected resonator frequency, the light frequency would "hop" to the adjacent longitudinal mode.

Laser frequency fluctuations present a problem for both DGV and pDv since they employ the absorption characteristics of iodine vapor to distinguish frequency changes. As the frequency of the laser drifts, the position on the calibration curve describing the transfer function of an IVC also changes, shifting the zero frequency or velocity reference point. To minimize the frequency drift, and maintain a single mode operation, techniques that actively control the length of the optical cavity have been developed.

Röhle and Schodl (1997), who developed a system that used a hyperfine structure in Iodine vapor to monitor the laser frequency, originally investigated the concept of active laser frequency stabilization. In response to deviations from the reference frequency setting, a Proportional Integral Derivative (PID) controller was used to manage a piezo-electric actuator mounted on the rear mirror of the laser cavity. This provided a means for adjusting the length of the laser cavity to return the resonator back to the desired reference frequency. This system provided laser frequency stability to within several kHz from the desired setting. However, the use of the hyperfine structure limited the usable dynamic range in the absorption line. For the present research, a similar system, shown in Figure 3-5, was constructed to maintain single frequency operation and avoid mode hops. This system did not use the hyperfine structure in the Iodine vapor to *lock* the laser, but instead used the transmission levels in the absorption line to maintain the reference frequency. The operating frequency of the laser was monitored through continuous measurements obtained at the LFM, which established the reference frequency. Real-time LFM frequency measurements were compared to the reference point enabling the frequency drift to be monitored. In response to deviations from the reference frequency setting, the resulting error signal was applied to a piezo-electric actuator mounted on the back of the rear mirror, Figure 3–3, enabling the optical path length of the laser cavity to be adjusted to restore the laser to the reference frequency. In this configuration, the resonating frequency

within the laser cavity was adjusted to match the frequency of the etalon resonator, which was held at a constant temperature to prevent thickness changes.
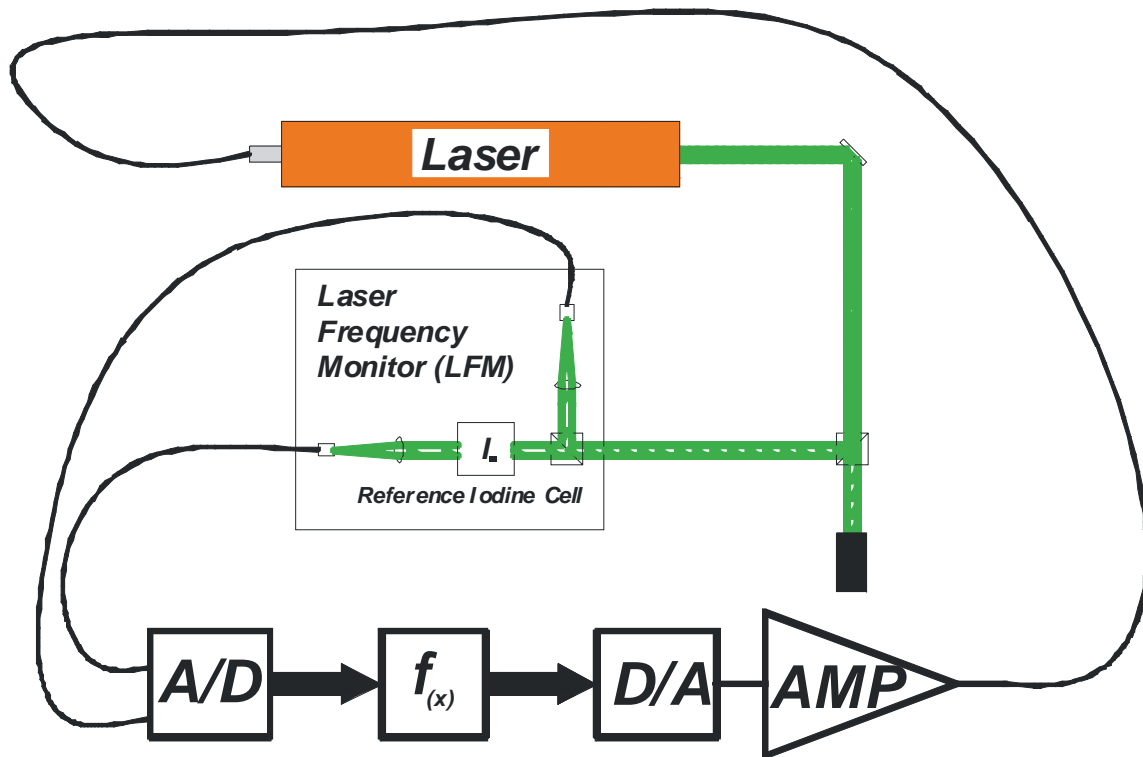
Figure 3-5 – Schematic of the laser frequency stabilization system.

Light exiting the Argon Ion laser was transmitted along two paths using a series of mirrors and focusing lenses to steer the beams shown in Figure 3-1. In one path a tightly focused laser beam was directed to the test area to illuminate particles passing through the probe volume. The second portion of the laser light was directed into the LFM system to facilitate laser frequency monitoring and laser stability control signals.

2. Iodine Vapor Cells

The key to the ability of pDv to measure particle velocities is based on the optical frequency absorption characteristics of Iodine vapor. As with DGV, the frequency discrimination characteristics of molecular iodine are realized in practice using temperature stabilized Iodine Vapor Cells (IVCs). In Figure 3-6, the temperature controller (A), Iodine Vapor Cell (B), and IVC mounted in the oven (C) are shown. The IVCs used in the present research were 76 mm (3 in.) long and 51 mm (2 in.) in diameter sealed glass cylinders with high quality, optically flat, glass cold-welded to each end.
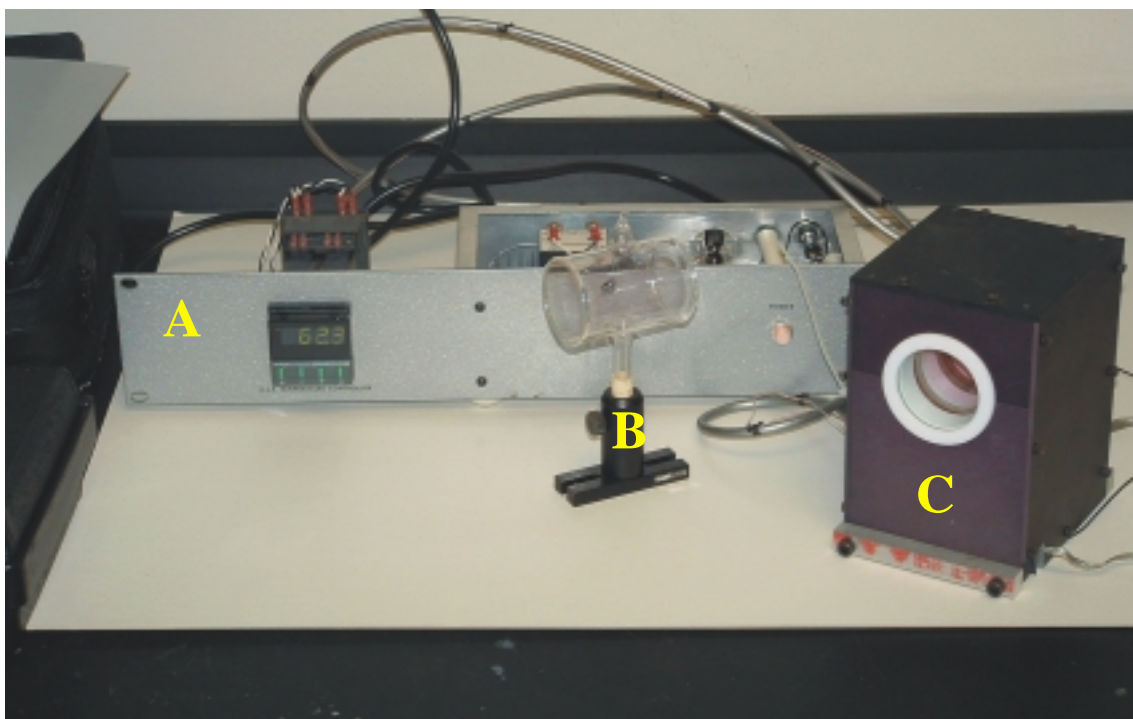
Figure 3-6 – Photograph showing the major components of IVC systems.

Two different IVC designs have been employed in pDv/DGV systems to distinguish light frequency variations. During early DGV research, IVCs designed to meet the needs of spectroscopy researchers were employed. For these cells the temperature of the stem (or *cold finger*) was kept constant to preserve the desired vapor pressure in order to maintain the absorption characteristics of the cell in wind tunnels. Testing concluded that these IVC implementations were not stable enough for pDv/DGV applications, as temperature controllers with 0.10°C resolution permitted absorption line variations. These variations were determined to be equivalent to ±3 m/s/0.1°C in resolved velocity measurement uncertainty. In addition, this method did not respond accurately to environmental changes because the heater hysteresis was too long; thus, the IVC transfer function in this configuration had unacceptable uncertainties.

The IVCs employed in the present research are commonly referred to as *starved-cells,* since no crystalline iodine was present within the cell during pDv experiments. The design of these cells is based on theory presented by Forkey (1996), which suggested that the greatest dynamic transmission range for an Iodine absorption line would be realized when the cell was heated to 40°C. Starved cells were constructed by first purging the vessels with an inert gas prior to placing a small quantity of crystalline iodine into them. A 150 mm (6-inch) cold finger used in the manufacturing process was then placed into a water bath at 40°C and the cell body heated to, and maintained at 60°C for 24 hours. Upon completion of the temperature stabilization period, all crystalline Iodine would deposit in the cold finger.

A 25 mm (1-inch) stopcock located midway along the length of the stem was shut to seal off the cold-finger and the crystalline iodine gravitated from the cell body. Thus, only iodine vapor remained within the barrel of the cell at a vapor pressure corresponding to 40°C. At this point, the cold-finger was welded between the body of the cell and the stopcock. During pDv operation, the IVC was heated to a temperature of 60°C, insuring that all of the Iodine was in the vapor state. At this setting, the Iodine vapor pressure would be constant in test facilities, where the ambient temperature could drop appreciably during the course of an experiment; e.g. Iodine vapor pressure was preserved in cases where the temperature dropped as much as 20°C.

Practical utilization of an IVC required that the cell be heated to and maintained at a stable temperature of 40°C or above in order to maintain a constant vapor pressure. This minimized the influence of temperature fluctuations in the surrounding environment and insured that the transfer function of the cell would be consistent. Temperature stability for an IVC was achieved by surrounding the body of the cell with a fitted, two-piece copper jacket held together with heater bands. The entire assembly was then mounted inside of an insulated box or oven. As shown in Figure 3-6, BK-7, anti-reflective glass windows were installed on each side of the oven. This allowed light to pass through the IVC, as it was mounted in the same axis as the other optical components. Stability of the IVC environment was maintained using a commercial PID based temperature controller that monitored the temperature of the cell by sampling the output of a thermocouple glued to the barrel of the IVC. Whenever the barrel temperature fell below the programmed setting of 60°C, the PID controllers pulsed the heater band power supply on and off until the temperature of the IVC was returned to the preset level. This feedback network kept the cell temperature stable to within ±0.1°C of the required setting, which was sufficient enough to maintain a full vapor state, given the 20°C temperature buffer.

3. Laser Frequency Monitor (LFM)

As discussed, ambient temperature changes about the pDv laser caused the operating frequency of the laser to drift in the vicinity of the desired setting. This behavior necessitated that the frequency of the laser be monitored and recorded in parallel with the acquisition of each velocity data point by the Laser Frequency Monitor (LFM). In addition to establishing the reference optical frequency from which the particle induced Doppler frequency shifts could be determined, the LFM provided feedback for the laser frequency stabilization system. Figure 3-7 is a schematic of the optical component arrangement used in the LFM. This system of optical components was mounted on an optical breadboard and housed within a temperature-controlled Plexiglas box, which shielded the system from extraneous light and minimized the influence of environmental temperature fluctuations.

pDv LFM Optical Components:
{A} Spatial Aperture (Filter)
{B} Half-Wave Plate (Polarizer)
{C} Adjustable Neutral Density Filter
{D} Bk7 Beam Sampler
{E} Microscope Objective (Reversed)
    Beam Expander
{F} Beam Splitter Cube

{G} Iodine Vapor Cell
{H} Focusing Lens
{I} Signal Leg PIN Photodiode
{J} Focusing Lens
{K} Reference Leg PIN Photodiode
{L} Beam Steering Mirror
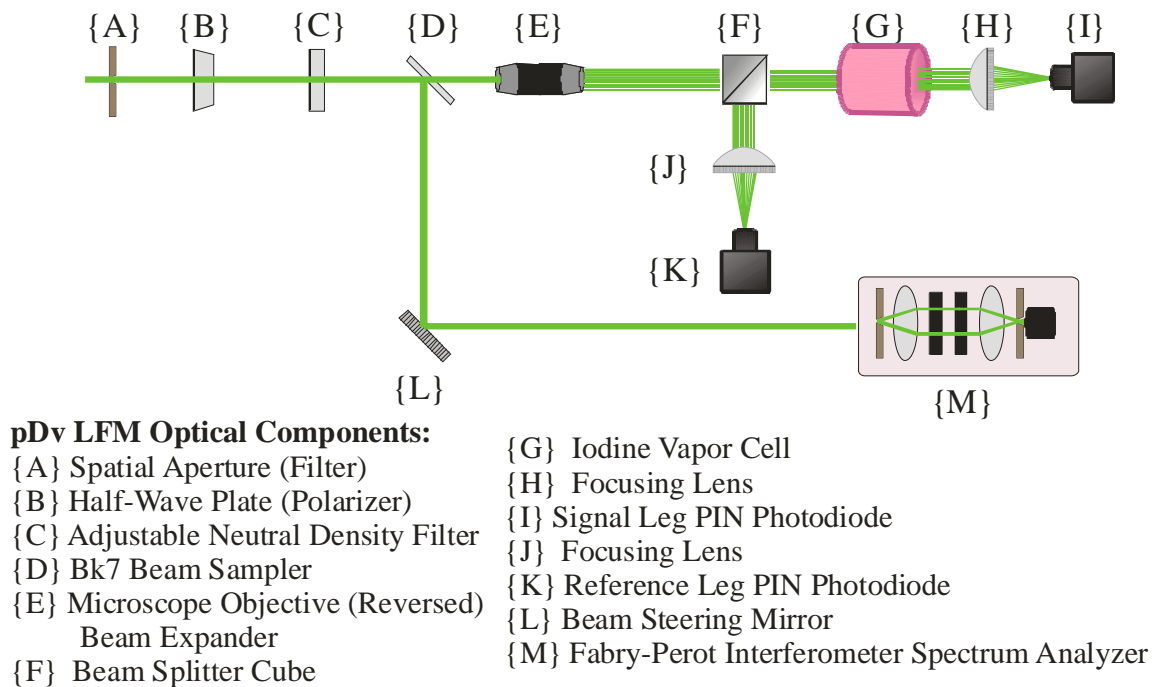{M} Fabry-Perot Interferometer Spectrum Analyzer

Figure 3-7 – Schematic of the pDv Laser Frequency Monitor (LFM).

In the manner of the velocity measurement component(s), the LFM employed the transfer function of Iodine vapor to measure optical frequency. However, since the rationale for using the LFM was to track laser behavior and supply feedback for the laser stabilization system, it measured the frequency of the laser beam directly and not that of the particle scattered light. To accomplish this, a small percentage of the laser energy exiting the laser, Figure 3-1 was steered directly through an aperture stop mounted in front of the LFM package (Figure 3-7(A)). The aperture stop minimized the influence of ambient light sources and provided a target for beam alignment. The beam then passed through a half-wave plate, Figure 3-7(B), used to balance the polarization of the laser light impinging on the surface of both the reference and the signal photodetectors. The half-wave plate was mounted in a rotating polarizer mount, which could be manually rotated as needed to match the voltage levels of both the reference and signal photodetectors in response to the incoming light. This adjustment was made with the laser tuned to a frequency lying outside of the IVC absorption region to negate the effects of the Iodine vapor.

The beam exiting the half-wave plate then passed through an adjustable Neutral Density (ND) filter, Figure 3-7(C), to attenuate the intensity of the beam and prevent saturation of the photodetectors. The attenuated beam then encountered a beam sampler, Figure 3-7(D), made of BK7 glass mounted at a 45° angle. This enabled approximately 10% of the beam to be picked off and directed towards a steering mirror that guided the beam to an optical spectrum analyzer, which will be discussed later.

The portion of the beam passing through the beam sampler continued on to an adjustable beam expander (Figure 3-7(E)). This beam expander was set to a 10:1 expansion ratio to distribute the energy contained within the approximately 2 mm laser beam across an area of about 2 cm in diameter to prevent local saturation within the IVC that was in the signal detector path. The expanded beam then passed through a 51 mm, 50/50-polarization insensitive beam splitter cube, Figure 3-7(F), that divided the light along two paths.

The portion of the beam deflected by the beam splitter was directed towards a 51 mm diameter lens (Figure 3-7(J)). This 51 mm focal length (FL) lens focused the beam down so that all of the laser energy would be directed onto the active area of the reference leg photodetector (Figure 3-7(K)). The portion of the beam passing through the beam splitter continued through the IVC, Figure 3-7(G), installed in the signal leg of the system, where it was attenuated according to the transfer function of the IVC. Light exiting the IVC was focused onto the signal leg photodetector (Figure 3-7(I)).

The photodetectors employed were fixed-gain, low-noise, Silicon PIN photodiodes with a 13 mm^2 active surface area. These photodiodes were capable of a maximum output voltage of 10.0 V and a bandwidth of 10 MHz.

The Fabry-Perot optical spectrum analyzer, Figure 3-7(M), in the LFM was used to visually monitor the laser frequency selection, verify the single-frequency stability and confirm the operation of the feedback network of the laser frequency stabilization system. Output signals for this device were connected to an oscilloscope configured to display the longitudinal modes around the 514.5 nm wavelength as discrete resonance peaks. Each peak represented a single lasing frequency being produced by the laser. This feedback was particularly useful when tuning the laser to the desired zero-velocity or reference frequency. As the etalon tilt angle was varied, the peaks would jump along the horizontal or frequency axis of the display indicating a hop to the next longitudinal mode or spectral line in the distribution shown in Figure 3-2. The amplitude of these peaks provided an indication of the laser output power level realized at a given mode. As each longitudinal mode was encountered, the optical frequency of the laser was determined by taking the ratio of the output levels of the LFM signal and the reference photodiodes. The actual operating frequency of the laser was then ascertained by reading the position in the frequency axis of the calibration curve describing the transfer function of the IVC that corresponded to the observed ratio.

Prior to the implementation of the laser frequency stabilization system, the output signals of the spectrum analyzer were monitored to verify that the laser was operating at the desired single frequency mode. Whenever the appearance of a second peak indicating a second resonating frequency

close to the initial single frequency setting or the laser frequency drifted significantly from the reference point, or a mode hop occurred, the tilt of the etalon was adjusted to return the laser to the desired frequency mode. This manual mode of operation defined the functionality required of the laser frequency stabilization system and made it possible to operate the laser at or near the same frequency setting for all of the collected data ensembles.

4. Measurement Component

The optical configuration shown in Figure 3-8, referred to as the pDv measurement component, measures the frequency of laser light scattered by particles passing through the sample volume. The arrangement of these optical components is identical to the LFM system configuration, except it employs higher sensitivity optics for light collection and high response PMTs, Figure 3-8(R&S), in place of photodiodes, Figure 3-8(I&K), for light detection. Like the LFM, the measurement component was housed in a Plexiglas box to minimize environmental effects.

pDv Measurement Component Optical Components:
{A&G} Beam Steering Mirrors
{B&C} 83.5mm F.L. Focusing Lens Combination
{D} 0.35mm Diameter Pinhole Spatial Aperture (Filter)
{E} 75mm F.L. Collimating Lens
{F} Polarization Insensitive Beam Splitter Cube
{H} -50mm F.L. Collimating Lens
{I} 200mm F.L. Focusing Lens
{J} Iodine Vapor Cell
{K} 1185mm F.L. Scattered Light Collection Lens
{L&M} 40mm F.L. Focusing Lens
{N&O} 514.5-nm optical bandpass filter
{P&Q} 0.45mm Diameter Pinhole Spatial Aperture (Filter)
{R} Signal Leg PMT
{S} Reference Leg PMT

Figure 3-8 – Schematic of the pDv measurement component optics package.

The fast response, high gain, PMT modules utilized in the measurement component were very sensitive to low particle-scattered light levels, especially in areas of low particle concentration. These PMT modules, Hamamatsu Model H6780, had an 8 mm^2 active surface area and were sensitive to wavelengths in the range of 300- to 850-nm. Each PMT module integrated its own isolated high-voltage power supply. Because PMTs produce a signal current representative of the intensity of the light impinging their photocathode surface, a current to voltage amplifier was used to condition the signal prior to interfacing it to the Analog Data Acquisition Board.

PMTs were selected to detect particle scattered light levels after other detector technologies were evaluated. The same PIN photodiodes used in the LFM component, ThorLabs PDA55A, were initially considered, as they were readily available, had integrated amplification electronics, were easy

to use/mount and were cost effective. Laboratory tests revealed however that these photodetectors were not sensitive enough to provide useful measurements for particle scattered light levels typical of pDv.

Avalanche Photo Diodes (APDs) from Analog Modules, Model 711-4-3A-DC, with a 0.5 mm^2 active area, peak wavelength of 830 nm, 1.8 MHz bandwidth and an integrated variable-gain, transimpedance amplifier were subsequently evaluated. These APDs were used in early pDv investigations and operated in the non-Avalanche mode. In this mode of operation, they produced a linear output signal making repeatable operation possible. However, it was later determined that in this mode they did not possess the sensitivity required to detect scattered light, when used in a 90 degree back scatter configuration. When operated in the Avalanche mode, the APDs had sufficient sensitivity for making single particle measurements. However, the non-linear output signal produced in the Avalanche mode introduced measurement uncertainties for the pDv application, which requires linear detector behavior, since velocity measurements are resolved through a normalization process.

At the front of the measurement component enclosure, a 76 mm diameter, 1185 mm FL lens, Figure 3-8(K), was used to gather the particle scattered light. This particular lens was selected because: (a) its focal length enabled the measurement component of the optics package to be located close to the sample volume, at a position where it did not interfere with the flow exiting the two-inch pipe, (b) it was large enough to collect sufficient scattered light for making a measurement, and, (c) its physical size was suitable for the form factor of the optics package. The collection lens, in combination with the 200 mm FL lens, Figure 3-8(I), that followed it, acted as a beam reducer concentrating the light onto the center of the 50 mm FL lens, Figure 3-8(H), that collimated the light into a 25-mm diameter beam.

The collimated beam was then turned 90 degrees using a beam steering mirror, Figure 3-8(A), mounted 45 degrees normal to the collimating lens. The deflected beam was then directed through a combination of optical elements, Figure 3-8(B-E), that acted as a spatial filter which served two purposes: First, the diameter of the aperture defined the size of the measurement sample volume. Secondly, the aperture minimized the contribution of secondary scattered or other (background light) originating from objects outside of the sample volume. The 75 mm FL lens, Figure 3-8(E), of the spatial aperture collimated the diverging light rays into a 25 mm diameter beam. The expanded beam continued to a 51 mm, 50/50-polarization insensitive beam splitter cube, Figure 3-8(F).

The portion of the beam passing through the beam splitter was directed towards the signal leg PMT, (Figure 3-8(R)). Prior to encountering the PMT, the light was passed through the IVC, Figure 3-8(J), where it was attenuated to the extent dictated by its transfer function. Light not absorbed by the IVC impinged on a 40 mm focusing lens, Figure 3-8(L), which focused the beam back to a point. Prior to reaching the 40 mm focal point, the converging light rays continued through a 514.5 nm optical bandpass filter, Figure 3-8(N), that served to filter out optical wavelengths other than those produced by the laser source. Light near the 514.5 nm wavelength, which passed through the bandpass filter, was directed through 0.35 mm aperture, Figure 3-8(P), to the surface of a PMT. The aperture was installed at this location to minimize the contribution of flare originating from reflections along the path of various optical components and the IVC.

The portion of the beam deflected by the beam splitter was turned 90 degrees toward the reference leg PMT by a steering mirror, Figure 3-8(G), mounted at a 45 degree angle normal to the beam splitter. Prior to reaching the PMT the same components less the IVC were used to condition and direct the beam onto the reference PMT surface.

5. *Data Acquisition and Signal Processing Hardware*

The sampling, management and monitoring activities necessary to obtain pDv measurements required the use of commercial and custom hardware systems. The configuration of the signal processing, data acquisition and system control components used in the presented research is shown in Figure 3-9. Custom software developed using the National Instruments LabVIEW programming environment and deployed on a PC class computer, was used to integrate, manage and control this

collection of custom and off-the-shelf systems. As this software represents a significant portion of the functionality of the data acquisition system and the presented research, it will be discussed in detail in Chapter 4.
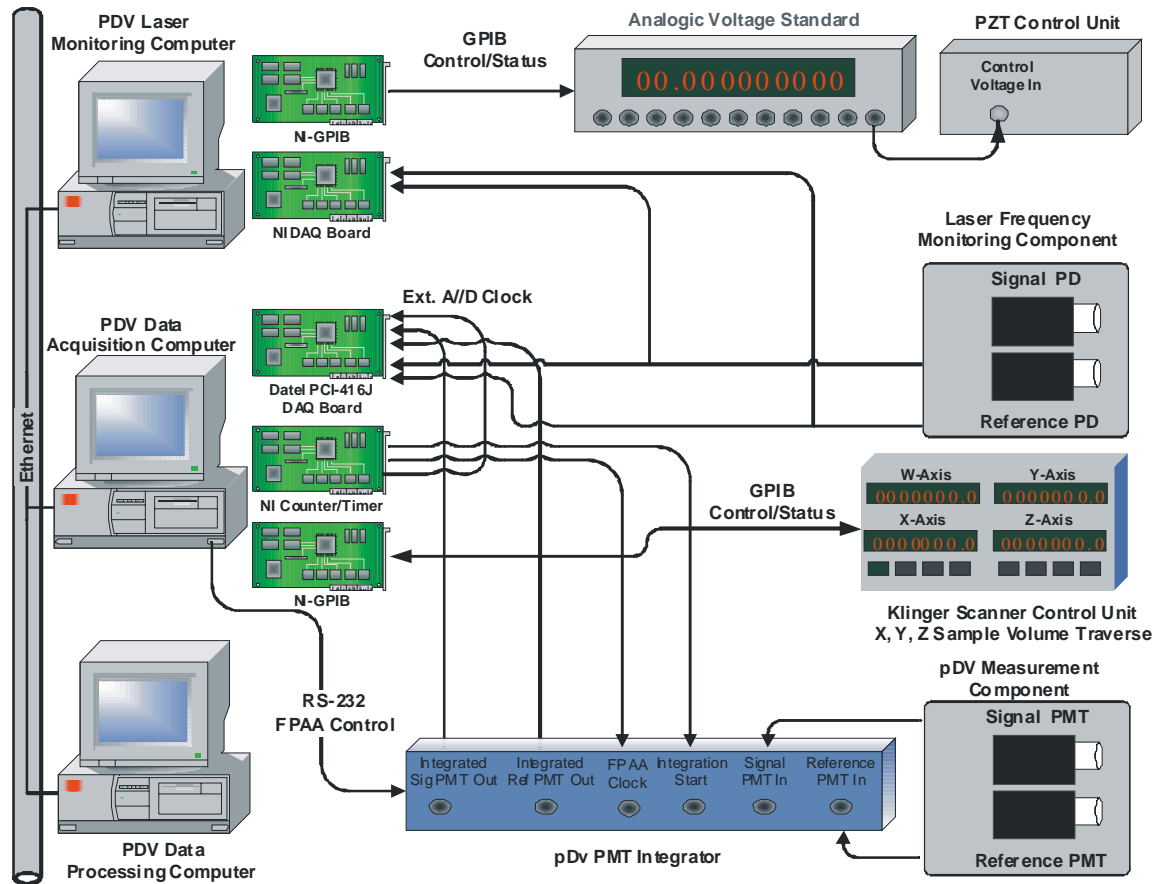
Figure 3-9 – Schematic of the pDv data acquisition/control hardware system.

The data acquisition computer hosted the General Purpose Interface Bus (GPIB), system-timing controller and an analog Data Acquisition Board (DAQ). The pDv positioning system and the pDv integrator were controlled over the GPIB and serial busses from the PC respectively.

a. *pDv Integrator*

The Poisson distributed passage of particles through the pDv sample volume suggests that there will be times when particle number density will be too low to scatter sufficient light for detection during the sampling interval. This becomes more of a concern when the probe volume is positioned in flow regimes where low particle concentrations are common such as in flow edges, shear regions and boundary layers. Failure to obtain data samples at the desired uniform rate will compromise the quality of flow spectral measurements.

To minimize the occurrence of these *holes* or *dropouts* in data records, the concept of integrating PMT output signals during the period between successive A/D sample clocks was investigated. In this way, the PMTs would emulate, in a fast response manner, the behavior of a single CCD camera pixel that integrates light impinging on its surface for a predetermined period. This eases the timing/sampling concerns and increases the signal-to-noise ratios due to the increased photon collection.

41

An ideal integrator for the pDv application would employ a high-speed A/D converter capable of integrating the input voltage signal during the period between successive sampling operations. Factors defining the duration of this integration period would include particle size distribution and number density, sample volume size and data acquisition rate. Traditional integrator circuits employing fixed value passive components were considered initially. This approach was abandoned, since a large number of integrating circuits capable of being easily switched into the PMT signal path would be required to accommodate the many flow condition variables that define optimum integration times. In consideration of these factors, the pDv integrator, shown in Figure 3-10 was developed around a programmable analog circuit referred to as Field Programmable Analog Array (FPAA). The FPAA, manufactured by Anadigm Inc., uses a switched-capacitor based sampling methodology to implement an array of user configurable, op-amp based, analog cells.
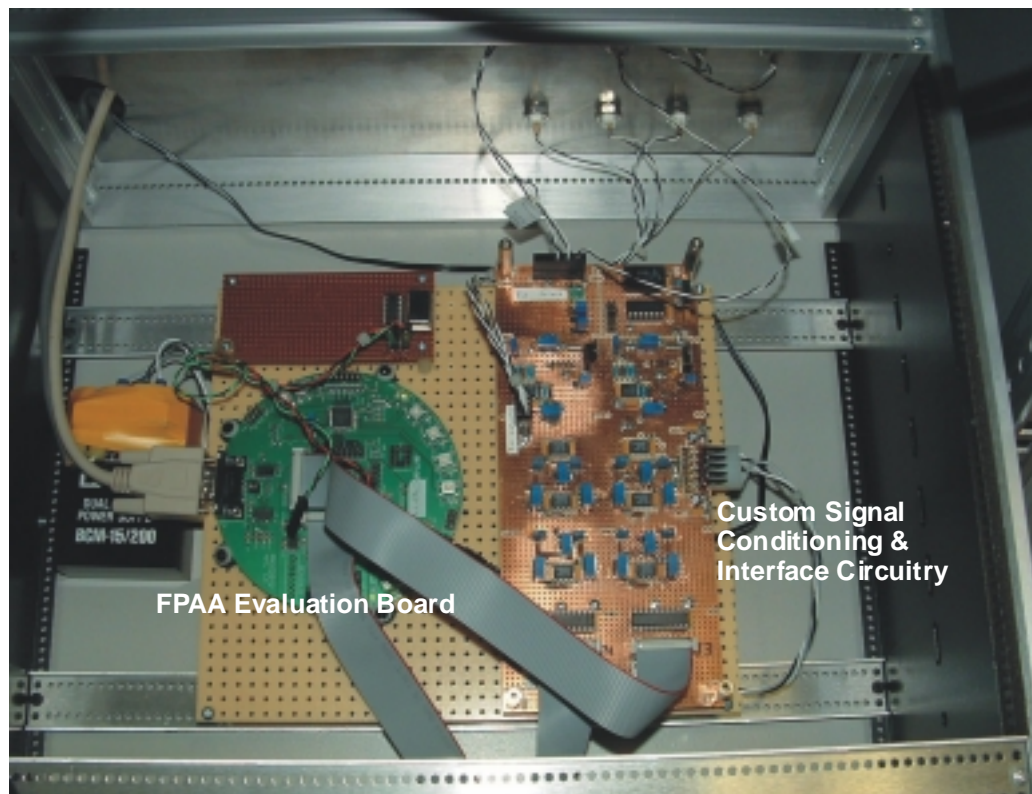
Figure 3-10 – **Photograph of the prototype pDv integrator.**

To support continuous integration, four of the twenty available FPAA cells referred to as IPModules were configured to operate as integrators. These integrators differed from the traditional op-amp/resistor/capacitor implementations, as they used a sampling approach and a programmable integration constant to integrate the input signal(s) in a digital manner. At the leading edge of each new master clock pulse, the input signal was sampled, multiplied by the gain constant and held. The number of samples used to integrate the PMT signal was dependent on the period between successive A/D sample clock pulses. Based on this time interval, the gain constant was adjusted so that the amplitude of the resulting integrated signal did not encroach upon the saturation region of the FPAA output amplifier.

Since the focus of the presented research was to mature the pDv technology and not the development of custom electronic instruments, the pDv integrator was implemented by constructing custom circuits around an FPAA mounted on an evaluation board. This also reduced

the time to deployment. Figure 3-11 is a block diagram of the pDv integrator, while Figure 3-12 is a timing diagram relating to system operation. Custom circuits were required to precondition pDv signals prior to interfacing them to the FPAA due to the manner in which the FPPA emulated the bipolar nature of a traditional op-amp. Since the FPPA used a single +5 VDC power supply, it referenced all signals to +2.5 VDC or Voltage Mid-Rail (VMR) - input signals below VMR were considered negative, while signals above VMR were interpreted as positive.
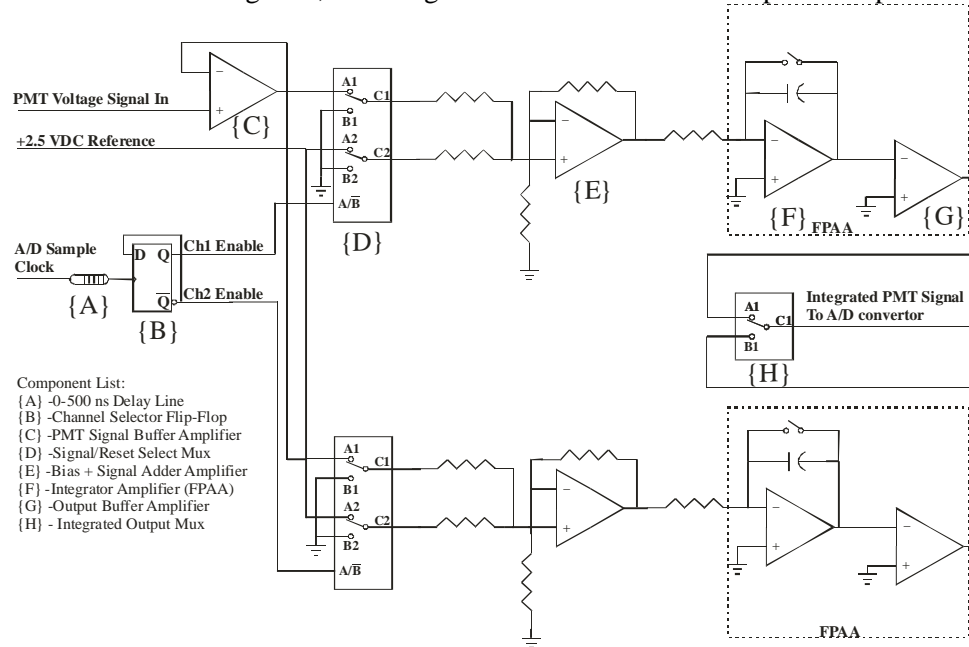
Figure 3-11 – Block diagram of the prototype pDv signal integrator.
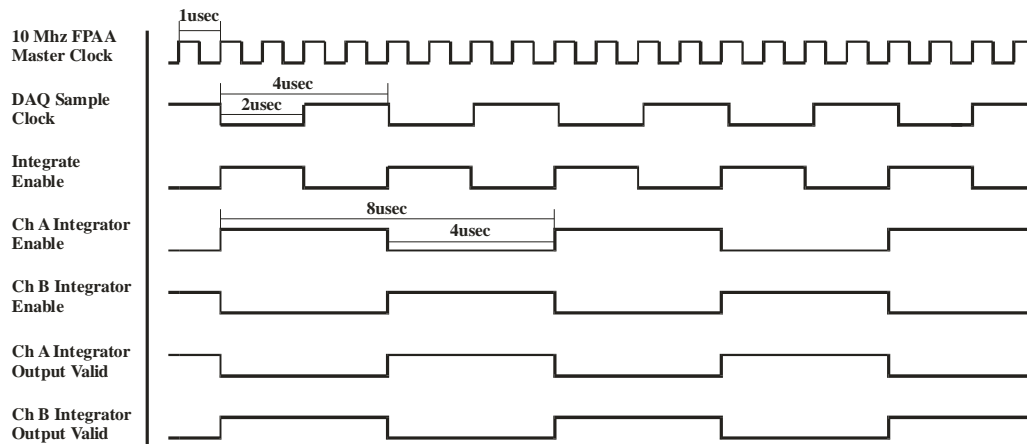
Figure 3-12 – Timing diagram for the pDv signal integrator.

Signal-conditioning circuits were used to condition PMT signals interfaced to the FPAA integrators, as the level of the input signal with respect to VMR controlled the integrating action. Integration was initiated once the input signal crossed VMR and continued until the input signal fell below VMR, where the integrator was reset to 0 VDC. Unfortunately, for the pDv application, this method of resetting the integrators posed a problem, since the PMT output had a maximum level of ~3.0 VDC and often fell below VMR, in response to discrete particle passages. To prevent the fluctuating PMT signal from resetting the integrator during the period between successive rising edges of the A/D sample clock, a +2.5 VDC biasing voltage was added to the PMT signal to maintain it above VMR (Figure 3-11(E)). Since the purpose of the pDv integrator

was to output a signal representing the average intensity of particle scattered light during the integration period, activation of the PMT biasing voltage was controlled by the A/D clock.

A ping-pong arrangement of two functionally identical integration channels was required (Channels 1 & 2 of Figure 3-11) to satisfy the requirement for continuous integration of the PMT input signal. The A/D sample clock controlled activation/resetting of isolated channels and input/output signal multiplexing.

The development and programming of the circuit designs for the FPAA was achieved using a software package called AnadigmDesigner. Within this environment, it was possible to wire, simulate and confirm the operation of various internal circuit designs. Configuration data describing the functionality of a validated design was downloaded over the serial port of the PC host computer to the FPAA via an RS-232 interface on the emulation board. To support the tuning of the integrator circuit integration time to match different test scenarios, several circuit designs were created, tested and archived, so that they could be downloaded to the FPAA during the course of laboratory testing. In this way, the operation of the integrator could be modified quickly. As the software package was an evaluation version, it was not possible to pre-compile and store FPAA configuration data in memory local to the FPAA device. This limitation required that the FPAA be programmed from within the AnadigmDesigner environment, precluding reprogramming of the device from within the pDv data acquisition program.

b. *Analog Data Acquisition Board*

Analog signals produced by the detectors employed in the LFM and integrators in the measurement components were sampled at regular intervals using a Datel, PCI-416J multifunction data acquisition (DAQ) board installed in the data acquisition computer. The specifications for this board were as follows:

- Low-noise, 12-bit digitization of Analog input signals (+/-10V)
- Simultaneous sampling of up to eight Analog input channels through the use of eight simultaneously clocked A/D converters
- Programmable sampling rates up to 250kHz/channel for eight channels.
- 16-bit Digital I/O.
- Two Analog Output channels
- High-speed PCI bus interface
- Windows 2000 compatible drivers
- LabVIEW and Visual C++ compatible software libraries

The selection of this data acquisition system was dictated by two factors. First, in order to maintain the temporal fidelity required to accurately measure the flow velocity, simultaneous sampling of all light detectors in the pDv system was essential. This was a primary requirement since the output signals levels of the signal and reference detectors of pDv measurement components were normalized in order to resolve flow related parameters. Any timing skew introduced when sampling these signals would result in a measurement error in normalized signal levels and consequently the measured velocities since the same flow conditions were not represented. For the one-component pDv system, four Analog input channels were used to sample the signal and the reference detector outputs for both the measurement and LFM components. As the pDv measurement capability becomes better established, the remaining channels will be used to sample signals produced by other pDv measurement components used to obtain multi-component velocity or cross correlation measurements.

The additional channels were used to sample analog signals produced by pitot-probes and/or a hot-wire anemometers in parallel with the acceptance of pDv measurements. This enabled pDv resolved velocities to be compared against these flow measurement standards in a time coincident manner.

A second pDv prerequisite, satisfied by this particular DAQ board was the Nyquist sampling requirements for measuring spectral quantities in a flow containing turbulence frequencies out to 100 kHz, as it exited a jet nozzle. The sampling rate of the PCI-416J was programmable and could be operated up to 250 kHz in the multiple channel configuration or as high as 400 kHz for single channel applications. The system also supported the use of an external A/D sample clock and triggering mechanisms to synchronize data acquisition activities with other instruments in the manner that it was used with the pDv integrator.

During pDv research activities, additional capabilities of the data acquisition board were also employed. For example, the digital I/O lines were used to control a mechanical shutter for the laser to block the light when background light level samples were acquired. In addition, one of the analog output signals was used to drive an LED used as an illumination source during PMT linearity testing.

c. *System Timing Controller*

Sampling activities of the DAQ board and the pDv integrator were synchronized using a National Instruments NI-6602, counter/timer board. The 80 MHz master time base of this PCI-bus based device maintained phase fidelity on up to eight programmable 32-bit counter/timer channels enabling the board to be used for event counting, period measurement, pulse-width measurement, frequency measurement, pulse generation, and pulse-train generation. Preservation of the temporal integrity necessary for pDv flow spectra characterization was achieved using three independent pulse generators of the NI-6602. The following three synchronous pulse trains controlled the integrator operation and synchronized it with the Analog data acquisition system:

- *Integrator Master Clock* – a 1 MHz pulse train drove the master sample clock of the FPAA installed in the pDv integrator. This assured that the same number of PMT input signal samples were obtained during each *integration aperture* (the time period between successive leading edges of the A/D sample clock).
- *DAQ Sample Clock* – this pulse train drove the sample clock of the A/D converter installed on the PCI-416J DAQ board. The frequency of this signal could be adjusted up to the 250 kHz maximum setting of the DAQ board, as dictated by the flow conditions.
- *Integration Start Signal* – this signal was a duplicate of the DAQ Sample Clock that controlled the multiplexing and sampling of the two integration circuits on alternating A/D sample pulses.

6. *pDv Sample Volume Positioning System*

A motorized scan-rig system with three degrees of freedom was employed to facilitate rapid relocation of the pDv measurement sample volume. The scan-rig provided the ability to reposition the sample volume anywhere within a ten-inch cube. As shown in Figure 3-13, the laser and the beam transmit optics along with the pDv measurement and LFM components were mounted on a system of three-inch, extruded aluminum rails. The scan-rig structure was mounted on caster wheels simplifying the relocation of the pDv system to different test areas.
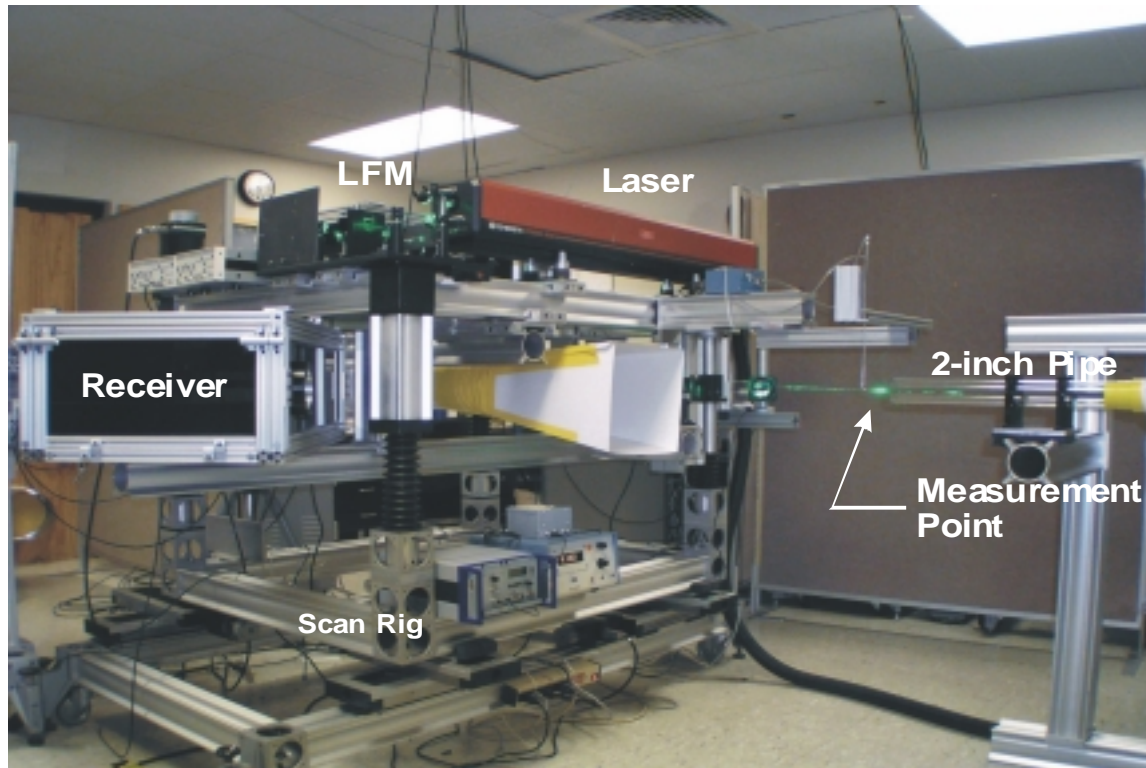
Figure 3-13 – Photograph of the pDv system installed in two-inch pipe facility.

Positioning of the pDv sample volume was controlled by commands issued to the scan-rig controller over an IEEE-488 (GPIB) interface from within the pDv data acquisition software. Since both the laser beam transmission and scattered light collection optics packages were mounted on the scan rig, optical alignment was maintained within the sample volume even when it was relocated. This minimized downtime between the acquisition of data records, since realignment was not required once the measurement volume was scanned to a new location.

In addition to supporting the positioning of the pDv optical systems, the scan rig was used to locate pitot probes and hot-wires during instrument comparison testing. By attaching these devices to the same traverse mechanism, it was possible to maintain the spacing relationship between the device and the pDv sample volume throughout the surveyed flow regions.

CHAPTER IV - pDv SOFTWARE DESIGN, DEVELOPMENT & VALIDATION

A. The Role of pDv Software

The ability of pDv to make accurate and repeatable velocity and spectral measurements requires the synchronized operation of an ensemble of tightly integrated hardware and software elements. These elements range from system to printed circuit board level components. The nature of pDv is such that the hardware and the software are inseparable; that is no phase of system operation can be achieved without each performing their respective functions in a systematic and coordinated manner.

Presented here is an overview of the pDv software system, which was designed in a manner that employs software functions to replace dedicated hardware components. This approach adds a degree of flexibility to the system since these software elements can easily be modified. In addition, system complexity and cost are reduced.

Developed software functionality was responsible for the initialization of the system hardware components and the orderly control of data acquisition and reduction activities. Custom software was used in conjunction with commercially available packages to make velocity and spectral measurements with pDv technologies in satisfaction of these requirements.

The developed software addresses three primary activities:

- *Hardware Interface and Control* – Software procedures that configure and control system hardware components prior to and during the course of pDv data collection activities. This includes the initialization of hardware and software drivers, communication ports and the synchronization of command and data transfers between the controlling software program and the targeted hardware system(s). Examples include the pDv integrator, scan rig, laser frequency stabilization and the file storage systems.
- *Data Acquisition* – Software components that synchronously manage an ensemble of diversified and complex hardware systems so as to sample signals produced by those systems in a manner that ensures time coherence, measurement accuracy and repeatability. These include the management of the analog data acquisition board, the digital oscilloscope, and the automated positioning of the pDv sample volume.
- *Data Processing* – Software subsystems that implement algorithms supporting the physics and mathematical basis of pDv enabling flow-related quantities to be extracted from raw voltage measurements. This includes converting raw data samples to velocity and spectra measurements, extracting temporal and statistical information pertaining to the investigated flow conditions, generating graphical representations of processed results and preserving intermediate and final processed data.

In addition to the functionality described, both the data acquisition and processing software packages support the following critical activities:

- *Data Archival* – Software mechanisms necessary for the management and storage of raw, intermediate and final data records.
- *Data Presentation* – Software functions required for user selection and graphical presentation of chosen raw, intermediate and final data records.

This chapter focuses on the custom software modules developed to support pDv research activities. Overviews of the development process, along with the purpose, requirements, implementation and validation of the various subsystems are provided.

B. Software Development Approach

In parallel with the evolution of the pDv hardware, the requisite software was developed using an incremental/prototype approach, as illustrated in Figure 4-1. The procedural sequence followed can best be described as a hybrid of the spiral and incremental models employed by software engineers.

Software elements were developed to support the integration of hardware subsystems during pDv instrument development. This research was conducted in three phases – each supporting the requirements of a particular development goal:

- *Construct a prototype, one-component, pDv instrument* – Incrementally incorporate hardware subsystems and develop associated control and processing software to characterize system functionality and gain experience with the practical application of novel scientific concepts. Validate system operation by measuring the rotational velocity of a rotating wheel that provides Doppler shifted scattered light frequencies based on two fundamental measurement standards: time and distance. The rotating wheel also provides a primary calibration and performance metric.
- *Assess and improve pDv measurement accuracy* – Authenticate pDv velocity and turbulence power spectra measurements for a flow exiting a two-inch pipe. Validate system accuracy by comparing the results against the measurements obtained using two flow measurement standards - the pitot probe (average velocity) and the hot-wire anemometer (spectra). Feedback obtained through system testing guides incremental system modifications to improve instrument measurement capability, and provides metrics to evaluate the accuracy and dynamic range of measurements as affected by the modification under investigation.
- *Improve system productivity* – Evolve data acquisition and processing software components into a distributed system employing efficient system control, data archiving, signal processing and data presentation capabilities via an easily navigable graphical user interface.
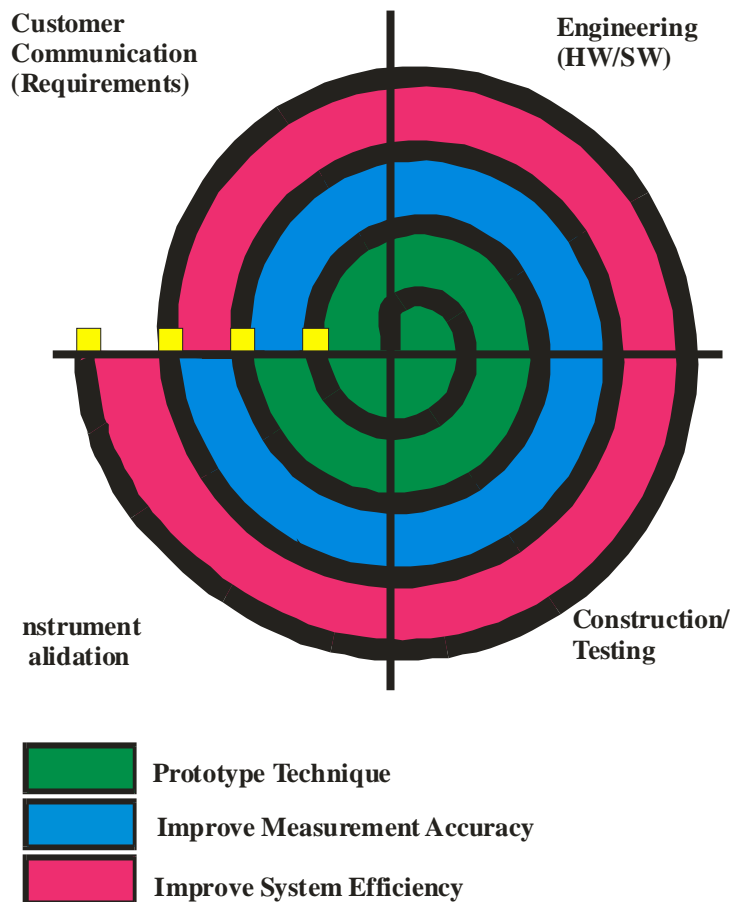

Figure 4-1 – Development model followed during pDv instrument research.

48

The research presented in this thesis concentrates on satisfying the first two phases to deliver a brassboard prototype of a non-intrusive instrument capable of making turbulence power spectra measurements.

C. pDv System Software Requirements

In order to support goals of the research activities, the following requirements were placed on the pDv software components:

- Robust, reliable, and automated operation
- Data acquisition instrumentation configuration and management facilities
- Convert raw data values to meaningful flow information
- Control for commercial and custom hardware/software components
- Flexible code modules facilitating reuse and expansion

To promote the timely development of pDv software and address the listed requirements, the National Instruments LabVIEW programming environment was chosen. LabVIEW possesses the characteristics needed to support the design/develop/test/ validate/deploy paradigm used:

- Extensive library of functions that support pDv hardware components
- Robust data/signal processing libraries
- Extensibility to support integration of custom C/C++ subroutines
- Facilities supporting the development of custom hardware drivers
- Integrated testing and debugging capabilities
- Modular development model that encourages component reuse
- Networking mechanisms for client/server applications
- Easy to use GUI development environment

The extensible nature of the LabVIEW environment enabled validated software procedures to be easily modified to support refinement of research objectives. This manner of development promoted the reuse of software components, with more versatility than traditional "library-based" functions that could be easily incorporated into the two planned versions of pDv software:

a. *Research Version*

Independent data acquisition and processing programs to facilitate system hardware control and testing and validate pDv physics and processing algorithms with maximum flexibility.

b. *Deployable Version*

Integrated data acquisition and processing modules that provide real-time velocity and spectral data. Controls providing low level and flexible instrument management necessary for instrument refinement activities will be removed to streamline system operation.

The research version of the pDv software will be addressed in this document, as the focus of this thesis is the development of the pDv instrument. Stand-alone pDv data acquisition and processing applications were created in consideration of project timelines and the need for functional and flexible software. Segregating the software in this manner provided platforms on which the capabilities of operation specific modules could be verified and tested. The characteristics of LabVIEW allow custom routines developed for these programs, once validated in the research version, to be incorporated into a single, deployable system. Wiring diagram examples depicting program execution and flow are presented in Appendix B.

D. System Software Organization

The organization of the software used during pDv technology development provides for the management of system components from power-up through the graphical presentation of flow

measurement and statistical data. This was accomplished through the sequence of processes outlined in Figure 4-2.
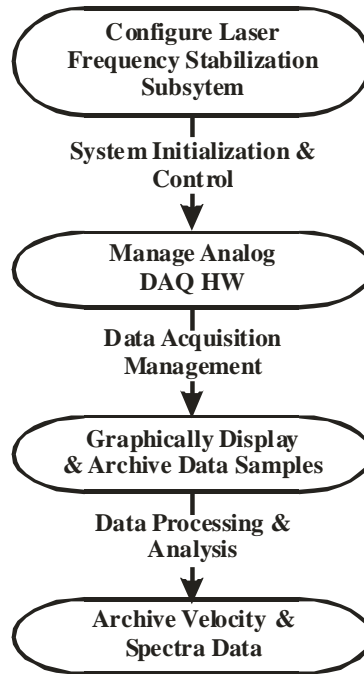
```
┌─────────────────────┐
│  Configure Laser    │
│ Frequency Stabilization │
│    Subsytem         │
└─────────────────────┘
          │
  System Initialization &
        Control
          ▼
┌─────────────────────┐
│   Manage Analog     │
│     DAQ HW          │
└─────────────────────┘
          │
   Data Acquisition
      Management
          ▼
┌─────────────────────┐
│  Graphically Display │
│ & Archive Data Samples │
└─────────────────────┘
          │
   Data Processing &
       Analysis
          ▼
┌─────────────────────┐
│  Archive Velocity & │
│    Spectra Data     │
└─────────────────────┘
```

Figure 4-2 – Sequence of pDv data acquisition and data processing operations.

E. System Initialization and Control Software

A collection of procedures, executed both from outside of and from within the custom data acquisition management program, prepared system hardware and software components for data acquisition operations (Chapter 3).

1. pDv Integrator Initialization & Control

The circuit configuration used to define the pDv integrator, described in section 3.D.5, was designed and verified from within the Anadigm, Field Programmable Analog Array (FPAA) CAD environment. Once validated, configuration data defining the circuit arrangement internal to the FPAA was compiled and uploaded to the FPAA evaluation board over an RS-232 connection. The FPAA circuit configuration was adjusted during pDv activities to tune the timing constants of the integrator circuits to match the data acquisition sampling rates for the flow conditions.

2. Flow Environment Control

During pDv research, the two-inch pipe flow used to validate instrument performance was operated at a single speed and managed manually. Future modifications for this facility will employ a computer controlled, variable speed, squirrel cage fan. This will enable the velocity of the flow exiting the pipe to be varied and make it possible to characterize the measurement capabilities of the pDv instrument over varying velocity regimes within the operating range of the fan driving the flow.

3. Laser Frequency Stabilization System Control

Frequency variations in the output beam of the Argon Ion laser had to be kept to a minimum in order to obtain accurate pDv velocity measurements. This was the purpose of the laser stabilization system (Chapter 3). Through the active adjustment of laser cavity length, this closed-loop system maintained the laser operating frequency within +/-5MHz of the reference setting established at the start of data collection activities. The reference frequency was achieved by manually tuning the laser,

so that the resultant frequency mode fell on the side of the IVC absorption line, where optical frequency shifts were measured. Custom, LabVIEW-based software, running on the pDv Laser monitoring computer (Figure 3-9), was used to maintain frequency stability by first sampling the LFM component Signal and Reference photodiode output signals (Figure 3-7) with the resident analog data acquisition board. Digitized signals were then normalized and the resolved frequency compared to the reference frequency. Based on the difference between the measured and the desired laser frequencies, the control software adjusted an error voltage signal driving a peizo-electric actuator mounted on the rear mirror of the laser. This allowed the laser cavity length to be dynamically varied in order to drive the output frequency back to the reference value.

4. *Scan Rig Initialization & Control*

To obtain an understanding of investigated flow-fields, data records at multiple spatial locations are required. The pDv sample volume positioning system (Chapter 3) enabled this data to be acquired in a repeatable and efficient manner. Custom subVIs operating under the user interface shown in Figure 4-3 managed the operation of this system. Commands and data transferred over a GPIB interface initialized the scan rig and positioned the sample volume to the X, Y and Z spatial locations required the test matrix during the course of the data collection activity

Figure 4-3 – pDv sample volume position control interface.

5. *Data Acquisition Hardware Configuration*

Custom software elements applied the settings of the controls presented on the pDv Data Acquisition Configuration tab (Figure 4-4) to configure and manage data acquisition activities of the Datel PCI-416J DAQ board and the NI-6602 counter/timer boards (Chapter 3). In addition, software functionality was provided to support the use of other instruments interfaced to the data acquisition computer via a GPIB interface. Some of the instrumentation employed during pDv research activities included a digital oscilloscope, a pulse counter and a voltage standard. This software initialized both the drivers needed to control these instruments and the parameters that defined their operation. Initialization involved defining signal-acquisition properties such as buffer memory allocation, sample rate, trigger signal definition and routing, channel number/measurement component associations, channel data type definition, record length and sampling intervals. The wiring diagram used to initialize the data acquisition hardware components is presented in Figure B-1, Appendix B.

Figure 4-4 –Data acquisition hardware initialization control interface.

6. *Data Source Definition*

An objective of the pDv research was to compare its velocity measuring capabilities to those of more mature technologies, such as the hot-wire and the pitot probe. Satisfaction of this goal required that signals produced by the pDv hardware and those of other instruments be sampled simultaneously (pitot probe) and sequentially (hot-wire) using the multiple channel capabilities of the Analog Data Acquisition board.

In order to identify the source of resultant digitized samples a labeling scheme was employed. Unique labels that identified the data source are described in Table 4-1 and the controls shown in Figure 4-5 provided an interface to a subVI that enabled the user to select the label describing the data source of a channel. Label strings generated via this interface that associated a transducer with a given A/D channel, were subsequently written to disk along with the acquired data. This information helped to automate the processing operations, since the data source mnemonic heading a given data column was used to activate instrument specific processing procedures.

pDv Data Source Labeling Scheme		
Instrument	**Mnemonic**	**Description**
pDv	AS	Component A Signal Leg Detector
pDv	AR	Component A Reference Leg Detector
pDv	BS	Component B Signal Leg Detector
pDv	BR	Component B Reference Leg Detector
pDv	CS	Component C Signal Leg Detector
pDv	CR	Component C Reference Leg Detector
pDv	DS	LFM Component Signal Leg Detector
pDv	DR	LFM Component Reference Leg Detector
Pitot Probe	Px	Pitot Probe signal, channel x
Hot Wire	Hx	Hot Wire signal, channel x
Kulite	Kx	Kulite pressure transducer signal, channel x
Microphone	Mx	Microphone transducer signal, channel x
PMT In Situ LED	Lx	PMT calibration LED voltage signal, channel x
Voltage	Vx	Misc voltage transducer signal, channel x
Other	Ux	User defined device signal, channel x
Disabled	XX	Channel not used

Table 4-1 – Data source identification mnemonics.
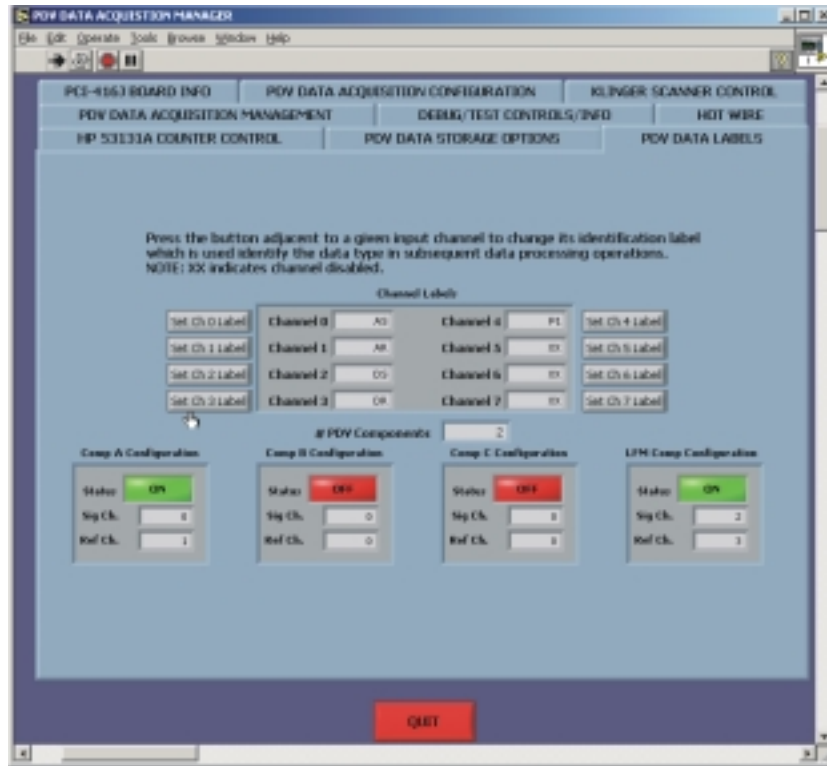
Figure 4-5 – DAQ board channel label assignment user interface.

7. *Data Acquisition Management*

Software functions activated in response to user interaction with the Data Acquisition Management panel shown in Figure 4-6 defined where, when and how pDv data records were acquired. This software supported the flexibility necessary to validate the performance of the prototype pDv system. Controls were provided to enable automatic positioning of the sample volume, number of records to acquire at each scan position and the time delay between the acquisition of successive records. With the activation of the Acquire Data control, data acquisition activities were commenced and continued until the required number of data records were acquired or the user activated the Stop Acquisition control. Data collection activities included enabling the timing signal generator, arming the data acquisition circuitry and monitoring the status of data acquisition hardware components (wiring diagram, Figure B-2, Appendix B).

Figure 4-6 – Interface used to manage data acquisition activities.

Three data acquisition modes were supported to give the program the versatility required of a system employed to investigate new concepts:

- *Continuous* – Data records were acquired continuously at the specified timing interval. This mode was used to verify system operation prior to initiating data acquisition operations.
- *Automatic* – The requested number of data records were acquired at the specified timing interval and saved to the disk. This mode was used once the system operation was verified and the sample volume was positioned at the desired location.
- *Manual* – A new data record was collected and saved to the disk each time the user activated the Acquire Data control. This mode supported the ability to acquire data records at irregular intervals as determined by the operator. For example, when velocity measurements were desired in an unstable flow region and particle seeding was not constant, the operator could initiate data acquisition once the seeding density became steady and reached levels where scattered light intensities were observed.

Four controls at the bottom of the sub-panel shown in Figure 4-6 provided the ability to reposition the sample volume and manage the storage of data records to minimize the inclusion of bad records in the data ensemble. These controls proved to be useful during testing, as they enabled data points to be repeated in situations where system anomalies were recognized. For example, records were reacquired when the laser frequency changed resonance mode or when seeding particle density was insufficient for attaining suitable signal levels.

System validation procedures incorporated into these processes afforded the ability to verify the completion of hardware specific operations. Whenever error conditions were identified, these functions alerted the operator, providing them with an opportunity to take corrective actions prior to proceeding with the predetermined test matrix.

F. Data Acquisition Software

These procedures, executed within the LabVIEW-based data acquisition program, concentrated on operations performed once signals output by the detectors in both the LFM and in the measurement components, as well as the Analog signals output by other instruments were digitized.

1. Data Retrieval

After initiating a data acquisition cycle, the control software entered a loop, where the status word for the Datel PCI-416J board was periodically retrieved and examined. Once the Memory Full bit of the status word was set, indicating that the number of samples acquired satisfied the number requested, the wait loop was exited. At this point, the digitized samples were transferred from the data acquisition buffers into pre-allocated 16-bit, unsigned integer arrays where archival and processing operations could be performed. The 16-bit integers held the sign extended version of the 12-bit data values produced by the A/D converter residing on the Analog data acquisition board. The sign bit, located in the most significant bit position of the digitized 12-bit value, was duplicated to the upper four bit locations of the 16-bit integers.

2. Data Storage Management

To accommodate the archiving of large numbers of samples acquired during a pDv experiment, a system capable of uniquely identifying and storing the data records was required. Software procedures developed to manage this task were geared for automated file path generation and fast pDv data storage with minimal user interaction. Parameters defining data storage formats and locations are shown in Figure 4-7. With the activation of the Configure Data Storage control, the pDv Data Storage Manager (Figure 4-8) was invoked. This interface provided fields and controls needed to define pDv data storage formats and locations. Based on user settings, this custom subVI generated a directory structure that conformed to path definitions, where the standalone pDv data processing program expected to find the calibration and data files. Prior to permitting these settings to be used, specified directory locations were scanned to determine if they contained data records having a filename prefix matching that entered by the user. When existing files were found, the user was alerted and controls supporting the ability to overwrite or move the files were activated thus giving the user an opportunity to delete or relocate previously archived files.
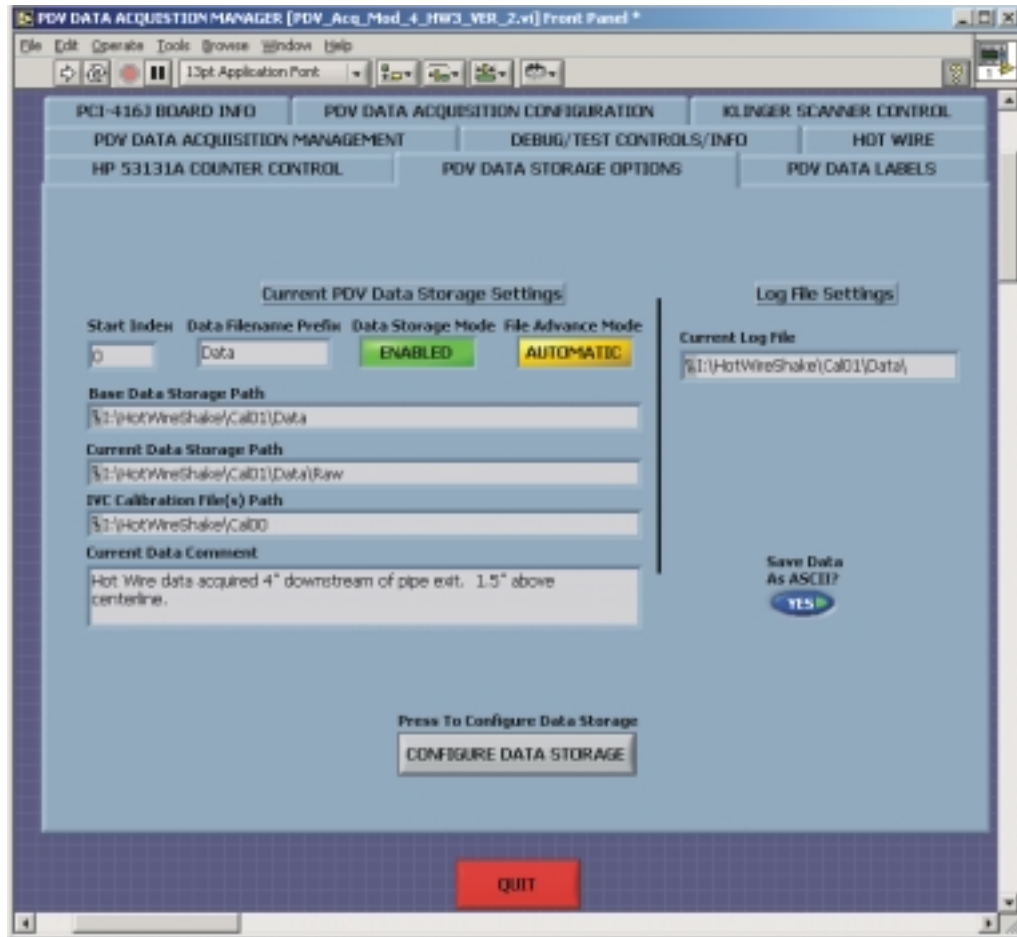
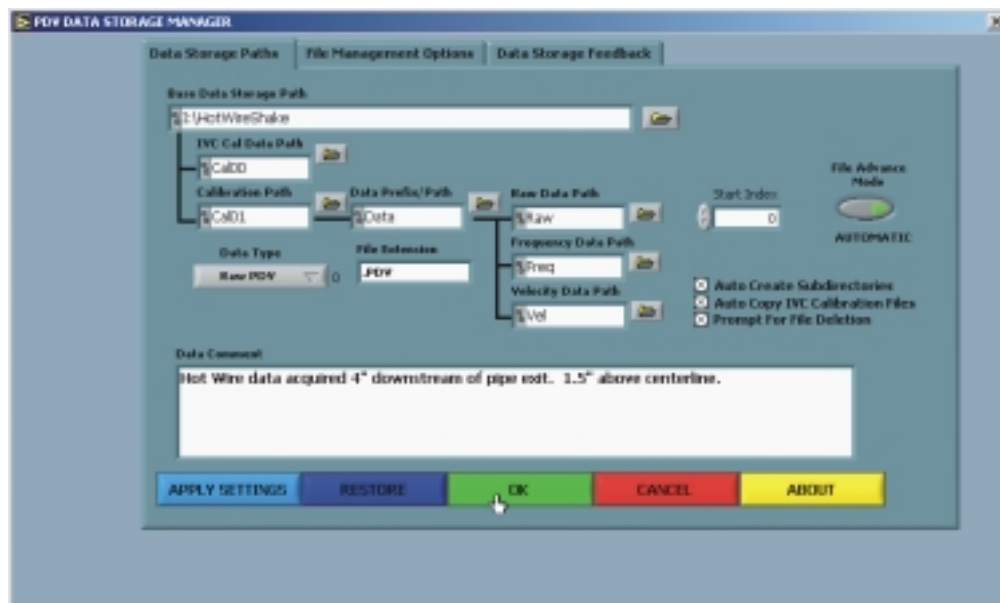**Figure 4-7 – Tab displaying data storage parameters.**

Figure 4-8 – Interface defining locations for raw data storage.

The Data Storage Manager dialog returned the following information:

- *Data Type* – Identified the data type to be one of background, flat field or raw pDv. Background and flat-field data sets were averaged enabling the corrections to be applied during on-line data processing operations.
- *Data Storage Format* – By default pDv data samples were saved in binary format; in addition, when the Save Data As ASCII? control of Figure 4-7 was enabled, data was also saved in an ASCII formatted file.
- *Data Storage Locations* – This information formed the root portion of the file path or *prefix,* where a succession of data sets was to be saved. The file prefix identified a series of data records acquired under similar flow conditions and simplified the grouping of these files. During the course of data acquisition operations, the cycle index value was appended to the file prefix to uniquely identify that data record.

3. Header Record Generation

The reduction of the contents of a given pDv data file was not possible without information detailing the manner in which the data was acquired. To address this need, software functions were developed to generate an ASCII formatted string or header record that described the conditions under which the data record was acquired (Table 4.2). Header strings were formed by prefixing data acquisition hardware settings culled from controls or indicators on LabVIEW VI front panels with descriptive labels. Additionally, sample volume position information was incorporated into these strings so that the origination point of the data and the rotational speed of the rotating wheel, when used, would be known. During off-line data processing operations, header information was parsed and applied to extract flow velocity data from the raw data values contained in that file.

4. Data Record Formatting

To facilitate the off-line analysis of pDv data records, software functions were developed to ensure that the data along with descriptive header information was written to disk in a uniform manner (Table 4.2). During early investigations, data was saved exclusively in tab delineated ASCII format as this enabled the data record to be interrogated from within Microsoft Excel. Data acquired from each of the enabled Analog input channels was organized in tab delimited, columnar order. The mnemonic labels presented in Table 4.1 were inserted at the row location preceding the actual data to identify the data source. This made it possible to archive data originating from instruments such as pitot probes and hot-wire anemometers in a single file along side pDv data samples. Subsequent interrogation of these labels simplified the task of identifying what processing operations were required to reduce a data subset into velocity or other information. As system operation became more refined and longer data records were acquired, a binary data storage capability was incorporated to reduce data storage requirements and recording time. In both the binary and ASCII formatted files, sampled data was preceded with header information in ASCII readable format. This enabled the user to obtain a quick overview of the data contained within a given file using word processing or spreadsheet programs.

E:\4In_Scan_1_13_03\Cal01\Data\Raw\Data02.pdv					
Monday, January 13, 2003	11:30:49 AM				
Data Acquisition Parameters:					
# Acquisition Channels:	5				
Record Length:	4096				
Total Acquired Records:	1				
A/D Sample Rate:	200				
A/D Board Trigger Source:	Internal				
A/D Board Trigger Rate:	1				
HP 53131A Reading:	0				
Wheel RPM:	0				
Atm. Pressure (in/Hg):	30				
Temperature (C):	25				
Scanner Positions:					
W-Axis:	5076.2				
X-Axis:	101600				
Y-Axis:	0				
Z-Axis:	0				
Flat Field Cal. Factors:					
Comp A:	1				
Comp B:	1				
Comp C:	1				
Comp D:	1				
Background Calibration Values:					
Comp A Signal:	0				
Comp A Reference:	0				
Comp B Signal:	0				
Comp B Reference:	0				
Comp C Signal:	0				
Comp C Reference:	0				
Comp D Signal:	0				
Comp D Reference:	0				
Scanner Comment:					
Sample Volume positioned 0.20" right of centerline.					
User Comment:					
pDv & Pitot Probe data acquired 4" downstream of 2-inch pipe exit					
Time	AS	AR	DS	DR	P1
0.00E+00	3.61E+00	4.45E+00	4.78E+00	6.86E+00	1.07E+00
5.00E-03	3.51E+00	4.18E+00	4.78E+00	6.91E+00	1.07E+00
1.00E-02	3.60E+00	4.43E+00	4.74E+00	7.01E+00	1.07E+00

Table 4-2 – ASCII formatted raw pDv data record – header data shaded.

G. Data Processing Software

Processing of pDv data was conducted on two levels:

- To support hardware management during data collection activities, some rudimentary, online, data processing operations were built into the data acquisition program for instrument monitoring purposes.
- More thorough data reduction operations were provided in the off-line and standalone, data processing program, Figure 4-9, that provided a means for computing flow velocity for acquired data sets.
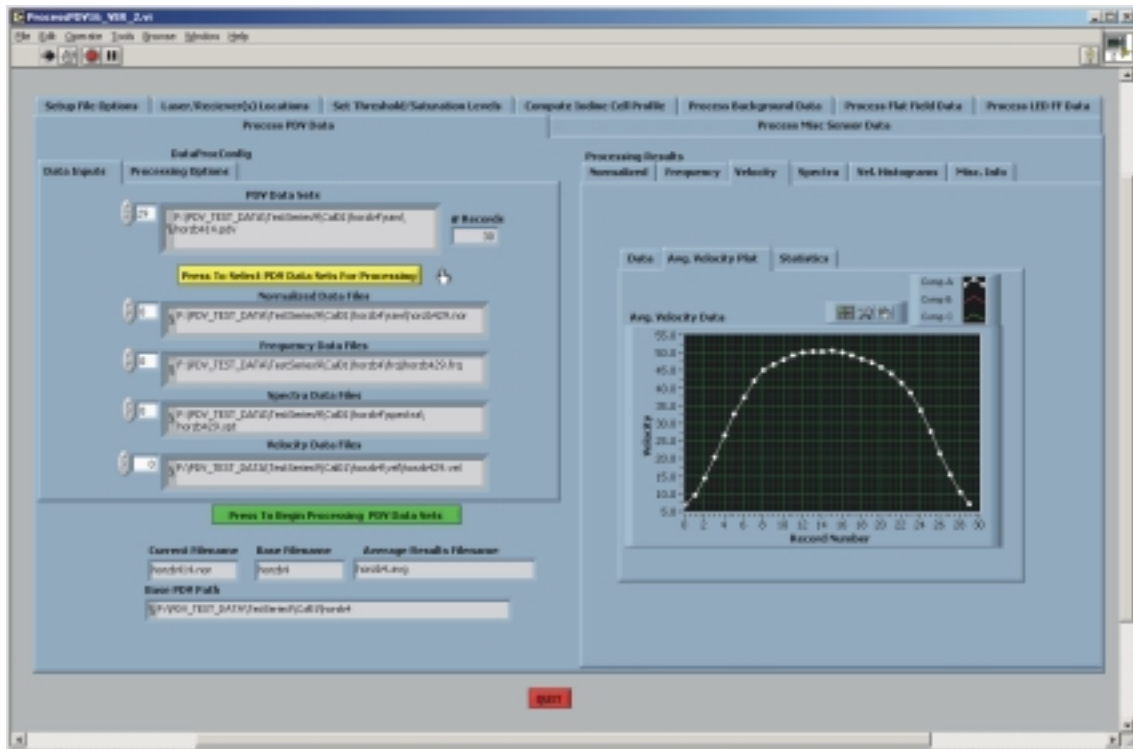
Figure 4-9 – User interface to the standalone pDv data processing program.

Since many of the tasks performed during the data acquisition phase were duplicated in the offline-processing program, no differentiation as to how the operation was performed will be made, unless clarification is warranted. On-line pDv data processing results were not used during the off-line processing sequence and data reduction procedures were repeated, as required, to insure that appropriate calibration data sets were applied. Data sets acquired under the same operating conditions were processed together to improve statistical accuracy and to enable an accurate assessment of velocity measuring capability.

1. Conversion to Voltage

Prior to processing acquired data records, each digitized data point was converted back into a voltage. A SubVI implementing the algorithm presented in the flow chart of Figure 4-10 enabled subsequent data processing operations to be performed using floating-point mathematical procedures.
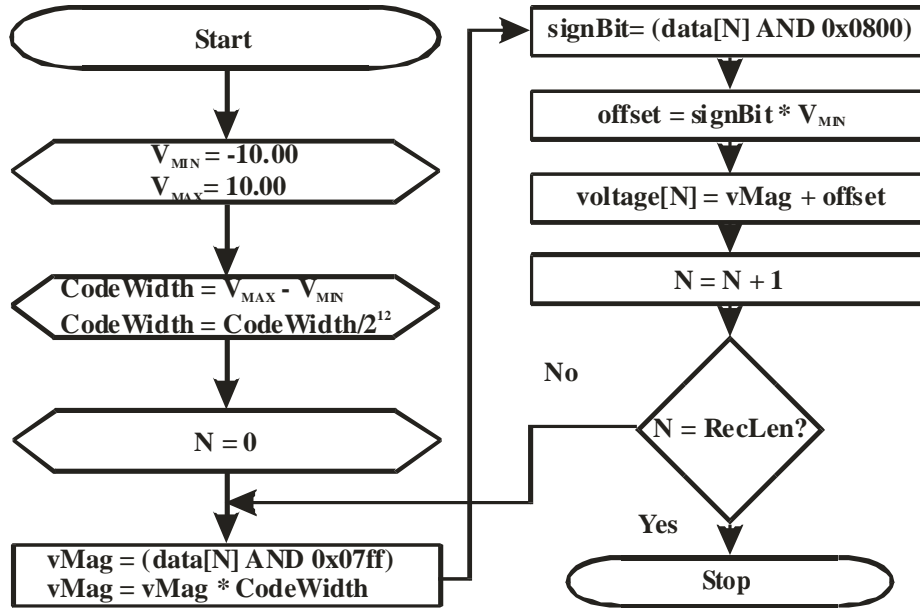
Figure 4-10 – Algorithm used to convert digitized values to voltage.

During the data acquisition phase, voltages resulting from this conversion were displayed in a time series plot window. This feedback enabled the researcher to verify that the incoming voltage signals, generated by the PMTs in response to varying scattered light levels, were within the predefined limits to achieve reasonable normalization levels that could be translated into accurate velocity measurements. The amplitude of these signals was such that they were high enough that variations due to particle movement could be distinguished from background light levels; yet low enough that they did saturate the PMTs or exceed the input voltage range of the A/D converter on the Analog DAQ board.

2. Calibration Data Management

Unless appropriate calibrations were applied, an accurate analysis of signals representing the light level fluctuations resulting from particles passing through the pDv sample volume was not possible. To improve velocity measurement accuracy, raw data samples were corrected to account for background light levels and mismatches along the optical paths (flat-field) of the reference and the signal detectors in both the measurement and the LFM components.

New background levels were required each time the pDv sample volume was scanned to a new location since the degree of light scattered by objects in the region where the data was collected varied. This required that multiple background data sets be acquired during a test sequence to enable appropriate position dependent corrections to be applied. Background data was collected prior to the initiation of data acquisition activities, before smoke particles were introduced into the flow, to account for model motion.

Typically, a single flat field calibration data set was acquired for a given data acquisition session and used to correct all data obtained during that time frame. Updated flat field calibrations were necessary only when the laser frequency changed resonance mode, requiring the laser reference frequency be manually reestablished.

Background and flat field calibration parameters were determined by computing the average of the individual data points in the data record. This averaging operation was performed automatically when the user specified the data type to be background or flat field. When possible, these average calibration values were applied to correct the raw data records online, as they were acquired.

Because the pDv optical configuration required adjustment when alternating between the acquisition of background, flat field and velocity data sets, a substantial amount of time was required

to complete a test matrix. To reduce the time needed to fulfill the testing requirements, and to minimize the risk of compromising system operation, background and flat field data sets were acquired either before or after the collection of the velocity data. Given this scenario, it was cumbersome to apply the correct calibration values to velocity data sets obtained during the data acquisition phase. The primary limiting factor in the application of calibration data in-situ was that the research version of the data acquisition program did not provide mechanisms the enabled the user to select the calibration data corresponding to the targeted sample volume position. In consideration of these issues, controls located on the data acquisition control panel allowed the user to apply a default background level of zero and a default flat field value of one, in cases where the application of the actual values was not possible. This enabled *ballpark* estimates of the normalized signal levels to be obtained, while expediting the data collection process.

In the standalone data processing program an interface to the file system was incorporated that enabled the user to match the appropriate background and flat field correction files to one or more pDv data records (Figure 4-11). This improved the accuracy of processed intermediate and finalized data sets.
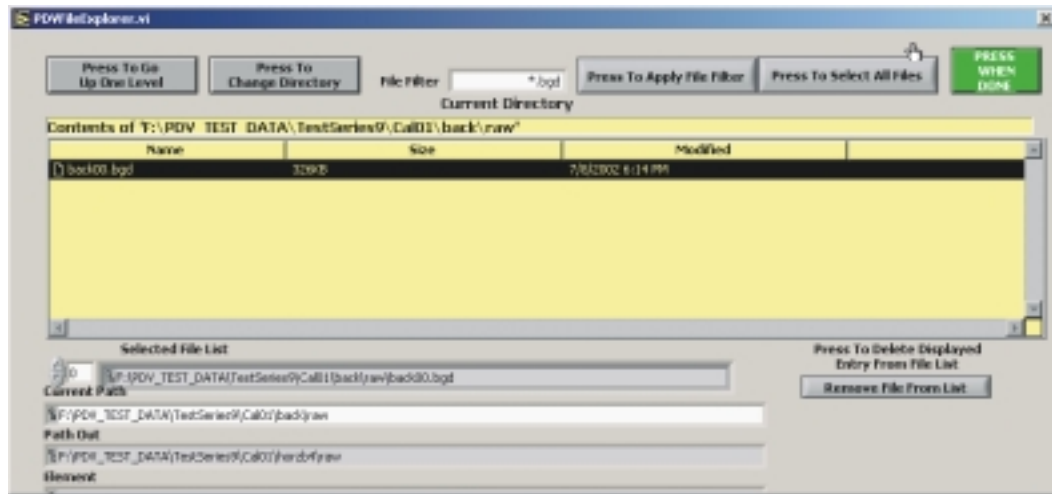

Figure 4-11 – pDv file navigation subVI front panel.

3. Data Normalization

Resolved Signal detector voltages were normalized by those determined from the Reference detector. Normalization accounted for scattering particle size and number density variations as well as intensity fluctuations in the illuminating laser beam. Elimination of these uncertainties produced a result that had a direct relation to the Doppler frequency measurement through the transfer function of the IVC.

As any error introduced during the normalization process becomes magnified during data processing, it was critical that the appropriate calibration parameters be applied to each acquired data point. Average backgrounds specific to the Signal or Reference leg detector and the flat-field correction levels for a given measurement component were applied to each element in the data record to improve the accuracy of the normalized result. Equation 4.1 was implemented in a custom LabVIEW sub VI to scale the normalized signal to 2048 to improve optical frequency resolution (wiring diagram Figure B-3).

$$N[i] = \left(\left[\frac{S[i] - BG_S}{R[i] - BG_R} \right] * \left[\frac{FF_R - BG_R}{FF_S - BG_S} \right] \right) * 2048 \qquad (4.1)$$
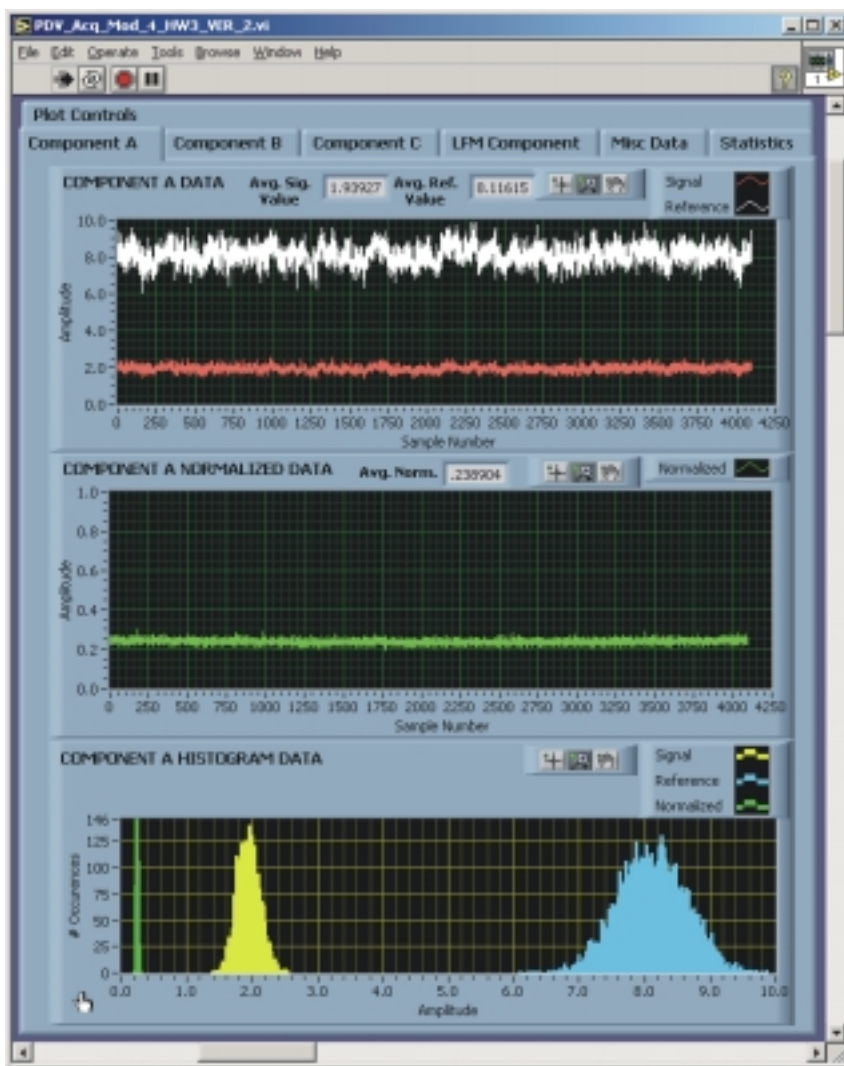
Figure 4-12 – Online presentation of raw, normalized and histogram data.

Normalization operations were performed during the data acquisition phase and the resulting values were plotted on the same XY time series plot as resolved Signal and Reference detector voltages (Figure 4-12) (wiring diagram Figure B-4). Presentation of the normalized data in this manner provided a means to evaluate data quality on-line. The visual feedback of the normalized signal levels made it possible to determine if particle induced scattered light frequency shifts were being measured in the linear region of the IVC absorption line.
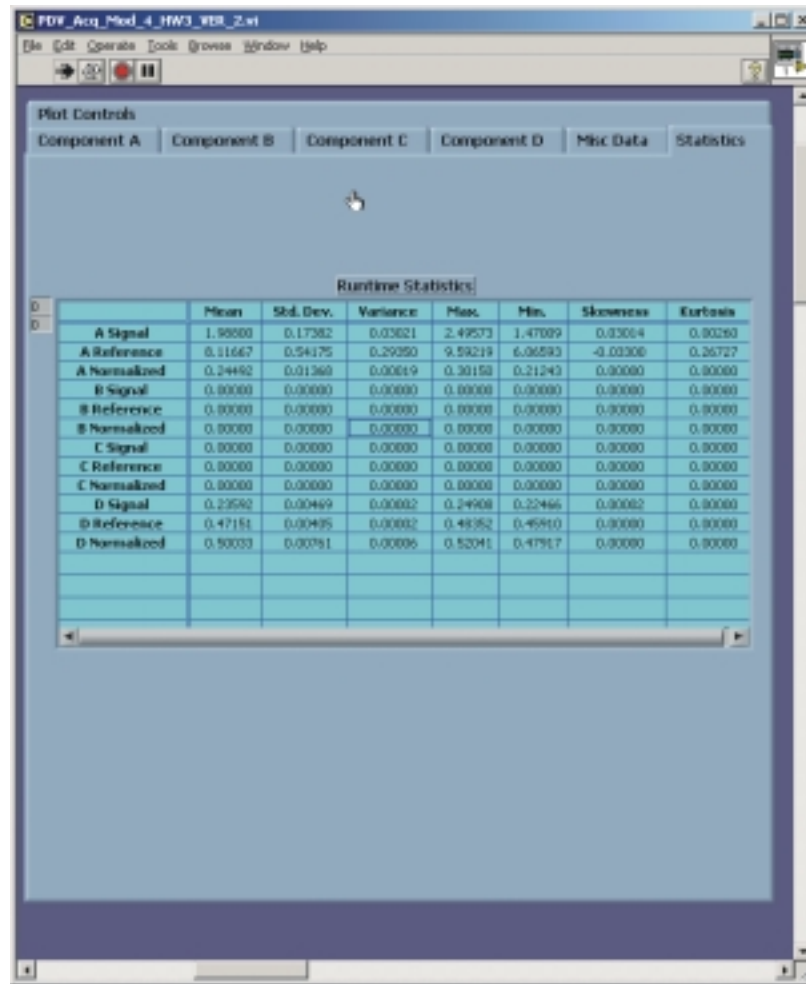
Due to the difficulties in applying pertinent calibration data, normalized values computed online were discarded. Normalization operations were repeated within the standalone data processing program where the file system navigation facilities made it possible to select and then apply the appropriate calibration files (Figure 4-11) to the raw data sets based on the notes recorded by the operator during data acquisition activities. Resultant normalized data records were saved to the disk and made available for additional processing.

4. Statistical Data Computation

To assess signal quality and system stability, statistical information was computed for raw and processed data sets. Statistical subVIs supplied with LabVIEW were incorporated into the custom subVIs providing data limiting (conditioning) features to determine the mean, standard deviation and

extremes for raw and processed data sets. In addition, histograms were computed and plotted, yielding feedback regarding the distribution of raw and computed data values (Figure 4-12).

As data records were collected, statistical information was computed (wiring diagram, Figure B-5, Appendix B) in real-time for uncorrected Signal, Reference and normalized data streams and then presented in a tabular form (Figure 4-13). Statistics were also calculated at each processing step within the data processing application. Finalized average and normalized frequency and velocity values for each active pDv component as well as the average velocity of the rotating wheel, computed by processing samples acquired from an optical tachometer, were presented on the user interface in numerical and graphical formats and archived.

	Mean	Std. Dev.	Variance	Max.	Min.	Skewness	Kurtosis
A Signal	1.98800	0.17382	0.03021	2.49573	1.47089	0.03064	0.00260
A Reference	8.11667	0.54175	0.29350	9.59219	6.06593	-0.03300	0.26727
A Normalized	0.24492	0.01360	0.00019	0.30158	0.21243	0.00000	0.00000
B Signal	0.00000	0.00000	0.00000	0.00000	0.00000	0.00000	0.00000
B Reference	0.00000	0.00000	0.00000	0.00000	0.00000	0.00000	0.00000
B Normalized	0.00000	0.00000	0.00000	0.00000	0.00000	0.00000	0.00000
C Signal	0.00000	0.00000	0.00000	0.00000	0.00000	0.00000	0.00000
C Reference	0.00000	0.00000	0.00000	0.00000	0.00000	0.00000	0.00000
C Normalized	0.00000	0.00000	0.00000	0.00000	0.00000	0.00000	0.00000
D Signal	0.23592	0.00469	0.00002	0.24908	0.22466	0.00062	0.00000
D Reference	0.47151	0.00405	0.00002	0.48352	0.45910	0.00000	0.00000
D Normalized	0.50033	0.00761	0.00006	0.52041	0.47917	0.00000	0.00000

Figure 4-13 – Online statistical data table.

5. *Histogram Limiting*

To reduce the influence of system noise and measurements obtained when large or no particles were within the pDv sample volume, a data limiting procedure based on the normalization value histogram was employed in the data processing program. The application of this concept improved the accuracy of computed statistical and average velocity information as outliers were eliminated during processing.
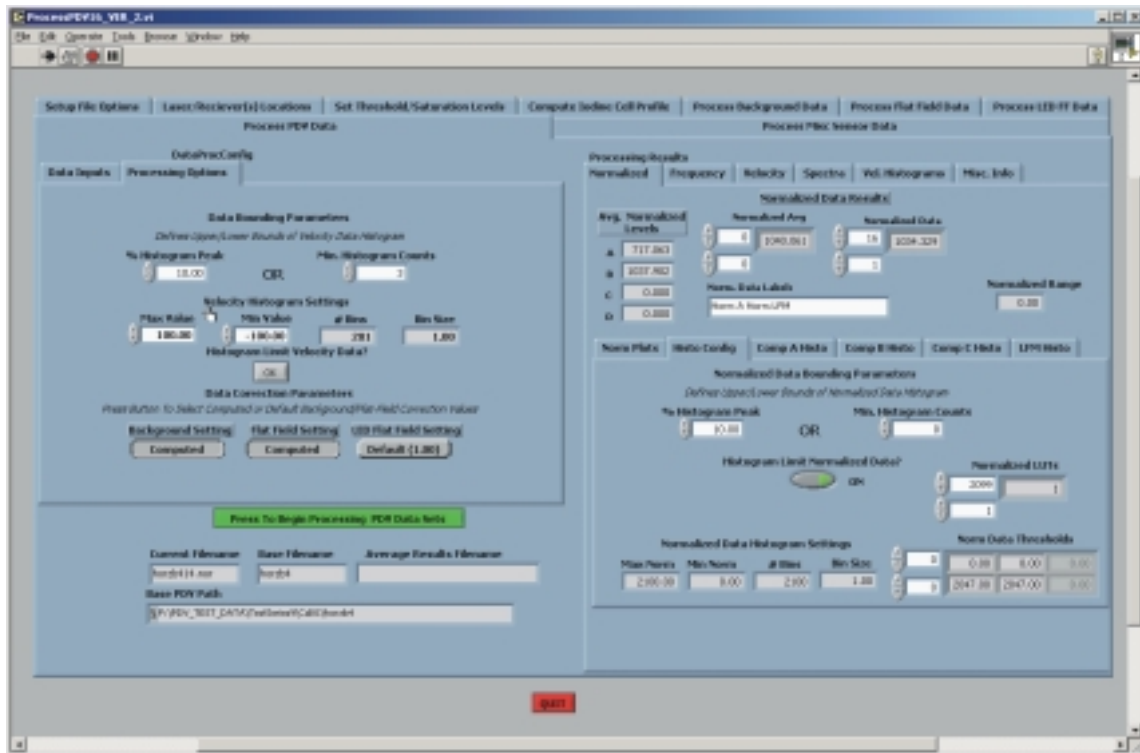
Figure 4-14 – Histogram limiting parameter definition controls.

The range of acceptable normalized data values was determined using the histogram definition of input values via the controls in Figure 4-14, through the implementation of the following operations:

- Compute the histogram for the data resulting from the pDv data normalization operations for each of the data records of interest.
- Sum all of the histograms generated for each processed data record.
- Plot the number of occurrences as a function of normalized value and locate the histogram peak value.
- Locate the upper and lower data value bins in the histogram not satisfying the user-defined number of occurrence criteria. The number of occurrence criteria was the lesser of a percentage (10% by default) of the histogram peak or a given count (default of three) and was set via the user interface.
- Determine if the total number of data value occurrences falling within the established bounds encompasses 95% of the data record. If the 95% criterion was not satisfied, the histogram was scanned further in an attempt to locate a second peak. A dual peak histogram was often encountered, when investigating shear regions in flow. For this second histogram, a second set of upper and lower data limits was identified.

Based on the established data bounds, measurement component specific, binary valued lookup tables were computed. The lookup table address locations matching the normalized values falling within the bounds of valid data values were set to one while out of bounds address locations were set to zero. During data processing, the data bounding look-up tables were applied as follows:

- Recall the result of the data normalization procedure from the disk.
- Use the normalized values to address the lookup table and multiply the value found at that location by the normalization value.
- In range normalized values were maintained, while outliers were set to zero and the resultant data record processed further to obtain velocity information.

65

6. Doppler Frequency Shift Determination

The Doppler frequency shift resulting from particle motion was determined by subtracting the optical frequency obtained at the measurement component from that measured at the LFM component (Equation 4.2):

$$\Delta v[i] = v_{MC}[i] - v_{LFM}[i] \tag{4.2}$$

Optical frequency was determined only in the standalone data processing program by using the normalized result to address the precomputed lookup tables (LUT) describing the optical frequency transfer function of the IVC employed in each component. To improve the accuracy of the resolved optical frequency a linear interpolation algorithm was employed (Equation 4.3):

$$f = \frac{n - n_1}{n_2 - n_1}(f_2 - f_1) + f_1 \tag{4.3}$$

Where:

f = resolved optical frequency

n = computed normalized value

n_1 = normalized value (LUT table index) preceding the computed value

n_2 = normalized value (LUT index) following the computed value

f_1 = frequency value obtained from LUT at address n_1

f_2 = frequency value obtained from LUT at address n_2

Frequency values obtained for both the measurement and the LFM components along with the computed Doppler frequencies were preserved in a single disk file.

Within the standalone data processing program, controls were provided, Figure 4-15, to enable the operator to associate precomputed LUTs, identified numerically, to the measurement component in which it was used during data acquisition. Code invoked with the selection of the Compute Iodine Cell Lookup Table control supported the loading of a precomputed or the computation of a new lookup table. The operation performed was dependent on the suffix of the selected file. If the selected file had a suffix of .lut, the data was retrieved from the file, loaded into a dynamically allocated array, and then used for optical frequency resolution.
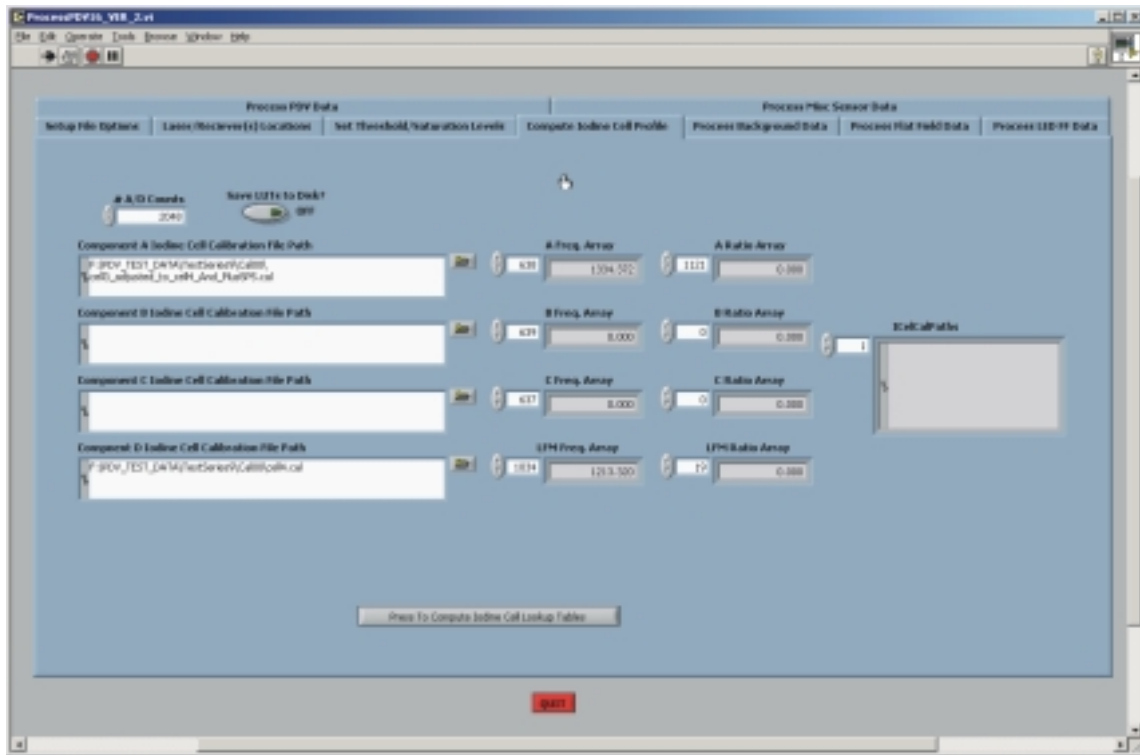
Figure 4-15 – Interface for IVC calibration table generation.

When the selected file had an .i2c suffix, the LUT was computed using four parameters describing the Boltzmann equation for an IVC transfer function. The Boltzmann equation was obtained by performing a Sigmiodal fit within Origin to smooth the curve describing the transfer function of the IVC, which was manually generated by aligning IVC calibration data subsets.

Generation of the IVC LUTs using the Boltzmann equation was useful during early investigations, when the LUT calibrations were tested to assess their accuracy. Provision of the ability to generate the LUTs dynamically simplified the iterative LUT generate/test cycle. Controls were provided that enabled the results of in-place LUT calculations to be preserved to disk for later retrieval. A complete description of the IVC development process is provided in Chapter 5.

The accuracy of the computed Doppler frequency shift was limited by errors related to the use of the LUTs describing the transfer function of IVCs. The first error is introduced by the fact that there is a difference between the frequency data contained in the LUT and the true frequency associated with the attenuation value observed. The frequency values contained within the LUT are the result of a calibration fit applied to values resolved from measurements obtained during the IVC calibration phase. The extent of this error becomes magnified since the resolved Doppler frequency shift is computed based on values extracted from independent LUTs used in the measurement and LFM components. The magnitude of this uncertainty is related through Equation 4.4:

$$u_f = \sqrt{\sigma_A^2 + \sigma_{LFM}^2} \tag{4.4}$$

Where:

u_f = Uncertainty in the resolved Doppler frequency

σ_A = Error resulting from the difference between the true frequency and that extracted from the measurement component (A) LUT

σ_{LFM} = Error resulting from the difference between the true frequency and that extracted from the LFM component LUT

7. Velocity Vector Determination

Since velocity is a vectorial quantity, the geometry of the pDv laser transmission and receiver optical packages with respect to the investigated flow must be considered when determining the velocity of the flow entrained particles. Within the standalone pDv data processing program controls were provided that enabled the user to enter information describing the optical configuration employed during the data acquisition process (Figure 4-16). The selection of the Process Location Data control invoked a custom subVI (wiring diagram Figure B-6) that implemented Pythagorean's theorem and the Laws of Sines and Cosines to determine the undefined distances and the measurement angles. This information was then returned to the main VI, where the magnitudes of the input vector (laser), the measurement component or output vector and the magnitude of the resultant velocity vector for each active component were computed.

Figure 4-16 – pDv system optical configuration definition tab.

8. pDv Velocity Resolution

Computed velocity vectors were applied to determine the instantaneous velocity of each sample contained within an acquired data record using a subVI (Figure B-7) that implemented Equation 4.5 within the offline data processing program only:

$$V[i] = \frac{\Delta v[i] * \lambda}{\left(\hat{o} - \hat{i}\right)} \qquad (4.5)$$

The collection of velocities resulting from this calculation were archived to disk and statistical and histogram information was computed for each velocity record. As data records acquired under similar test conditions were batch processed, average velocities for each data record along with the sum of the individual histograms were presented graphically (Figure 4-17).
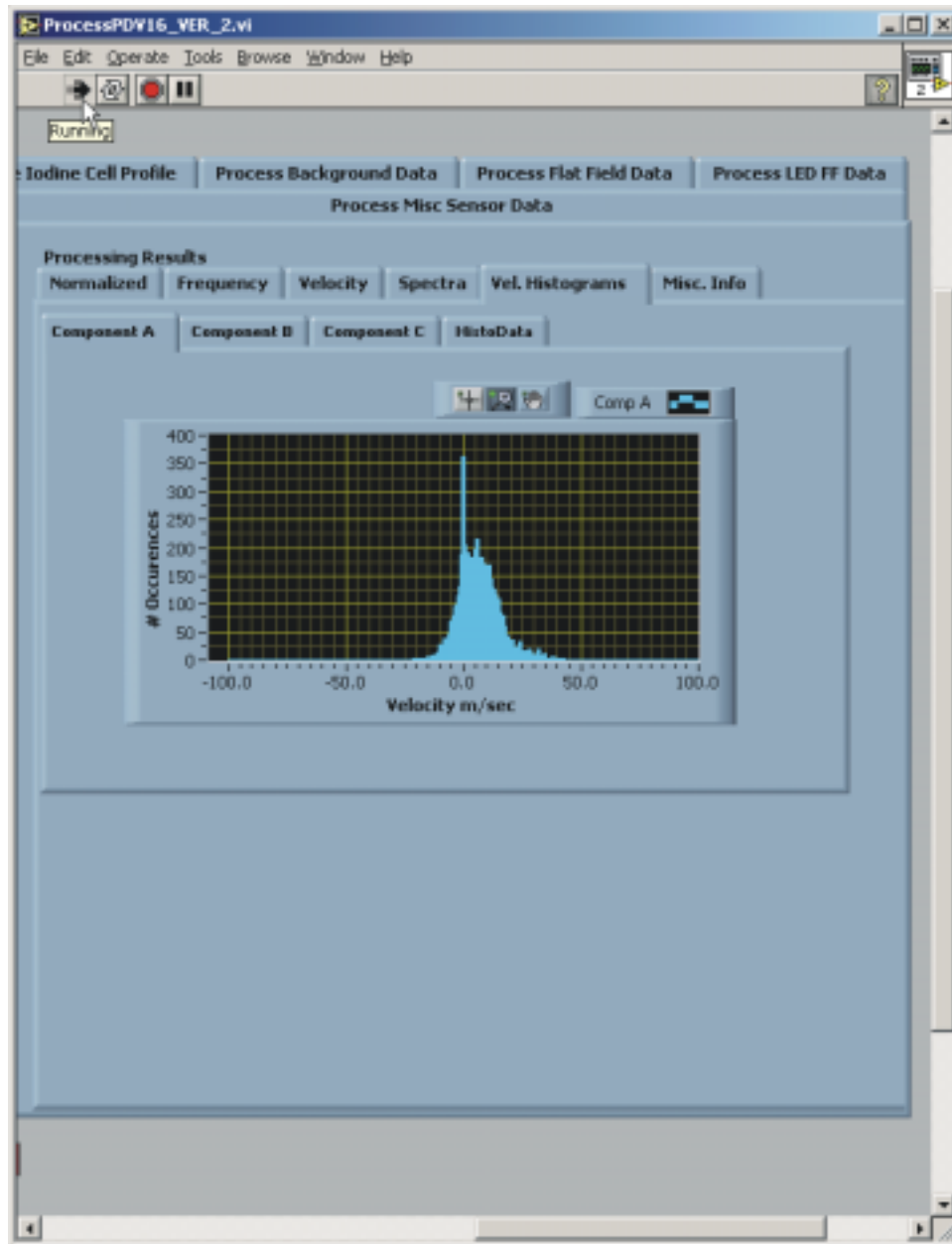

Figure 4-17 – Presentation of pDv velocity data histogram.

9. Velocity Data Bounding

Procedures were incorporated into the off line data processing program to determine the optimum scaling to use for displaying velocity histograms. By presenting data plotted on the same scale, the researcher, with a quick glance could assess velocity data distribution across several measurement components by noting the shape of the plotted histogram.

For a collection of data records, the maximum and minimum velocity values for each processed record were preserved in order to determine the appropriate scales on which to plot velocity histograms. At the completion of the processing cycle, arrays holding the identified minimum and maximum values were examined to locate extremes in the collection of processed records. These extremes were then used to define the scaling for the graphs on which the velocity data records were to be plotted.

10. Pitot Probe Data Processing

Individual pitot probe pressure transducer output signal samples, acquired simultaneously with the pDv data were converted to velocity and averaged. As the flow produced by the two-inch pipe is incompressible, a custom subVI called by the offline data processing program implemented this conversion through the following steps:

- Convert the measured voltage, $V_{PP}[i]$, (0.10V = 1Torr), to differential pressure p_D in N/m^3 (1 Torr = 133.324N/m^3);

$$p_D = V_{pp}[i]*1333.24 \qquad (4.6)$$

- Apply temperature and atmospheric pressure values entered into the appropriate fields provided on the data acquisition user interface of (Figure 4-4) to determine air density:

$$\rho = \left(\frac{\left(\frac{p_{AM}}{p_A} \right)*1.013}{(T_M + 273)*R} \right) N/m^2 \qquad (4.7)$$

- Compute the exit velocity using Bernoulli's equation:

$$V_P = \sqrt{\frac{2 p_D}{\rho}} \qquad (4.8)$$

Where, p_D represents the differential pressure measured with the pitot probe which is the difference between the total pressure, p_T and the static or atmospheric pressure, ρ_s:

$$p_D = p_T - p_S \qquad (4.9)$$

Instantaneous pitot probe velocity measurements and the computed statistical information were presented in both numerical and graphical formats then preserved to disk. This information was analyzed off-line to gauge how well pDv was able to measure flow velocity as compared to the pitot probe, an accepted velocity measurement standard.

11. Hot-Wire Data Processing

In the manner of converting the voltage signals generated by the pitot probe pressure transducer, it was necessary to convert the voltages sampled at the output of the hot-wire anemometer to velocity. A fourth-order polynomial (Equation 4.10) was implemented in the data acquisition program to convert the sampled voltages to velocity:

$$v_{HW}[i] = K + Ae[i] + Be[i]^2 + Ce[i]^3 + De[i]^4 \qquad (4.10)$$

Where: $v_{HW}[i]$ is the instantaneous velocity of the sample point; *e[i]* is the voltage measured at the hot-wire anemometer output; and, *K,A,B,C* and *D* are constants describing the heat-transfer relationship of the hot-wire as determined using King's Law.

From the collection of measurements obtained, the turbulent fluctuations were enhanced by subtracting the average velocity for the time series data from each individual data point:

$$v_{RMS}[i] = v_{HW}[i] - \bar{v}_{HW} \qquad (4.11)$$

The results of this procedure were then used to compute the power spectrum for the data record. The power spectra was computed from 239 records; each with a record length of 4096. These records were obtained by sub-sampling the data records containing 491520 individual measurements using a record overlapping approach. The spectral data resulting from the hot-wire data sets was compared to that obtained with pDv. Based on this information, the pDv system was optimized further in order to better match the hot-wire results.

As the hot-wire data was processed on-line, a tab within the data acquisition program (Figure 4-18) was created that provided fields for entering the constants used in the voltage-to-velocity conversion equation and for recording overlap percentage. Data processing results (wiring diagram Figure B-8, Appendix B) were also presented on this tab in numerical and graphical formats.
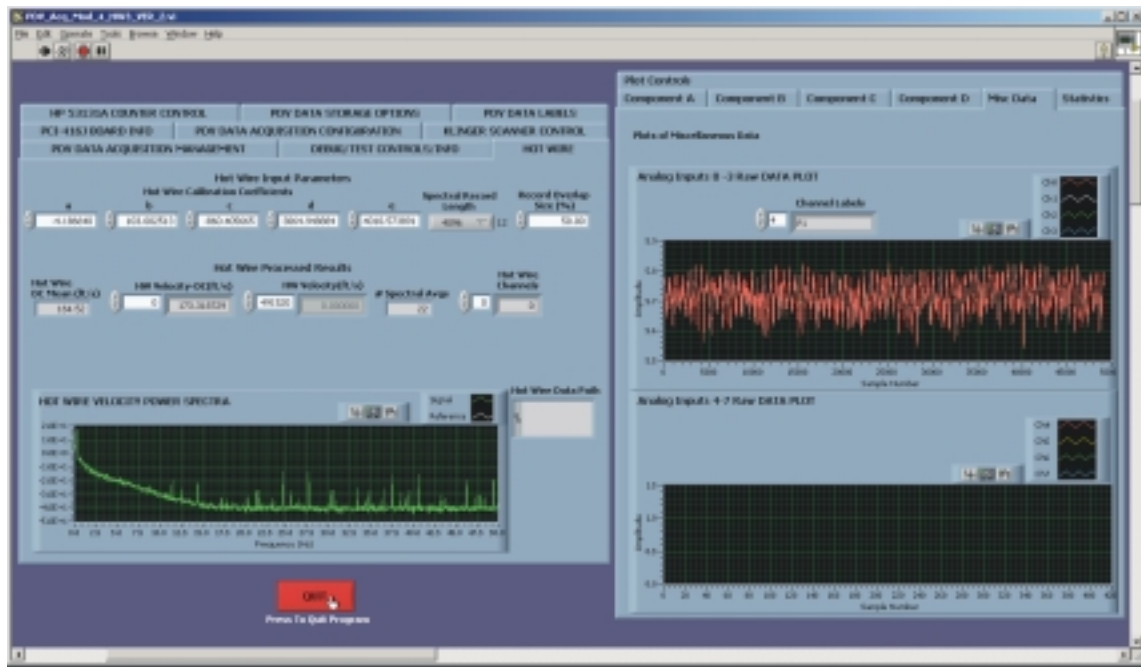
Figure 4-18 – Online hot-wire data acquisition/presentation tab.

12. *Rotating Wheel Velocity Computation*

Since the rotating wheel was used as a primary standard to determine the accuracy of pDv velocity measurements, it was necessary to compute the velocity of the wheel for each radial location where pDv data was collected. In addition, knowledge of the actual wheel velocity was fundamental to developing calibration curves describing the laser light transmission to optical frequency transfer function for employed IVCs.

The rotational speed of the rotating wheel at the time that the data record was acquired was determined within the standalone pDv data processing program. In order to perform this calculation,

it was necessary to record both the rotational speed of the wheel at the instant the sample was acquired and the radial position of the sample volume along the wheel surface. Wheel speed was measured using a digital pulse counter that counted the pulses generated by an optical tachometer. The counter was interfaced to the pDv data acquisition computer over a GPIB interface and sampled at the completion of a data record acquisition sequence. Pulse frequency measurements in Hertz were recorded with the acquisition of each data record. The radial location along the surface of the wheel where the pDv sample volume was positioned was known since the w, y, z spatial coordinates used to locate the sample volume were recorded in the header portion of each data record.

The configuration presented in Figure 1-3 was employed to first develop the IVC calibration data which was then used to verify the accuracy of pDv velocity measurements. Custom subVIs within the off-line data processing program used the resultant velocity vector computed from position information entered into the fields of the user interface of (Figure 4-17) to establish wheel velocity. Applying the unit vectors î and ô for the resultant velocity vector along with the wheel speed and scan location information extracted from the header record, the wheel velocity was determined as follows:

Determine the wheel angle in radians:

$$\theta_w = \tan^{-1}\left(\frac{\hat{i}}{\hat{o}}\right) * \frac{180}{\pi} \tag{4.12}$$

Applying the computed wheel angle, the i and j plane wheel velocities were determined for each of the investigated radial locations:

$$\vec{V}_W = (2\pi * r_w * 0.0254) * \frac{RS_w}{60} * \sin\left(\pi * \frac{\theta_w}{180}\right) \tag{4.13}$$

As the velocity vector resulting from the employed configuration was primarily in the horizontal plane, only the î plane velocity was considered for comparison purposes and preserved. The wheel velocities obtained through this procedure were stored in a file containing the average velocities resolved using pDv.

13. Power Spectra Computation

Through the computation of the power spectra for the time dependent raw pDv data sets, it was possible to provide insight into the frequency content of a flow. Presentation of the spectral information in graphical format provided another means of verifying system operation during two-inch pipe investigations (Figure 4-19). Spectral results for data obtained near the center of the flow exiting the pipe exhibited peaks centered about a single frequency as the flow was primarily laminar while data acquired near the flow edges demonstrated multiple frequency peaks due to increased flow turbulence in these regions.

Custom subVIs employed the FFT Power Spectrum subVI supplied with LabVIEW to compute the spectral information. During data collection activities, the average power spectra of the raw Signal and Reference detector signals for each active component was computed then presented graphically (Figure 4-12). This information was then discarded since the appropriate calibration data was not applied.

During off-line processing operations, the power spectra for the flow velocities observed in the active measurement component(s) were computed for each data record. Spectral information for the individual data records as well as the average spectra for a collection of related data records was computed on a channel by channel basis and saved to disk

Controls provided in both the data acquisition and processing programs enabled the user to define the manner in which spectral information was computed and presented (Figure 4-19). These controls enabled the user to select one of several common time domain windows, configure averaging parameters and set the desired plotting format.
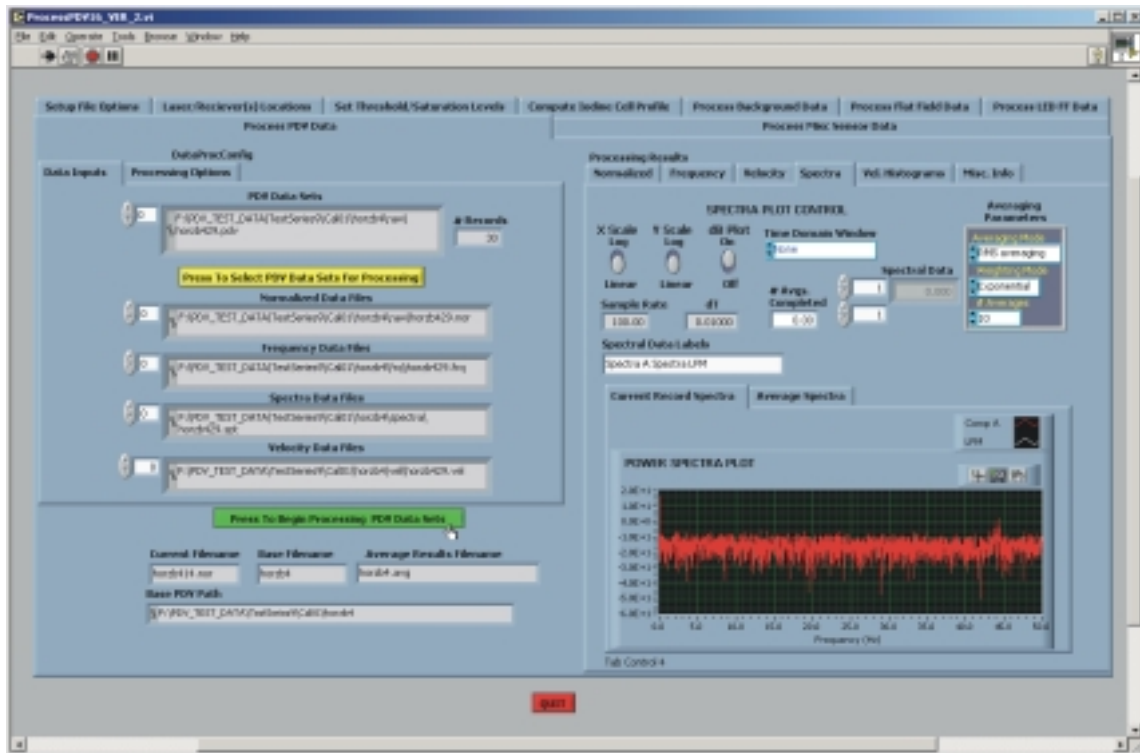
Figure 4-19 – pDv spectral data processing control panel and results.

14. *Graphical Data Presentation*

The graphical presentation of raw and processed pDv data sets during an experiment provided the researcher with visual feedback regarding system operation making it possible to evaluate signal quality and identify patterns, discontinuities and anomalies in the data records. To accommodate the large number of plots generated on the limited display area, a tabbing system, Figure 4-12, was employed to hold the component specific plot data. Graphing subVIs supplied with LabVIEW were incorporated into custom subVIs to produce the following plots:

a. *XY Series Data Plots*

During data acquisition activities, time history plots of measurement and LFM component signals were generated for each acquired data record. Signal, Reference and normalized data traces for each component were displayed in the same plot window (Figure 4-12). In addition, time-series data produced by other transducers such as hot-wire anemometers or pitot probes was plotted on the two generic data graph windows shown in Figure 4-20.

Figure 4-20 – Misc. sensor raw data presentation tab.
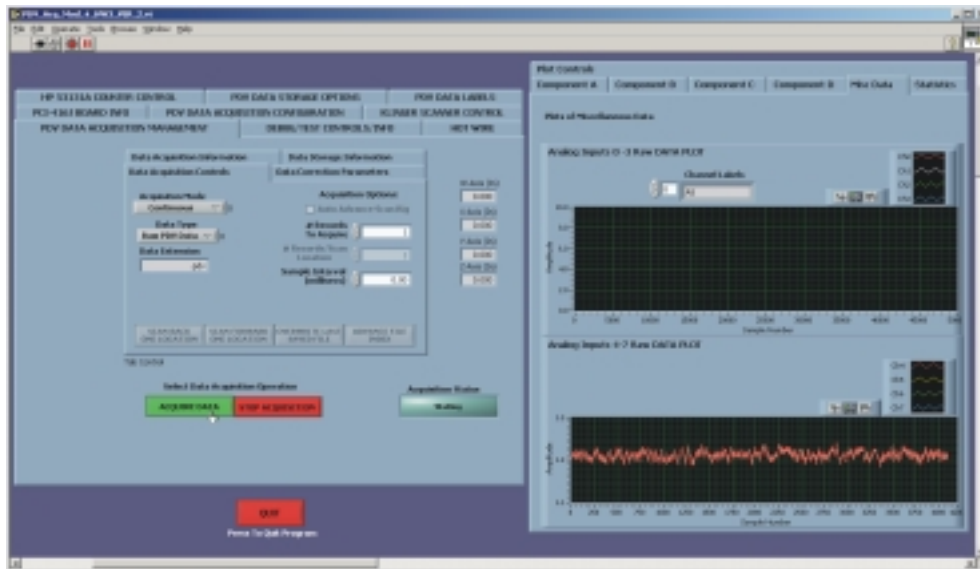
b. *Average Data Plots*

In the standalone data processing program, the average, normalized, frequency and velocity values computed for each processed data record were plotted as in Figure 4-21, Figure 4-22 and Figure 4-9 respectively.
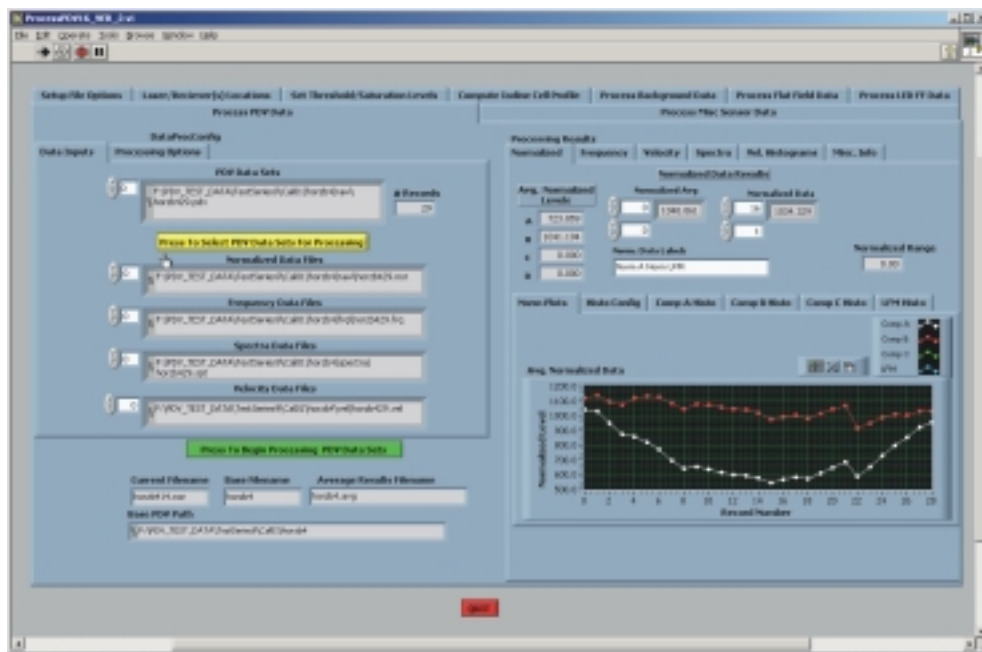

Figure 4-21 – Average processed normalized data presentation tab.
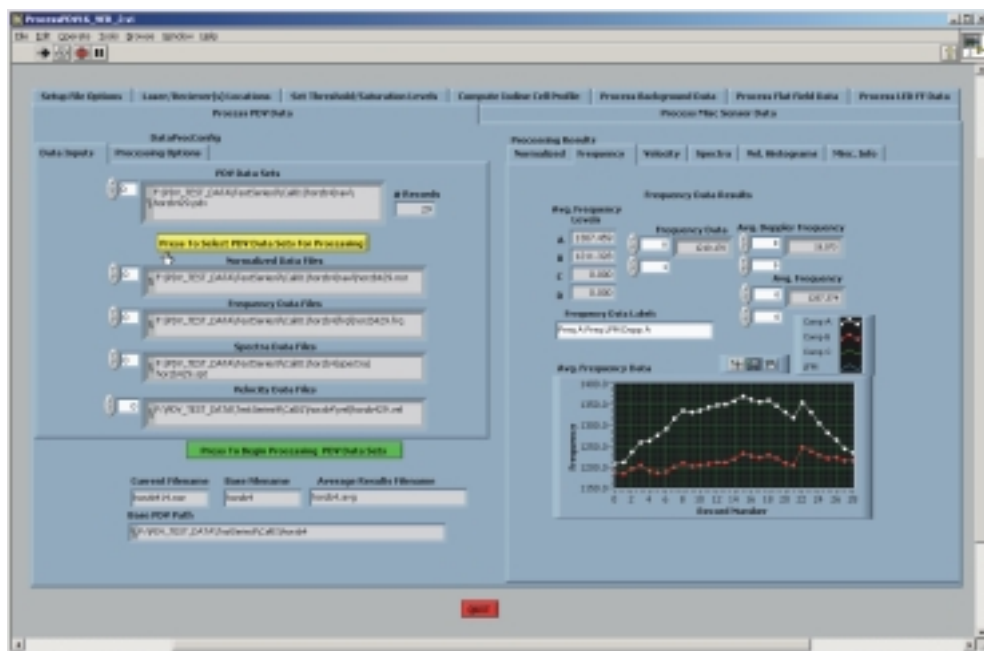
Figure 4-22 – Average processed frequency data presentation tab.

c. *Spectral Data Plots*

The power spectra for each individually processed record, along with the average spectra computed for a collection of processed records, was presented to the user to provide insight into the frequency content (turbulence quantities) of the studied flow (Figure 4-19).

d. *Histogram Data Plots*

Histograms computed during the acquisition and the processing stages were presented in graphical format to give the user insight into the distribution of data values. During the data acquisition phase, histograms computed for raw Signal and Reference data and normalized results were plotted within one hundred bins, with an interval of 200mV over the +/-10V input voltage range of the A/D converter. Within the standalone data processing program, histograms of data resulting from normalization and velocity, (Figure 4-17), calculations were presented, as they were computed.

Figure 4-23 – Processed normalized data histogram.

15. *Processed Data Archival*

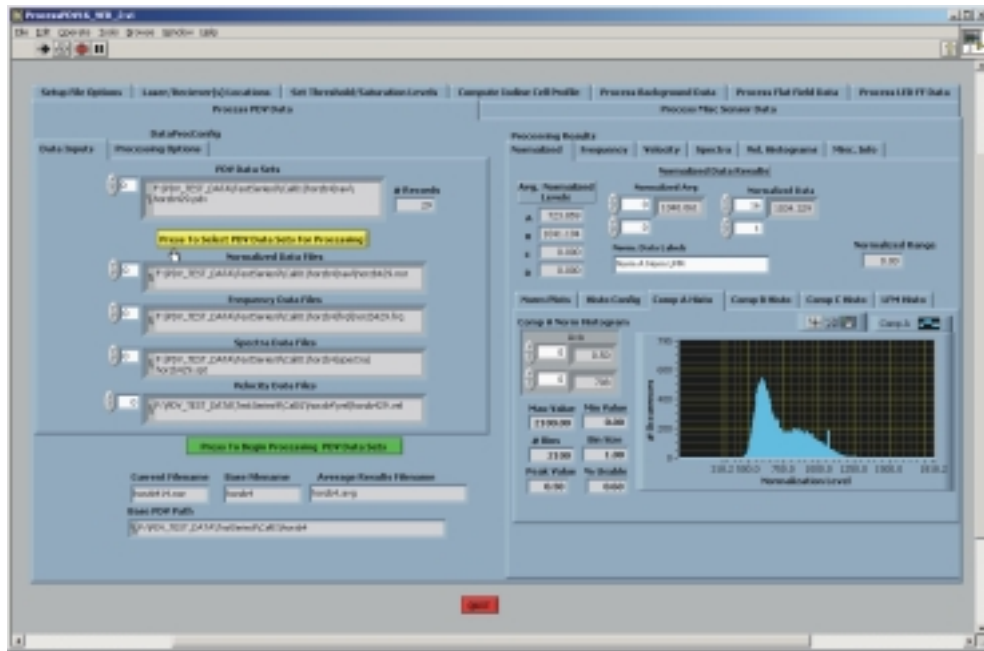Data produced during off-line processing operations was archived to the disk for evaluation and presentation purposes. Both the finalized and intermediate pDv data processing results were saved to files with filename prefixes matching those of their *raw* data counterparts in the same directory structure.

Results obtained resulting from the various pDv data processing steps; normalization, frequency and velocity were permanently archived to tab delimited ASCII files. Measurement component specific data was saved in columnar order with each column prefaced with a mnemonic, Table 4-2, that identified the data source. The velocity measurements resolved with the pitot probe and hot-wire were also preserved to disk in the same manner.

Archival of data in this manner served two purposes. First, in order to evaluate the system performance, data extracted from these files was plotted and the resultant graphs examined to determine how well the data matched the expected results. Secondly, the results obtained with the implemented software routines were compared to values obtained through manual calculations. This provided a means to verify if the software was operating properly.

CHAPTER V - pDv INSTRUMENT VALIDATION AND RESULTS

A. System Testing Objectives

The primary objective of the pDv research activity was to integrate hardware and the physics principals to form a foundation along the lines of established laser based flow quantification technologies such as those developed for LV, PIV and DGV. These concepts were combined with classical signal processing algorithms to investigate the ability of the resulting instrument to measure flow-related quantities. This required that a methodical sequence of validation activities be performed to develop a working knowledge of system principles, characteristics, measurement capabilities and limitations. Using the information compiled during this process, alternative approaches, intended to improve system operation, were developed and implemented under controlled conditions and the results evaluated.

In this chapter, the purpose, execution and results of tests conducted during this phase of research are presented. Problems in system functionality encountered during these activities and the workarounds incorporated to overcome them are discussed. Finally, the results of comparative tests conducted alongside matured flow characterization instruments are presented.

B. pDv Instrument Validation Activities

In line with the incremental/prototype model presented in Figure 4-1, validation of the pDv system progressed from evaluating components individually to verify that collectively they made it possible to attain the capabilities suggested by the underlying physics (Figure 5-1). Thus, the instrument was constructed incrementally using the components and subsystems evaluated under controlled conditions prior to being incorporated into the system.

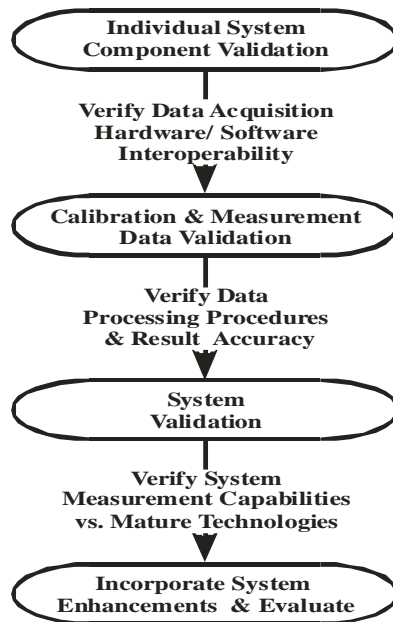**Figure 5-1 – pDv system validation sequence.**

Since the pDv software was tightly integrated with the ensemble of instrument subsystems (Chapter 3), this testing also provided opportunities to validate the functionality of the initial versions. Software problems identified during the course of the testing were corrected as encountered and the functionality of the solution(s) validated through further testing.

1. Component Validation

A series of bench tests was performed to investigate the capabilities of the individual components employed in the pDv instrument. The results of these experiments were evaluated to determine if the candidate components satisfied both pDv instrument requirements and manufacturer specifications. In this way, it was possible to identify measurement limitations, systematic error sources, and to quantify the extent of any inherent errors. This information was subsequently applied to develop calibration procedures for data sample correction and error minimization, thereby improving the prospects of attaining pDv measurements with accuracies approaching those of matured technologies. The major components and subsystems tested were:

a. Analog Data Acquisition Subsystem

As the Datel, PCI-416J multifunction data acquisition (DAQ) board was the primary signal sampling instrument in the system, it was essential that its capabilities be assessed before proceeding to other research activities. Bench top signal generators provided the stimulus necessary to verify the digitization capabilities of the DAQ board as follows:

Static Signal Testing – A series of DC voltages produced by a high-precision voltage standard were applied to each of the analog input channels to verify the quantizing capabilities of the A/D converters residing on the DAQ board. As the analog input range for the DAQ board was ±10 V, positive and negative representations of the following signals were applied: Full Scale (FS), (FS - 1 LSB), ½ FS, ¼ FS, 0 V (system ground), (0 V - 1 LSB), (0 V + 1 LSB) where 1 Least Significant Bit (LSB) for the 12-bit A/D converter equaled 4.88 mV and FS represented either positive or negative 10 VDC. Data records of length 4096 samples were collected at a 200 kHz sample rate for each stated input voltage condition and analyzed in an attempt to identify anomalies or limitations. A time history trace of a data record acquired with all analog input channels grounded is shown in Figure 5-2(a).
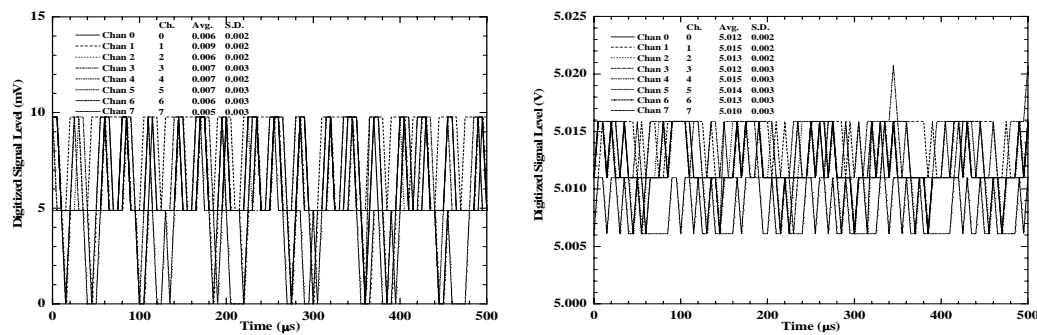

Figure 5-2 – PCI-416J DAQ board static signal performance.

For this data set, the average digitized signal level was about 10 mV (~2 LSB) higher than the zero voltage level expected indicating an offset inherent to the system. A second time history trace, this one with all of the channels connected to +5 VDC, also demonstrated an offset of about 10 mV from the expected +5 VDC (Figure 5-2(b)). Analysis of other data records acquired during this exercise demonstrated similar offsets in the applied input signal, suggesting that it was constant across the DAQ board input range. This offset was accounted for and removed from the acquired data records through the background calibration procedure.

Further processing of the presented data sets demonstrated a standard deviation in the digitized values of less than one LSB. This indicated that the contribution of system noise components was negligible, since it was within the uncertainty expected from any A/D conversion. The uncertainty in the mean resolved voltages across all channels for the data records shown in Figure 5-2 was computed using Equation 5.1 and found to be better than 0.0032%:

$$\sigma_M = \sigma/\sqrt{N} \qquad (5.1)$$

Where:

σ_M = Uncertainty in the mean resolved voltage level

σ = Standard deviation of the measurements in the data record

N = Number of statistically independent measurements in the data record

Dynamic Signal Testing – Sine and square waves of several different frequencies and amplitudes produced by a bench top signal generator were applied to characterize the ability of the DAQ board to digitize, then faithfully reconstruct time varying signals. Error analyses of these results indicate the expected performance with unknown input signals.

For the first test series, a sine wave was applied to all DAQ board analog input channels to investigate its simultaneous sampling capabilities. A single cycle of a +5 V, 25 kHz sine wave sampled at 250 kHz is shown in Figure 5-3(a). Data from each channel is presented in this plot and visual inspection shows little phase misalignment in the digitized signals. In addition, a statistical cross correlation analysis was performed to determine how well time coherence (phasing) of the input signal was being maintained across the analog input channels. Figure 5-3(b) is a plot of the standard deviation in the digitized values across the eight input channels for each discrete time sample. The average standard deviation for the presented data plot was 0.0027 or approximately ½ LSB, indicating no phasing skew in the sample clock driving the eight independent A/D converters.
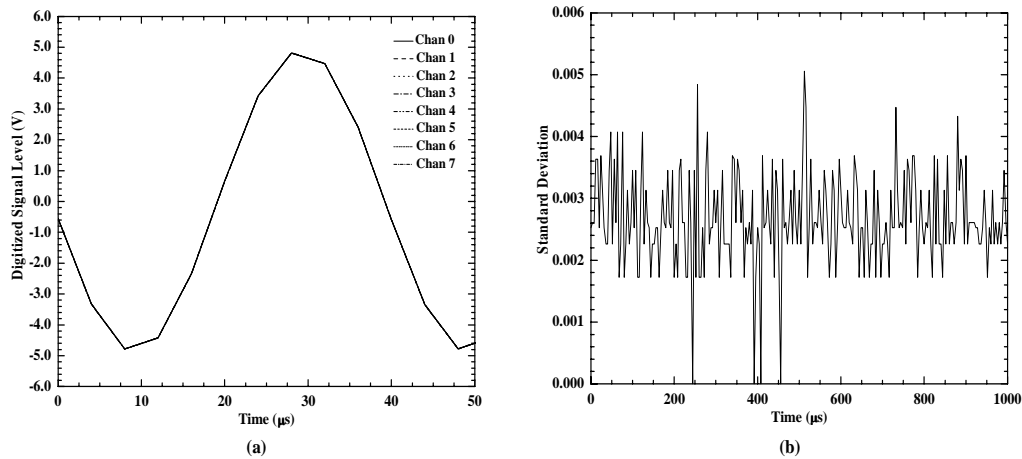

(a)

(b)

Figure 5-3 – PCI-416J DAQ board response to a dynamic input signal.

The second series of experiments was conducted to investigate if and/or how a signal on one channel affected the operation of the other channels. The presence and extent of this characteristic, commonly referred to as channel-to-channel crosstalk was investigated by applying a square wave signal to each of the eight Analog input channels of the DAQ board sequentially. With the test signal applied to a targeted channel, the remaining channels were connected to system ground. An alternate test was conducted with the test signal applied to the even numbered channels, while the odd channels were grounded. The test was then repeated with the signal applied to odd channels, while even channels were grounded. Off-line statistical analyses of the acquired data sets showed that the grounded channels demonstrated an offset of approximately two LSB from the ideal zero-volt level. This bias was consistent with earlier results that also demonstrated a 10 mV offset from the expected levels.

A better understanding of the extent of crosstalk was obtained by performing a spectral analysis of the data set. The spectra computed for a data record consisting of 4096 samples of a 50 kHz

square wave applied to the odd channels of the DAQ board is shown in Figure 5-4. This data record was sub-sampled to 15 records of 512 bytes, each with a 50% overlay to emphasize the frequency spikes in the spectra. As shown, odd numbered channels demonstrated strong signal peaks at the primary 50 kHz and second harmonic 100 kHz frequencies. The even channels exhibited a flatter distribution of signal strength suggesting that channel crosstalk was minimal. In addition, the average digitized level for the even channels was about ½ LSB with a standard deviation of approximately one LSB, another indication that the signal bleed from one channel to the next was minimal.
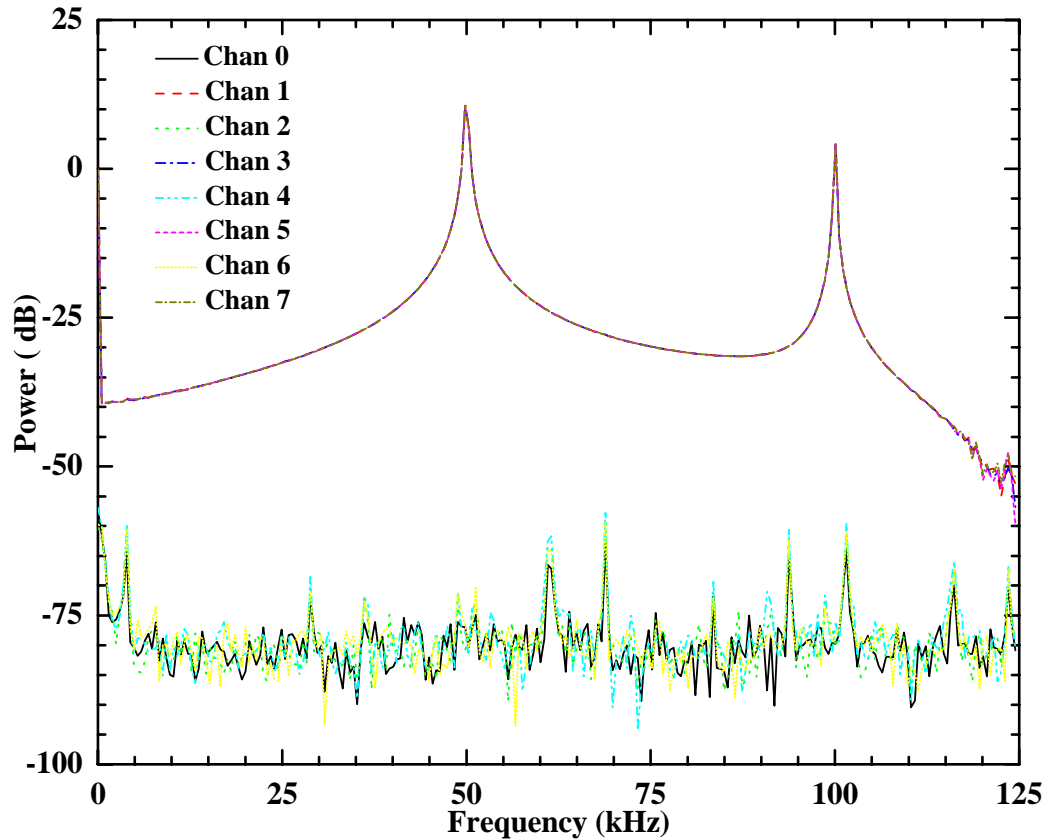

Figure 5-4 – PCI-416J DAQ spectral response to a 50 kHz square wave.

b. *Photodetectors*

Faithful representation of the passage of particles through the sampling volume is vital to making accurate velocity and spectral measurements. Thus, the detector used in pDv must have the sensitivity to detect varying light levels and output a voltage or current signal proportional to the amount of light impinging on its surface in a linear manner. As discussed in Chapter 3, several different detector types were evaluated before settling on PMTs for the measurement component(s).

The most extensive detector bench testing related to the work presented was conducted using two Avalanche Photodiodes (APDs), which were available at the time testing was conducted. These devices were characterized using flashlight bulbs and LEDs as illumination sources, which provided better control in these tests than the particle scattered light, since their operation could be established using electronic signals. This made it possible to correlate the output signals produced by the APDs with a known signal rather than random, time varying signals that resulted from particles passing through a light beam. The investigated APDs had integrated

transimpedance amplifiers that converted their current output to a voltage. The signals were then buffered using laboratory voltage amplifiers prior to being interfaced to the data sampling hardware. In this configuration, it was possible to investigate the operating characteristics of the data acquisition system as a whole. The following APD characteristics were investigated:

Noise – Quantification of the output signal produced by an APD with no light impinging on its surface was necessary to obtain an understanding of the dark current characteristics for of the device. Dark current refers to the current produced only from the spontaneous emission of electrons within the detector system.

To quantify the dark current levels, a strip of black electrical tape was applied across a lens mount installed in front of the APD and room lights were turned off. APD output signals were then sampled using the Datel PCI-416 DAQ board. The first one hundred samples of a 4096 sample record are shown in Figure 5-5. For this data set, the Signal APD had an average dark level of 11.8 mV (~ 3 LSB) and a standard deviation of 2.42 mV (~ 0.5 LSB). The Reference leg APD exhibited an average dark level voltage of 7.44 mV (~ 1.5 LSB) with a standard deviation of 2.46 mV (~ 0.5 LSB). As the other nine data records acquired during this experiment exhibited similar signal and standard deviation levels, it was concluded that the APD dark current levels were relatively low and stable. The dark current contributions are removed from the acquired data records during processing through the background calibration procedure.
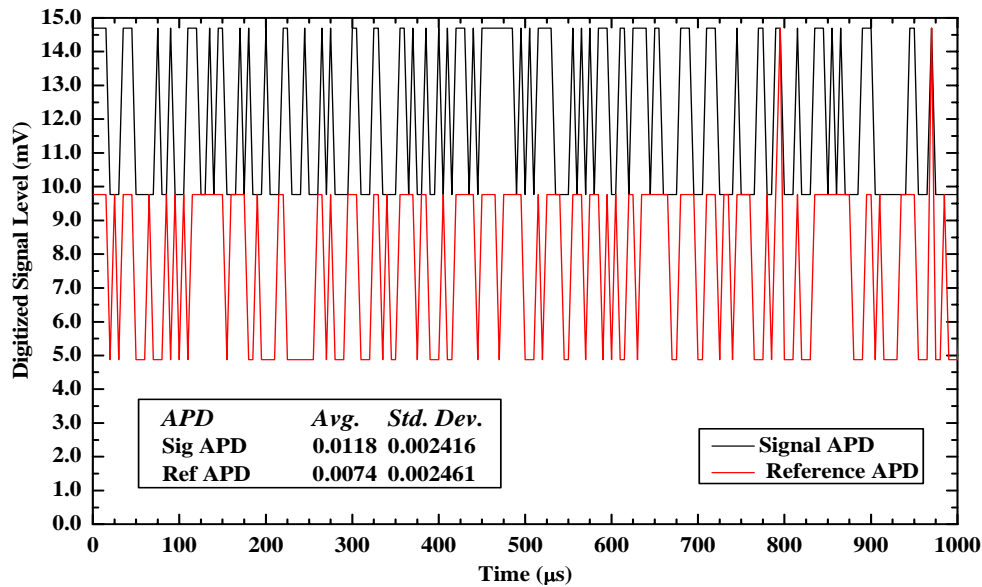
Figure 5-5 – Dark current performance of investigated APDs.

Sensitivity, Linearity & Stability – The detectors used in pDv systems must be capable of predictable operation over a wide range of scattered light conditions. Ideally, the selected detector should possess the following traits:

(a) Sensitivity – the detector should respond to the low intensities of particle-scattered light.

(b) Linearity – the detector should provide a linear output signal over a wide range of scattered light levels.

(c) Stability – the detector output signal should be stable in spite of inherent shot noise. This shot noise is due to the random process of photon arrivals, and low level AC

noise components that result from: a) thermal fluctuations, b) incident background light, and c) dark current.

Two independent experiments were performed to characterize the response of the APDs to different light level conditions. In these tests, the flashlight bulb was driven with a 2.5 VDC signal originating from a stable laboratory voltage standard. The first data set was acquired using a Tektronix TDS744A digital oscilloscope operated at three different sampling rates: 2.5-, 25- and 250-kHz. A second set was collected using the PCI-416J DAQ board at sampling rates of 200 Hz, 2 kHz, 20 kHz and 200 kHz. For each sampling rate setting, the intensity of the light originating from the light source was varied by installing Neutral Density (ND) filters in the optical path of the APD. Four different intensity conditions were investigated; full (No ND filter) and 93%, 50% and 11% of light transmission.

By acquiring data sets using two different data acquisition systems, it was possible to isolate the operation of the APDs from that of the voltage amplifiers and the digitizing hardware. The results of these experiments are shown in Figure 5-6, where the average signal levels for the two APDs were linear as light intensity levels increased for both data acquisition systems. This behavior was repeatable as the sample rate was increased, indicating that the APDs and the digitizing hardware behaved linearly over the investigated intensity and output voltage ranges (0 to 0.7 Volts). The investigated range represented a limited degree of the capabilities of both the APDs and the digitizers and did not reflect the signal levels encountered during later velocity measurement experiments. A more thorough linearity test would include increasing light intensity incrementally until either detector or digitizer saturation was reached.
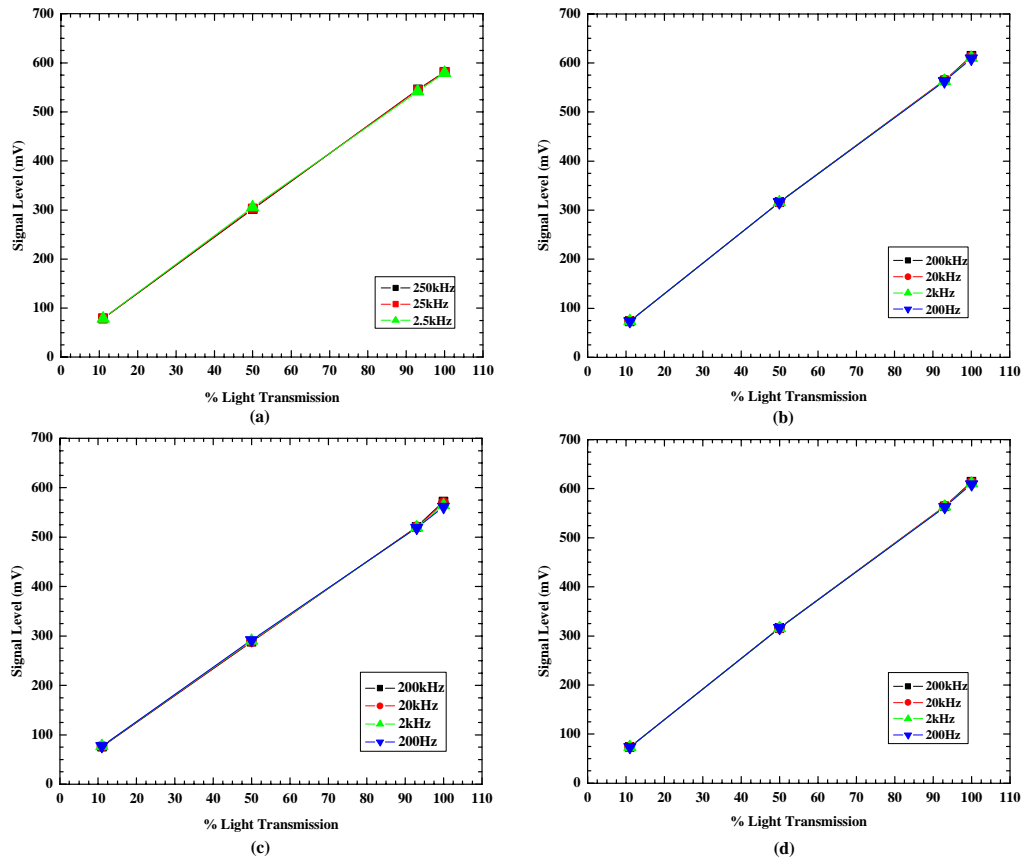

Figure 5-6 – APD response to continuous illumination.

A statistical analysis was performed on the acquired data ensembles to assess system performance. Standard deviations for data sets acquired using the digital scope varied with light intensity and sample rate and did not demonstrate any particular trend (Figure 5-7 (a) & (b)). The measurement uncertainties for these data sets were on the order of 0.03%. The standard deviations for data sets acquired with the PCI-416J (Figure 5-7 (c) & (d)) had a more predictable trend, as standard deviation levels increased with signal level. These data sets had a measurement uncertainty of ~0.005%.
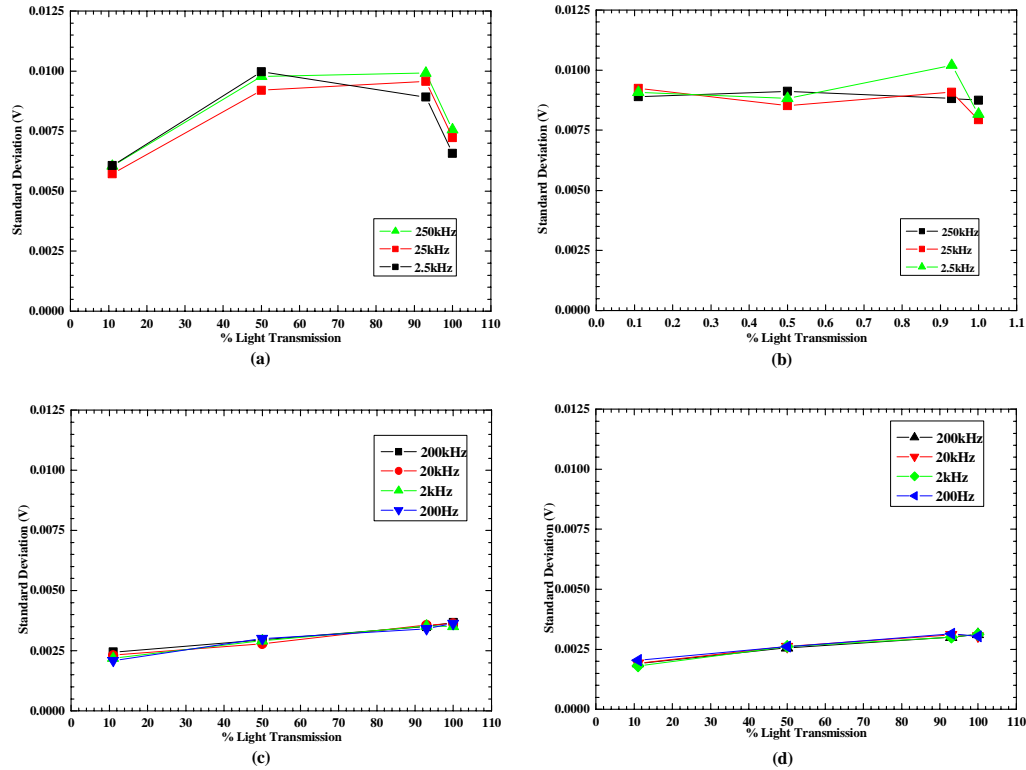
Figure 5-7 – Standard deviation of APD response to continuous illumination.

<u>Dynamic and Frequency Response</u> – In order to make accurate pDv measurements, the employed detector must respond quickly to varying light intensities, which can swing from low light (single particle) to near saturation (multiple particles) conditions instantaneously. In addition, a fast response capability is mandatory for characterizing flow frequency and turbulence quantities, as the transition time of the particles through the sample volume can be short (on the order of a microsecond or less). Thus, the detectors and supporting electronics must provide the capability to acquire velocity measurements at a rate sufficient to determine the flow turbulence power spectra, which may be on the order of several hundred kilohertz. These bandwidth considerations led to the selection of the APD, which in combination with its integrated transimpedance amplifier had a unity gain bandwidth of 1.8 MHz.

Accurate evaluation of the detector also required performance characterization of the signal conditioning and sampling subsystems through which the output signal was passed. These devices must not modify the original signals by bandwidth limiting or by introducing electronic noise artifacts. Accordingly, the detection system was scrutinized as a whole to assess its dynamic response and bandwidth capabilities. This was accomplished by acquiring then analyzing records of light produced by an LED driven with a sine wave signal. This provided a means of evaluating the system under the best case of a noise-free scenario. Records were collected for sine wave frequencies between 100 Hz and 100 kHz with the APD output being sampled at rates of 2-, 20-,

and 200-kHz with the Datel DAQ board. Figure 5-8(a) presents the first fifty samples of a data record acquired at 200 kHz, while the LED was driven with a 20 kHz sine wave. Visual inspection of the plotted data shows good phase response between the LED and the detection system indicating successful tracking of the light fluctuations. The spectral plot for this data set, Figure 5-8(b), shows a frequency peak at 20 kHz and harmonics at 40-, 60- and 80-kHz. This confirmed that the detection system was tracking and responding to frequency variations in the amplitude modulated light and little noise was being introduced by the components in the system.
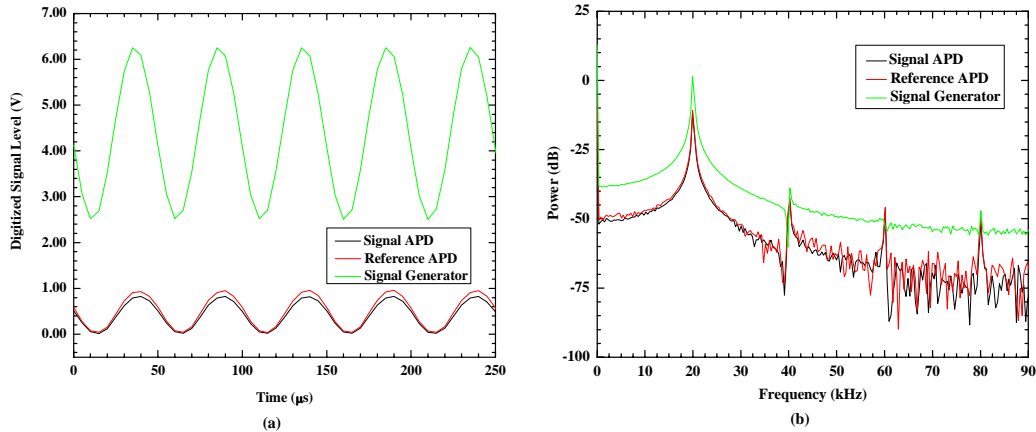

Figure 5-8 – PMT response to light scattered by a sine wave driven LED.

System spectral performance was investigated by acquiring data sets while the LED was driven with a white noise signal (flat rms/Hz range of 0 to 600 kHz). This represented a more realistic scenario of the light scattered by flow driven particles. APD output signals representing the fluctuating input light levels were sampled at a 200 kHz rate with the DAQ board. To isolate frequency information present in the collected light from the noise artifacts in the system hardware, a scheme of bandwidth limiting the original white noise signal prior to its application to the LED was employed. In this way, any significant system noise components with frequencies outside of the band of frequencies driving the LED would easily be identified during spectral analyses. Bandwidth limiting was achieved by using low-pass and high-pass filters in tandem to pass only a band of frequencies approximating a targeted center frequency.

Spectral performance data for the bandwidth limited noise experiments was obtained by sub-sampling the original 100 data records of 4096 samples into 1500 records with a length of 512 samples. A 50% overlap was used to accentuate frequency spikes. The results are presented for the 20-, 40-, 80- and 100-kHz bandwidth limited cases in Figure 5-9(a-d), respectively. These plots indicate that the detected frequencies were in agreement with those of the signal driving the LED with peaks close to the center of the bandwidth-limited signal. For the most part these plots indicate minimal system noise source contributions. However, as can be seen, the reference leg response had several spikes that are not present in the signal leg plot. Also note that the frequency spikes at ~1.5 kHz and 6 kHz correspond with those in the LED response data, but do not show up in the signal APD response plot. These discrepancies in response indicated that the reference APD was more sensitive than the signal APD.
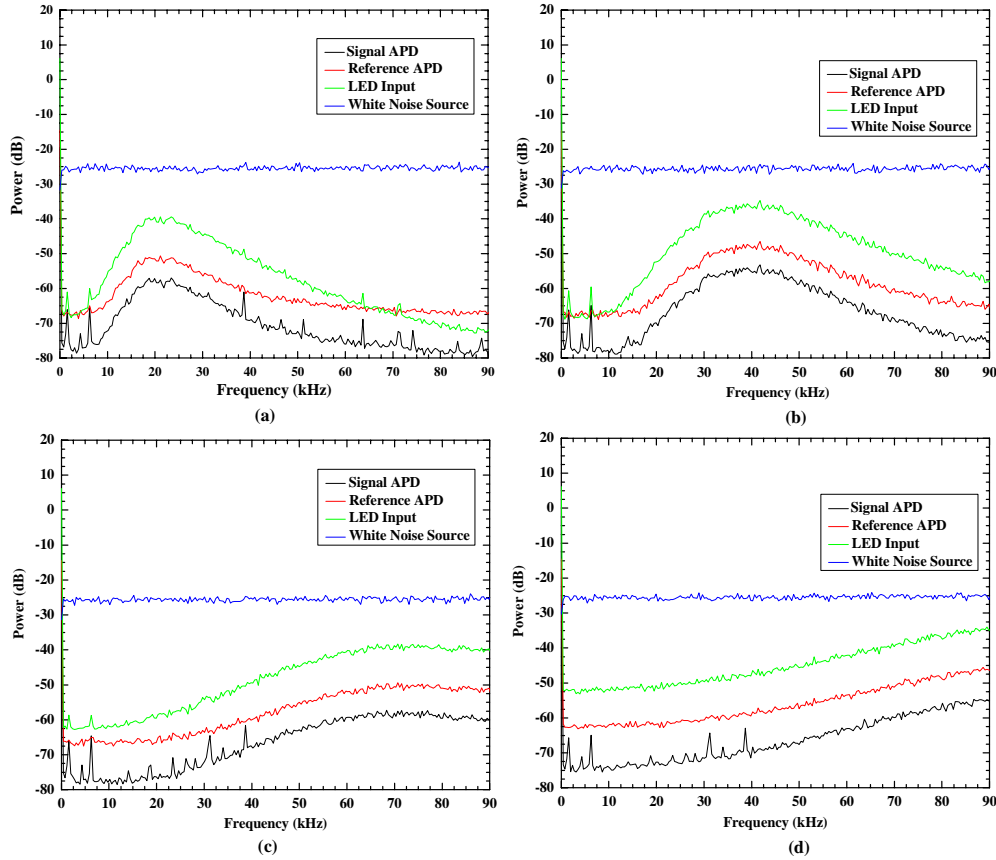
Figure 5-9 – Spectral response of PMT to bandwidth limited noise.

Another area of concern for the detection system is *phase mismatches* in the detection and digitization of signal and reference light levels. Any phase difference, whether it be caused by the optical system, signal processing electronics or digitizers, between the recorded signal and the reference samples, introduces an error in the normalization process. Because the passage of particles through the sample volume is random, and the digitizers are sampling at regular intervals, it is impossible to determine the pulse phase, when the sample is accepted. This limitation is outlined in Figure 5-10 for a single particle passing through the sample volume in a constant velocity flow. Figure 5-10(a) presents an ideal situation, where no phasing difference exists in the detection system, so the resulting normalized values at sample times A and B are equal (0.52). Figure 5-10(b) presents a situation where a phasing mismatch exists in the detection system. In this case, the normalized value at sample points A (0.49) and B (0.547) are different. Taking the example a step further and applying the geometric configuration used to investigate the flow exiting the two-inch pipe (Figure 1-1), demonstrates the consequences of phase mismatches. For the situation shown in Figure 5-10(a), the Doppler frequency is 25.7 MHz, which translates to 36.51 m/s for both samples A and B. The ratios obtained in Figure 5-10(b), produced different Doppler frequencies; 43.3 MHz (sample A), and, 8.93 MHz (sample B). Thus, the velocity for sample A is 61.5 m/s and for sample B is 12.7 m/s, resulting in a very large velocity measurement uncertainty.
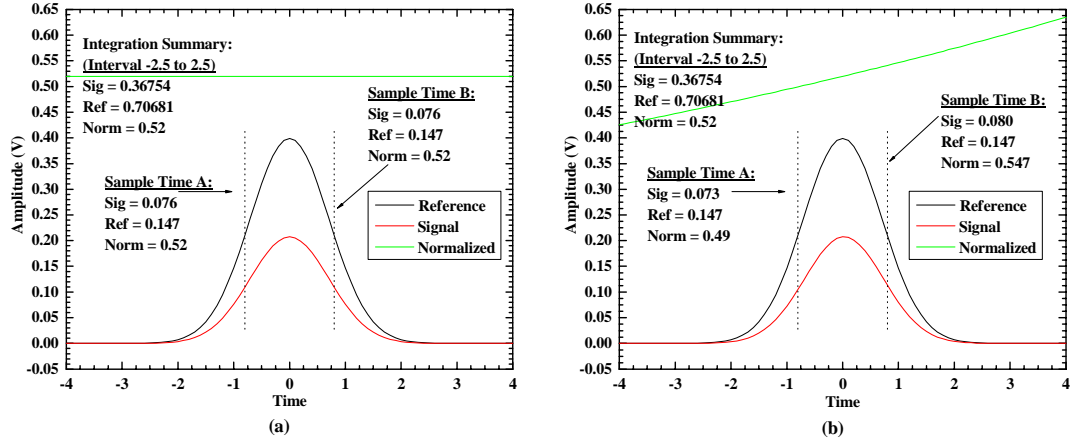
Figure 5-10 – Detection system phase mismatch example.

Analysis of data sets acquired during the pDv research did not demonstrate the velocity errors of the magnitude presented in this example. However, it was recognized that errors introduced by phase mismatches could limit measurement accuracy. Therefore, integration techniques were investigated and applied to reduce the effects of these errors. As shown for the two sampling conditions of Figure 5-10, the results of normalizing the integral of the signal and reference light level samples respectively is the same (0.52), matching the ratios of points A and B in Figure 5-10(a). This translates to a velocity measurement of 36.5 m/s in both cases. Thus, integration before normalization greatly reduces measurement uncertainties. Initially integration was incorporated into the system with a boxcar integrator and later with the custom-built pDv integrator.

2. Iodine Vapor Cell (IVC) Calibration Development and Verification

An accurate calibration of the light attenuation-to-light frequency (A/F) transfer function of the IVCs was required prior to attempting velocity measurements, since this is the sensing element of the pDv technique. Two major sources of measurement uncertainty error in pDv are related to the consistency and accuracy of the calibration established for the true absorption profile of an IVC (Meyers and Lee, 2000). The calibration curves developed during these exercises represented only the left-hand side of the selected absorption band in the proximity of the 514.5 nm wavelength of the Argon Ion laser.

Because it was difficult to measure the absolute frequency of the laser light using other techniques, an alternative method was employed to develop calibrations of the A/F transfer functions for the IVCs. A 12-inch diameter rotating wheel, arranged in the geometric configuration shown in Figure 5-11 was employed to develop IVC calibrations for the DGV system (Chapter 2). The wheel was used to induce a Doppler shift in the frequency of the light emitted by the laser (Figure 5-11(a)).
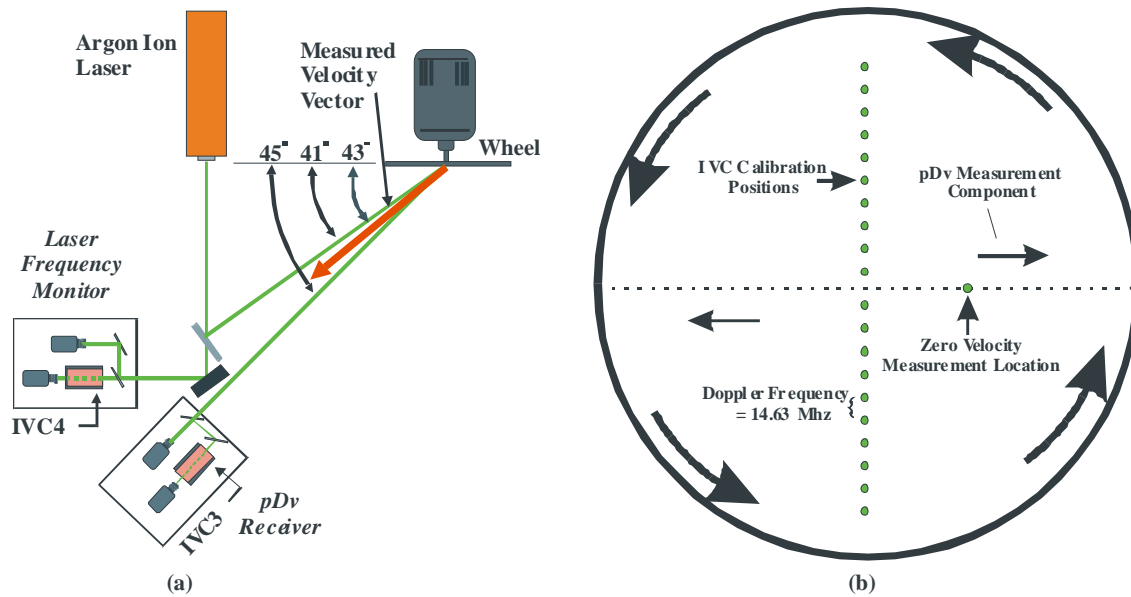
Figure 5-11 – (a) Geometry, and (b) rotating wheel used for IVC calibrations.

In this configuration, the velocity vector measured at the point where the light beam impinged the wheel surface was in the horizontal plane. CCD cameras, used in the DGV system to detect the Doppler shifted light scattered by the wheel surface, were replaced with APDs to measure the Doppler shift at a point. The laser beam was scanned vertically across the wheel surface in evenly spaced increments to map out a single segment of the absorption profile. The laser was tuned to an appropriate frequency mode located within the absorption band prior to mapping each segment. The laser beam was then scanned vertically in 0.50-inch increments beginning 1.25-inches from its top edge and continuing 9.5-inches downwards, Figure 5-11(b), to map out a single segment of the absorption profile. Scanning the laser beam across the wheel surface in this manner resulted in a change in the Doppler shift at each 0.50-inch increment of 14.63 MHz in the unknown light frequency emitted by the laser. The Doppler frequency shift at each scan location was computed given that the geometric configuration of the transmission and receiver optics packages, the radial position of the beam striking the wheel and the rotational speed of the wheel were known (Chapter 2). Complementary radial locations along the vertical diameter of the wheel provided positive and negative Doppler frequency shifts about the incident laser frequency with a total segment frequency range of ~280 MHz. By tuning the laser through sixteen longitudinal modes in the range of the selected absorption band, and repeating the scan sequence, it was possible to obtain a continuous mapping of the transfer function in a piecewise manner (Figure 5-12).
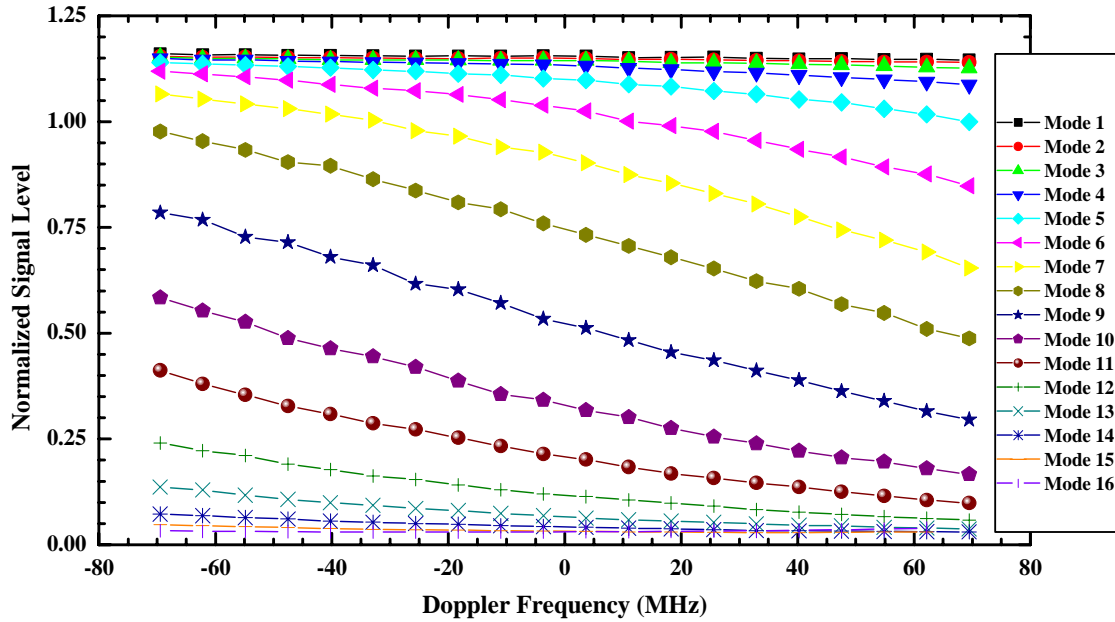
Figure 5-12 – IVC light attenuation profiles for sixteen laser frequency modes.

The laser must be operated and maintained at a single frequency in order to map an absorption profile segment. Each frequency mode was selected by mechanically tuning the temperature-stabilized etalon. Single frequency selection/stability was visually monitored using a Fabry-Perot optical spectrum analyzer (Figure 3-7(M)) installed in the LFM. Development of an IVC calibration profile was initiated by tuning the laser to a stable and nearly repeatable starting point. This reference point was the laser *flash point*, which occurred when the front surface of the etalon was perfectly orthogonal to the optical axis of the laser. With the etalon in this position, a second laser resonator cavity producing all frequency lines (multi-mode) was created. Tilting the etalon broke resonance until a longitudinal mode was reached where lasing occurred, when optical resonance was attained in both the laser resonator and the etalon. After finding the flash point of the laser, the etalon was adjusted two longitudinal mode positions higher in frequency and the first absorption profile segment was mapped. Once the last radial scan position on the rotating wheel was reached, the laser was set to the next longitudinal mode, increasing in optical frequency and the next segment mapped. The separation between each of these longitudinal modes was approximately 129 MHz, representing nearly one-half of the total Doppler frequency shift induced by the rotation of the wheel. This provided sufficient overlap to combine adjacent frequency segments. The ability to overlap adjacent absorption profile segments in this manner removed the necessity of knowing the true laser frequency. Frequency tuning was concluded when the resident iodine vapor absorbed a majority of the collected scattered light, making any further detection impossible with the APDs.

Data records generated for each investigated frequency mode were post-processed using custom sorting and interleaving algorithms to develop continuous IVC calibration curves. A LabVIEW program implementing these algorithms was used to overlap the calibration segments representing the transfer function for each IVC. For example, from Figure 5-12, the absorption profile segment for mode eleven was adjusted in frequency by about 45 MHz, which brought the first point in this segment into close proximity of the seventh point of the absorption profile segment for mode ten. This manner of sliding absorption profiles in frequency using least squares minimization (Figure 5-13), improved the radial position overlap between adjacent mode settings, thus improving Doppler frequency resolution. Interleaving operations were repeated for each of the sixteen A/F transfer function segments to develop the continuous profile shown in Figure 5-14.
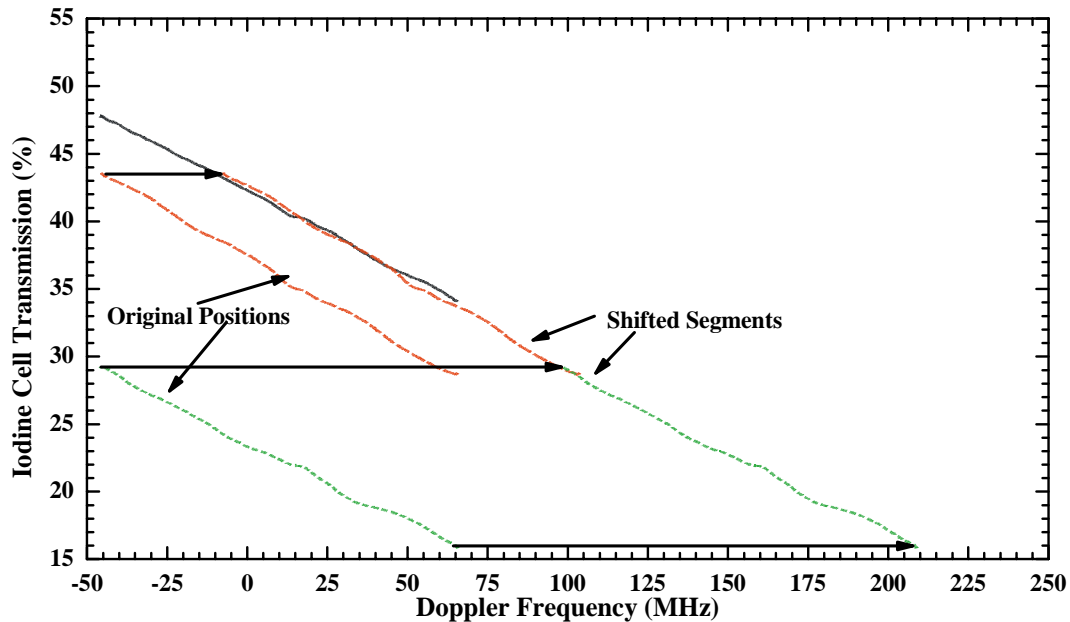
Figure 5-13 – IVC absorption profile frequency alignment process.

The initial calibration curve resulting from the interleaving operation had a shape resembling the expected profile. However, a close examination of the calibration data sets showed that in some areas, even after using rms error minimization, the fit between adjacent points was not smooth and demonstrated a good deal of jitter (Figure 5-14). This was because the overlapped regions of adjacent segments did not always have similar slopes, and/or the spacing between individual points that together formed each segment was not uniform. These variations were caused by laser frequency drift, which occurred during the course of data collection. Resulting segment alignment jitter produced multiple frequency values for a given ratio, which if left uncorrected would make unique optical frequency determination impossible.

Figure 5-14 – IVC calibration curves developed using attenuation profile segments.

Calibration jitter was overcome using two different curve-fitting algorithms. The first chosen was a Sigmoidal fit since its shape was similar to the absorption profile of the Iodine va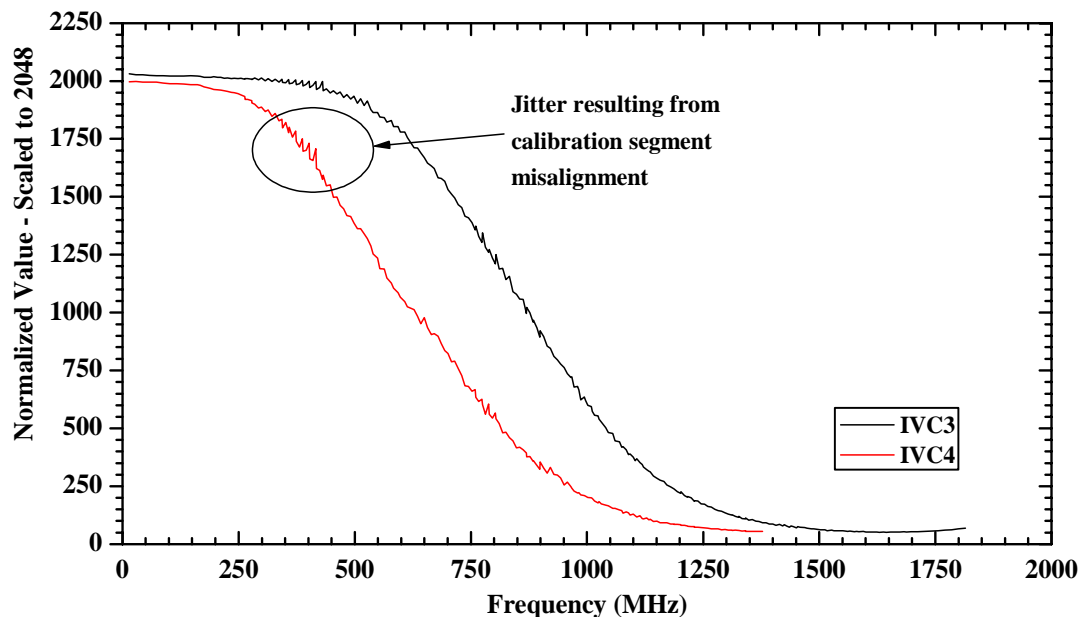por. This fitting procedure returned the coefficients of a Boltzmann equation describing the fit of the individual points in the calibration data set. By observing the Coefficient of Determination value (r^2) returned along with these coefficients, it was possible to gauge the *goodness of fit* for the developed curve. The start and end points, defining the portion of the calibration curve where the Sigmoidal fit was to be applied were adjusted in order to approach the ideal r^2 value of 1.00 (fit passes through all points). This process was repeated until an acceptable r^2 value was found and the resultant Boltzmann coefficients archived. At the start of pDv processing operations these coefficients were recalled from storage and applied to the Boltzmann equation to generate a lookup table (LUT) describing the transfer function of the IVC (calibration curve) (Equations 5.2 & 5.3). To increase the processing speed, the table was maintained in local memory so that it could be quickly addressed and interpolated with appropriately scaled normalized signal values.

Sigmoidal Fit Frequency Equation:

$$Frequency = x_0 + dx\left(\ln\left(\frac{(A_1 - Ratio)}{(Ratio - A_2)}\right)\right) \tag{5.2}$$

Normalization Ratio Equation:

$$Ratio = A_2 + \frac{(A_1 - A_2)}{\left(1 + \exp\left(\frac{Frequency - x_0}{dx}\right)\right)} \tag{5.3}$$

Where:

A_1 = Sigmoidal fit initial value scaled to 2048

A_2 = Sigmoidal fit final value

X_0 = Sigmoidal fit center value

dx = Sigmoidal fit slope

$Frequency$ = Frequency corresponding to the computed ratio value

$Ratio$ = 0 to 2048 (Signal Value / Reference Value * 2048)

This method was used to develop the absorption profile calibrations for four different IVCs. The resultant plots, relating the calibrations developed for the IVCs were placed side by side and their shapes were compared. The two IVC calibrations most similar in shape were selected for use in the LFM and measurement components respectively.

Although the calibration curves for the two selected IVCs were visually similar, a frequency offset existed between them. This was a consequence of the differences in the iodine vapor pressures between the selected cells and to a lesser extent, variations in the laser output frequency at the time the calibrations were developed. The computed difference between the two calibrations was added to the frequency values present in the measurement component's IVC calibration table (Component A), effectively sliding it in frequency to better overlay the calibration for the IVC residing in the LFM. Once the calibrations were aligned, it was possible to make Doppler frequency measurements.

This difference in frequency between the two calibration sets was determined experimentally by measuring the frequency of the light scattered by the surface of the rotating wheel. In this experiment, the laser beam was scanned to a point slightly off the wheel center in the horizontal axis of the wheel (Figure 5-11). At this location the Doppler frequency shift in the scattered light was zero for the horizontal velocity component. Under these conditions, both the measurement component and the LFM would measure the same optical frequency; i.e. the laser frequency, as the Doppler shift is zero.

Therefore, any difference between the two resolved frequencies represented the offset between the two calibrations.

Frequency measurements were obtained with the wheel stopped and rotating at speeds of ~600 rpm (slow) and ~2400 rpm (fast). For each wheel condition, data records were acquired at three adjacent laser modes, near the center of the calibrated side of the absorption profile. The laser frequency mode near the center of the absorption curve was typically used during pDv investigations since it provided the greatest dynamic range for measuring frequency variations in the collected scattered light.

A plot of the average frequency difference observed between the IVCs installed in Component A and the LFM for the three investigated mode and speed conditions is presented in Figure 5-15(a). As can be seen, the average delta between the three laser modes was approximately 130 MHz – nearly the Free Spectral Range (FSR) of the laser. This indicated that the output frequency of the laser had changed about one mode position between calibration sequences - most likely due to ambient temperature differences that changed the optical cavity length of the laser. The calibration obtained by applying the Sigmoidal fit to the Component A IVC data was shifted by 130 MHz. This was the average frequency difference of five points near the center of the IVC absorption profile. Application of the new IVC calibrations produced the results shown in Figure 5-15(b). Here the average frequency difference from the ideal zero was approximately 2.5 MHz between adjacent modes for the slow and fast speed cases.
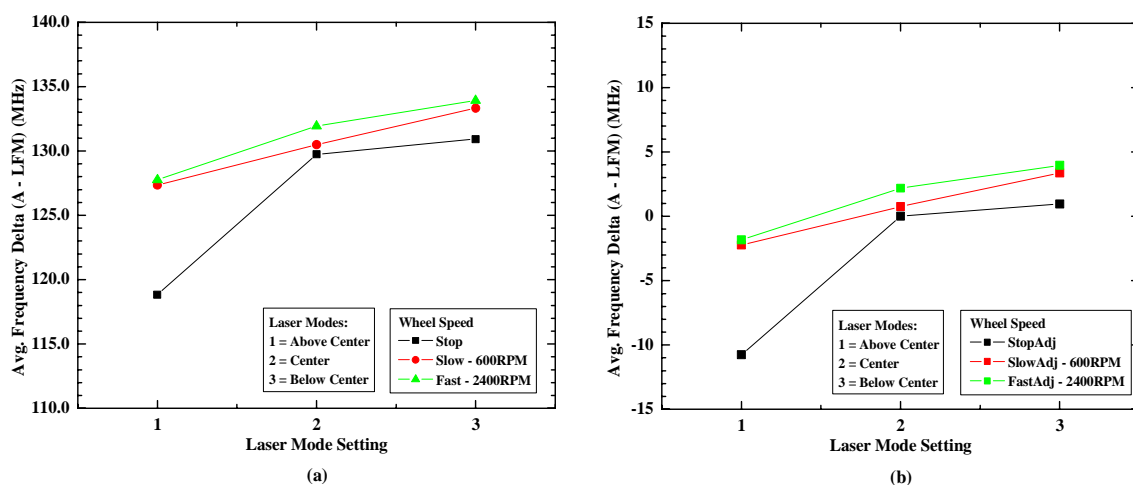

Figure 5-15 – Frequency differences between Iodine Vapor Cells 3 and 4.

Additional adjustments in these calibrations were made without observing any significant improvement and it was concluded that a better overlay of the two calibrations would be impossible for the following reasons:

- Although the same manufacturing process was used, the absorption characteristics of each IVC were different, since their vapor pressures were not matched
- The Sigmoidal fitting process only approximated the calibration data and imposed artificial restrictions on the data

A B-Spline curve fit was then investigated to determine if the calibrations could be improved further. The shapes of the calibration curves resulting from the application of the B-Spline fit algorithm were more accurate than the earlier results. This was because the B-Spline fit method assumed the best fit in the calibration data regardless of its shape, thus overcoming the restrictive approach of the Sigmoidal fit.

As with the calibration curves developed using the Sigmoidal fit, those resulting from the B-Spline fit process also required frequency adjustment before they could be used. The alignment

between the calibrations improved by subtracting 136 MHz from the results of the B-Spline curve fits. Velocities resolved using these calibrations at the same off center locations previously discussed for the three investigated modes and wheel speeds of 300-, 1500- & 3000-rpm are shown in Figure 5-16. These results indicated that at the center laser frequency mode and one laser frequency mode lower, the average resolved velocity was within 1 m/s of the expected zero velocity.
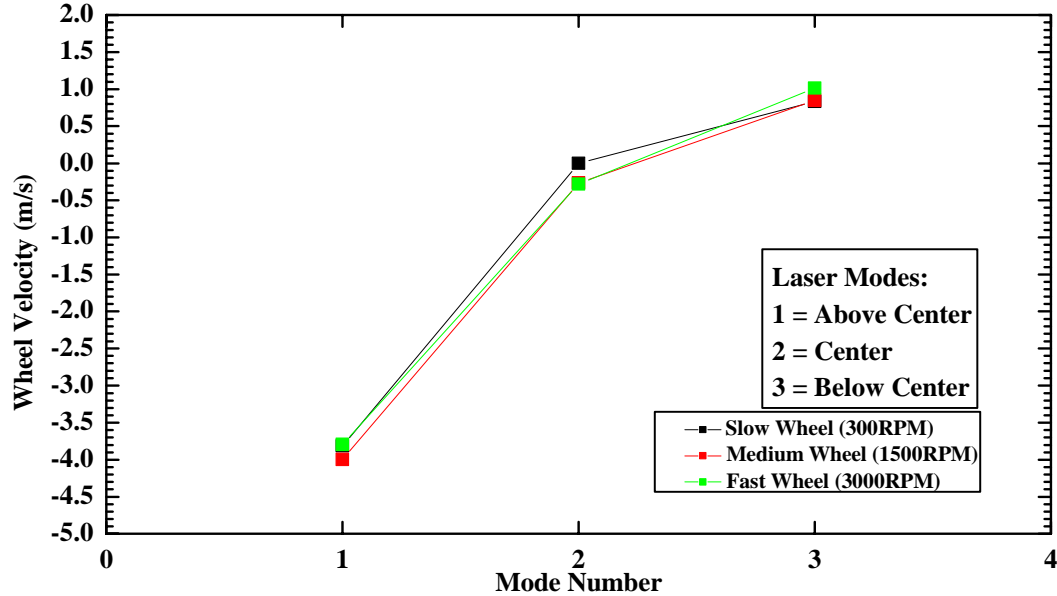
Figure 5-16 – pDv velocities measured at three wheel speeds and three laser modes.

Having improved the level of accuracy in the calibration profile that better approximated the true frequency response of the IVC, the calibrations were verified by measuring the velocity profile along the vertical diameter of wheel as a circular crosscheck. Data sets were acquired at the center and one mode below laser frequency settings, at a wheel speed of 2400 rpm. The laser point was scanned 10-inches across the surface of the wheel, starting two inches from its edge in 0.50-inch increments. At each position, 4096 sample records were acquired at a 5 kHz rate and the wheel speed was recorded in parallel with each data point. Average pDv resolved velocities were in good agreement with computed wheel velocities (Figure 5-17).

Figure 5-17 – Vertical velocity profiles of a rotating wheel measured using pDv.

3. Water Flow Investigations

Measurement of the velocity of particles suspended in water was investigated after the pDv technique demonstrated its ability to provide 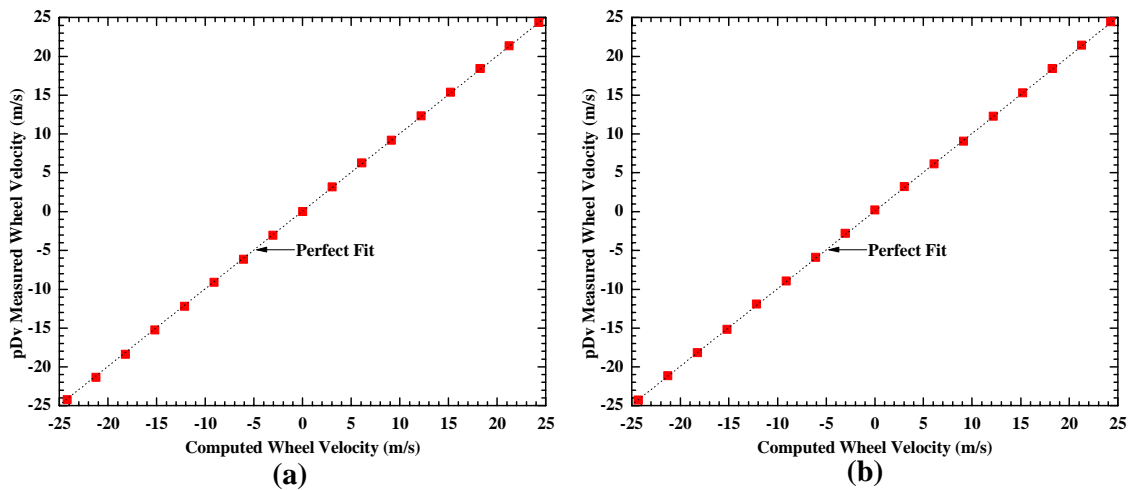acceptable wheel velocities. A small amount of coffee creamer was added to an aquarium filled with distilled water to act as a scattering medium and a small drill pump was used to circulate the water and move the particles. In this test, it was found that the APDs were not able to detect the light scattered by the particles. Increasing the dynamic range of the APDs, which placed them in their avalanche mode, did result in scattered light detection. However, the APDs are non-linear in this mode and thus can not be used in pDv applications. The APDs in the measurement component were replaced with Hammamatsu Photomultipliers (PMTs), which had detection capabilities better suited for the low scattered light conditions, typical of flow regimes for which pDv was intended. The operational characteristics of the PMTs were investigated using the same evaluation tests as those used for the APDs and compared favorably (Figure 5-18(a) Center mode and, (b) one mode above center).
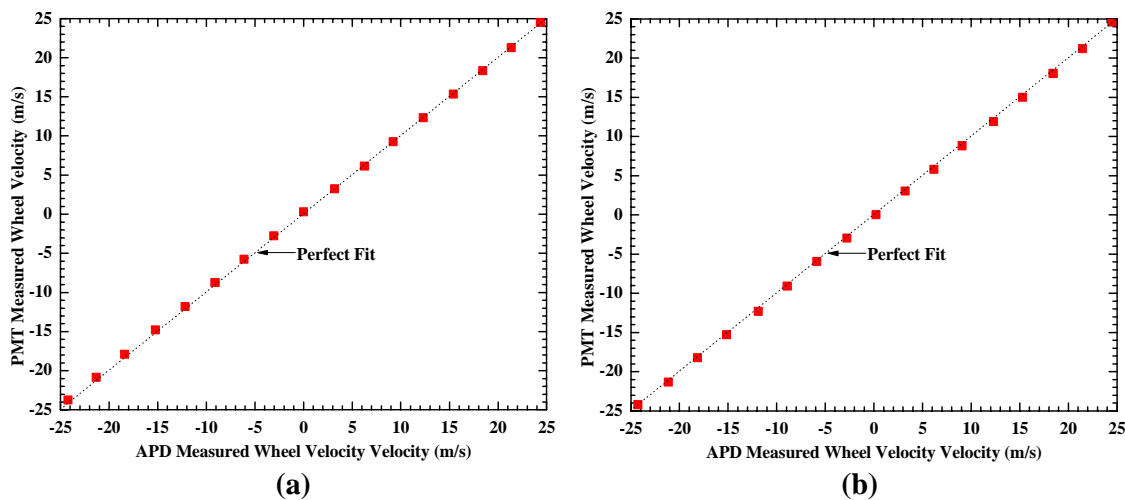

(a)   **(b)**

Figure 5-18 – Comparative testing results for PMTs and APDs.

Once the PMTs were characterized, aquarium testing was resumed. Three conditions were investigated: (a) before, (b) during, and, (c) post pump operation. This provided static, steady state flow, and decreasing flow test conditions. The average velocity measured for the last two conditions was approximately 4.0 m/s. No conclusions were drawn from this qualitative test, except that the pDv system was able to measure particle velocities. The ability of the instrument to measure particle velocities in a fluid was an important project milestone.

4. Air Flow Investigations

The next step in the research effort was to assess pDv measurement capabilities in air; thus, the pDv system was arranged to measure the directed flow exiting a two-inch pipe. System performance was evaluated for statistical and temporal measurement accuracy. The results were compared to those obtained using two flow measurement standards - the pitot probe (average velocity) and a hot-wire anemometer (statistics and temporal) for the same flow conditions. This enabled measurement accuracy and repeatability to be assessed. The results of these investigations will be discussed in chronological order to emphasize the test/modify/validate paradigm followed.

A schematic of the two-inch jet flow is presented in Figure 5-19. A motor operating at 3550 RPM was used to drive a 10.625-in. diameter, six-bladed blower. Mineral oil smoke particles, produced by a commercial smoke generator, were drawn into the blower via the air inlet. The flow exiting the

blower was pumped through a 12.5-foot section of a 4-inch diameter PVC pipe. This was followed by an 8-inch section of PVC pipe, where straws could be added to modify the flow. A 4- to 2-inch coupling was used to interface a 20-inch section of 2-inch diameter glass pipe that produced the jet flow. Particles exiting the pipe were exhausted through a door via an 11-foot section of 6-inch diameter PVC pipe. On the opposite side of the door, a 25-foot section of 12-inch diameter flex hose was connected to a commercial exhaust fan, which, when running, cleared the room of smoke particles.
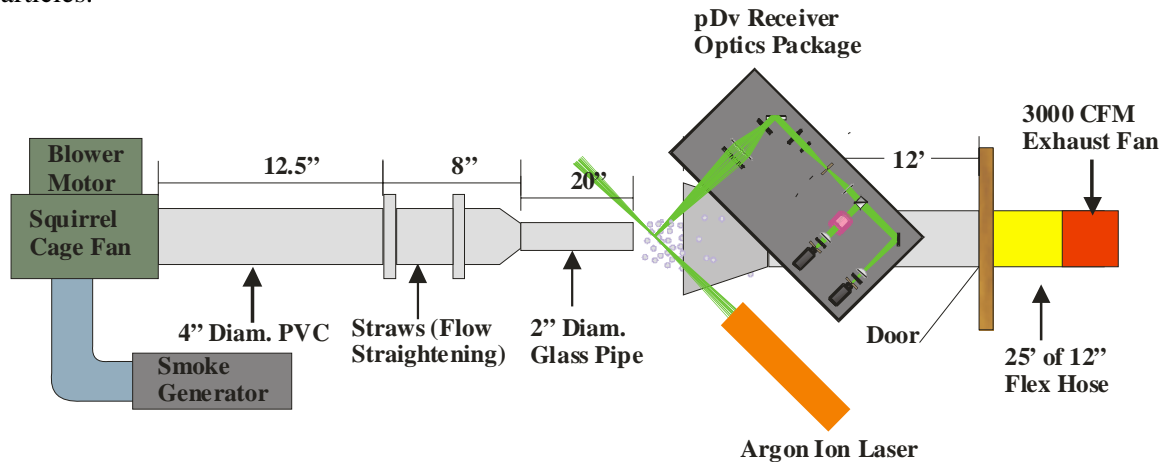
Figure 5-19 – Schematic of two-inch jet flow.

5. *Mean Velocity Investigations*

Average velocity measurements for the flow exiting the pipe were simultaneously acquired with pDv and a pitot probe located 0.12-inches downstream of the pDv measurement volume. This separation distance was necessary so that the presence of the probe would not influence the flow at the pDv measurement location (>2 pipe diameters upstream). Horizontal velocity profiles were acquired at locations of x/D equal to 0, 0.125, 0.250, 0.50, 1.00, 2.00 and 4.00 downstream of the pipe exit. Data collection at these stations commenced at pipe center and proceeded to the right of the pipe exit (facing downstream) in r/R = 0.10-inch increments to r/R = 2.0. The sequence was repeated in the left-hand direction after scanning the sample volume scanned to flow centerline (r/R = 0). This manner of scanning the probe volume was followed in all subsequent testing.
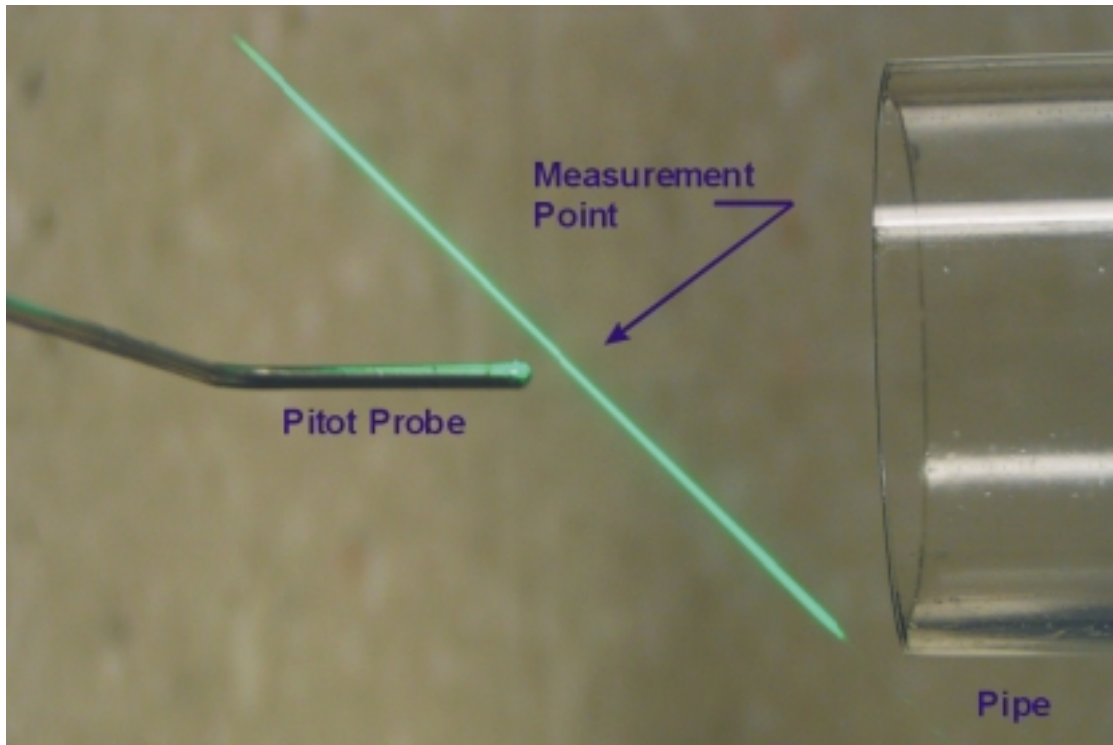
Figure 5-20 – Pitot probe and pDv sampling volume locations for two-inch pipe.

Prior to initiating pDv comparative testing, the unseeded flow exiting the pipe was calibrated using a pitot probe. Horizontal velocity profiles were acquired for the presented test matrix. Differential pressure obtained with the pitot probe was measured using a Barocell pressure sensor connected to an electronic manometer with an output sensitivity of 0.10 V/Torr. The resolved average radial velocity profiles demonstrated classical turbulent pipe flow shapes and had a centerline velocity of approximately 52 m/s (Figure 5-21). The smoothness of the developed profiles confirmed the flow to be stationary with time. Note that as the flow progressed downstream the centerline velocity dropped and the width of the flow increased as the primary flow mixed with entrained air at the flow edges.
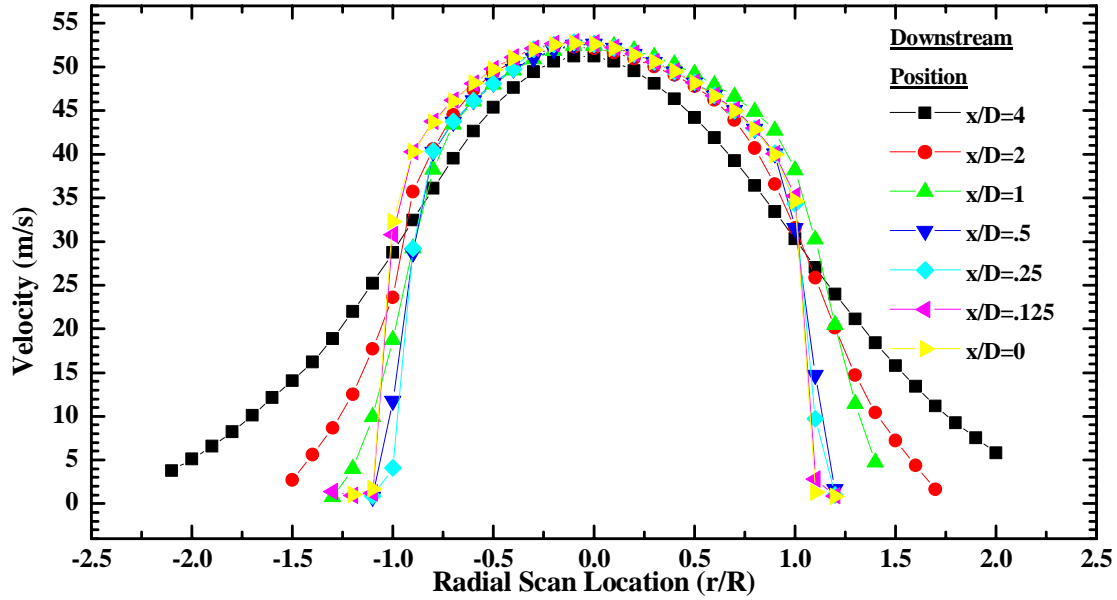
Figure 5-21 – Pitot probe measured axial velocity profiles for the two-inch pipe.

pDv velocity measurement assessment was then commenced using the geometry shown in Figure 1-1. The symmetric orientation of the pDv receiver and the laser about the flow centerline in this configuration yielded a direct measure of the streamwise velocity (u-component). The results of the initial pDv comparative test with the pitot probe conducted at the $x/D = 2$ downstream station are shown in Figure 5-22. Here each point represents the average of 4096 velocity measurements, acquired at a 100 Hz rate. As shown, the presence of seeding particles did not affect the pitot probe measurements. Turbulence Intensity (T.I.) was computed using Equation 5.4:

$$TI_{CL} = \frac{\sigma_v}{v_{CL}} * 100 \tag{5.4}$$

Where:

TI_{CL} = Turbulence intensity based on the centerline exit velocity

σ_v = Standard deviation for resolved local velocity

v_{CL} = Centerline velocity at pipe exit

Figure 5-22 – First pDv velocity and turbulence intensity measurements at x/D=2.

The pDv velocity data sets showed good agreement with the pitot measurements in shape and the developed turbulence intensity profile was typical of this type of flow. Flow turbulence intensity at centerline was low and gradually increased symmetrically towards the flow edges at the shear region between the direct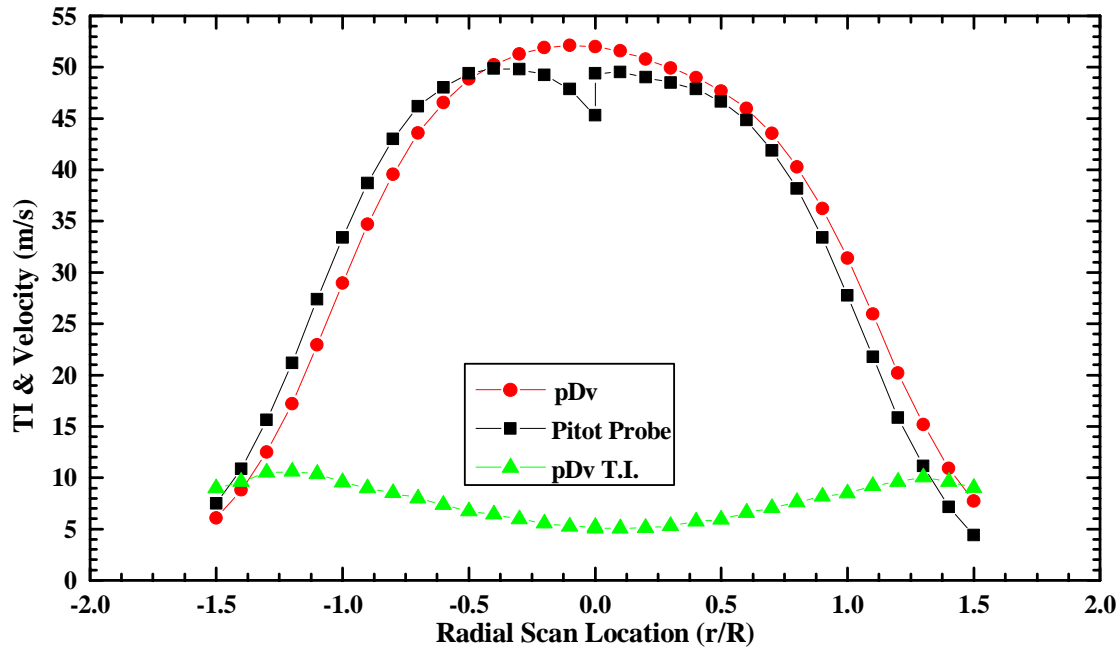ed pipe flow and the entrained air. For this particular experiment, velocity measurements were made outboard to the r/R = 2.0 stations on both sides of the pipe. Results obtained further out than r/R = 1.5 are not presented due the unreliability of the pDv measurements because only part of the flow was being measured; i.e., only the seeded main flow was measured and not the clean entrained air. The consequences of this condition, commonly referred to as sampling bias (Meyers, 1991), limited the ability of the instrument to make accurate velocity measurements. This was because mixing causes the measurements to be biased toward the pipe flow velocity, since the entrained flow was not measured.

pDv and pitot probe velocity measurements differed by an average of 0.87 m/s over the entire horizontal scan profile and the magnitude of the local differences changed sign between the right hand and left hand scan directions. Of particular note is that the average pDv velocity measured dropped significantly during the time between the acquisitions of the first and second data points at the flow centerline. In addition, velocities measured at several other positions left of centerline did not agree with the symmetric velocity measurements made to the right of centerline. The fact that the pitot probe measurements did not demonstrate a change in velocity confirmed that the flow was stable over time, indicating a problem with the pDv measurement.

Once the acquired pDv data sets were processed, it was observed that the laser frequency drifted about 80 MHz during the time it took to survey the velocity profile to the right of the pipe exit. This drift resulted in different regions of the IVC calibration curves being used to resolve Doppler frequency shifts over the course of the profile scan. These results reinforced earlier predictions that the two primary error sources in the pDv system would be associated with (a) maintaining the laser at a single frequency, and, (b) IVC calibration accuracy.

At the time this data was collected and analyzed, a lack of knowledge about the nuances of the pDv technology, and the degree to which laser frequency variations could affect measurement accuracy, was overlooked. It was assumed that:

- Because the LFM measured the output frequency of the laser directly, any deviation form the laser set point would be tracked and accounted for in the normalization process
- As long as the laser was set to operate in a linear region of the IVC absorption band, accurate Doppler frequency shifts could be measured
- Since the employed IVCs were used to obtain velocity measurements comparable to those computed for the rotating wheel (Figure 5-17), small variations in laser frequency could be tolerated and relatively accurate velocity measurements could still be made.

The presented results proved that these assumptions were incorrect and indicated that the laser frequency drift would have to be kept to a minimum before accurate measurements could be obtained. What was not understood at the time was that the ambient temperature variations would cause the absolute operating frequency of the laser to vary, in turn causing the relative laser longitudinal mode positions to be different with time. Thus, adjusting the tilt of the etalon did not guarantee that a particular portion of the linear region of the IVC would be used throughout the test or during the calibration of the IVCs. The consequence of this was that laser frequency could drift into areas, where the misalignment in the calibrations between the employed IVCs, would be significant enough to generate errors in resolved Doppler frequencies.

Additional experimentation provided more insight into the actual causes of this behavior and generated ideas about minimizing or eliminating these problems. However, without the wisdom of experience, these tests addressed what turned out to be symptoms and not the problem sources. In hindsight, this testing was not an exercise in futility, since it provided valuable hands-on experience with the pDv technique and a better understanding of the physics that guided testing towards the problem sources.

Since laser frequency drift was identified as the primary source of measurement error during early flow velocity characterization activities, testing was focused on identifying the cause(s) for this behavior in order to develop methods for minimizing its effects. A short-term solution was to closely monitor the laser and manually adjust it prior to the acquisition of each data record. This resulted in a better match between pDv and pitot probe measurements; however the ability of pDv to provide repeatable measurements was suspect since successive runs produced different and inconsistent results. Many of the experimental data sets demonstrated results similar to those of Figure 5-22 suggesting a fundamental error source. In an attempt to identify the cause of this behavior, several items were examined and minor system modifications were incorporated including:

- The alignment of the laser beam was checked and confirmed to be correct
- The current-to-voltage conversion circuits, consisting of a 10K resistor connected across the output of each PMT and a voltage amplifier, were replaced with current amplifiers over a concern that the PMT signals may be bandwidth limited
- 50 mV of electronic noise riding on the PMT bias voltage supply was suppressed with a 0.10 µF capacitor placed across the power supply rails

The incorporation of these modifications did not result in a substantial improvement in system performance. Subsequently the operation of the PMTs employed in the system was investigated. As a means of checking PMT performance, the employed IVCs and the laser etalon were removed and the remaining receiver package elements were left intact. This eliminated light frequency dependency as an error source. The response of the PMTs to laser light scattered off a stationary sheet of fine grit sand paper attached to the end of the pipe was then characterized. The PMT response, Figure 5-23(a), was compared to the LFM photodiode samples, Figure 5-23(b), to insure that the detectors tracked the laser power variations. The results of this test demonstrated that intensity variations due to laser power fluctuations appeared in both the measurement and LFM components as expected. A closer look at these plots highlights a problem with the Signal leg PMT: specifically, that the average voltage output level increased over time and there was a definite increase in slope enhanced by the linear fit. In contrast, the Reference PMT output had a gentler decreasing slope. This behavior could have potentially compromised the normalization process and consequently produced errors in velocity

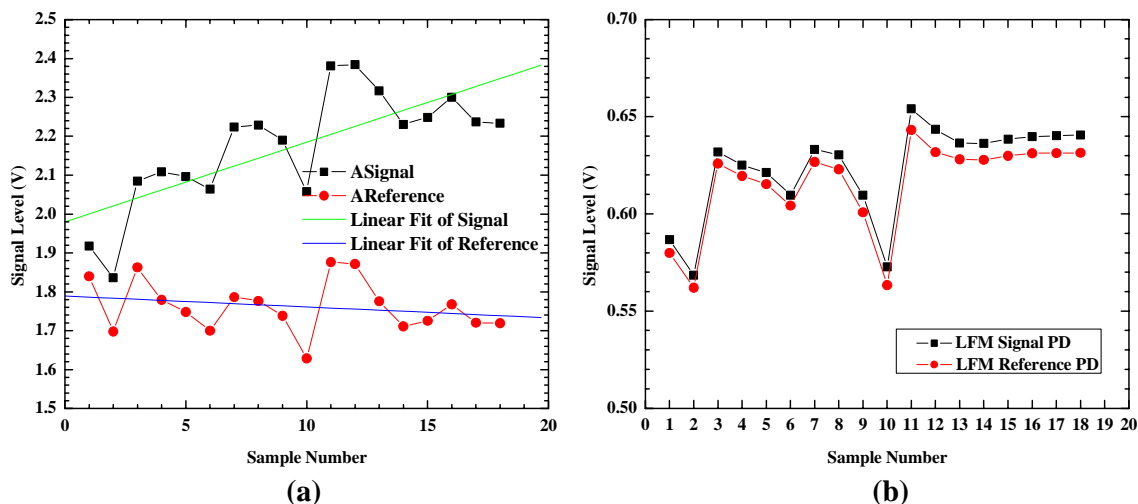measurements, since the PMT responses were not stationary, shifting in opposite directions at different rates.

Figure 5-23 – PMT and LFM response to light scattered by fine grit sandpaper.

As the Signal PMT exhibited a more dramatic drift in the output signal, it was suspected that the problem was isolated to this particular PMT. The suspected *bad* PMT was then replaced and testing resumed. The replacement device also exhibited similar behavior, but not to the extreme found previously. The manufacturer of the PMTs was then contacted for more insight into the laboratory observations. The response given was that this behavior was typical until the device went through its *burn in* period and the extent of drift would decrease over time. It was recommended that the PMTs be exposed to continuous light for several hours prior to use to achieve better detector stability. Although the PMTs were being used regularly, the intensity of the scattered light was not sufficient to satisfy this requirement. Hence, the PMTs were exposed to fluorescent room light for a period of five days before testing was resumed. In addition, prior to initiating each experiment, the PMTs were exposed to room lighting for one hour.

Having accommodated PMT burn-in requirements, the system was deployed in a modified configuration, where boxcar integrators were installed at the output of each PMT. The boxcar integrator acted as a wide bandwidth low-pass filter by integrating the real-time signal (200 MHz bandwidth) to 67 kHz. This reduced the transient signal properties of individual particles passing through the pDv sample volume, yet it was above the 20 kHz flow turbulence bandwidth.
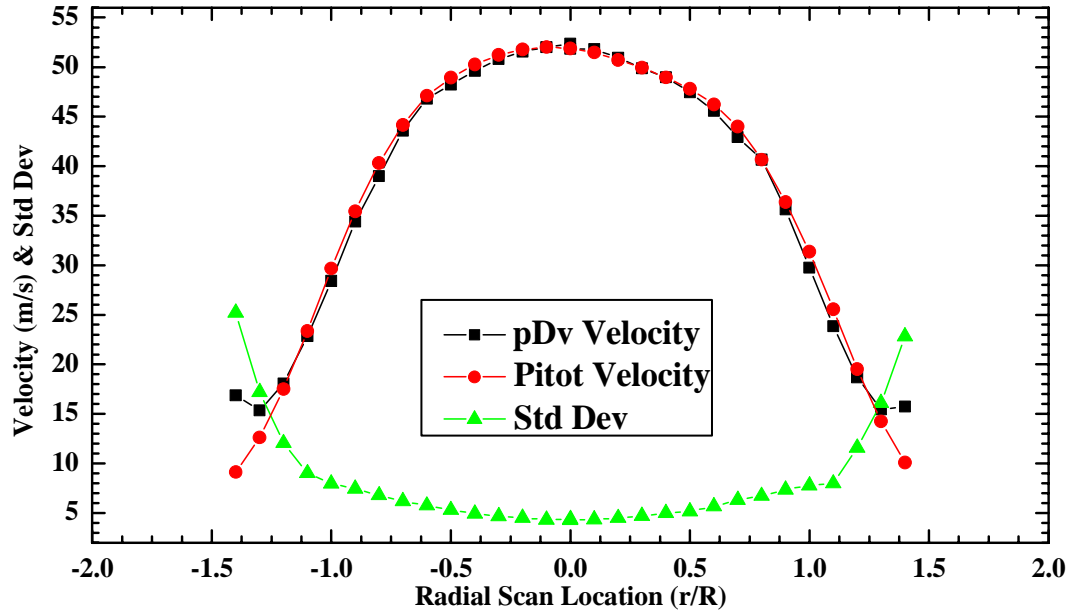
Figure 5-24 – Horizontal plane velocity profiles measured at x/D = 2 station.

As can be seen in Figure 5-24, the obtained pDv velocity measurements were in excellent agreement with those of the pitot probe. Also, the standard deviation of the pDv measurements was about 5% of the velocities measured in the core region of the flow and increased at the flow edges as expected in the shear region of the flow. This level of deviation indicated that the pDv resolved velocities at the flow centerline were reasonably accurate, since they were close to the 3.5% turbulence intensity levels typical of a classical pipe flow.

Although the burn-in of the PMTs and the manual tracking of the laser frequency provided good measurements, additional testing still showed variations at the flow centerline. Looking closely at the centerline data point the plot of Figure 5-24, a variation is present. A remaining concern was that pDv measurements were not always reliable, because results comparable to those of Figure 5-22 were occasionally obtained. This supported the earlier assessments that the observed problems were primarily due to laser frequency drift, which caused the Doppler frequency and the velocity measurements to fluctuate, since different regions of the IVC calibrations were being used over time. An attempt to quantify the effects of laser frequency drift over time was made by measuring the velocity of a stationary piece of Mylar. Theoretically, the velocity measured should be zero, however as shown in Figure 5-25 the resolved velocity started at 0.5 m/s and drifted to about –1.7 m/s over the 30 minute test.
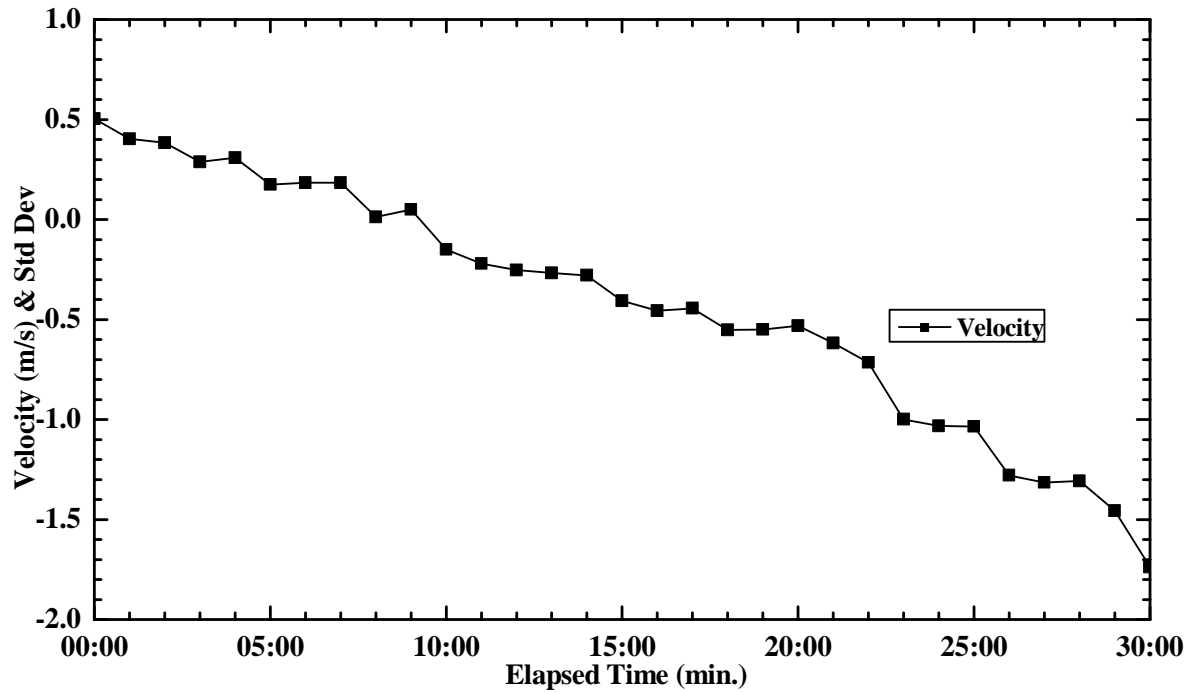
Figure 5-25 – Deviation from zero velocity due to laser frequency drift.

These results in combination with those of Figure 5-24 indicated that laser frequency drift was an error source that would have to be resolved, before accurate and reliable measurements could be realized. After contemplating what procedures could be followed to obtain accurate measurements, it was decided that an active method of controlling the laser frequency would simplify system operations and provide more consistent results. This led to the development of the laser drift minimization system discussed in Chapter 3 (Lee and Meyers, 2005).

Figure 5-26 – Simultaneous pitot probe and pDv measurements at x/D = 2.

Characterization of the flow exiting the two-inch pipe was resumed after the laser drift minimization and pDv integrator systems were refined and incorporated into the pDv instrument. Figure 5-26 shows the radial velocity profile measured at the x/D = 2 downstream location. Note that the shape of the flow in this plot differs from those presented earlier, because these data sets were acquired after straws were inserted into the pipe (Figure 5-19) to reduce low frequency turbulence. As with the ea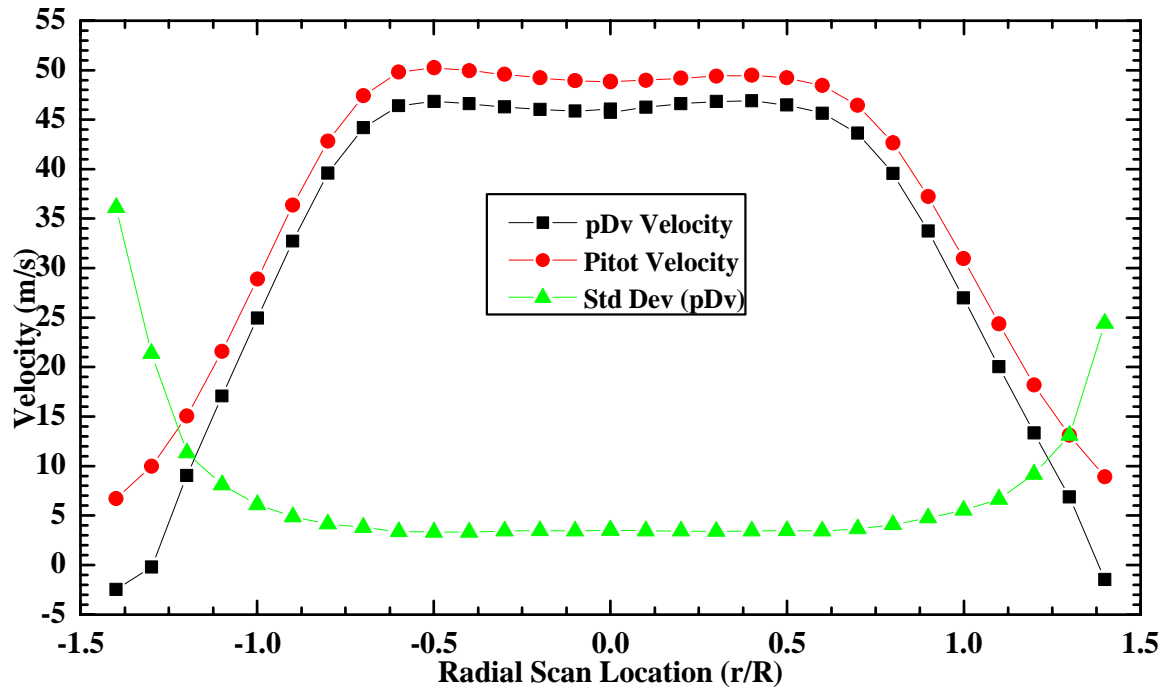rlier data sets, pDv velocities differed from those of the pitot probe, however, the delta was more consistent in the core of the flow and gradually increased closer to the flow edges. When these data sets were collected and examined, it was concluded that the primary cause for the discrepancies in the velocity measurements was related to the differences in the calibrations developed for the IVCs residing in component A and the LFM. This conclusion was reached after making the following observations:

- Laser frequency was being maintained by the laser frequency stabilization system which was capable of keeping drift to less than 1 MHz/minute and the region of the IVCs being used during testing was fairly consistent
- The difference in the velocity measurements was nearly uniform, particularly in the core region of the flow.

Follow-on studies conducted after developing a better feel for the subtleties of pDv, led to a more appropriate explanation based on system physics, for the offset between the pitot probe and pDv measurements this data set. This will be discussed in a later section.

Although the pDv-measured velocities did not match those of the pitot probe, the presented results were nonetheless very encouraging. The improvement in data indicated that incorporation of the system used to minimize laser frequency drift and integration of the PMT output signals had diminished the effects of the previously identified problems. Further evidence that system operation was improved was apparent in follow-on testing, which yielded higher quality measurements, as noted by the lack of velocity differences in the centerline measurements.

102

6. pDv Spectral Quantity Measurement Validation

The potential capability of pDv to resolve flow spectral quantities in turbulent flows was the most attractive aspect of the technique to the aerodynamicists. Their interest was in using pDv to characterize the flow exiting a high-speed jet so that the flow turbulence quantities, which are responsible for fluid friction losses and fluid induced noise, could be better understood (Jorgensen, 2002). Hot-wire measurements indicated that this flow contained frequency components of up to 100 kHz. This was the primary criterion for designing the pDv system to have sampling capabilities of up to 250 kHz. In preparation for this testing, the spectral content of the flow exiting the 2-inch pipe was quantified with pDv. The pDv results were then compared to the hot-wire measurements for the same flow conditions to cultivate a level of confidence that pDv was capable of making the required measurements. Because smoke particles will change the cooling rate of the hot-wire and subsequently its calibration, it was not possible to make these measurements simultaneously. Rather, the data sets were acquired independently in back-to-back experiments.

(a)

(b)
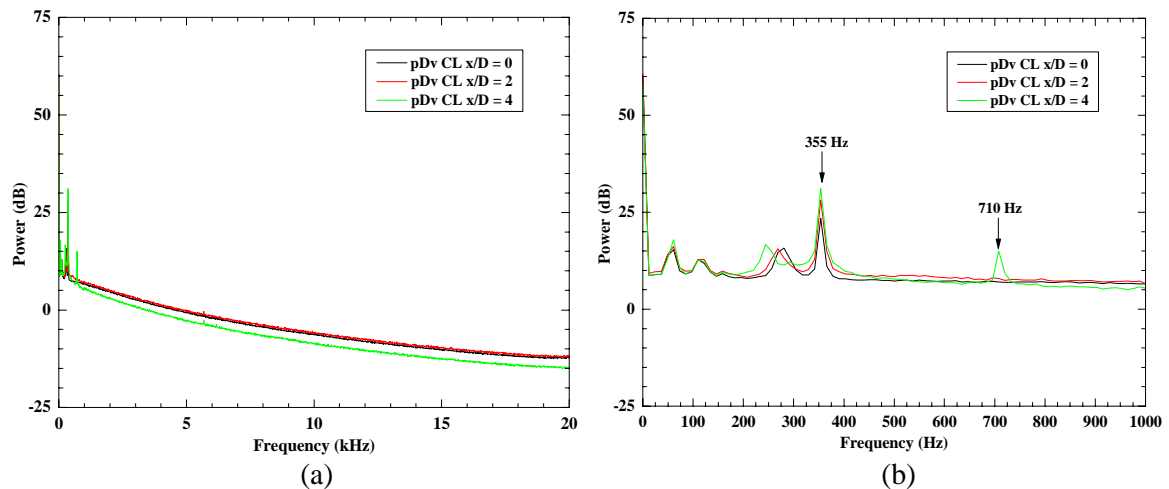
Figure 5-27 – Spectral content of flow exiting two-inch pipe measured using pDv

Prior to initiating the hot-wire experiments, data sets were acquired using pDv to assess its frequency measuring capabilities and validate spectra processing software. Data sets were acquired along the pipe centerline at the $x/D = 0$, 2 and 4 downstream stations at a rate of 50 kHz (Figure 5-27). The resultant spectral plots were analyzed and the following observations made:

- A spike was identified at 355 Hz for all three downstream locations. This frequency coincided with the rate of blade passages of the six-bladed fan driving the flow, the speed of which was measured to be 3550 RPM, using a strobe during normal operation.
- A strong peak at 710 Hz was identified in the $x/D = 4$ spectral record. This frequency indicated that the second order harmonic of the fan blade passages was also being measured.

Data was then acquired using a hot-wire at the same downstream locations characterized using pDv and data records of 500k samples were collected at a rate of 50 kHz. Spectral plots for each downstream station showed a frequency spike at 355 Hz and a spike at 710 Hz for the $x/D = 4$ station only.
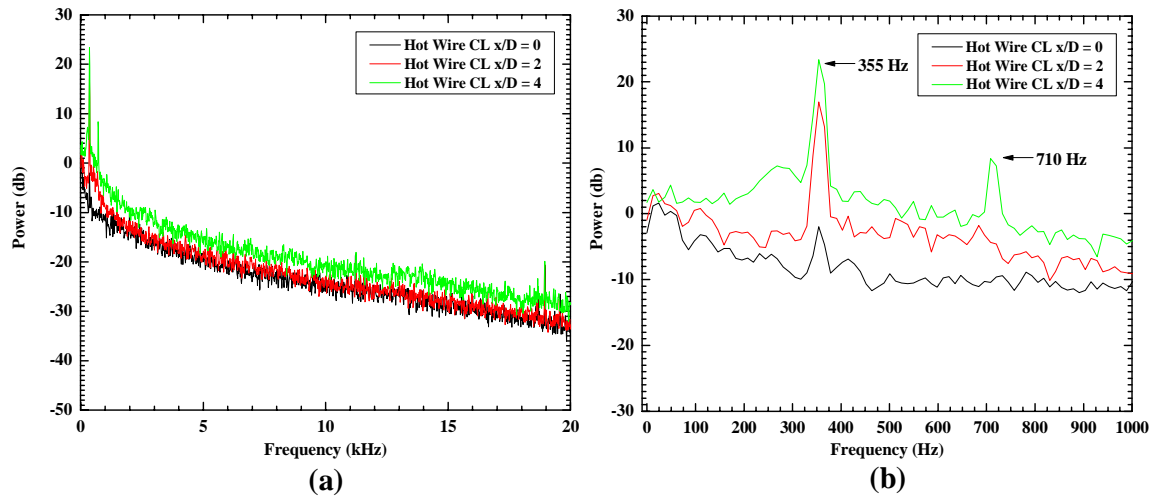
Figure 5-28 – Hot wire spectral measurements of flow exiting two-inch pipe.

The fact that the pDv and the hot wire spectral plots contained the same spikes at both the fundamental (355 Hz) and secondary (710 Hz) harmonic frequencies of the fan driving the pipe flow, confirmed that pDv was indeed capable of measuring the frequency content of a flow. An area of concern with the pDv measurements was that the noise floor was higher than that of the hot wire, Figure 5-29, which limits the dynamic range of pDv. Later analyses of the pDv data sets, discussed subsequently, did provide a hint into the possible causes of the higher than desirable noise floor. This information will be used in future investigations to improve the pDv spectral measurement performance.

Figure 5-29 – Comparison of pDv and hot wire spectra measurements

7. *pDv Measurement Capability Review*

The mean velocity and turbulence spectral measurement results demonstrated the ability of pDv to accurately measure particle velocities with a limited degree of repeatability. At the time when the bulk of the presented research was conducted, no single cause for the inability to make repeatable and reliable measurements was identified. As the first phase of pDv research concluded, it was obv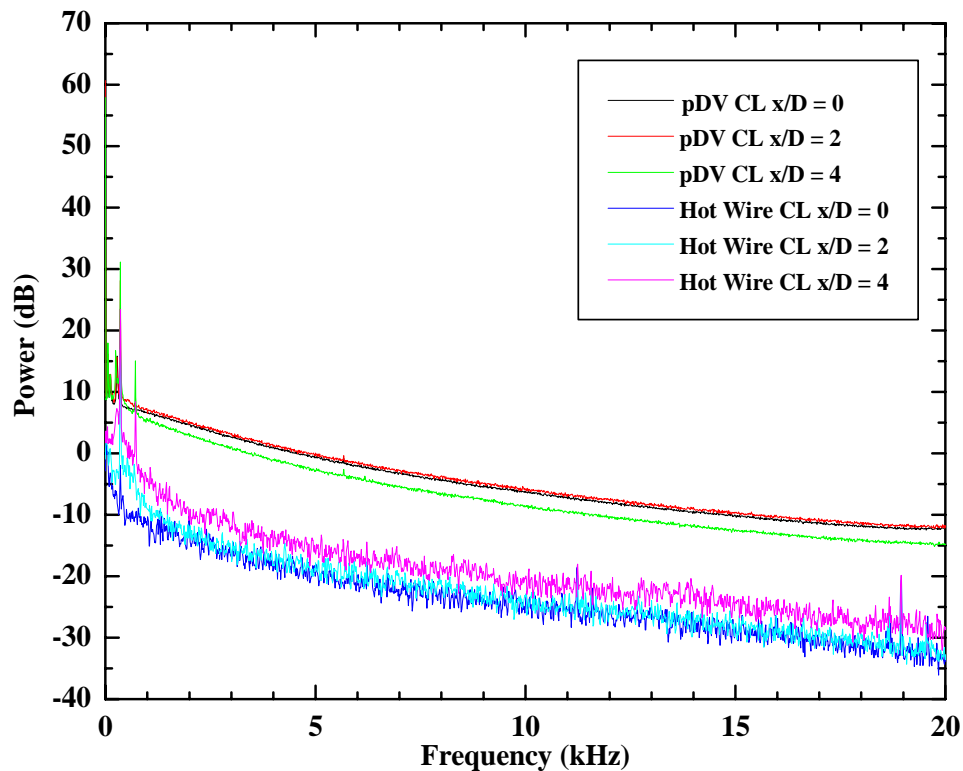ious that further work would be required to increase measurement confidence so that the pDv technique would be attractive to researchers. After reviewing the breadth of data gathered during this research, the primary identified error sources, in order of difficulty were:

- Laser frequency instability
- IVC calibration mismatches
- Sample phase mismatch
- Optical system alignment
- PMT saturation

Subsequent research was focused on addressing the first two items since they were identified at project onset as the most difficult to control. Integration techniques were investigated as a possible solution to the sample phase mismatch errors. Concerns with the optical alignment dissipated with further hands-on experience and learning the effects of various components and configurations, through a series of cross checks incorporated in the optical setup procedures. Further work on the pDv activity was concentrated on gaining a better understanding of these error sources so that solutions geared towards improving measurement accuracy and repeatability could be implemented.

a. *Laser Frequency Instability*

The ability to maintain single frequency operation with a laser satisfying the power requirements needed to illuminate a seeded flow is difficult, because these lasers are susceptible to changes in their operating characteristics with ambient temperature variations. This problem was minimized with the development of a closed-loop, feedback system that adjusted the optical cavity length of the laser to compensate for temperature variations, which kept the laser close to the desired operating frequency. Results obtained using this system for a few experiments conducted towards the end of the pDv research activity demonstrated a marked improvement over early pDv measurements. As a point of comparison, the laser frequency drifted about 80 MHz while acquiring the data shown in Figure 5-22 and only 8 MHz for the experimental results of Figure 5-26. This was a strong indication that laser frequency drift could be minimized, so no further research was conducted in this area other than to confirm that frequency instability compromised measurements in early data sets.

b. *IVC Calibration Mismatches*

The errors associated with inaccuracies between the developed IVC calibrations and the true absorption properties of the resident iodine, and the mismatches between the calibrations of the IVCs residing in the measurement and the LFM components were investigated further. IVC calibrations developed using pDv methodologies were limited in accuracy; a result of the discrete sampling of collected data points, sparse data sets, laser frequency drift, and measurement position uncertainty. It was theorized that improved measurement accuracy might be obtained if the IVCs were calibrated using the DGV technique. The DGV approach resolves each absorption segment by computing the Doppler frequency shift at every pixel location falling along the vertical diameter of the wheel. This was possible since the employed CCD cameras measured the Doppler frequency shifts over the entire wheel surface, at the same time providing simultaneous measurement of the entire vertical profile. A calibration describing the complete absorption profile was obtained by tuning the laser to the individual frequency modes and acquiring multiple images. The resulting average image yielded the Doppler frequency shifts of the absorption

segment for that mode setting. To summarize, A/F calibrations obtained using DGV by their nature are more accurate than those achieved using the pDv approach primarily because:

- Absorption profile segments resolved with DGV were more sensitive to frequency response trends, since they were developed using a higher spatial resolution than the pDv method; i.e. ~100 points/inch vs. 2 points/inch.
- The time required for resolving an absorption profile segment was short (less than one second), so the effects of laser frequency drift were minimal. For the pDv method, the accuracy of the resolved frequency was compromised because the laser tended to drift during the time required (~75 minutes) to acquire a set of data points comprising a calibration segment.

Thus, DGV generated IVC calibrations were applied to the data set obtained at the x/D = 2 downstream station of the 2-inch pipe exit (Figure 5-24) to determine if an improvement in measurement accuracy would be realized. As can be seen in Figure 5-30, the velocities obtained using DGV calibrations were an average of 5.25 m/s faster than those previously resolved. In contrast, the average difference between the pitot probe and the pDv velocity measurements obtained with the original calibrations was only 0.16 m/s.
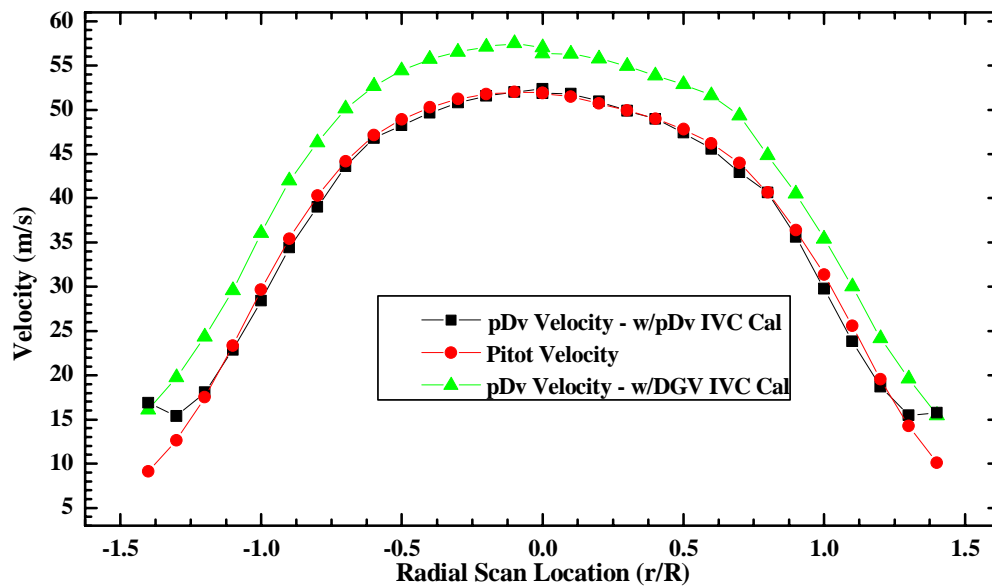

Figure 5-30 – First pDv measurements reprocessed with DGV calibrations.

The results were not as expected and hence suggested that one of the original conclusions, tying a majority of the measurement errors to the IVC calibrations was invalid. Proof of this is the fact that the application of either DGV or pDv calibrations produced similar flow profiles that had a nearly uniform offset between them. If the error were strictly the result of calibration mismatches, this offset would be more inconsistent. Analyses of these results and those of Figure 5-26 indicated that some other systemic error was being overlooked, which might cause such a uniform offset between data sets.

After reconsidering the sequence of procedures followed to make the pDv velocity measurements, an explanation for this offset was identified. It tied the observed offset errors to the laser frequency setting at the time flat-field data sets were acquired. Recall that the flat-field correction factors account for unique differences in the optical, detector and signal conditioning paths between the signal and the reference legs in both the measurement and the LFM components (Chapter 2). It was assumed that once the laser frequency was tuned outside of the

absorption line to acquire the flat-field data, the ratio was independent of frequency. This assumption was based on the theoretical models of iodine absorption spectra and on exactly matching the laser frequency used to acquire the flat-field data during IVC calibration was not a concern. If this were not true, the scale factor would be different, thus yielding an apparent bias error. This could explain the relatively constant offset (ratio) between the pDv and pitot probe velocities in the core.

The selection of the laser frequency for flat-field data acquisition is critical and setting the laser frequency at "top of curve" should not be set casually. The selected mode must be as close as possible to the mode used to develop the IVC calibrations. From Figure 5-31 the *ideal* frequency mode (blue) should be used since the induced Doppler shift during flat-field calibration would not cause the collected scattered light to be absorbed, resulting in the most accurate flat-field correction factor. If one of the *suspect* mode settings (red) is selected, the Doppler shift induced by particle motion could cause some of the particle-scattered light to be absorbed. This was not the case during IVC calibration, as the component velocity could be set to 0 m/s by positioning the measurement point on the horizontal diameter of the wheel. This results in a flat-field correction value that introduces velocity biases similar to those observed.
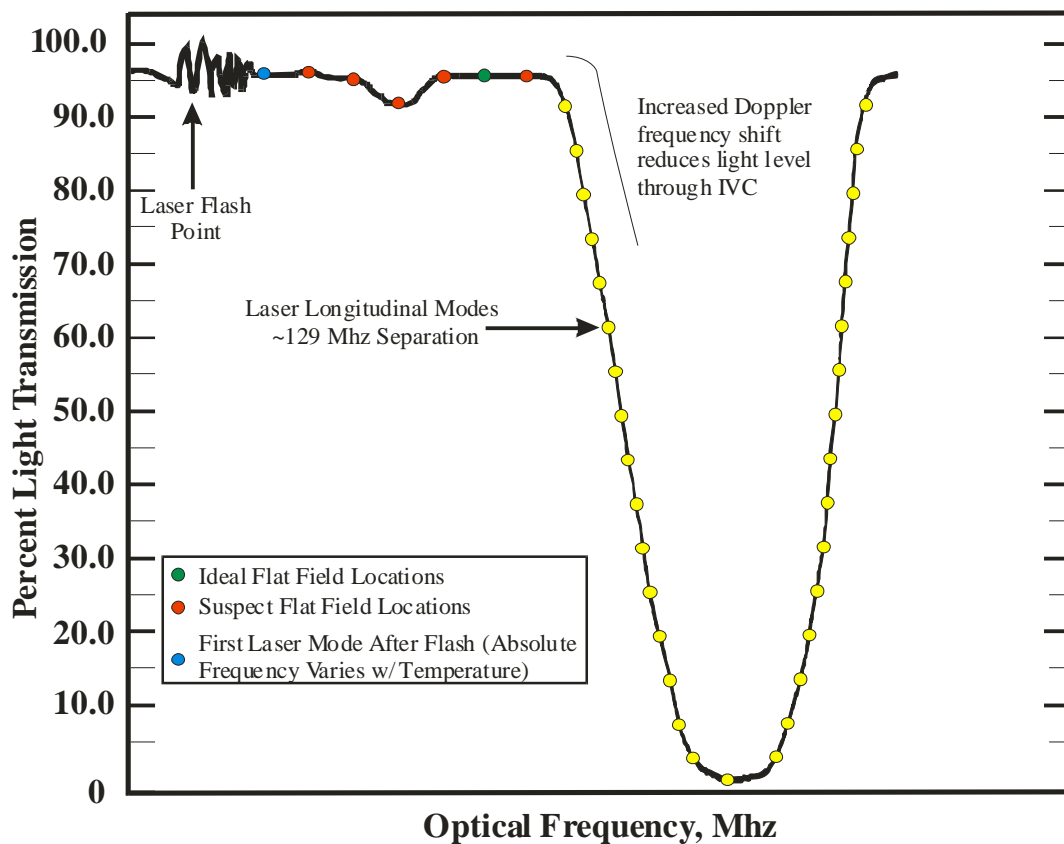
Figure 5-31 – IVC absorption profile showing frequency modes.

As a means of validating the premise that the flat-field mismatches were the cause of the observed offset errors, the data sets of Figure 5-26 and Figure 5-30 were reexamined. The average ratio between the pDv and the pitot probe measurements in the core region (r/R = +/-0.7) was computed and applied to the data values to determine if the resulting profiles would overlay each other.

Figure 5-32 (a) shows the results of multiplying the pDv data values computed using the DGV IVC calibrations (Figure 5-30) by the ratio of these measurements to the pitot probe

measurements (0.93), Figure 5-32. (b) shows the results of multiplying the pDv data values of Figure 5-26 by the ratio of these measurements to the pitot probe measurements (1.07). As shown, the scaled pDv data sets overlay the pitot set, within the expected measurement error, particularly in the core regions. The results of these adjustments verified the conclusion that mismatches in the portion of the IVC absorption band used to develop the flat-field correction factors for data sets and the IVC calibration were different.
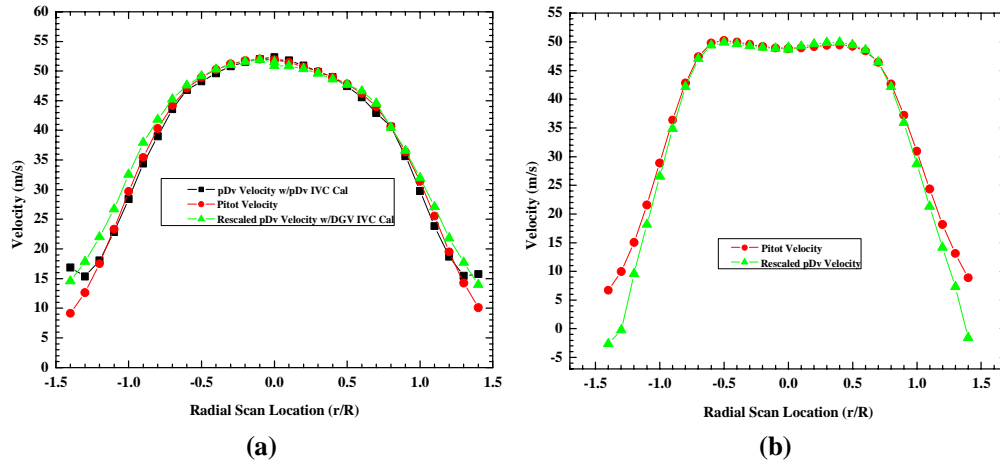

(a)   **(b)**

Figure 5-32 – Results of scaling data to correct for flat-field mismatches.

c. *PMT Saturation*

During pDv spectral measurement characterization tests, the performance of the system PMTs was investigated due to concerns about the high noise floor and unacceptable standard deviation levels in resolved velocities. In these studies, the PMT output signal, in response to light originating from an LED, was measured in order to establish saturation levels based on energy output as a function of time. It was observed that the output of the PMTs remained linear as the intensity of the LED was increased until the PMT reached steady state saturation at ~2.0 VDC output.

Further testing with dynamic signals was required because the light scattered by particles passing through the pDv sample volume is a combination of a dynamic component (occasional large particles) riding on top of a DC component (many smaller particles). To determine if the PMT saturation level remained at the same voltage under particle scattering conditions, the LED was driven with squared pulses of various widths and duty cycles with the PMT output being monitored on a digital oscilloscope. It was observed that as the pulse duty cycle was decreased, the magnitude of the voltage applied to the LED could be increased to supply more light to the PMT before saturation occurred. This sequence was continued until the peak of the PMT output pulse was no longer flat. This dynamic saturation occurred when the voltage reached levels much higher than the 2 V limit found at steady state. Since the levels appeared to correlate with pulse length, it seemed that energy limits were defining the saturation point. Integration of acquired data samples found that saturation occurred at the energy level of 2.5 V/ms.

The non-linear behavior exhibited by the PMTs under dynamic light input was caused by photoelectron depletion, which changed the quantum efficiency (QE) of the PMT, as the intensity of the impinging light increased beyond saturation. The QE of a PMT, a wavelength dependent quantity, is a measure of the probability that an incident photon will cause a photoelectron to be released (normally expressed as a percentage). The QE was found to be constant when the incident light levels were low. However, if the intensity of the impinging light exceeds the device threshold, the QE is compromised. When the detector encroaches upon saturation, it behaves non-

linearly because it can no longer produce the same number of photoelectrons for a given number of incident photons. This limitation is the result of the inability of the employed power supplies to provide sufficient current to generate the photoelectrons needed to maintain a constant QE at high incident photon rates. Having gained a better understanding of the response characteristics of the PMTs, the raw voltage levels for the first pDv data set acquired at the x/D = 2 location (Figure 5-22), were reexamined to determine if saturation was the cause of the observed behavior. This data set was selected since no signal conditioning circuitry, other than a 10K-load resistor, required to convert the PMT current output to a voltage, was installed between the PMTs and the DAQ board. This enabled the true response of the PMTs to be investigated without the influence of signal conditioning circuits used in later experiments. A running integration with time was performed on raw signal and reference records for the selected data set to determine if the energy exceeded the established saturation threshold. When the energy within the integration aperture (1 ms) was greater than 2.5 V/ms, it was eliminated from the statistical calculations. The resulting mean velocity values did not change significantly from the original results. Thus, of the potential error sources investigated, the contribution of laser frequency drift appears to be the major source of measurement errors.

Although PMT saturation was insignificant for mean measurements in the current investigations, it may be a major contributor to the noise floor presented in the spectra results. Knowledge that the PMT operation can become non-linear will be applied in future activities as a guide for adjusting the laser power and/or particle concentration to keep the PMTs operating below their saturation regions.

CHAPTER VI - CONCLUSIONS AND FUTURE WORK

The development of a one-component Point Doppler Velocimeter has been described and its ability to provide accurate and repeatable flow velocity and spectral measurements has been demonstrated. This level of capability was achieved through a methodical sequence of tests. By overcoming several significant obstacles, it was possible to design a collection of tightly integrated hardware and software elements into a system capable of measuring the velocity of a rotating wheel and the velocity of particles exiting a two-inch pipe. Further research will be required however to improve system reliability before the instrument can be deployed in flow research facilities.

A modify/test/analyze approach was employed to construct the system incrementally by combining the technologies and the physics that form the basis of Laser Velocimetry (LV), Particle Image Velocimetry (PIV) and Doppler Global Velocimetry (DGV) with modern signal processing methodologies. This model made it possible to identify and minimize systemic error sources, by assessing the capabilities and limitations of each hardware element using known signal sources, prior to its incorporation into the system. The same paradigm was followed in the development of the required software packages. The functionality of this software was verified in parallel with the testing of individual hardware components, managing velocity measurement experiments and the reduction of output voltage samples into flow related measurements.

Development of instrumentation systems of the magnitude of pDv would be a tedious and difficult process without the use of software to automate data collection and processing. Accordingly, this portion of the research was the most time consuming aspect of the project since the pDv instrument is approximately ninety-percent software. This effort did not consist solely of authoring working code, but also of validating its operation through the rigorous testing conducted while maturing the measurement capabilities of the instrument.

Custom software elements produced during the course of pDv research addressed the requirements for component and system control, and data collection and reduction. This was achieved in a manner that provided the flexibility needed to accommodate system modifications during the evolution of the instrument. To support the level of functionality required in the pDv instrument, software was developed at several levels. This included using a schematic like drawing environment to program the FPAA used in the pDv integrator and developing C language programs for algorithm development and verification and offline data analysis. The ensemble of custom software elements and device drivers were then integrated into a cohesive, easy-to-use package created in the LabVIEW programming environment. The modular approach to the software made the transition from research versions to production level software straightforward. The developed software packages proved to be reliable and stable throughout the operating envelope of the instrument.

Developed software was segregated into two distinct standalone packages that served the two functions of data acquisition and data processing. The primary operations provided in the data acquisition module focused on managing the various hardware components, during the course of testing. Along with acquiring the data samples obtained from these components the software also displayed the data graphically and archived the results for off-line analyses. The data processing package was designed to convert raw voltage samples into flow velocity and turbulence quantities during off-line processing. Resolved measurement data was presented to the user in an easy-to-interpret graphical format and placed in permanent storage.

By leveraging two of the primary strengths of LabVIEW, its instrumentation interfacing and signal processing capabilities, it was possible to rapidly bring the requisite software online. Custom procedures were developed by integrating well-tested functions within the LabVIEW libraries and manufacturer supplied hardware drivers with custom algorithms. Prior to incorporating "off the shelf" library routines into the system, their functionality was verified to determine if they satisfied pDv instrument requirements. Routines not providing the desired functionality were discarded and replaced with customized functions. During operation, the developed software was controlled via

production quality Graphical User Interfaces (GUIs) that were created with controls provided in LabVIEW.

The process of developing a system that was capable of achieving the reliability and measurement accuracies of instruments, considered as flow measurement standards was not straightforward. Problems with iodine vapor cell (IVC) calibration, laser frequency stability, and detector performance slowed system progress and compromised measurement accuracy. Nonetheless, the instrument, which was very unstable initially, was matured to the point that it provided velocity measurements comparable to those obtained with a pitot probe in a two-inch pipe flow.

Before investigating the velocity measurement capabilities of the pDv instrument, a calibration describing the light attenuation to optical frequency transfer function of the iodine vapor cells (IVCs) was required. These calibrations, which quantify the Doppler shift in the original laser light, were developed in a piecewise manner using a rotating wheel, since the absolute optical frequency of the laser light was not easily measured. The wheel induced a known Doppler shift in the frequency at the point where the laser light impinged on the surface of the wheel. The Doppler shifted light was collected by the pDv measurement component and sampled. Collected data sets were then correlated with the frequency shifts computed for each scan location to develop the calibration tables.

The ability of pDv to make velocity measurements was first assessed by using the instrument to measure the velocity of a rotating wheel, which provided two measurement standards of time and distance. Initially, feedback from these investigations was used to refine IVC calibrations. Once an acceptable level of confidence in the calibrations was attained, data collection activities were initiated and pDv resolved velocities were compared to theoretical values based on scan position and rotational speed measurements. This activity, which was also a crosscheck of the IVC calibrations, provided average velocity measurements along the vertical diameter of the wheel, that differed from the computed velocities by less than 1 m/s.

The progression of using pDv to measure the velocity of a rotating wheel, to the measure of smoke particles within a fully developed, turbulent pipe flow, proved to be challenging. Simultaneous acquisition of pDv and pitot probe data at the investigated flow locations enabled average pDv velocity measurements to be compared with an accepted flow velocity measurement standard. Initial measurements were inconsistent, deviating unpredictably from the pitot probe results. Feedback from these experiments helped to identify three primary error sources; (a) Argon Ion laser frequency instability caused by temperature fluctuations and vibrations, (b) measurement offsets resulting from IVC and flat field calibration mismatches, and, (c) photomultiplier saturation.

Laser frequency fluctuations limited the accuracy and repeatability of resolved velocities. An example of this problem can be seen in Figure 5-22, where the two velocity measurements made at the centerline flow position during the same experiment differed by 4 m/s. To diminish the effects of this problem, a closed-loop, laser frequency drift minimization system was developed. This improved velocity measurement repeatability and yielded flow profiles that matched that of the pitot probe. However, the system sometimes exhibited a uniform offset from the pitot probe values. The observed offset, on the order of 3 m/s, was at first attributed to two inaccuracies in the IVC calibrations. First, the calibrations developed for the IVCs residing in the measurement component and the Laser Frequency Monitor (LFM) did not overlay each other exactly, a direct cause of errors in Doppler frequency resolution. The second limitation was that the developed calibrations did not represent the true absorption profile for the IVCs with the precision required to make accurate velocity measurements.

As a means of verifying that the IVC calibrations were the source of the observed measurement offset, calibrations for the IVCs, developed using the DGV method were applied. It was hypothesized that the velocity measurements would be improved for two reasons. First, each calibration segment used to develop the DGV calibrations is created from a collection of tightly packed pixels. This provides better spatial resolution and eliminates uncertainties in laser beam positioning on the wheel surface, which improves segment-to-segment overlap accuracy. Secondly, since the time required to collect data for each segment is short, the effects of laser drift are

minimized. The average velocity measurements obtained by applying the DGV generated calibrations (Figure 5-30) were about 5.25 m/s faster than those measured using pDv calibrations. These results suggested that something else was causing the errors in the resolved measurements.

Upon reviewing the results of applying the DGV IVC calibrations, the entire pDv instrument – hardware and software inclusive was examined to search for the cause of the induced bias. Since the bias was nearly uniform, the flat-field correction factor was suspected. If the flat-field factor used to scale the velocity data sets was not the same as the flat field factor used to produce IVC calibration data, a bias would be present in the resolved velocity data sets. This problem and the method used to verify that flat-field mismatch was the source of observed problems, was presented in Section 5.B.7.b.

The ability of the pDv instrument to quantify the spectral components of a flow was also investigated and the results were compared to measurements obtained using a hot-wire, an accepted standard for measuring flow turbulence quantities. Spectral data obtained using both techniques clearly showed the same frequency spikes at 355- and 710-Hz, which were induced by the blower driving the pipe – confirmation that pDv was capable of measuring turbulence spectral quantities. A limitation in the pDv results however, was related to the high magnitude of the broadband noise floor, which limited the measurement dynamic range.

Through a methodical process of problem identification and resolution, a pDv system has been developed that fulfills many of the promises of its underlying physics. Additional work is required however to improve measurement accuracy and system reliability. Several areas such as improving online data processing, IVC calibrations, PMT saturation monitoring and sampling phase mismatch will be investigated further to determine if the technology can be improved.

The functionality provided in the developed software packages simplified the operation of the pDv instrument through an easy to use interface. This enabled research time to be focused on improving system measurement capability and not on support processes. Offline data processing procedures to provide feedback that guided follow-on research after-the-fact, is a limitation. Future software development will concentrate on combining data acquisition and processing procedures to provide the researcher with real-time feedback that can be used to guide research activities and in-situ production testing.

An improvement in IVC calibration accuracy may be possible using an alternative calibration method developed by Lee & Meyers (2005). This scheme used Acousto-Optic Frequency Shifters (AOFS) or Bragg cells to map the transfer function of an IVC directly instead of with a rotating wheel. This approach is preferred, since it produces a known and repeatable offset in the original laser frequency and a bandwidth sufficient to map the top, bottom and gap regions of the iodine absorption band (Figure 1-2). Further, the overlapped regions were found to be less disjointed.

The use of integration techniques has proven to minimize PMT saturation and sampling phase bias effects. Research will continue in this area to advance the operation of the pDv integrator by extending its dynamic range and sampling speed. An alternative method under consideration will use a high-speed digitizer to sample the PMT outputs at a high rate, sub-sampling the digitized record to a user defined size, and then applying software integration techniques to resolve the measurements. The primary objective of this work will be to determine if the noise floor in pDv spectral measurements can be reduced.

The advances made in pDv technology by the described research has led to its selection as the method to measure the flow angle of cryogenic nitrogen, as it enters the
2.5 m x 2.5 m test section of the NASA Langley Research Center National Transonic Wind Tunnel (NTF). Currently no technique exists which can provide this critical information for a semi-span model. Optical fibers will be used to transmit laser light into and receive scattered light from the test section in order to keep the optical system outside of the cryogenic environment.

APPENDIX A - THE DOPPLER EFFECT

1. The Doppler Effect and Sound

The Doppler effect describes the shift in tone that occurs with the relative motion between a radiating source and an observer, which was first explained by Christian Doppler in 1842 (Davidson, 2004). This phenomenon is represented in Figure A-1, where the sound waves produced by a moving train's whistle impinge on the ears of Al, Bob and Carl, who are standing at three different positions relative to the train's direction of travel. As shown, the train is moving away from Al and towards Bob and Carl. Note that the distance between the successive sound waves that impinge on Al's ears is greater than the distance between wave fronts impinging on the ears of both Bob and Carl. The distance between these waves is called the *wavelength* and the rate of arrival of successive waves is referred to as *frequency*. As the train gets closer to Bob, sound waves produced by the train's whistle bunch up so Bob detects a higher pitched sound, since the wavelength is decreasing and the wave fronts impinge on his ears at a higher frequency. In the same manner as Bob, Carl also perceives an increase in pitch, however it differs from that heard by Bob since he is standing at a location that makes an angle, θ, relative to the oncoming train. Meanwhile, Al observes the opposite effect, since the train is moving away from him and the wave fronts become more spread out. The pitch of the train's whistle sounds lower to Al, since the wavelength is increasing and the wave fronts are detected at a lower frequency.
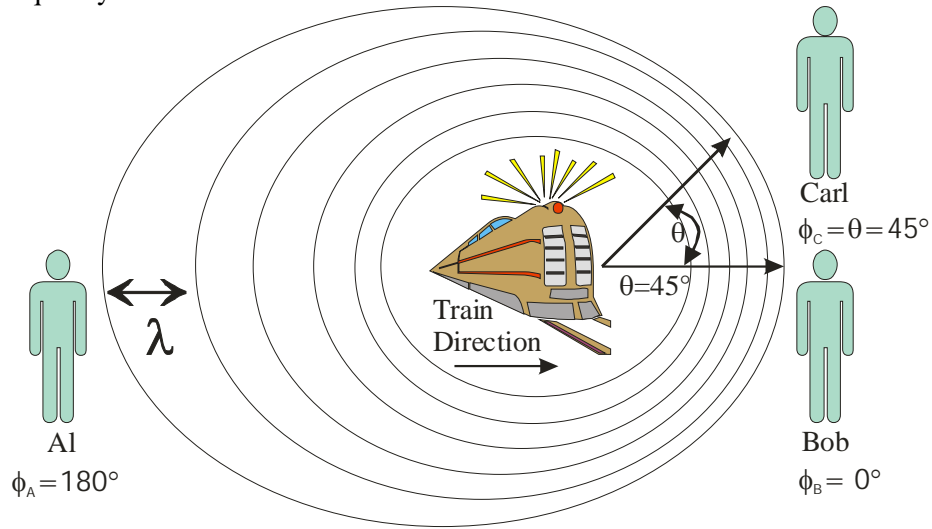

Figure A – 1 – Diagram depicting the travel of sound waves produced by a moving train's whistle.

Changes in pitch are observed whenever a source or an observer move with respect to each other as follows: a) when the sound source moves towards/away from the observer; b) when the observer moves towards/away from the sound source; and, c) when both the sound source and the observer move towards/away from each other (Young, 1992).

In order to compute the change in pitch, Δf, detected by an observer, the frequency, f_O, of the arriving sound waves must be determined. To establish f_O, consider the case where a stationary observer, such as Bob, in Figure A-1, is at a location directly in front of the oncoming train. The relationship between the frequency of the sound emitted by the train's whistle and the pitch detected by the stationary observer is:

$$f_S v_{SM} t = \left(v_{SM} - \left| \vec{V}_S \right| \right) f_O t \qquad (A.1)$$

Where:

f_S the frequency of the sound source

v_{SM} velocity of sound in the medium

t time period of consideration

$\left|\vec{V}_S\right|$ velocity magnitude of the sound source

f_O frequency of sound detected by the observer

Rearranging Equation A.1 yields the equation for f_O, the frequency detected by the observer:

$$f_O = \frac{f_S v_{SM}}{v_{SM} - \left|\vec{V}_S\right|} \tag{A.2}$$

In addition, as shown in Figure A-1, the changes in pitch, such as those observed by Carl, will be different as the angular position of the observer with respect to the sound source changes. Taking into consideration the angular displacement between the source and the observer, ϕ_O, Equation A.2 can be rewritten to determine the frequency of the sound waves reaching an observer regardless of the direction the source travels in with respect to the observer:

$$f_O = \frac{f_S v_{SM}}{v_{SM} - \left|\vec{V}_S\right|\cos\phi_O} \tag{A.3}$$

Equation A.3 can be applied to the situations of Figure A-1 to determine the frequency of the pitch detected by Al, Bob and Carl. First, consider, f_A, the frequency observed by Al who is located at a position where $\phi_A = 180°$ relative to the train's direction of travel:

$$f_A = \frac{f_S v_{SM}}{v_{SM} - \left|\vec{V}_S\right|\cos 180°} = \frac{f_S v_{SM}}{v_{SM} + \left|\vec{V}_S\right|} \tag{A.4}$$

Recognize (in Equation A.4) that the frequency, f_A, detected by Al will decrease as the train moves away.

Next, consider Bob, who is located at position $\phi_B = 0°$ relative to the approaching train:

$$f_B = \frac{f_S v_{SM}}{v_{SM} - \left|\vec{V}_S\right|\cos 0°} = \frac{f_S v_{SM}}{v_{SM} - \left|\vec{V}_S\right|} \tag{A.5}$$

As shown in Equation A.5, when the train moves towards Bob, an increase in the frequency, f_B, will be observed.

Lastly, the frequency, f_C, observed by Carl, who is standing at a location that makes an angle of $\theta = 45°$ with the approaching train is determined.

For $\phi_C = 45$-degrees, f_C is:

$$f_C = \frac{f_S v_{SM}}{v_{SM} - \left|\vec{V}_S\right|\cos 45°} = \frac{f_S v_{SM}}{v_{SM} - 0.707\left|\vec{V}_S\right|} \tag{A.6}$$

Thus, Carl observes an increase in frequency, f_C, since he is also in front of the train. However, the frequency, f_C, is less than that observed by Bob, f_B, since he is located at an angular position of 45°. Note here that as the train continues towards its destination, the angle, θ, between the train and Carl will increase to 90°, where $f_C = f_S$, and then onward where θ increases to 180° and $f_C => f_A$.

Another relationship that must be considered when discussing the Doppler effect is that of an observer who is moving relative to a stationary sound source. This scenario is depicted in Figure A-2, where Don is changing position with respect to the sound source, S. Don will detect a change in pitch as he moves towards/away from the sound source in the vector direction î. In addition, note Ed, who is at vector location, ô with respect to Don. The sound observed by Ed is that of the sound waves produced by the stationary source as they deflect off Don. Thus as Don moves around, Ed, too, will detect changes in pitch.
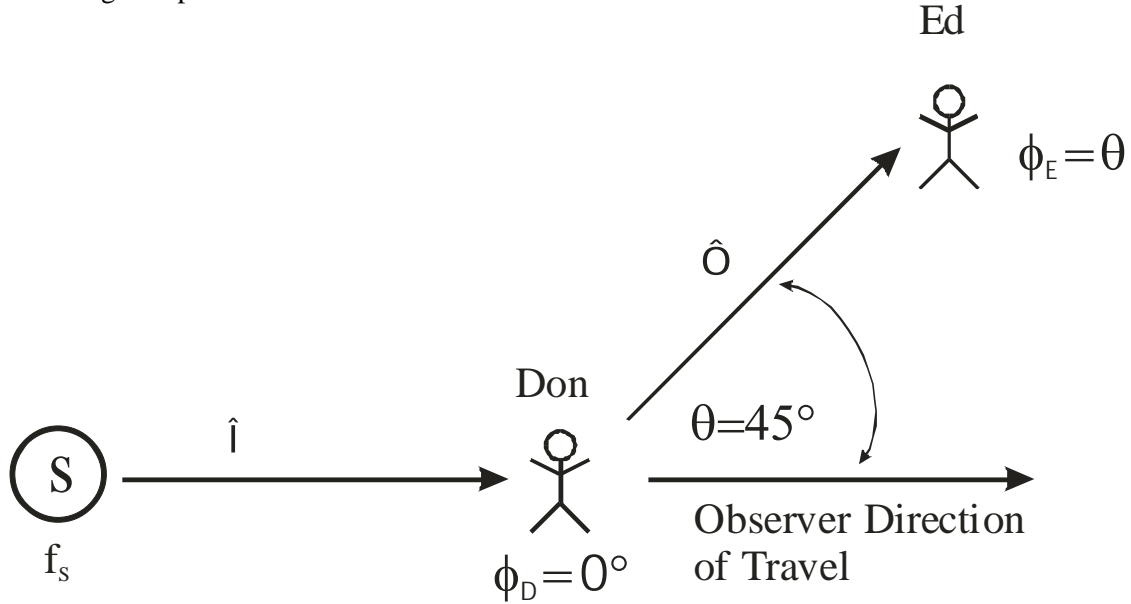

Figure A – 2 – Vectorial depiction of direction of travel of sound waves produced by a stationary source, S, towards moving observer Don in direction î and those deflecting off of Don towards stationary observer Ed in direction ô.

The relationship between the frequency perceived by the moving observer and the stationary sound source is:

$$f_O v_{SM} t = \left(v_{SM} - \left| \vec{V}_O \right| \right) f_S t \tag{A.7}$$

By rearranging Equation A.7, the formula for determining the frequency detected by the moving observer, f_O, becomes:

$$f_O = \frac{f_S \left(v_{SM} - \left| \vec{V}_O \right| \right)}{v_{SM}} \tag{A.8}$$

As with Equation A.3, Equation A.8 can be modified to accommodate the angular displacement between the source and the observer, ϕ_O :

$$f_O = \frac{f_S \left(v_{SM} - \left| \vec{V}_O \right| \cos \phi_O \right)}{v_{SM}} \tag{A.9}$$

Equation A.9 can be applied to the case presented in Figure A-2 to determine the frequency perceived by the observer regardless of the direction of travel. First, consider the case of the frequency observed by Don who moves away from the sound source in angular direction $\phi_D = 0°$:

$$f_D = \frac{f_S \left(v_{SM} - \left| \vec{V}_D \right| \cos 0 \right)}{v_{SM}} = \frac{f_S \left(v_{SM} - \left(\left| \vec{V}_D \right| * 1 \right) \right)}{v_{SM}} \tag{A.10}$$

From Equation A.10 it can be seen that as Don moves away from the sound source, he perceives a decrease in frequency f_D.

If Don moves towards the sound source, in angular direction $\phi_D = 180°$ he detects an increase in frequency, f_D:

$$f_D = \frac{f_S \left(v_{SM} - \left| \vec{V}_D \right| \cos 180 \right)}{v_{SM}} = \frac{f_S \left(v_{SM} - \left(\left| \vec{V}_D \right| * (-1) \right) \right)}{v_{SM}} \tag{A.11}$$

Next, consider the frequency of the sound, f_E, observed by Ed, who is in a stationary position and hears the sound of the source after it has been deflected off Don in angular direction, $\phi_E = \theta = 45°$. To accommodate this situation, Equation A.3 is modified to make Don the sound source:

$$f_E = \frac{f_D v_{SM}}{v_{SM} - \left| \vec{V}_D \right| \cos \phi_E} \tag{A.12}$$

Substituting Equation A.9 for f_D, A.12 becomes:

$$f_E = \left[\frac{v_{SM}}{v_{SM} - \left| \vec{V}_D \right| \cos \phi_E} \right] * \left[\frac{f_S \left(v_{SM} - \left| \vec{V}_D \right| \cos \phi_D \right)}{v_{SM}} \right] \tag{A.13}$$

which simplifies to:

$$f_E = \left[\frac{f_S \left(v_{SM} - \left| \vec{V}_D \right| \cos \phi_D \right)}{v_{SM} - \left| \vec{V}_D \right| \cos \phi_E} \right] \tag{A.14}$$

With the frequency of the observer established, the Doppler shift frequency, Δf, can be determined:

$$\Delta f = f_O - f_S \tag{A.15}$$

Applying Equation A.15 to the situation depicted in Figure A-2, the Doppler shift frequency is:

$$\Delta f = f_E - f_S \tag{A.16}$$

Substituting Equation A.14 (f_E) into Equation A.16:

$$\Delta f = \left[\frac{f_S \left(v_{SM} - \left| \vec{V}_D \right| \cos \phi_D \right)}{v_{SM} - \left| \vec{V}_D \right| \cos \phi_E} \right] - f_S \tag{A.17}$$

and thus:

$$\Delta f = f_S \left[\frac{\left(\left| \vec{V}_D \right| \cos \phi_E - \left| \vec{V}_D \right| \cos \phi_D \right)}{v_{SM} - \left| \vec{V}_D \right| \cos \phi_E} \right] \tag{A.18}$$

An alternate method for determining the frequency detected by an observer is through the application of unit vectors to describe the direction of travel of sound waves. Unit vectors can be substituted for angular quantities using the following relationship:

$$\vec{V}_S \bullet \hat{i}_O = \left| \vec{V}_S \right| \left| \hat{i}_O \right| \cos \phi \tag{A.19}$$

Applying this relationship to the activities of Don and Ed in Figure A-2, the angular relationship of Don who is moving with respect to the stationary sound source in vector direction $\hat{i}$, can be expressed in terms of vectors as:

$$\vec{V}_S \bullet \hat{i} = \left|\vec{V}_S\right|\left|\hat{i}\right|\cos\phi_D \tag{A.20}$$

Likewise, the vectorial relationship for Ed who detects the sound from the source after it deflects off Don in vector direction $\hat{o}$ is:

$$\vec{V}_S \bullet \hat{o} = \left|\vec{V}_S\right|\left|\hat{o}\right|\cos\phi_E \tag{A.21}$$

Substituting vectorial quantities into Equation A.18 the Doppler shifted frequency can be determined by:

$$\Delta f = f_S\left[\frac{\left[\left(\vec{V}_D \bullet \hat{o}\right) - \left(\vec{V}_D \bullet \hat{i}\right)\right]}{\nu_{SM} - \left(\vec{V}_D \bullet \hat{o}\right)}\right] \tag{A.22}$$

which reduces to:

$$\Delta f = f_S\left[\frac{\vec{V}_D \bullet \left(\hat{o} - \hat{i}\right)}{\nu_{SM} - \left(\vec{V}_D \bullet \hat{o}\right)}\right] \tag{A.23}$$

2. The Doppler Effect and Light

The Doppler effect, commonly associated with sound waves, also holds true for electromagnetic sources such as light and radio waves. As applied to light waves, the Doppler effect is sometimes referred to as the Fizeau effect, after Armand Fizeau, who is credited with being the first person to develop a reliable method for measuring the speed of light. (Davidson, 2004).

The equations relating the Doppler effect as applied to sound can also be used to determine the shift in light frequency that occurs with the motion of a light source and a detector. Since the source of the radiation is light, the speed of sound in the medium is replaced with the speed of light represented by c. In addition, when discussing light, the symbol typically used to represent frequency is ν. Equation A.18 which is used to compute the Doppler shift in sound, can be modified for determining light frequency as:

$$\Delta\nu = \nu_S\left[\frac{\left(\left|\vec{V}_D\right|\cos\phi_E - \left|\vec{V}_D\right|\cos\phi_D\right)}{c - \left|\vec{V}_D\right|\cos\phi_E}\right] \tag{A.24}$$

Further, since the speed of light is many times faster than the moving object:

$$c \gg \left|\vec{V}_D\right|\cos\phi \tag{A.25}$$

The velocity of the object is negligible in the denominator, and Equation A.24 is rewritten as:

$$\Delta\nu = \nu_S\left[\frac{\left(\left|\vec{V}_D\right|\cos\phi_E - \left|\vec{V}_D\right|\cos\phi_D\right)}{c}\right] \tag{A.26}$$

or, in terms of unit vectors:

$$\Delta\nu = \nu_S\left[\frac{\vec{V}_D \bullet \left(\hat{o} - \hat{i}\right)}{c}\right] \tag{A.27}$$

By convention, light waves are typically explained in terms of wavelength, which is inversely proportional to frequency:

$$\lambda_S = \frac{c}{\nu_S} \qquad \text{(A.28)}$$

Expressing Equation A.27 in terms of wavelength, λ:

$$\Delta \nu = \left[\frac{\vec{V}_D \bullet (\hat{o} - \hat{i})}{\lambda_S} \right] \qquad \text{(A.29)}$$

3. Applying the Doppler Effect to Measure Particle Velocities

The Doppler effect associated with light has been employed to measure particle velocities as this phenomenon is also observed, when a laser source and a light detector maintain stationary positions and particles pass through a laser light beam or sheet. Transitory particles scatter the laser light, resulting in a change in the wavelength or frequency of light waves impinging on a detector, as depicted in Figure A-3.
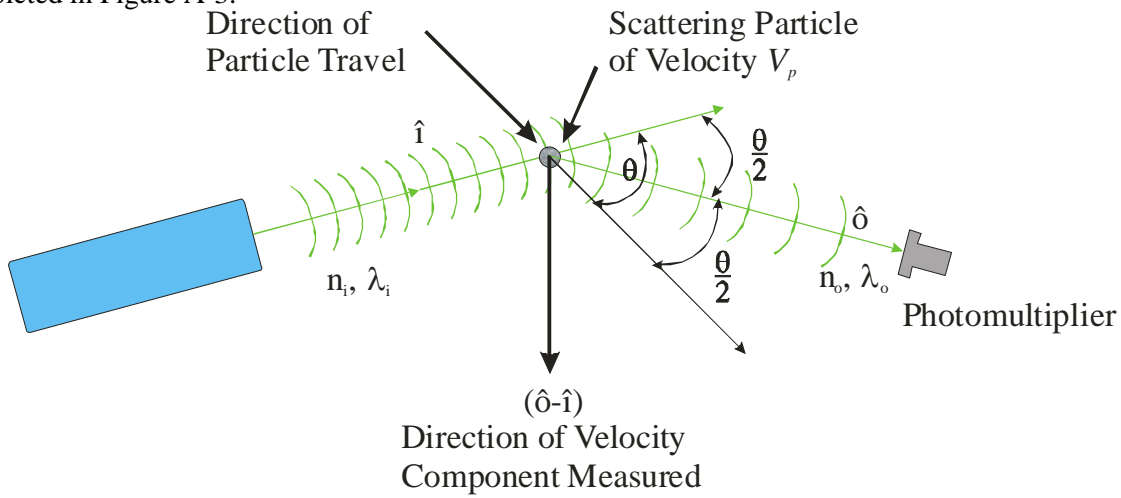
Figure A – 3 – Depiction of the interaction of wave fronts emitted by a stationary laser in direction î with a moving particle.

The manner in which these particle velocity measurements are made is best presented by first describing the interaction of the particle with the emitted laser light and then explaining the detection of the particle scattered light by the photomultiplier. In Figure A-3, light, of wavelength of λ_i, emitted by a laser, impinges on a particle moving at velocity V_p; a scenario that is identical in principle to that depicted in Figure A-2. Relating the components in Figure A-2 and Figure A-3; the laser replaces the sound source as the wave front generator, the particle replaces the moving observer, Don, and the photomultiplier tube (PMT) replaces the stationary observer, Ed. Rewriting Equation A.29 to represent the Doppler shift observed at the PMT:

$$\Delta \nu = \left[\frac{\vec{V}_P \bullet (\hat{o} - \hat{i})}{\lambda_L} \right] \qquad \text{(A.30)}$$

Where:

$\vec{V}_P$ velocity of the moving particle

$\hat{i}$ unit vector direction of laser light wavefronts towards particle

$\hat{o}$ unit vector direction of scattered laser light wavefronts towards PMT

λ_L the wavelength of the laser light source

APPENDIX B - LabVIEW WIRING DIAGRAMS

This appendix presents a sampling of the many wiring diagrams implementing the custom functions developed to support the user controls presented on the user interface diagrams presented in Chapter 4.
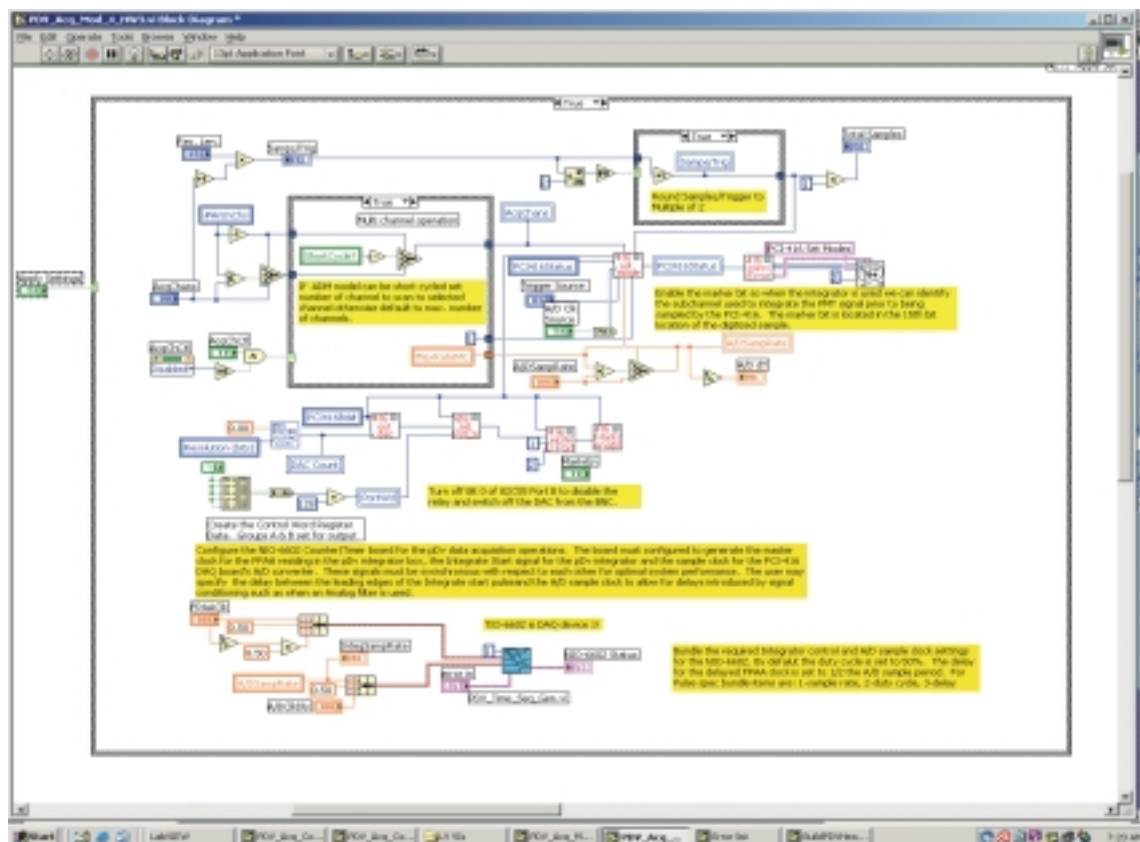

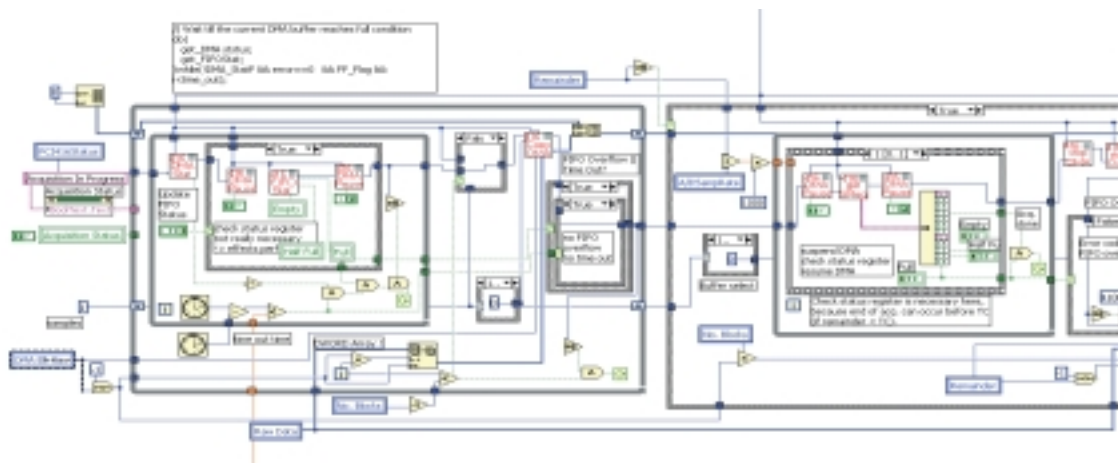**Figure B – 1 – Wiring diagram of pDv hardware initialization operations.**

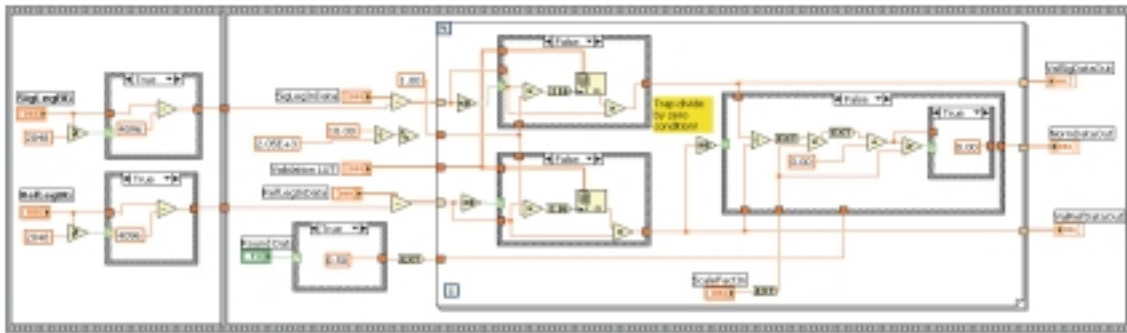**Figure B – 2 – Wiring diagram of pDv data acquisition operations.**

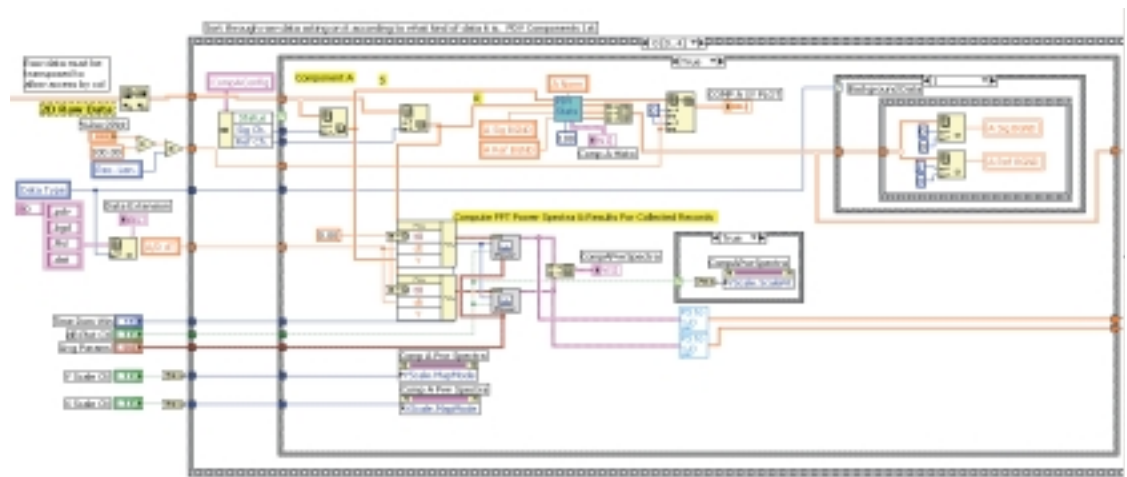**Figure B – 3 – Wiring diagram of pDv data normalization operation.**

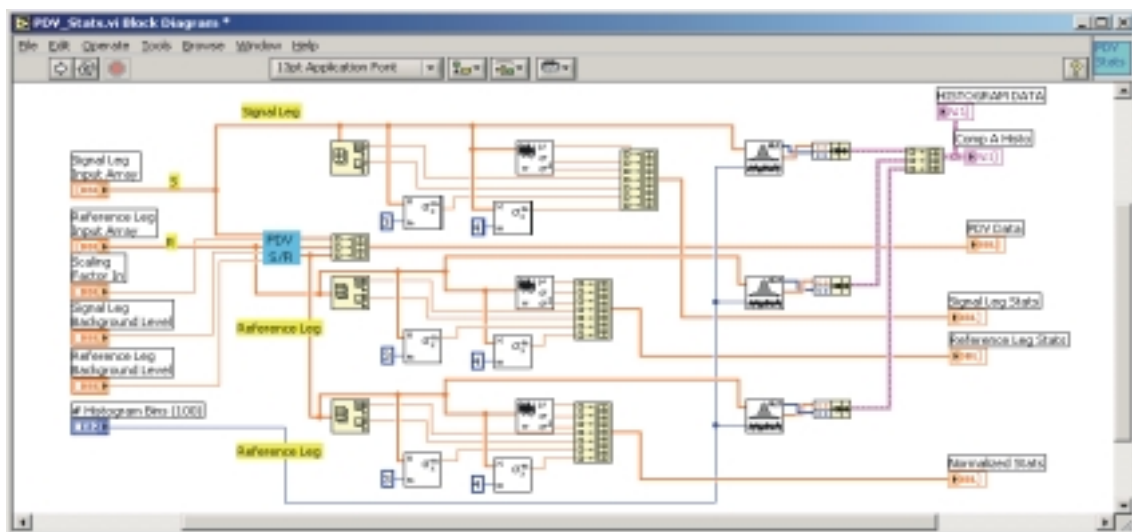**Figure B – 4 – Wiring diagram online data presentation operations.**

Figure B – 5 – Wiring diagram of the pDv statistical data generation process.
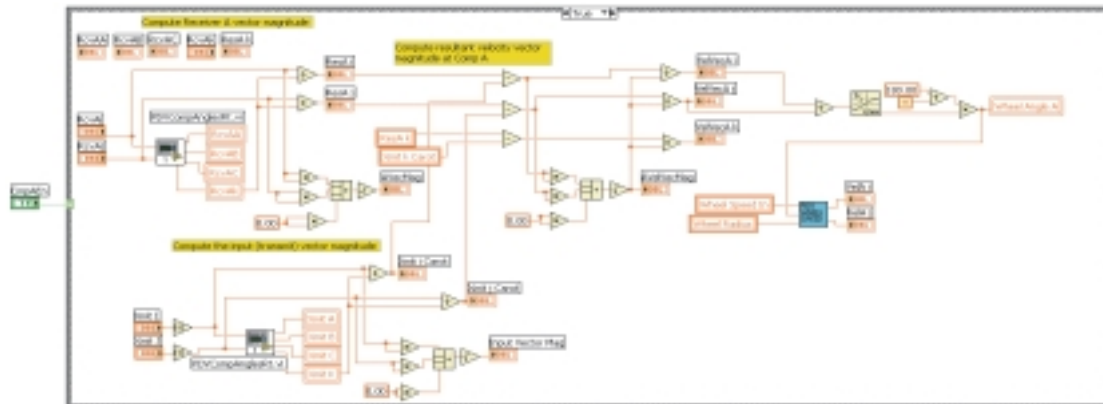
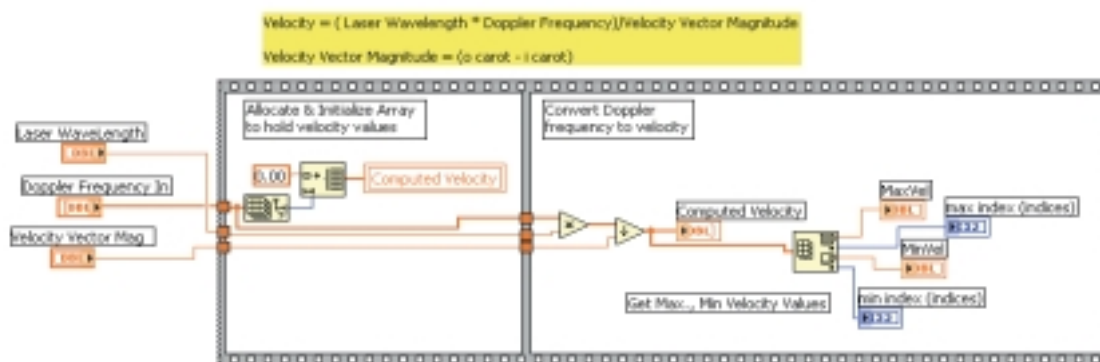**Figure B – 6 – Wiring diagram of pDv velocity vector determination.**

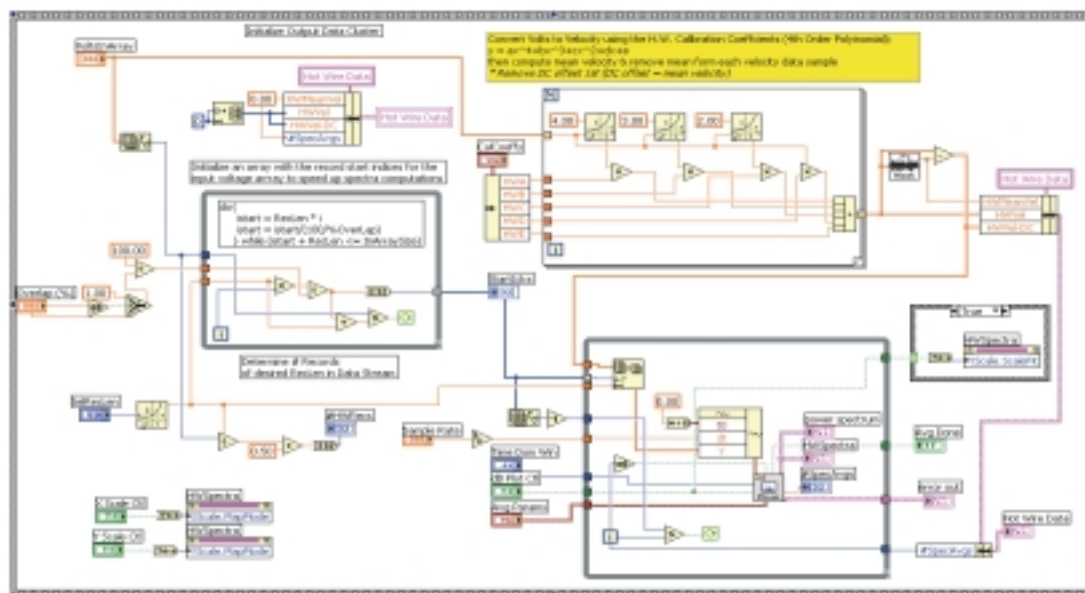**Figure B – 7 – Wiring diagram of pDv velocity data computation procedure.**

Figure B – 8 – Raw voltage data to HW velocity/spectra data conversion process.

REFERENCES

Adrian, R.J. and Yao, C.S., "Development of Pulsed Laser Velocimetry for Measurement of Turbulent Flow," *Proceedings of the 8th Biennial Symposium on Turbulence*, Univ. of Missouri, Rolla, pp. 170-186,1983.

Asher, J.A., "Laser Doppler Velocimeter System Development and Testing," *Symposium on Instrumentation for Airbreathing Propulsion*, Naval Postgraduate School, Monterey, California, September 19-21, 1972.

Baker, G.D., Meyers, J.F., and Murphy, R.J., "An Adaptive LDV Signal Processor," *Proceedings of the Fourth International Symposium on Applications of Laser Anemometry to Fluid Mechanics*, Lisbon, Portugal, paper 22.5, July 11-14, 1988.

Beutner, T.J., Elliott, G.S., Williams, G.W., Baust, H.D., Crafton, J., Carter, C.D., "Forebody and Leading Edge Vortex Measurements Using Planar Doppler Velocimetry," *Measurement Science Technology*, pp. 378-394, January 2001.

Brayton, D.B., Goethert, W.H., "A New Dual Scatter, Laser, Doppler Shift velocity Measuring Technique," *Instrumentation in the Aerospace Industry*, Vol 16, pp 14-26, 1970.

Brayton, D.B., Kalb, H.T., and Crosswy, F.L., "A Two-Component, Dual-Scatter Laser Doppler Velocimeter with Frequency Burst Signal Readout," *Project Squid Workshop on The Use of the Laser Doppler Velocimeter for Flow Measurements*, Purdue University, March 9-10, 1972.

Cavone, A.A., Sterlina, P.S., Clemmons, J.I., Jr., and Meyers, J.F., "A High Speed Buffer for LV Data Acquisition," *Proceedings of the 12th International Congress on Instrumentation in Aerospace Simulation Facilities*, College of William and Mary, Williamsburg, VA, June 22-25, 1987, pp. 113-120.

Clemmons, J.I., Jr., "Laser Velocimeter Autocovariance Buffer Interface", *NASA TM 83110*, May 1981.

Davidson, M.W., "Molecular Expressions: Science, Optics, and You – Timeline- Christian Doppler" (The Florida State University, 1995-2004) [Online], available from http://micro.magnet.fsu.edu/optics/timeline/people/doppler.html (accessed 25 February 2004).

Davidson, M.W., "Molecular Expressions: Science, Optics, and You – Timeline- Armand Fizeau" (The Florida State University, 1995-2004) [Online], available from http://micro.magnet.fsu.edu/optics/timeline/people/fizeau.html (accessed 25 February 2004).

Fleming, G.A., Editor, "Unified Instrumentation: Examining the Simultaneous Application of Advanced Measurement Techniques for Increased Wind Tunnel Testing Capability," *22nd AIAA Aerodynamic Measurement and Ground Testing Conference*, St. Louis, Missouri, June 24-26, 2002.
Foreman, J.W., Jr., George, E.W., and Lewis, R. D., "Measurement of Localized Flow Velocities in Gases with a Laser Doppler Flowmeter," *Applied Physics Letters*, Vol. 7, No. 77, pp. 77-78, August 1965.

Forkey, J.N., "Development and Demonstration of Filtered Rayleigh Scattering – A Laser Based Flow Diagnostic for Planar Measurement of Velocity, Temperature and Pressure," *Princeton University Department of Mechanical and Aerospace Engineering Technical Report 2067*, 1996.

Friedman, J.D., Meister, K.A. and Young,R.M. "Wide Band Frequency Trackers in Laser Doppler Velocimeter Systems," *ISA - 17th National Aerospace Instrumentation Symposium*, Las Vegas, Nevada, May 10-12, 1971.

Goldstein, R.J., and Kreid, D.K., "Measurement of Laminar Flow Development in a Square Duct Using a Laser Doppler Flowmeter," *Journal of Applied Mechanics*, Item 32, Series E, pp. 813-818, December 1967.

Grant, G.R., and Orloff, K.L., "Two-Color Dual-Beam Backscatter Laser Doppler Velocimeter," *Applied Optics*, Vol. 12, No. 12, pp. 2913-2916, December 1973

Hoffenberg, R., and Sullivan, J.P., "Filtered Particle Scattering: Laser Velocimetry Using an Iodine Filter," *ASME-FED*, Vol. 161, pp. 135-8, June 20-24, 1993.

Humphreys, W.M., Jr., "A Histogram-Based Technique for Rapid Vector Extraction from PIV Photographs," *Proceedings of the Fourth International Conference on Laser Anemometry – Advances and Applications*, Cleveland, Ohio, August 5-9, 1991.

Huffaker, R.M.; Fuller, E. E.; and Lawrence, T. R., "Application of Laser Doppler Velocity Instrumentation to the Measurement of Jet Turbulence," *International Automotive Engineering Congress*, 690266, January 13-17, 1969.

Jorgensen, F.E. "How to Measure Turbulence with Hot-Wire Anemometers – A Practical Guide," Dantec Dynamic Skovlunde, Denmark, 2002.

Komine, H., "System for Measuring Velocity Field of Fluid Flow Utilizing a Laser Doppler Spectral Image Converter," U.S. Patent No. 4,919,536, April 24,1990.

Kuhlman, J.M., and Scarberry, T., "Point Doppler Velocimeter (pDv) Jet Data Using Avalanche Photodiodes (APD's)," *22nd AIAA Aerodynamic Measurement and Ground Testing Conference*, St. Louis, Missouri, June 24-26, 2002.

Kuhlman, J.M., Burton, L., and Scarberry, T., "Doppler Global Velocimetry Data in Circular Jets," paper 6.3, presented at *IEEE 19th ICIASF Conference*, Cleveland, Ohio, 2001.

Kuhlman, J.M., Naylor, S., James, K., and Ramanath, S., "Accuracy Study of a 2 Component Point Doppler Velocimeter (pDv)," paper AIAA-97-1916, presented at *AIAA 28th Fluid Dynamics Conference*, Snowmass, Colorado, June29-July 2,1997.

Lennert, A.E., Brayton, E. B., Crosswy, F. L., "Summary Report of the Development of a Laser Velocimeter to be Used in AEDC Wind Tunnels," TR-70-101, 1970, Arnold Engineering Development.

Lennert, A.E., Brayton, D. B., Goethert, W. H., Smith, F. H., "Laser Applications for Flow Filed Diagnostics," *Laser Journal* March/April 1971.

Lennert, A.E., Smith, F. H., and Kalb, H. T., "Application of Dual Scatter, Laser Doppler Velocimeters for Wind Tunnel Measurements," *4th International Congress In Aerospace Simulation Facilities, von Karman Institute for Fluid Dynamics*, Rhode-Saint-Genese, Belgium, June 21-23, 1971

McKenzie, R.L. "Planar Doppler Velocimetry for Large Scale Wind Tunnel Applications," AIAA Paper 97-0498, presented at *35th Aerospace Sciences Meeting*, Reno, Nevada, January 1997.

Meyers, J.F., "Investigation and Calculations of Basic Parameters for the Application of the Laser Doppler Velocimeter," *NASA TN D-6125*, April 1971.

Meyers, J.F., "Biasing Errors and Corrections," *von Karman Institute for Fluid Dynamics, Lecture series 1991-08*, Brussels, Belgium, Laser Velocimetry, June 10-14, 1991.

Meyers, J. F., "Review of Typical Applications - Wind Tunnels," *von Karman Institute for Fluid Dynamics, Lecture series 1991-08*, Brussels, Belgium, Laser Velocimetry, June 10-14, 1991.

Meyers, J.F., "Doppler Global Velocimetry, The Next Generation?," presented at the *AIAA 17th Aerospace Ground Testing*, Nashville, TN, July 6-8, 1992.

Meyers, J.F.: "Doppler Global Velocimetry - The Next Generation?," AIAA *17th Aerospace Ground Testing Conference*, paper AIAA-92-3897, Nashville, TN, July 6-8, 1992.

Meyers, J.F.; Clemmons, J. I., Jr.; Stoughton, J. W.; Kanetkar, S. V.; and Savakis, A. E., "Frequency Domain Laser Velocimeter Signal Processor," United States Patent 4, 786, 168, November 22, 1988.

Meyers, J.F.; and Clemmons, J. I., Jr.: "Frequency Domain Laser Velocimeter Signal Processor - A New Signal Processing Scheme," *NASA TP-2735*, September 1987.

Meyers, J.F., Komine, H., "Doppler Global Velocimetry – A New Way to Look at Velocity," presented at *ASME Fourth International Conference on Laser Anemometry*, Cleveland, Ohio, August 3-9, 1991.

Meyers, J.F., Lee, J.W., "Identification and Minimization of Errors in Doppler Global Velocimetry Measurements," presented at 10th International Symposium on Applications of Laser Techniques to Fluid Mechanics, Lisbon, Portugal, July 10-13, 2000.

Meyers, J.F.; and Wilkinson, S.P.: "A Comparison of Turbulence Intensity Measurements Using A Laser Velocimeter and A Hot Wire In A Low Speed Jet Flow." *Proceedings of the International Symposium on Applications of Laser-Doppler Anemometry to Fluid Mechanics*, Lisbon, Portugal, paper 17.4, July 5-7, 1982.

Reinath, M.S., "Doppler Global Velocimeter Development for the Large Wind Tunnels at Ames Research Center," NASA Ames Research Center, *NASA TM-112210*, September 1997.

Roehle, I., Schodl, R., "Evaluation of the Accuracy of the Doppler Global Technique," *Proceedings of Optical Methods and Data Processing in Heat and Fluid Flow*, London, England, April 14-15, 1994.

Roehle, I., Schodl, R., "Applications of Three Dimensional Doppler Global Velocimetry to Turbo Machinery and Wind Tunnel Flows," *Proceedings, 7th Intl. Conf. On Laser Anemometry Advances and Applications*, pp.387-395, Karlsruhe, Germany, 1997.

Rudd, M.J., "A Self Aligning Laser Doppler Velocimeter," *ICO-8, Optical Instruments and Techniques*, Oriel Press, pp. 58-166, 1969.

Schodl, R., Willert, C., Roehle, I., Heinze, J., Foerster, W., Fischer, M., Beversdorff, M., "Optical Diagnostic Techniques In Turbomachinery," *22nd AIAA Aerodynamic Measurement and Ground Testing Conference*, St. Louis, Missouri, June 24-26, 2002.

Schodl, R., Roehle, I., Karpinsky, G., Foerster, W., Krain, H., "3-Component-Doppler-Laser-Two-Focus Velocimetry Applied to a Transonic Centrifugal Compressor," presented at *10th International Symposium on Applications of Laser Techniques to Fluid Mechanics*, Lisbon, Portugal, July 10-13, 2000.

Smith, M.W., "Application of Planar Doppler Velocimetry System to a High Reynolds Number Compressible Jet," AIAA Paper. 98-0428, *36th AIAA Aerospace Sciences Meeting and Exhibit*, Reno, Nevada, January 12-15, 1998.

Sydenham, P.H., *Measuring Instruments: Tools of Knowledge and Control*, Peter Peregrinus Ltd. Stevenage (1979).

Wernet, M.P., "3-Component Planar PIV Utilizing Fuzzy Inference," *AIAA Advanced Measurement and Ground Technology Conference*, New Orleans, Louisiana, June 18-20, 1996.

Wernet, M.P., "A Flow Field Investigation in the Diffuser of a High-Speed Centrifugal Compressor Using Digital Particle Imaging Velocimetry," *Measurement Science Technology*, pp. 1007-1022, February 2000.

Yanta, W. J. and Ausherman, D.W., "A 3-D Laser Velocimeter For Use In High-Speed Flows," *7th Biennial Symposium on Turbulence*, University of Missouri-Rolla, September 21-23, 1981.

Yeh, Y. and Cummins, H.Z.: "Localized Fluid Flow Measurements with a He-Ne Laser Spectrometer," *Applied Physics Letters*, Vol.4, No. 10, pp. 176-178, May 1964.

Young, H.D., *University Physics*, 8th Edition, Addison-Wesley Publishing Company, pp. 551-553, 593-596 and 1085-1087, 1992.

REPORT DOCUMENTATION PAGE

1. REPORT DATE *(DD-MM-YYYY)*	2. REPORT TYPE	3. DATES COVERED *(From - To)*
01- 11 - 2008	Contractor Report	

4. TITLE AND SUBTITLE

The Development of Point Doppler Velocimeter Data Acquisition and Processing Software

5a. CONTRACT NUMBER

NNL07AA00B

5b. GRANT NUMBER

5c. PROGRAM ELEMENT NUMBER

6. AUTHOR(S)

Cavone, Angelo A.

5d. PROJECT NUMBER

5e. TASK NUMBER

NNL07AM34T

5f. WORK UNIT NUMBER

599489.02.07.07.06.02

7. PERFORMING ORGANIZATION NAME(S) AND ADDRESS(ES)

NASA Langley Research Center
Hampton, VA 23681-2199

8. PERFORMING ORGANIZATION REPORT NUMBER

9. SPONSORING/MONITORING AGENCY NAME(S) AND ADDRESS(ES)

National Aeronautics and Space Administration
Washington, DC 20546-0001

10. SPONSOR/MONITOR'S ACRONYM(S)

NASA

11. SPONSOR/MONITOR'S REPORT NUMBER(S)

NASA/CR-2008-215545

12. DISTRIBUTION/AVAILABILITY STATEMENT

Unclassified - Unlimited
Subject Category 35
Availability: NASA CASI (301) 621-0390

13. SUPPLEMENTARY NOTES

Langley Technical Monitor: Kenneth D. Wright

14. ABSTRACT

In order to develop efficient and quiet aircraft and validate Computational Fluid Dynamic predications, aerodynamic researchers require flow parameter measurements to characterize flow fields about wind tunnel models and jet flows. A one-component Point Doppler Velocimeter (pDv), a non-intrusive, laser–based instrument, was constructed using a design/develop/test/validate/deploy approach. A primary component of the instrument is software required for system control/management and data collection/reduction. This software along with evaluation algorithms, advanced pDv from a laboratory curiosity to a production level instrument. Simultaneous pDv and pitot probe velocity measurements obtained at the centerline of a flow exiting a two-inch jet, matched within 0.4%. Flow turbulence spectra obtained with pDv and a hot-wire detected the primary and secondary harmonics with equal dynamic range produced by the fan driving the flow. Novel,hardware and software methods were developed, tested and incorporated into the system to eliminate and/or minimize error sources and improve system reliability.

15. SUBJECT TERMS

Doppler global velocimetry; LabVIEW; Laser velocimetry; Particle image velocimetry; Point doppler velocimetry; Anemometer; Data acquisition; Fluid flow instrumentation; Hot-wire; Pitot probe

16. SECURITY CLASSIFICATION OF:			17. LIMITATION OF ABSTRACT	18. NUMBER OF PAGES	19a. NAME OF RESPONSIBLE PERSON
a. REPORT	b. ABSTRACT	c. THIS PAGE			STI Help Desk (email: help@sti.nasa.gov)
U	U	U	UU	142	19b. TELEPHONE NUMBER *(Include area code)* (301) 621-0390